



UNIVERSITÉ DE STRASBOURG
France

UNIVERSITÉ DE FREIBURG
Allemagne



ÉCOLE DOCTORALE Physique et Chimie-physique
Institut Charles Sadron (UPR22-CNRS) Strasbourg

THÈSE EN COTUTELLE présentée par :
Charchit KUMAR

Soutenue le : **28 mai 2019**

Pour obtenir le grade de : **Docteur de l'Université de Strasbourg**
&
Docteur de l'Université de Freiburg

Discipline/ Spécialité : *Biomécanique*

**Quantitative and qualitative investigation of adhesion
and friction on textured surfaces: inspiration from
insect-plant interactions**

THÈSE dirigée par :

Prof. LE HOUEROU Vincent
Prof. SPECK Thomas

Professeur, Université de Strasbourg
Professeur, Université de Freiburg

RAPPORTEURS :

Dr. RESTAGNO Frédéric
Dr. FEDERLE Walter

Chargé de recherche, Université Paris-Sud, Paris
Docteur, Université de Cambridge

EXAMINATEURS

Prof. RÜHE Jürgen
Prof. BUENO Marie-Ange

Professeur, Université de Freiburg
Professeur, Université de Haute-Alsace, Mulhouse

DISSERTATION

Quantitative and qualitative investigation of adhesion
and friction on textured surfaces: inspiration from
insect-plant interactions

Inaugural-Dissertation

to obtain the Binational Doctoral Degree

Faculty of Biology, Albert-Ludwigs-Universität Freiburg, Freiburg im Breisgau, Germany
&
Doctoral School of Physics and Physical Chemistry, Université de Strasbourg, France



Presented by

Charchit KUMAR
Born in Pheena, Bijnor, India

Freiburg im Breisgau
(March 2019)

Diese Arbeit wurde erstellt unter der Leitung von

Herrn Prof. Dr. Thomas Speck
an der Albert-Ludwigs-Universität zu Freiburg
Fakultät für Biologie
Schänzlestraße 1
79104 Freiburg im Breisgau, Germany

Herrn Prof. Dr. Vincent Le Houérou
An der Université de Strasbourg
Laboratoire ICube UMR 7357
IUT Robert Schuman - Dpt Génie Civil
72 route du Rhin, Illkirch, France
und dem zugehörigen Institut Charles Sadron (ICS)
CNRS UPR022, 23 rue du Loess, BP 84047,
67034 Strasbourg Cedex 2, France

Dekan der Fakultät:	Prof. Dr. Wolfgang Driever
Promotionsvorsitzender:	Prof. Dr. Andreas Hiltbrunner
Betreuer der Arbeit:	Prof. Dr. Thomas Speck Prof. Dr. Vincent Le Houérou
Referent:	Prof. Dr. Thomas Speck
Koreferent	
Drittprüfer:	

Tag der Verkündung des Ergebnisses:

...memories of my grandparents

Mr. CHARCHIT KUMAR was a fellow member of the International Doctoral Programme of the University of Strasbourg during his PhD, from 2016 to 2018. He has benefited from specific financial support by the fellowship and, has attended several transversal training courses on the topics of general European interest presented by international experts. Mr. KUMAR's thesis was recognised as a Cotutelle de thèse promotion from the Franco-German University (Université franco-allemande/ Deutsch-Französische Hochschule) and received thesis sponsorship and mobility funding.

This PhD research project has been conducted as a part of cotutelle (bi-national) agreement between the University of Freiburg and the University of Strasbourg.

This thesis project was carried out under the framework of International Research Training Group (IRTG) "Soft Matter Science: Concepts for the Design of Functional Materials", a joint Doctorate program. This thesis was prepared: in the Botanical Garden and Faculty of Biology, University of Freiburg and in the Freiburg Centre for Interactive Materials and Bioinspired Technologies (FIT); in the Institut Charles Sadron (ICS, CNRS UPR-022) associated with the Université de Strasbourg.

Preface

This dissertation is written in a cumulative style. A large part of the results of this doctoral thesis has been presented in four manuscripts (A, B, C and D), which can be found in Chapter 6. Manuscript A was published in March 2018 in the *Royal Society Open Science Journal*. Manuscript B was published online in December 2018 in the journal *Philosophical Transactions of the Royal Society A*. At the time of thesis submission, Manuscript C was in the submission process. Manuscript D is a ‘ready to submit’ draft on the last study (friction investigation) done in this thesis.

This dissertation is written mainly in English, and an abstract in German and French along with a summary in French are supplemented. The structure of this dissertation is divided into six chapters. Chapter 1 contain a general introduction to the thesis topic, a state of the art, and a description of the objectives of this work. Chapter 2 describes the materials and methodology used in this work and adds some further information to the details of experiments, that are not included in the manuscripts. Chapter 3 presents results and discussion of the important results accomplished in this work. This is followed by a summary of insights gained and an outlook, in Chapter 4. Finally, a bibliography is presented in section 5 of the dissertation. An appendix is attached at the end of this thesis.

This thesis was carried out as a part of a broad research theme “Soft Matter Science: Concepts for the Design of Functional Materials” of International Research Training Group (IRTG) and funded by the German Research Foundation (Deutsche Forschungsgemeinschaft, DFG).

Acknowledgements

The quest for facts and truth spirit of scientific philosophy has always been a great attraction and inspiration for me. I am well-pleased to get an opportunity to explore a tiny bit of it during my PhD research. This would not be possible without the continuous guidance, support and encouragement from both my supervisors (doktorvater), Prof. Vincent Le Houérou and Prof. Thomas Speck. Dear Vincent, you were always there to support me in all odd and even situations during this thesis and very patiently corrected my mistakes. Dear Thomas, your cheering-up and positive attitude towards new ideas, irrespective of discipline, always encouraged me. I express my sincere gratitude to both of you for believing in me and carving my scientific skills throughout these years. I would like to extend my thanks to Dr. Holger Bohn for his close guidance at the very beginning of my PhD, in particular for introducing me to the plant biology. It was a great pleasure working with you.

In general, working and living in both Germany and France have been a great experience, which taught me a lot of new things and sharpened my personality. I would like to thank each and everyone who accompanied and supported me throughout this amazing journey.

I am deeply grateful to every (former and current) member of the Plant Biomechanics Group and the Botanical Garden for being extremely supportive and helpful throughout these years. Especially Amar, Anna, Falk, Kathi, Marco, Max-2, Sandra and Tim, you all were not only just colleagues but also became good friends. *Herzliches dankeschön* for a great time together and invaluable support in countless ways. A special thanks go to Alejandro, a master student I co-supervised with pleasure, and both student assistants (Hiwi) Ramesh and Rajesh for helping me in various experiments.

This thanksgiving will be incomplete without extending my gratitude towards Birgitta and Jana (coordinator IRTG), you both extraordinarily helped me throughout these years. I would also like to thank all institute administrators, technical and secretarial staffs, financiers (IRTG, IGA Freiburg, and PDI Strasbourg) for their active support. I extend my special thanks to Odile for her generous support, especially during the Freiburg to Strasbourg transition period.

From Strasbourg side, I would like to express my gratitude to the whole PMTP team members for their support. A special thanks to Damien, our lab engineer, for helping me to plan and design my contact mechanics experiments. How can I forget to mention my international lunch group (Amparo, Andrea, George, Jean, Justine, Laure, Maryam, Othmene, Randy, Rigoberto,

Vaibhav and Vishnu); each and every one of you for being dear and very supportive over the years. *Merci du fond du coeur* for enriching my French skills and for endless fun everyday over the lunch table. I owe my gratitude to Tathagata, Manish and Suresh sir for their constructive advice and proof-reading. My heartfelt thanks go to my dear friends outside the institute, Antoine, Bechara, Chockalingam Damien, Elsa, Elisabetta, Farouk, Laura, Lydia, Marc and Shree for sharing the delighting and joyful moments during these years in Strasbourg. Indeed, I am blessed to have met Muthu and Satish, earnest thanks for extraordinarily supporting and helping me in multitudinous ways. I am in debt to my close friends from IIT days; Amit, Arjun, Jitu, Sandeep and Satish, for cheering me and being together during many struggles.

Finally, my brother, Kamal, who is very close and beloved to me, and always there with me irrespective of time or situation. I would also like to express my deepest gratitude to all our common friends and the family members (Ankur, Bittu, Dolly, Gaurav, Lala, Neeraj, Sushant, Sweeta di, Vishal and Vikas) for their enormous love and support.

Ultimately, back home in my village (Pheena) in India, my parents for their infinite love and indispensable support, irrespective of the circumstances. I am not audacious enough to express my gratitude in words; the best would be to follow the way of life they taught me.

- *Danke Schön, Merci Beaucoup, Thank you, and धन्यवाद (Dhanyavād)* –

Contents

Preface	VI
Acknowledgements	VIII
List of Figures	XII
Abbreviations and Symbols	XIV
Abstract	XVI
Kurzzusammenfassung	XVIII
Résumé	XX
1 Introduction	1
1.1 Insect-plant interactions	1
1.1.1 Plant surfaces.....	1
1.1.2 Insect’s adhesive pads	3
1.2 The state-of-the-art: replication techniques.....	4
1.3 Contact mechanics.....	6
1.3.1 Adhesion mechanics.....	6
1.3.2 Friction mechanics	11
1.4 Aims and scope of this work	15
2 Materials and Methodology	18
2.1 Model plant leaves	18
2.2 Plants leaf surface replication	19
2.3 Model adhesive system	20
2.4 Surface morphology characterization.....	21
2.4.1 Scanning electron microscopy.....	21
2.4.2 Confocal laser scanning microscopy.....	22
2.5 Strategy to accomplish real contact visualization	22
2.6 Modified adhesion force tester	23
2.7 Friction force tester	24

2.8	Image processing and analysis	25
3	Results and Discussion	26
3.1	Plants leaf replication	26
3.2	Adhesion mechanics investigation	29
3.3	Friction mechanics investigation.....	33
4	Summary	37
5	References	43
6	Publications and Manuscripts	51
6.1	Manuscript A.....	53
6.2	Manuscript B	62
6.3	Manuscript C	85
6.4	Manuscript D.....	116
	List of Publications	139
	Appendix	141

List of Figures

Figure 1.1 Simplified schematic representing a general construction of the outermost layers of the plant epidermis cells and their major components.	1
Figure 1.2 Simplified model of epidermis cell cross sections representing different bases leading to patterning of plant leaf surfaces.	2
Figure 1.3 Schematic review of the most prominent functions of the plant boundary layer on a hydrophobic micro-structured surface.....	3
Figure 1.4 SEM images exhibiting adhesive pad morphology of (a) a male dock beetle (<i>Gastrophysa viridula</i>) and (c) an Indian stick insect (<i>Carausius morosus</i>).	4
Figure 1.5 Schematic sketch of a model contact between two spheres of radii R_1 and R_2 are compressed together by the application of an external force P	7
Figure 1.6 Schematics illustrating three main adhesion mechanics theories (Hertz, JKR and DMT)....	8
Figure 1.7 The transition between the DMT theory and the JKR theory.	11
Figure 1.8 Schematic sketch of a model sliding contact between a sphere and smooth substrate, under an application of normal load (F_n).	13
Figure 1.9 Master curves for the friction coefficient of the acrylonitrile-butadiene rubber C on four surfaces.	14
Figure 1.10 Comprehensive recapitulation of this work strategy.	16
Figure 2.1. Photographs of original plant leaves (a, b, c), and their SEM images (d, e, f), and CLSM microscope images (g, h, i).	18
Figure 2.2. Simplified schematic sketch of the two-step replication process.....	19
Figure 2.3. (Left) Stereo microscope image of tarsus of a stick insect (<i>Carausius morosus</i>) with paired claws and the intervening smooth adhesive pad (Arolium). (Right) Photograph of the model adhesive system with a half- spherical PDMS tip is embedded within the tip holder.....	21
Figure 2.4. Simplified schematic sketch (left) exhibiting how the <i>in-situ</i> real contact visualization was achieved.....	22
Figure 2.5. (Left) Schematic of a typical pull-off tests for adhesion force investigation. (Right) Photograph of the modified nanoindenter with force measurement head.	23
Figure 2.6. (Left) Schematic of sliding friction test on textured surfaces together with <i>in-situ</i> real contact visualization. (Right) Photograph of the modified nanoindenter setup with friction configuration.....	25

Figure 3.1. SEM images of original plant leaf surfaces (<i>a- c</i>) and their PDMS replicas (<i>d- f</i>) developed using Epoxy-PDMS replication technique.	26
Figure 3.2. Qualitative comparison of replication quality of three techniques for <i>L. chinensis</i> leaf. ...	27
Figure 3.3. (Up) Representative force-time (displacement) curve obtained for a typical adhesion test curve for a whole test cycle on smooth PDMS sample, at a pre-load (F_L) of 1.5 mN. Different points of interest (<i>a-f</i>) are marked on the curve and their corresponding <i>in-situ</i> images (down).....	29
Figure 3.4. Force- displacement curve (pull-off retraction part) obtained at different normal pre-load conditions as indicated in mN.	30
Figure 3.5. High definition real contact images recorded, at full pre-load loading stage, on all four surfaces.	32
Figure 3.6. <i>In-situ</i> real contact images during sliding friction tests (under shear state) on all four substrates, at a normal load of 1.5 mN and a sliding speed of 16.67 $\mu\text{m/s}$	34
Figure 3.7. Friction coefficient versus sliding distance for all four surfaces investigated, at a constant normal load (1.5 mN) and sliding speed (16.67 $\mu\text{m/s}$).	35

Abbreviations and Symbols

Abbreviations:

CLSM	Confocal laser scanning microscopy
DI	Deionized water
DMTA	Dynamic mechanical thermal analysis
Epoxy	Epoxy resin
IPA	Isopropyl alcohol
PDMS	Polydimethylsiloxane
PMMA	Poly(methyl methacrylate)
PVS	Poly-vinyl siloxane
SEM	Scanning electron microscopy
UV	Ultraviolet light

Symbols:

A_{ap}	Apparent contact area (μm^2)
μ	Coefficient of friction
K	Combined (effective) elastic modulus (MPa)
a	Contact radius (μm)
a_d	Contact radius at absolute zero load condition in adhesion investigation (μm)
a_e	Contact radius at lowest force point where contact abruptly vanished to zero (μm)
$ACCF_{MAX}$	Cross-covariance function ratio
Z_0	Equilibrium separation in Lennard-Jones potential (nm)
P or F_n	Applied normal force (mN)
T_g	Glass transition temperature ($^{\circ}\text{C}$)
A_n	Normalized contact area
N	Number of tests
ν	Poisson's ratio
F_L	Pre-load in adhesion investigation (mN)
F_{ad} or P_{off}	Pull-off adhesion force (mN)
R	Radius of curvature (μm)
A_r	Real or true contact area (μm^2)
D_s	Relative topography difference
V	Sliding speed ($\mu\text{m/s}$)
σ	Stress (Pa)
γ	Surface energy (mJ m^{-2})
μ_T	Tabor's parameter
F_t	Tangential (friction) force (mN)
W	Work of adhesion (mJ m^{-2})
E	Young's modulus (MPa)

Abstract

Adhesion and friction exist in many technical systems as well as in natural ones. Both phenomena have a profound influence on the durability and efficiency of technical systems, of particular note are micro-contact applications with high surface to volume ratio. A well-recognised approach to precisely tune these characteristics - besides altering the physicochemical properties - is the micro and/or nano-structuring of the interacting surfaces. Inspiringly, plant leaf surfaces are often decorated with diverse and species-specific surface morphologies, and so show remarkable surface functionalities: slipperiness, self-cleaning and anti-adhesive, just to name a few. However, these biological surface functionalities are driven by an interplay of surface structuring and chemistry, making it a highly intricate system to investigate with many unsolved questions. Altogether, this interdisciplinary work aimed to perform a systematic investigation of adhesion and friction mechanics on micro-structured surfaces directly replicated from the surface of plant leaves, in contact with a model adhesive system which is inspired from the adhesive pad (Arolium) of an insect.

Three different model plant leaves and a technical surface, with variable size range (0.5 - 100 μm), shape and complexity (hierarchical levels) of their surface morphologies, were chosen in this work. Surface morphologies of the fresh leaves were directly transferred onto a soft viscoelastic polymer. For this, three different replication approaches were established and comprehensively investigated. Scanning electron microscopy was utilised to analyse the surface morphology of the leaves and to qualitatively compare the replication accuracy of the replication techniques. Furthermore, a quantitative evaluation of the replication quality was performed, by applying two model parameters (cross-covariance function ratio and relative topography difference) on the line profiles and the surface profiles recorded with confocal laser scanning microscopy. Both qualitative and quantitative investigations came out well in-line, confirming the precise replication ability of Epoxy-PDMS technique.

For the contact mechanics investigation, a high-resolution (load or displacement control) nanoindenter was modified, with incorporating a unique feature to record the *in-situ* real-contact images. A JKR (Johnson, Kendall and Roberts) contact mechanics based pull-off force test, at a low force range, was performed on the bio-replicated samples by forming contact against a model adhesive tip. A series of tests were carried out to quantitatively evaluate and thoroughly understand the effect of pre-load on adhesion force characteristics. A significant enhancement in adhesion force with increasing in pre-load was observed on *Hevea* replica (fine micro-structuring) and *Litchi* replica (complex hierarchical morphology), unlike the other two

surfaces: no specific influence was noted on smooth PDMS and *Ludisia* replica (coarse conical shape patterns). An overall comparison between the surfaces clearly demonstrated significant differences in the resulting adhesion force, discussed according to each surface's topographic profile. Furthermore, results from real-time synchronization of the exact real contact image with corresponding force value pointed out distinct attachment-detachment modes, based on different pre-load conditions and distinct surface topographies.

Next study was achieved to investigate the friction mechanism on all four substrates that were utilised in the preceding study of adhesion mechanics. Friction tests were carried out in the unidirectional sliding configuration (with the same nanoindenter apparatus used in previous section), to examine the effect of normal load and sliding speed on the friction characteristics. All surfaces showed a decrease in friction coefficient with increasing the normal load, however, each surface exhibited distinct decreasing behaviours. Examination of synchronized *in-situ* videos revealed the different real contact evolution behaviours and the distinct sliding mechanisms, arising from surface-specific topographies. A clear dependency of the friction response on sliding speed was recorded for all surfaces, attributed to the rate-dependent viscoelastic behaviour of PDMS. Accordingly, the friction behaviour was correlated and analysed with the PDMS loss factor in the same frequency range. The overall comparison manifests, the *Ludisia* and *Litchi* replicas significantly lowered the friction coefficient as compared to the smooth PDMS and *Hevea* replica.

The replication technique advancement achieved in this work may represent an effective alternative for future bio-replication studies. In addition, insights and concepts gained from this study may provide valuable assistance for designing the bio-inspired functional surfaces, particularly to fine tune the adhesive and frictional characteristics of smart surfaces.

Kurzzusammenfassung

Adhäsion und Reibung kommen sowohl in vielen technischen als auch natürlichen Systemen vor. Beide Phänomene haben einen großen Einfluss auf die Haltbarkeit und Effizienz technischer Systeme, insbesondere bei Mikrokontakt-Anwendungen mit hohem Oberflächen-Volumen-Verhältnis. Ein anerkannter Ansatz zur präzisen Abstimmung dieser Eigenschaften ist - neben der Veränderung der physikalisch-chemischen Eigenschaften - die Mikro- und/oder Nanostrukturierung der interagierenden Oberflächen. Die Oberflächen pflanzlicher Blätter besitzen oftmals eine Vielzahl artspezifischer Morphologien, die bemerkenswerte Eigenschaften aufweisen und als Inspirationsquellen dienen können: Rutschfestigkeit, Selbstreinigung und Antihafte Wirkung sind nur einige Beispiele. Diese biologischen Oberflächeneigenschaften basieren auf dem komplexen Zusammenspiel von Oberflächenstrukturierungen und chemischen Eigenschaften wodurch sich ein sehr komplexes System ergibt, bei welchem es noch viele ungelöste Fragen zu erforschen gibt. Die vorliegende interdisziplinäre Arbeit zielte darauf ab, eine systematische Untersuchung der Adhäsions- und Reibungsmechanik auf mikrostrukturierten Oberflächen, direkt repliziert von der Oberfläche von Pflanzenblättern, durchzuführen. Hierfür wurde ein Modell-Haftsyste, welches den Haftpolstern (Arolien) von Insekten nachempfunden wurde, entwickelt.

Blattoberflächen dreier verschiedener Pflanzenarten sowie eine technische Oberfläche, deren Oberflächen-Morphologien in Bezug auf Größe (0,5 - 100 μm), Form und Komplexität (hierarchische Ebenen) variierten, wurden für diese Arbeit ausgewählt. Frisches Blattmaterial diente als Vorlage zur direkten Übertragung der Oberflächen-Morphologien auf ein weiches, viskoelastisches Polymer. Hierfür wurden drei unterschiedliche Replikationsansätze etabliert und umfassend untersucht. Darüber hinaus wurden rasterelektronenmikroskopische Untersuchungen durchgeführt, um die Oberflächenmorphologie der Blätter zu analysieren und die Genauigkeit der drei Replikationstechniken qualitativ zu vergleichen. Eine quantitative Bewertung der Replikationsqualität wurde ebenfalls durchgeführt, indem zwei Modellparameter (das Kreuzkovarianzverhältnis und die relative Topographiedifferenz) auf die Linienprofile und die mit der konfokalen Laserscanning-Mikroskopie aufgenommenen Oberflächenprofile angewandt wurden. Sowohl die qualitativen als auch quantitativen Untersuchungen haben sich in der Praxis bewährt und bestätigen die hochpräzise Replikationsfähigkeit der Epoxy-PDMS-Technik.

Für die kontaktmechanischen Analysen wurde ein hochauflösender Nanoindenter (Last- oder Auslenkungskontrolle) mit einer einzigartigen Funktion ausgestattet, die eine *in-situ*

Aufzeichnung der realen Kontaktflächen ermöglicht. Haftkraftmessungen (Abzugsversuche) auf Basis der JKR (Johnson, Kendall und Roberts) Kontaktmechanik wurden für einen niedrigen Kraftbereich an Replikaten biologischer Proben durchgeführt, nachdem Kontakt zum Modellhaftsystem hergestellt worden war. In weiteren Untersuchungen wurde der Einfluss der Vorspannung auf die Eigenschaften der Haftkraft quantitativ nachvollzogen und bewertet. Eine signifikante Verbesserung der Haftkraft mit zunehmender Vorspannung wurde bei *Hevea*- (feine Mikrostrukturierung) und *Litchi*-Replikaten (komplexe, hierarchische Morphologie) beobachtet, wohingegen auf den übrigen Oberflächen, glattes PDMS und *Ludisia*-Replikat (grobe konische Formmuster), kein spezifischer Einfluss festgestellt werden konnte. Im Gesamtvergleich zeigten alle vier Oberflächen signifikante Unterschiede in ihren Haftkräften, die den jeweiligen Oberflächenprofilen zugeordnet werden konnten. Darüber hinaus zeigten die Ergebnisse der Echtzeit-Synchronisation des realen (*in-situ*) Kontaktbildes mit den korrespondierenden Kraftwerten eindeutige Anhaftungs- und Ablösungsmodi auf, die auf unterschiedlichen Vorspannbedingungen und Oberflächentopographien basierten.

In einer weiterführenden Studie wurde der Reibungsmechanismus auf allen vier Substraten, die in der vorangegangenen Studie zur Adhäsionsmechanik verwendet worden waren, untersucht. Mit demselben Nanoindenter, der bereits in der vorherigen Studie verwendet worden war, wurden unidirektionale Reibungstests in der Gleitkonfiguration durchgeführt, um den Einfluss der Normallast und der Gleitgeschwindigkeit auf die Reibungseigenschaften zu untersuchen. Alle Oberflächen zeigten eine Abnahme des Reibungskoeffizienten mit zunehmender Normallast, wobei die tatsächliche Abnahme von Oberfläche zu Oberfläche verschieden war. Die Auswertung des synchronen *in-situ* Videomaterials zeigte verschiedenartige Entwicklungen der realen Kontaktfläche und der Gleitdynamik unter Scherung, die sich aus oberflächenspezifischen Topographien ergaben. Auf allen Oberflächen konnte eine eindeutige, schrittweise Abhängigkeit zwischen der Gleitgeschwindigkeit und dem Reibungsverhalten festgestellt werden, die auf das ratenabhängige viskoelastische Verhalten von PDMS zurückzuführen ist. Dementsprechend wurde das Reibungsverhalten mit dem PDMS-Verlustfaktor des gleichen Frequenzbereichs korreliert und analysiert. Ein Gesamtvergleich zeigte, dass *Ludisia*- und *Litchi*-Replikat deutlich niedrigere Reibungskoeffizienten im Vergleich zu denen des glatten PDMS und der *Hevea*-Replikat besitzen.

Die in dieser Arbeit erzielte Weiterentwicklung der Replikationstechnik kann eine effektive Alternative für zukünftige Bio-Replikationsstudien darstellen. Darüber hinaus können die Erkenntnisse und Konzepte aus dieser Studie ein wertvolles Hilfsmittel bei der Gestaltung bioinspirierter, funktionalisierter Oberflächen, sowie bei der präzisen Einstellung der Adhäsions- und Reibungseigenschaften zahlreicher „intelligenter“ Oberflächenanwendungen sein.

Résumé

L'adhérence et le frottement existent dans de nombreux systèmes techniques ainsi que dans les systèmes naturels. Ces deux phénomènes ont une influence profonde sur la durabilité et l'efficacité des dispositifs techniques, en particulier concernant les applications de micro-contacts avec un rapport surface/volume élevé. Une approche reconnue pour ajuster précisément ces caractéristiques - outre le fait de modifier les propriétés physico-chimiques - est la micro et/ou la nanostructuration des surfaces en contact. Les surfaces des feuilles de plantes sont souvent décorées avec des morphologies de surface diverses et spécifiques à chaque espèce, et présentent ainsi des fonctionnalités de surface remarquables : glissantes, autonettoyantes et anti-adhésives, pour n'en citer que quelques-unes. Cependant, ces fonctionnalités biologiques peuvent résulter d'un couplage entre la structuration et la chimie de la surface, ce qui en fait la plupart du temps un système très complexe à étudier. Ce travail interdisciplinaire visait à réaliser une étude systématique de la mécanique de l'adhérence et du frottement sur des surfaces microstructurées, directement répliquées à partir de surfaces de feuilles végétales, en contact avec une sonde adhésive modèle qui s'inspire de l'organe adhérent (Arolium) d'un insecte.

Trois feuilles de plantes modèles et une surface technique, de morphologies de surface de taille variable (0,5 - 100 μm), de forme et de complexité (niveaux hiérarchiques) différentes, ont été choisies dans ce travail. Les morphologies de surface des feuilles fraîches ont été directement transférées sur un élastomère viscoélastique. Pour ce faire, trois différentes approches de reproduction ont été utilisées et ont fait l'objet d'une étude approfondie. La microscopie électronique à balayage a été mise en œuvre afin d'analyser la morphologie de surface des feuilles et de comparer qualitativement la précision de reproduction des trois techniques. Une évaluation quantitative de la qualité de reproduction a également été réalisée, via l'estimation de deux paramètres topographiques (rapport de covariance croisée et différence topographique relative) appliqués à des profils et surfaces issus de microscopie confocale à balayage laser. Les résultats cohérents des études qualitatives et quantitatives ont confirmé la précision de la technique de reproduction Epoxy-PDMS.

Concernant l'étude de la mécanique des contacts, un nano-indenteur (pilotage en force ou en déplacement) a été modifié, permettant d'enregistrer les images *in situ* des contacts réels. Un test de décollement du contact (de type JKR - Johnson, Kendall et Roberts -) entre une sonde modèle et les surfaces étudiées a été mis en œuvre à faible charge sur les échantillons bio-répliqués. Une série d'essais a été menée afin d'évaluer quantitativement l'effet de la précharge

sur la force d'adhérence. Une augmentation significative de cette dernière avec l'augmentation de la pré-charge a été observée sur la réplique d'*Hévéa* (micro-structuration fine) et de *Litchi* (morphologie hiérarchique complexe), contrairement aux deux autres surfaces : aucune influence spécifique n'a été notée sur le PDMS lisse et la réplique de *Ludisia* (formes grossières et coniques). La comparaison entre les surfaces a clairement démontré des différences significatives dans la force d'adhérence résultante, discutées en fonction de chaque profil topographique. De plus, la synchronisation des images *in-situ* du contact réel avec le signal de force a mis en évidence des modes de collage/décollement distincts en fonction des conditions de pré-charge et des topographies de surface différentes.

L'étude suivante a été consacrée au frottement sur les quatre substrats utilisés dans l'étude d'adhérence. Des essais de frottement ont été effectués dans la configuration de glissement unidirectionnel (avec le même appareil nano-indenteur utilisé dans la partie précédente) afin d'examiner l'effet de la charge normale et de la vitesse de glissement sur les caractéristiques de frottement. Toutes les surfaces présentaient une diminution du coefficient de frottement avec l'augmentation de la charge normale, mais les surfaces présentaient des comportements distincts. L'examen des vidéos synchronisées *in-situ* a révélé les différents comportements d'évolution du contact réel et du mécanisme de glissement vis à vis des topographies spécifiques de surface. Une nette dépendance de la réponse au frottement à la vitesse de glissement a été enregistrée pour toutes les surfaces et attribuée au comportement viscoélastique du PDMS. Les comportements de frottement ont été ainsi corrélés et analysés à l'aide du facteur de perte du PDMS dans la gamme de fréquences considérée. La comparaison globale montre que les répliques de *Ludisia* et de *Litchi* ont considérablement réduit le coefficient de frottement par rapport à celui des répliques de PDMS lisse et d'*Hévéa*.

Les avancées obtenues dans le cadre de ces travaux en termes de technique de reproduction pourraient présenter un intérêt certain pour de futures études sur la bio-reproduction. De plus, les enseignements et les concepts issus de cette étude peuvent fournir une aide précieuse pour la conception des surfaces fonctionnelles bio-inspirées, notamment pour ajuster précisément les caractéristiques adhésives et de frottement de surfaces intelligentes.

1 Introduction

1.1 Insect-plant interactions

Contact mechanics of insect-plant interactions is mutually influenced by both sides which involves, on one side insect attachment organs, and on other side plant surfaces [1, 2]. Both counterparts comprise highly diversified chemical and physical properties, including complex geometries [3–5]. Following sections shed some light on both sides in turn.

1.1.1 Plant surfaces

Structural diversity of plant leaf surfaces: Approximately more than 400 million years of land plants evolution led to a vast diversity of structures on plant surfaces [4]. The plant surfaces are organized with a large variety of surface structuring, over a wide size range (from nano- to macro-scale), with distinct morphologies, and including several hierarchical levels [4, 6, 7]. Since the recent development of the electron microscopy technique, diverse morphologies of plant leaf surfaces has been classified and studied by researchers. Notable work on developing a detailed SEM micrographs database of plant surfaces was done by Barthlott and co-workers at the university of Bonn, Germany [8–10].

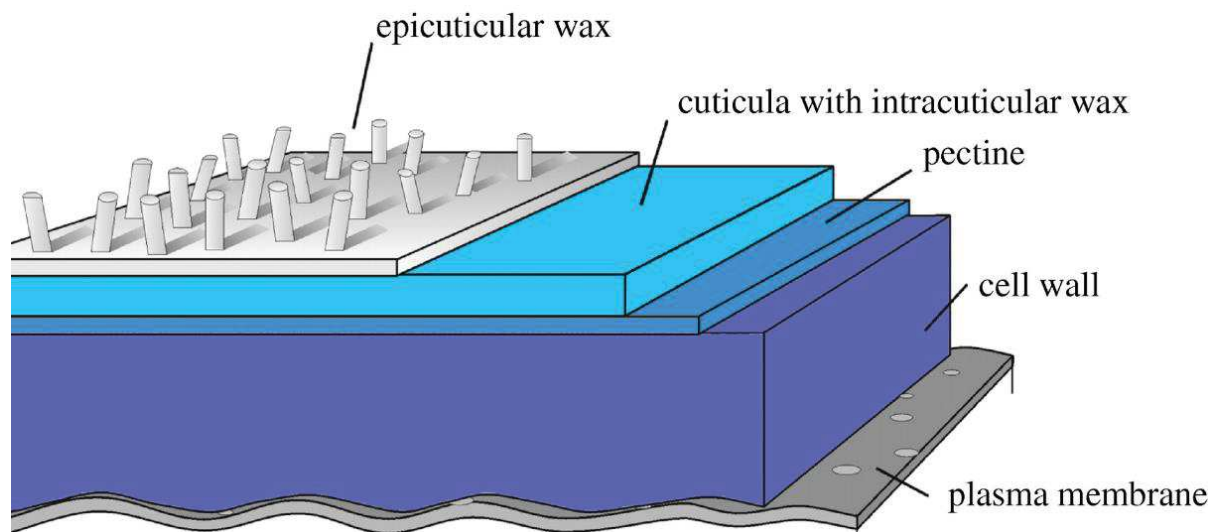


Figure 1.1 Simplified schematic representing a general construction of the outermost layers of the plant epidermis cells and their major components. Modified after [4].

The great structural diversity of plant leaf surfaces arises from the cell shapes, cell surface structures, and by the formation of multi-cellular structures [4]. The epidermis is the outermost cell layer of the primary tissues of all plants leaves. A basic and simplified structuring model

of an epidermal cell is presented in Figure 1.1. The cuticle, a thin extracellular membrane, is the outermost layer at the outside of an epidermal cell, which consists of cutin, polysaccharides and intracuticular wax, and superimposed with epicuticular waxes [4]. In general, epidermal cells create micro-scale surface morphologies, which can be classified in three different categories on the basis of the cell curvatures as described in detail by Koch *et al.* [4]: tabular (flat cells), concave (inside arched) and convex (outside arched). The convex cell is the most common cell type, which are found on leaves, flower-leaves and stems [11]. Epidermal cells are also decorated with different types of surface structuring. Most fine surface structuring within a single epidermis cell can lie in the range of less than one micrometre to several micrometres. Koch *et al.* [4] describes these cells surface structuring, on the basis of different sources of their development, in four different categories as schematically reported in Figure 1.2. Normally, cuticular folds are frequently found on flower petal surfaces [4].

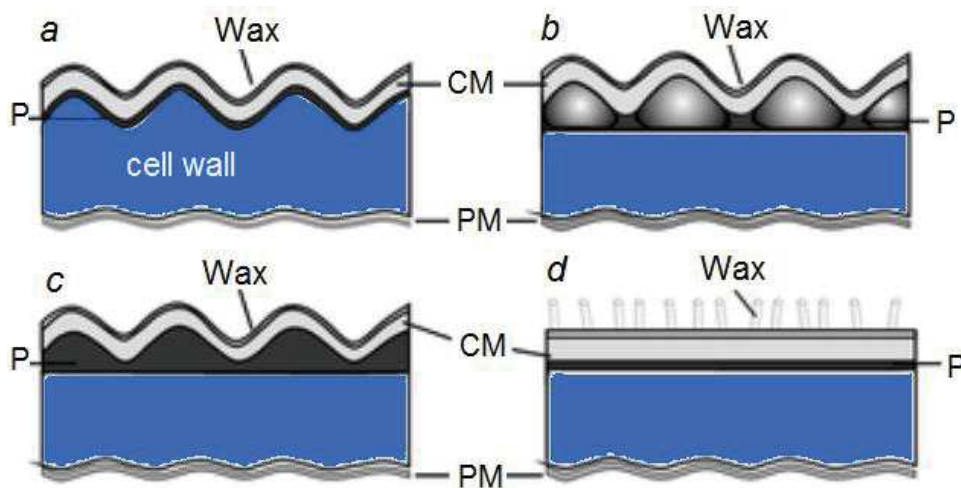


Figure 1.2 Simplified model of epidermis cell cross sections representing different bases leading to patterning of plant leaf surfaces. (a) The surface patterns are induced due to undulations of the underlying cell wall, (b) due to insertion of sub-cuticular minerals, (c) by folding of the cuticle and (d) by epicuticular waxes, positioned on top of the cuticle. CM = cuticular membrane, P = pectin, PM = plasma membrane. Modified after [4].

Multifunctional surfaces of plant leaves: The diverse surface structuring and the surface chemistry of plant leaves give rise to a variety of remarkable and inspiring functionalities, which have attracted a great attention, not only in biology but also in other disciplines, leading to get inspired, investigate and thus implement in bio-mimetic surface applications [11–13]. The plant cuticle provides various functional properties to plant leaves, as illustrated in Figure 1.3, and reviewed in-detail by Koch *et al.* [7, 11]. For instance, the slippery surface in some carnivorous plants (e.g. *Nepenthes alata* Blanco) for insect catching is caused by hierarchical

surface structuring and anti-adhesive properties against insects attachment of the rubber tree (*Hevea brasiliensis*) leaves result from their fine micro-structuring [14–16]. The well-known self-cleaning ability of the leaves of sacred lotus (*Nelumbo nucifera*) arise from the remarkable de-wetting ability due to the complex hierarchical surface structuring [17, 18]. The air retention ability of the floating fern *Salvinia molesta* is caused by the unique hairy surface morphologies (the Salvinia effect) [19, 20]. On flower leaves, the surface micro-structures (cuticular folding) assumed to be creating a prejudicial favourable path for insect pollinators to walk [4]. However, the relationship between structures and functionalities is not straight forward, as almost all these surface functionalities are driven by a complex interplay of heterogeneous material composition, surface chemistry and diverse surface structuring, and lead to a highly sophisticated system to investigate [11, 21, 22].

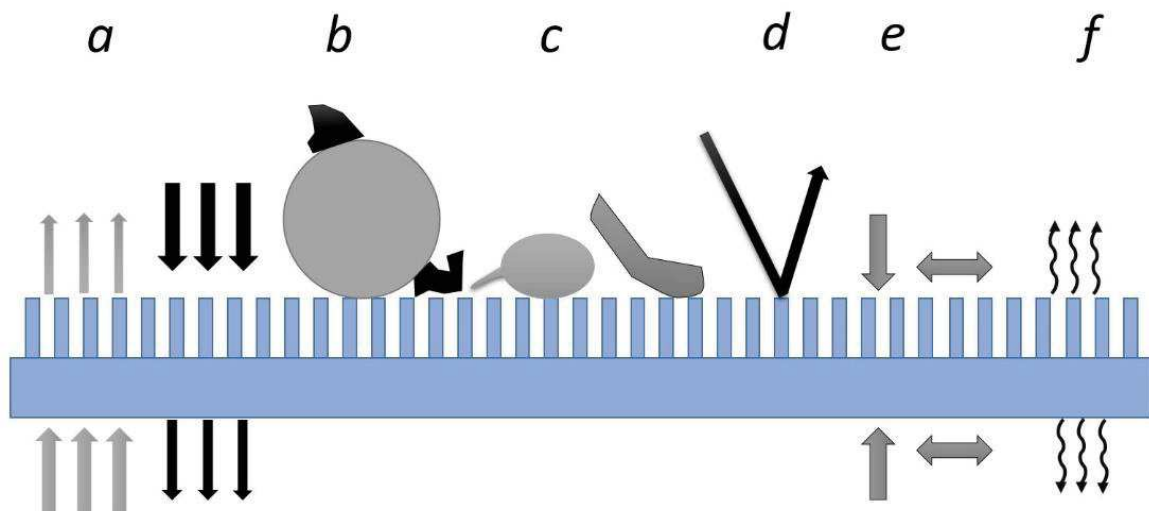


Figure 1.3 Schematic review of the most prominent functions of the plant boundary layer on a hydrophobic micro-structured surface. (a) Transport barrier: limitation of uncontrolled water loss from interior, (b) surface wettability and self-cleaning, (c) anti-adhesive, reduction of contamination pathogen attack and controlling of insect attachment/locomotion, (d) optical properties: protection against harmful radiation, (e) mechanical properties: resistance against mechanical stress and physiological integrity maintenance, and (f) signalling: cues for host–pathogen/ insect recognition and epidermal cell development. Modified after [11].

1.1.2 Insect’s adhesive pads

Like plant surfaces, insects have also evolved with having a vast kind of attachment structures. Attachment systems of insects facilitate climbing on, sticking to, running on or walking over different surfaces (e.g. on plant leaves or flowers) [23]. Interestingly, attachment systems developed in such a way, so that they provide a strong attachment to avoid falling and at the same time they enable easy detachment to able the insects to move [3, 24].

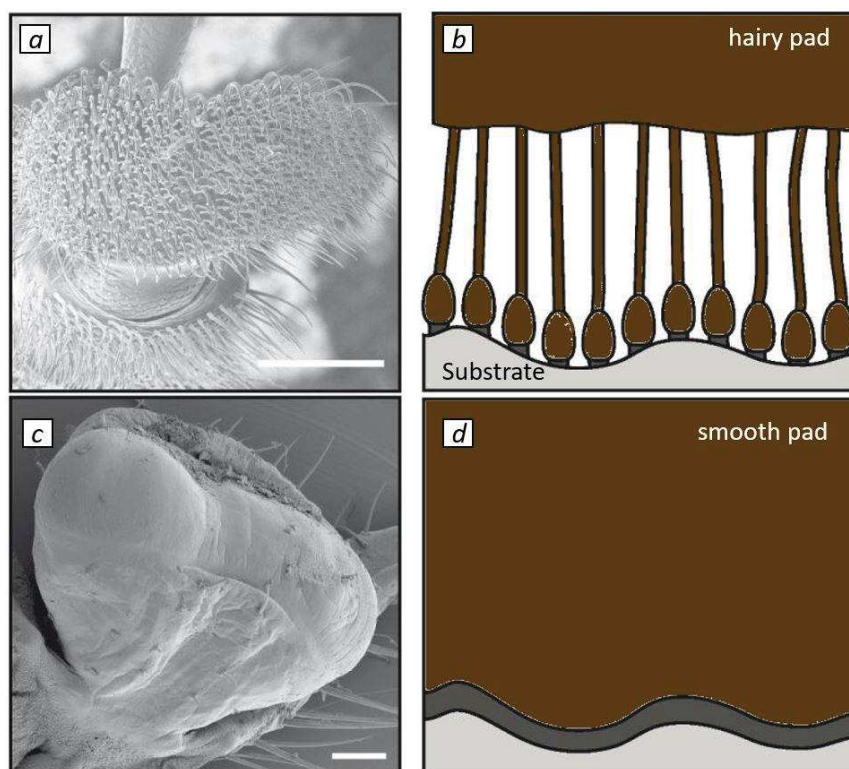


Figure 1.4 SEM images exhibiting adhesive pad morphology of (a) a male dock beetle (*Gastrophysa viridula*) and (c) an Indian stick insect (*Carausius morosus*). Simplified sketches of the close contact formation by the hairy (b) and smooth pads (d) to a non-smooth substrate. Modified after [25, 26].

In a broad classification, adhesive systems of insects can be divided into two principle types: “smooth” and “hairy” (fibrillar) pads [25, 27–29]. In the present research project, we took inspiration from smooth adhesive pad as a model attachment system. The surface of these adhesive pads appears smooth under a microscope, containing a soft (“pillow-like”) and specialized adhesive cuticle which can accommodate surface irregularities, as schematically shown in Figure 1.4 [30, 31]. The main mechanical characteristic of smooth attachment pads are the deformability and the softness of the pad material having viscoelastic properties [3, 28, 32, 33].

1.2 The state-of-the-art: replication techniques

In the past recent decades, bio-replication techniques have drawn an increasing interest from biologist as well as from the technical industry. Techniques to develop bio-replicas include atomic layer deposition, imprint lithography and replica moulding, physical vapour deposition methods, and sol–gel technique [34]. However, replica moulding is relatively advantageous as compared to other bio-replication techniques, on account of its easy, straight-forward and inexpensive procedure. It also allows direct utilisation of an original plant leaf as a master sample [34]. In general, the replica moulding is performed by filling a liquid polymeric material

onto a plant leaf (bio-template) master to generate a negative mould. Afterwards, this negative mould is used to transfer the surface structure onto a second material (positive replica) [21, 35–45]. The replication accuracy and quality largely depend on the choice of materials used for the negative mould and the positive replicas, respectively.

Back in 1987, Williams *et al.* [44] introduced a replication technique using a dental impression material (polyvinyl siloxane) to develop the negative mould and an epoxy resin for the positive replica. Later, this (PVS-epoxy) technique has been extensively investigated by several other researchers [21, 35, 39]. In this technique, a fresh leaf was covered with the PVS mixture and then manually pressed down with a flat slide. Fast curing at room temperature (approximately 2-5 minutes) of PVS and low adherence to leaf samples is useful to prevent artefacts [35]. However, quick polymerization of PVS could cause air to get trapped inside the micro-structure cavities, at the interface of mixture and leaf surface [35]. Recently various studies have utilised polydimethylsiloxane (PDMS) mixture to produce both negative mould and positive replicas (PDMS- PDMS) [37, 38, 41, 46, 47]. Here, in order to develop a negative mould, the fresh leaf sample was filled up with PDMS mixture and cured at high temperature (80-90°C) [37, 38]. The treatment of plant leaves with high temperatures is likely to facilitate shrinkage or collapse of surface topographies, due to evaporation of water from the cells during the process [48]. Furthermore, PDMS-PDMS technique also involves an additional intermediate step of an anti-stiction treatment on the negative mould by organosilane monolayer deposition, allowing for easy demoulding [37, 41, 46, 47]. For performing the organosilane monolayer deposition, the PDMS moulds need additionally to be treated under plasma, which can cause surface damage or instability [49]. Furthermore, during silane vapour deposition, aggregations of silane molecules can induce surface roughness [46, 50]. In general, an anti-stiction surface treatment degrades with time and replication cycles (production of three or four positive replicas) [47]. In another replication approach, positive replicas were developed on PMMA polymer from PDMS negative mould [40]. In this approach, plant leaves were also exposed to high temperature during the development of negative mould. Few other replication techniques comprise of the negative mould development on nickel template using sputtering and electroforming, and then the structures from the negative mould were further transferred to acrylonitrile–butadiene–styrene copolymer or to a UV-curable photopolymer [51, 52]. In these methods, the substrate surface was first metallized with gold sputtering and patterned by nickel electroforming [51]. The substrate needs to be exposed under vacuum for the gold sputter coating, which might induce cell shrinkage artefacts (surface distortion) [48, 53]. Altogether, each replication technique has its own advantage- disadvantages, and limitations according to

the specific application of the final replicas. However, a versatile replication technique would be one with the ability to replicate complex three-dimensional hierarchical structures, having high reproduction and precision, using simple and straightforward protocol, limiting intermediate treatments, and able to produce multiple replicas from a same negative mould.

1.3 Contact mechanics

Contact mechanics refers to the study when two bodies (or media) are brought into contact [54, 55]. When dealing with the insect-plant interactions, their contact could be better addressed thanks to contact mechanics involving two bodies: attachment system of insects and plant surfaces [1, 2]. In this contacting system, the contact mechanism is mutually determined by both sides material characteristics, chemical property, and surface structuring. It is important to bear in mind that the real situation of insect-plant interaction is further more complex [1]. Nevertheless, to make a meaningful and systematic study, one could consider to simplify this complex system by limiting or generalizing some parameters [21, 22, 56]. In the scope of this work, we emphasized two major issues of contact mechanics: adhesion and sliding friction, are introduced with related fundamentals in next sections.

1.3.1 Adhesion mechanics

Adhesion is the action or process of attraction between two free surfaces when they are brought into contact. In contrast, cohesion indicates the strength of like molecules to stick to each other within one material. The most common model system, when studying contact mechanics, can be conceptualised as a contact interaction of two spherical bodies, as illustrated with the simplified presentation in Figure 1.5. Three main theories of contact mechanics, Hertz, JKR and DMT with their stress distribution profiles, are presented in this section and for a convenient comparison, are schematically illustrated in Figure 1.6. The two latter involve adhesion phenomenon.

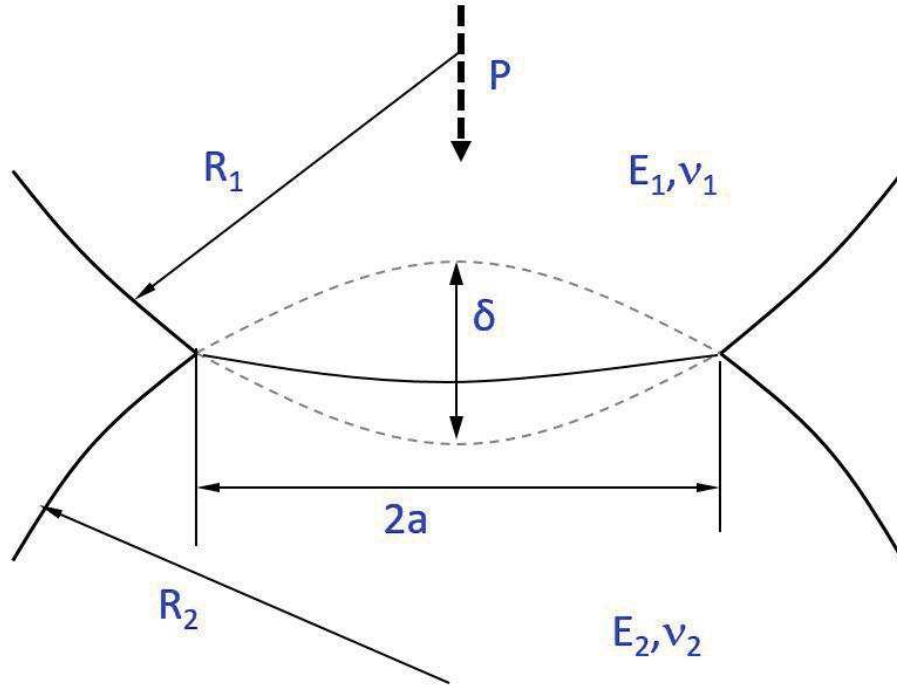


Figure 1.5 Schematic sketch of a model contact between two spheres of radii R_1 and R_2 are compressed together by the application of an external force P . $2a$ is the diameter of the resulting contact area and δ is the indentation depth.

Hertz theory: The very first work in the field of contact interaction of two bodies is credited to Heinrich Hertz [54, 57]. Back in 1882, Hertz studied, as a part of this graduate research, the contact interference patterns of a contact formed between two glass lenses, when pressed together. He gave a theory to quantitatively determine the radius (a) of contact caused by the externally applied normal load P , as described by equation 1:

$$a = \left(\frac{3PR}{4 E^*} \right)^{1/3} \quad (1)$$

where, R is the effective radius of curvature, calculated with equation 2, and E^* is the combine elastic modulus and can be estimated with equation 3.

$$\frac{1}{R} = \frac{1}{R_1} + \frac{1}{R_2} \quad (2)$$

$$\frac{1}{E^*} = \left[\frac{1 - \nu_1^2}{E_1} + \frac{1 - \nu_2^2}{E_2} \right] \quad (3)$$

where, E_1 , ν_1 and E_2 , ν_2 are Young's modulus and Poisson's ratio of contacting body 1st and 2nd, respectively. One need to cautiously note that, the Hertz's model is well applicable only for linear elastic and isotropic materials. This model assumed the radius of contact is considerably smaller as compared to the sphere radius and completely neglected the surface interactions such as contact adhesive forces (adhesion) [57–60]. So, as per this model, the interactions between surfaces can act only within the contact area. The contact restores back to zero contact area, as soon as the externally applied normal load is removed (Figure 1.6.a).

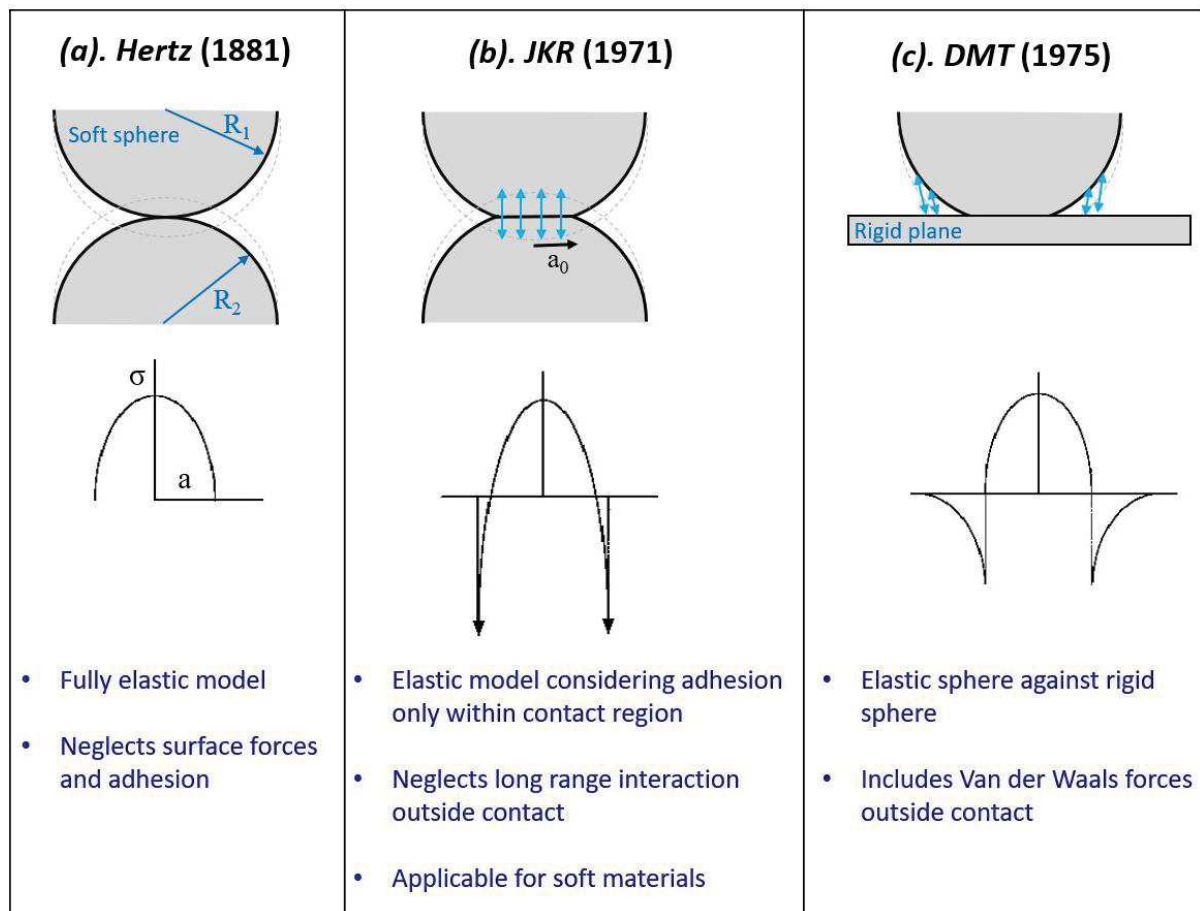


Figure 1.6 Schematics illustrating three main adhesion mechanics theories (Hertz, JKR and DMT) given for two spherical bodies in contact with their stress profiles under compressive load and key features. Adapted from [54, 61].

The JKR theory: To overcome limitations of Hertz's theory, in 1971, Johnson, Kendall and Roberts demonstrated a new model that considers the effect of adhesive forces in between two elastic spheres when brought in contact [58]. As of now, this is of the most popular adhesion mechanics theory for soft elastic contact, and known as 'the JKR theory'. Actually, Johnson *et al.* motivated their model by their experimental observations demonstrating a significantly larger contact area to that of measured from Hertz's theory [58]. They witnessed a finite area

of contact at the zero load condition during the unloading cycle (Figure 1.6.b). The JKR theory was obtained by correlating the area of contact to the elastic energy, mechanical potential energy and interfacial interaction strength (surface energy) [58]. Accordingly, JKR theory predicts the radius (a) of contact under an applied normal condition, as given by:

$$a = \left(\frac{R}{K} \left[P + 3\pi WR + \sqrt{6\pi WRP + (3\pi WR)^2} \right] \right)^{1/3} \quad (4)$$

where, K can be estimated with $4E^*/3$, and W accounts to the work of adhesion and can be related to Dupré's energy equation given below:

$$W = \gamma_1 + \gamma_2 - \gamma_{12} \quad (5)$$

γ_1 and γ_2 are the surface energy of interacting bodies (1st and 2nd respectively) and γ_{12} is the interfacial energy. Considering the JKR theory characteristics, a minimum negative (tensile) force is needed to separate the surface below zero load during the unloading cycle. This force is defined as the critical load or pull-off force (JKR), and is given by:

$$P_{\text{off(JKR)}} = -\frac{3}{2}\pi WR \quad (6)$$

Furthermore, by utilising the equation 4, one can estimate the value for the contact radius (a_0) at zero external load condition ($P = 0$).

$$a_0 = \left(\frac{6\pi WR^2}{K} \right)^{1/3} \quad (7)$$

Interesting to note here that, by neglecting the adhesive interactions ($W = 0$) between two bodies, the solution of JKR theory precisely matches with the Hertz's theory results. The JKR theory works well with soft materials, large objects and for high attractive interactions, and it has been well established by many experimental research [59, 60, 62–65].

The DMT theory: Shortly after, in 1975, Derjaguin, Muller and Toporov presented a complementary theory (DMT) assuming the contact stress profile same as in Hertzian

configuration, but including the van der Waals attraction outside the elastic contact region (Figure 1.6.c) [66]. DMT theory leads to the following equations for the radius of contact (a):

$$a = \left(\frac{R}{K} (P + 2\pi WR) \right)^{1/3} \quad (8)$$

and the pull-off force can be estimated with:

$$P_{\text{off(DMT)}} = -2\pi WR \quad (9)$$

Tabor's parameter: The question of applicability of JKR and DMT theories was open for a while in the contact mechanics community. Actually, there has been a heated contradiction where to use JKR model or DMT model, as both theories are valid, but for two opposite ends of adhesive contact [60, 67]. Therefore, to discriminate a JKR contact or a DMT one, Tabor [68] proposed a dimensionless physical parameter, popularly known as Tabor's parameter (μ_T), and given in Equation 10:

$$\mu_T = \left(\frac{RW^2}{E^* Z_0^3} \right)^{1/3} \quad (10)$$

here, Z_0 is the equilibrium separation of the surfaces in the Lennard-Jones potential and usually comes in between 0.3 and 0.5 nm [62, 69]. Moreover, in physical understanding, μ_T could be relate to the ratio of normal elastic deformation (due to adhesion without of external normal load) to the spatial range to the adhesion forces themselves [60]. For the appropriate application the JKR or DMT model, the usual transition appears in between 0.1 and 5 value of μ_T . If μ_T is larger than 5 then the JKR model can utilised and for the μ_T value less than 0.1 then the contact system well described using DMT theory [68, 69]. The DMT theory is well applicable for hard solids with week attractive interactions, whereas the JKR theory decently agrees for soft materials with strong adhesive forces [60, 67]. Later on, Maugis [67] introduced a composite model (known as The Maugis-Dugdale model), nicely establishing a continuous transition between the JKR and DMT limits for the entire range of materials with a transition parameter (λ), which is similar to the Tabor's parameter (μ_T) [60].

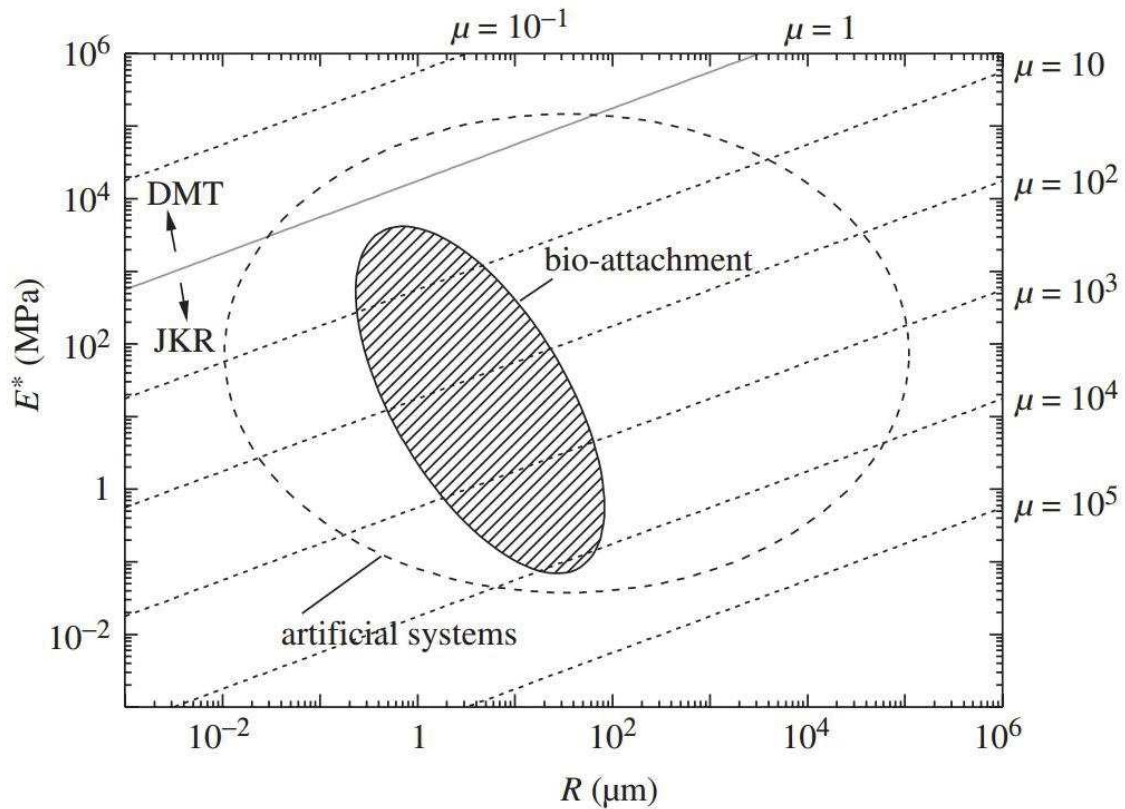


Figure 1.7 The transition between the DMT theory and the JKR theory (indicated by the solid line). R , μ and E^* are reduced contact radius, effective modulus and the Tabor's parameter, respectively. The two ellipses represent roughly the range of parameters in natural attachment devices and the range accessible by artificial attachment systems [70].

In the context of contact mechanics of biological attachment systems, it is worthwhile to mention a comprehensive work by Spolenak *et al.* demonstrating that the most natural attachment system can be well treated within the framework of the Johnson- Kendall- Roberts (JKR) theory [70]. They evaluated the Tabor's parameter based on contact radius and reduced modulus of natural attachment devices and delineate the transition region between the two theories (JKR and DMT), as shown in Figure 1.7.

1.3.2 Friction mechanics

Friction describes the force resisting the relative motion of two bodies when sliding against each other. Friction is a crucial aspect right from the design stage of every engineering system involving contacting surfaces [71, 72]. Two forms of friction processes are usually described: the static friction is the force at the onset of sliding and kinetic (or sliding) friction is defined as the force required to keep the contacting bodies in motion. Usually, static friction is greater than the kinetic friction [71]. Classically, the friction phenomenon during sliding could be formulated in three laws, are as follows. The first law of friction was given by Amontons in

1699, which states that the frictional force (F_t) between two macroscopic bodies is proportional to the applied load (F_n) [73]. This can be expressed with the simple equation 11.

$$F_t = \mu F_n \quad (11)$$

where the proportionality coefficient ‘ μ ’ is called the coefficient of friction. Amontons’ second friction law holds that the friction force between two bodies is independent of the macroscopic (apparent) contact area. However, in later years, it was realized that the macroscopic contact (or apparent contact; A_{ap}) is most of the time rough and thus comprises of a large number of small real contact asperities (A_i) with various geometries [71, 74, 75]. The total real contact area ($A_r = \sum A_i$) comes out smaller than macroscopic contact [75, 76]. Finally, the third law of friction was proposed by Coulomb (1736-1806), which says that the kinetic friction force is independent of the sliding speed [71]. These friction laws do not always hold adequately true, especially when dealing with small scale friction, lubricated contact or the sliding interaction of polymeric materials (or at least one of the contacting body is a polymer), which has significantly different features than that of typical engineering materials (wood and metals for example): visco-elasticity and adhesion may be involved [72, 77–79].

Broadly mentioning, mechanism of friction force generation is so complex, that it is still not fully understood, though several competing theories came out over the years. Back in around 1930s, Bowden and Tabor, for the first time, pointed out the adhesive force contribution to friction, and proposed an analytical model to describe the connection of adhesion forces with friction forces [71, 75, 80]. Their model associated the adhesive force required to shear real contacting junctions under elastic and plastic deformations [75]. Later on in 1963, the pioneering work of KA. Grosch on polymer materials (rubber), demonstrated that the description of total friction response could be determined as a contribution of two distinct mechanisms (Equation 12): the adhesion component and the deformation component, as illustrated in Figure 1.8.

$$F_t = F_{adh} + F_{def} (F_{plast}; F_{visco}) \quad (12)$$

where, F_{adh} is the adhesive component of friction and F_{def} is the viscoelastic contribution to friction [81–83]. Another contribution to friction force is given by Bowden and Tabor [84], which described as the ploughing term (one can also consider it under deformation as the plastic component, F_{plast}), and it accounts the contribution from ploughing of a hard body (asperities)

through a softer surface (contact of rigid body against soft polymer). It originates due to the induced plastic flow on the softer material in contact [71, 84]. The same was analysed and elaborated by Lafaye *et al* on hard polymers [85]. This component would become relatively insignificant when the contact is formed between two bodies of a same soft polymer (soft-soft type contact) under low pressure (no plastic deformation).

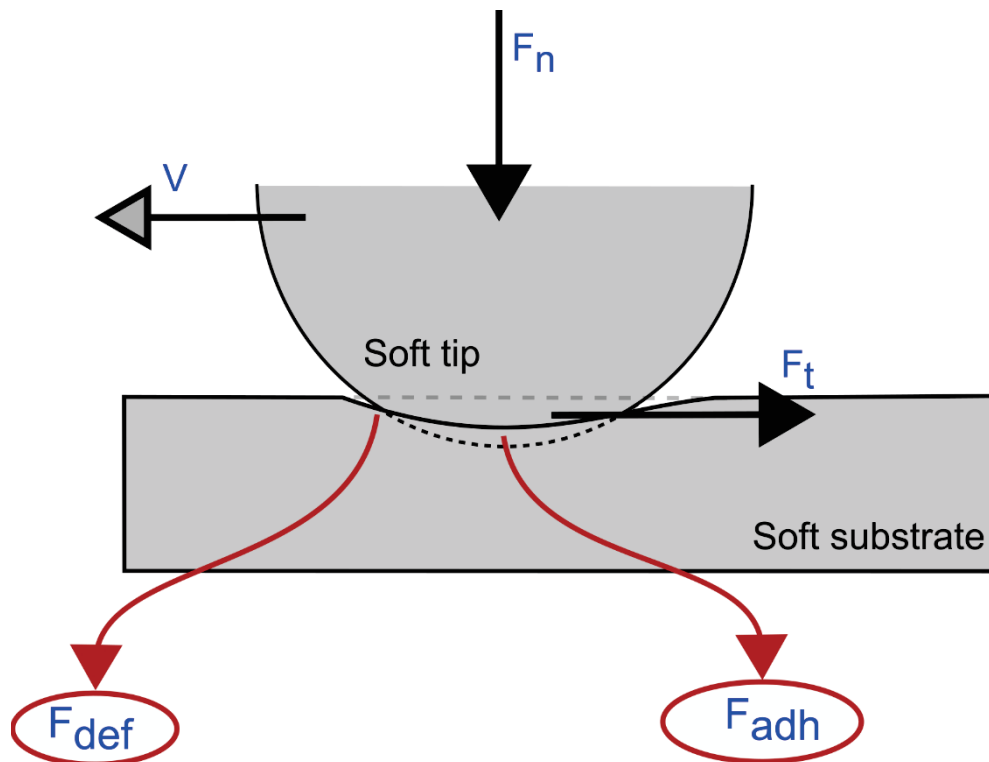


Figure 1.8 Schematic sketch of a model sliding contact between a sphere and smooth substrate, under an application of normal load (F_n). V is sliding speed and F_t is tangential friction force. F_{adh} and F_{def} are two key mechanism contributing to the friction force.

The adhesion component, which has already been introduced earlier, occurs between two surfaces in contact, due to their interatomic attractive force (van der Waals forces) [86]. Usually, the adhesion (molecular) component shows comparably major contribution in regard to the interaction of polymeric materials [87]. In the beginning, it was believed that the adhesive contribution to the friction force comes just from the energy needed to break the molecular adhesive bond [88]. However, later on, it came out too short as compared to the friction magnitude [72, 89]. The work of Grosch established that adhesive contribution of friction (for polymers) is rate dependent and largely influenced by polymer's viscoelastic component [81, 83]. Moreover, in regard to the deformation component (F_{def}) mechanism of friction response, it holds to the energy losses arising from the deformation of the polymer.

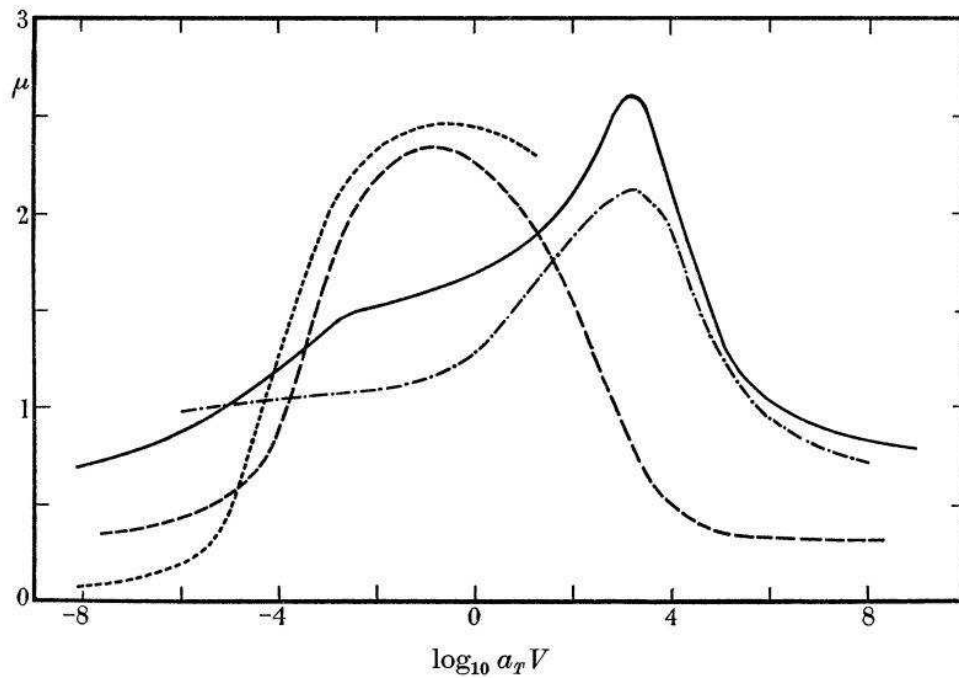


Figure 1.9 Master curves for the friction coefficient of the acrylonitrile-butadiene rubber C on four surfaces: Solid line (clean silicon carbide), small dashed line (polished stainless steel), dash-dotted line (dusted silicon carbide) and large dashed line (wavy glass). All curves obtained at 20 °C [81].

Remarkably, Grosch's work experimentally demonstrated a high dependency of the friction response on sliding speed and temperature, as shown in Figure 1.9. That would also be represented by a master curve describing the velocity dependence (at a constant temperature), and a universal temperature function whose only parameter (T_s), is related to the material's glass transition temperature. This transformation showed a close agreement with the Williams-Landel-Ferry (WLF) model [81, 90].

1.4 Aims and scope of this work

Interfacial contact phenomena (adhesion and friction) are widespread in most technical as well as in natural systems. These phenomena are encountered in everyday life, such as stick notes, scrolling your finger over laptop touchpad, knee joints motion or insects walking on plants, just to name a few. In particular regard to the growing field of micro- and nano-technology, where enormously increased surface- to- volume ratio results in high surface forces, it becomes crucial to precisely tune frictional and adhesive properties right from design considerations. Apart from the substrate's material property and chemistry, the surface texturing was found to be a strategic tool to control these phenomena. Both, adhesion and friction, play an influencing role in many processes in nature; on a particular note is the interaction of biological systems with the inanimate environment. However, almost all biological surface phenomena are governed by a composition of highly diverse and unique surface texturing and chemistry. Through a modern bio-inspiration strategy, one could go forward by simplifying the complex biological systems (simplified topography), to develop a clear understanding on biological contact behaviour and critically examine the adhesion and friction mechanism arising from their complex surface morphologies. The developed understanding might better contribute to improved functional surfaces in the future. Altogether, this work aims to integrate these considerations in a larger study which addresses frictional and adhesion properties of micro-textured soft polymeric surfaces (directly replicated from plant leaf surfaces; Figure 1.10.c) in contact with a polymeric probe (inspired from insect's feet; Figure 1.10.b). A comprehensive sketch of this work's context is illustrated in Figure 1.10.

This thesis involves three different approaches / sub-projects to achieve the overall project aim. In the first part of this work; after doing a comprehensive morphological survey of various plant leaves surfaces, three different plant leaves, comprising surface structures with variable size (0.5– 100 μm), distinct shape and complexity, were selected as model bio-templates. However, to simplify the complexity of plant leaf surfaces, a potential strategy would be to precisely transfer the surface morphologies of plant leaves onto a known material. Thus, enabling us to methodically examine the morphological influence on adhesion and friction characteristics; excluding physiochemical properties. In addition, another objective of *in-situ* real contact visualization could only be achieved by developing a micro-replication technique to transfer the complex micro- and/or nano-structures of model plant leaves onto a highly transparent soft polymer material.

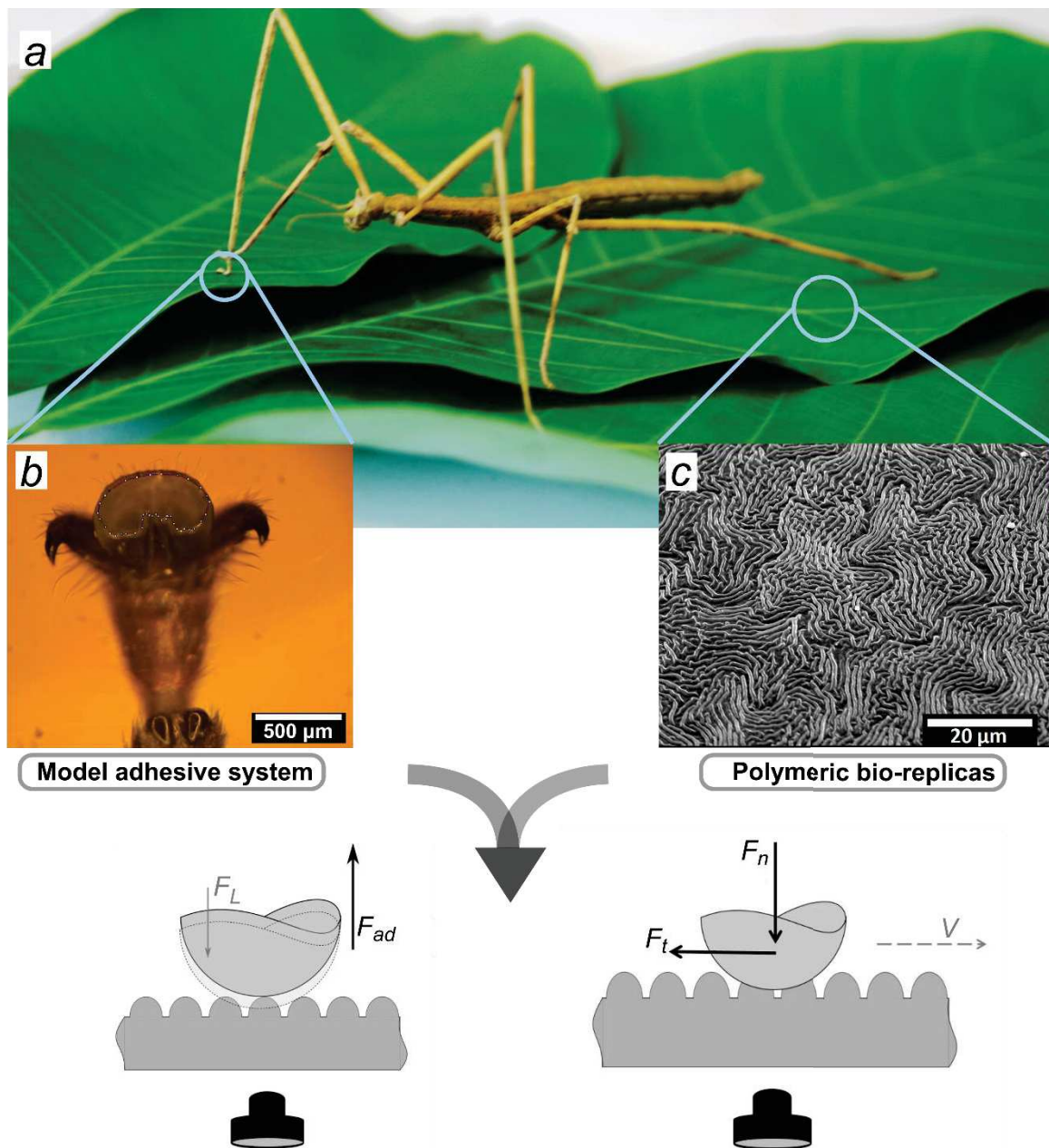


Figure 1.10 Comprehensive recapitulation of this work strategy. (a) Photograph of a stick insect (*Carausius morosus*) trying to find a perfect hold on the leaves of rubber tree (*Hevea brasiliensis*). (b) Optical microscope image of a tarsus of a stick insect with a smooth adhesive pad (Arolium), which was used as an inspiration for designing model adhesive system. (c) SEM image of *H. brasiliensis* leaf surface. (Down) Schematics of a pull-off adhesion test and a sliding friction test, coupled with *in-situ* real contact visualization.

To investigate the uttermost limitation of the replication technique, a fourth plant leaf with three-dimensional dense arrangement of perpendicularly oriented long wax platelets was studied. Three different replication techniques (with different materials for mould and intermediate treatments) were extensively investigated, qualitatively and quantitatively compared. Scanning electron microscopy was used for qualitative morphological

characterization and comparison (original leaf and polymeric replica). Line and surface profile data sets on original templates (three plant species and one technical surface), their negative moulds and positive replicas were assessed using a confocal laser scanning microscope. Two model parameters were utilised to quantify the replication quality. This study confirmed the best replication ability of Epoxy-PDMS technique, therefore the PDMS replicas developed from this technique were further utilised for contact mechanics investigation in the next two parts.

In the second study, we aimed a systematic (quantitative and qualitative) investigation of adhesion mechanics on each PDMS replicas and on a smooth PDMS surface as a reference. To permit to perform adhesion measurements at a low force range (few mN, that corresponds to the insect-plant interactions), an ultra-nanoindenter setup with high load and displacement precision, was modified. To our knowledge, the *in-situ* real contact visualization on complex biological micro-structured surfaces (down to sub-micron sized cuticular fold level) could not be achieved before. An innovative *in-situ* contact visualization (along with real-time data synchronization) system was developed and successfully incorporated into the adhesion setup, to get an in-depth understanding of true contacts and attachment/ detachment mechanisms. The adhesion force characteristics was quantitatively evaluated, and analysed how it influenced by pre-load conditions. The surface-specific attachment-detachment phenomena were also described, arising from their unique surface morphologies.

The objective of the last (third) part of this work was to investigate the sliding friction mechanism on the complex surface topographies (the same leaf replicas used as in the second part). For this purpose, a nano-scratcher was used, performing uni-directional linear sliding tests. This study was also performed in conjugation with *in-situ* visualization technique (from the previous part) to visualise the distribution of real contact regions and their propagation during sliding movement. Tests were carried out to investigate the friction coefficient dependence to the applied normal load. Furthermore, we also evaluated the effect of sliding speed on the frictional characteristics and correlated it with the visco-elastic properties of contacting materials.

2 Materials and Methodology

This section of the dissertation consists of materials, samples preparation techniques, data analysis, and various experimental procedures that were utilised in this thesis.

2.1 Model plant leaves

After achieving an extensive screening of various plant species, three model plant leaves Jewel orchid (*Ludisia discolor*), Rubber tree (*Hevea brasiliensis*) and Lychee (*Litchi chinensis*) were chosen in this work, on the basis of a wide size range (0.5 μm to few 100 μm), distinct topography and complexity of their surface structures (Figure 2.1). *L. discolor* (adaxial surface) shows circular cone-like shaped microstructures (50-100 μm), *H. brasiliensis* (adaxial surface) represents two levels of structuring consisting of epidermal cells covered with fine cuticular fold microstructures (0.5-2 μm), and *L. chinensis* (abaxial surface) shows a highly complex hierarchical surface structuring, made up of undercuts and overhanging patterns. In addition, a technical (PMMA) micro-structured surface decorated with regularly arranged circular dimples (depth of 5 μm and radius of 25 μm) was selected, which was utilised for the quantitative evaluation of replication ability (Manuscript B).

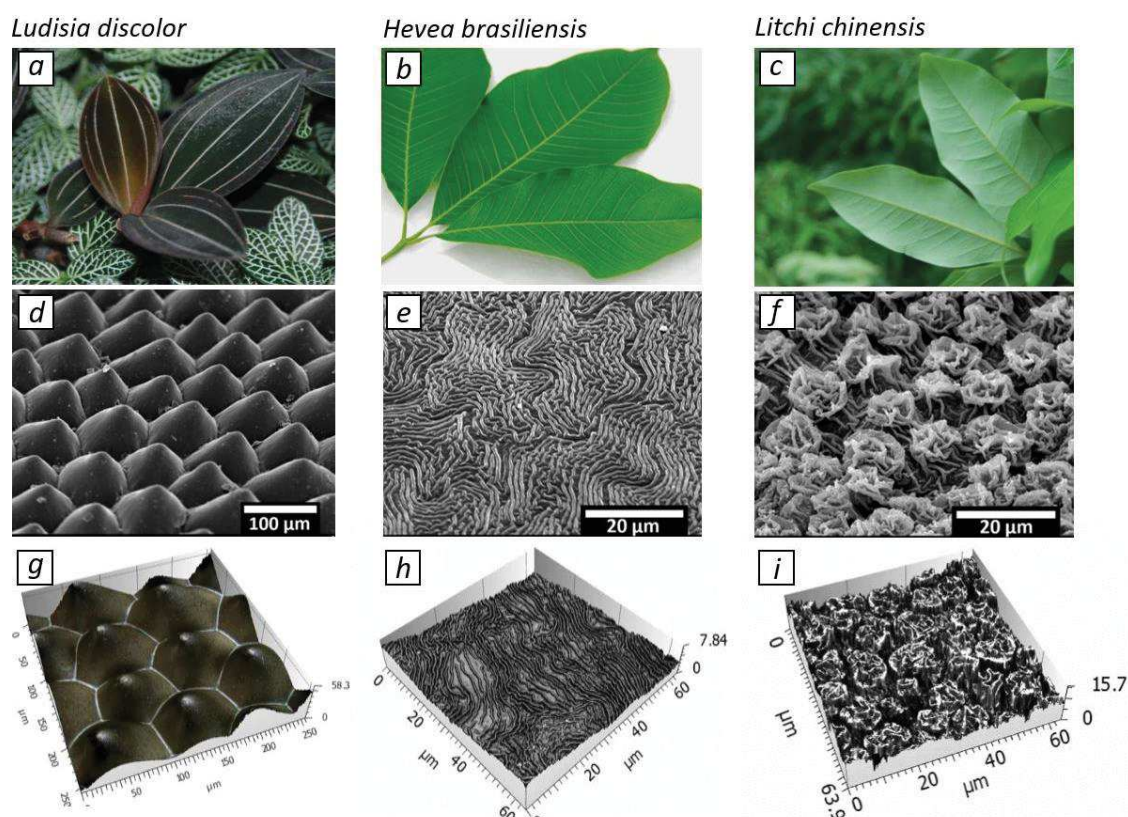


Figure 2.1. Photographs of original plant leaves (a, b, c), and their SEM images (d, e, f), and CLSM microscope images (g, h, i). (a) *Ludisia discolor* (adaxial, upper side surface), (b) *Hevea brasiliensis* (adaxial, upper side surface) and (c) *Litchi chinensis* (abaxial, lower side surface).

2.2 Plants leaf surface replication

After selecting the model plant leaves, the foremost and essential step of this work was to precisely transfer the surface topography from plant leaves to a polymeric surface. Studies on investigating the mechanical characteristics of plant leaves at cellular level show their Young's modulus in the scale of few MPa, nevertheless plant leaves are made-up of a highly complex and heterogeneous material composition [91–93]. Considering this, the PDMS, a soft matter polymer ($E \approx 0.5\text{--}4$ MPa, alter with varying the monomer to cross-linker ratio), appears to be an interesting candidate for developing positive replicas and to further perform contact mechanics investigations [94]. Notably, it displays high optical transparency over a wide spectrum of UV light, thus a perfect material for achieving *in-situ* contact visualization [95]. Furthermore, it offers numerous key advantages: low cost, widely commercially available, easy handling, non-toxicity, and a low surface energy (22 mJ m^{-2}) [94–96]. PDMS gets easily cross-linked to a very stable elastic network ($T_g = -120$ °C), shows strong chemical stability at room temperature, and has no explicit significant interaction with other materials [97]. Moreover, one may also note the PDMS has high surface energy to elastic modulus (γ/E) ratio. Therefore it appears very appropriate for adhesive contact mechanics studies and has been extensively studied in various previous studies [62, 98–102].

To achieve the replication objectives, we principally followed a two-step double casting replication approach. At first, a negative mould was produced directly from a fresh plant leaf, and then the patterns from the negative mould were replicated onto PDMS surfaces, as shown in Figure 2.2. The replication processes are described in more details in manuscript A and manuscript B.

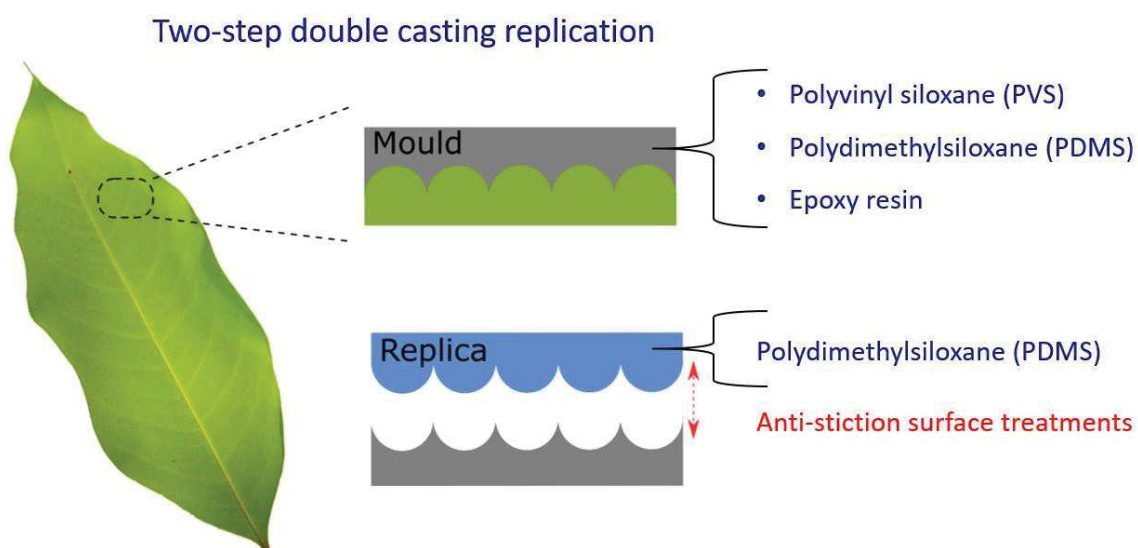


Figure 2.2. Simplified schematic sketch of the two-step replication process. Fresh plant leaf was used to develop negative mould, which was further utilised to transfer the surface micro-structures on to the positive replica.

Three different replication approaches (with different materials for mould and intermediate anti-stiction surface treatments; soft- soft, soft- soft and hard- soft as summarized in Table 1) were comprehensively investigated and compared. As one of the prerequisite to achieve the *in-situ* visualization was to get the final replica on a highly transparent polymer as previously mentioned, therefore the final replicas were always developed on PDMS in all the three techniques. The interfacial anti-stiction treatment was required to facilitate the smooth separation of positive replica from a negative mould, application depend on the mutual affinity of both materials. PVS-PDMS and Epoxy-PDMS replication techniques were originally established in this thesis.

Table 1. A complete description of three replication techniques, utilising different materials for mould and anti-stiction surface treatments.

Mould material	Final replica material	Intermediate anti-stiction treatment	Process abbr.
PVS (soft)	PDMS (soft)	Gold thin film coating (15-20 nm)	PVS-PDMS
PDMS (soft)	PDMS (soft)	Trichloro 1H,1H,2H,2H perfluorooctyl silane (FOTS) monolayer	PDMS-PDMS
Epoxy (soft)	PDMS (soft)	Potassium hydroxide aqueous solution (KOH, 60 wt%)	Epoxy-PDMS

In all three techniques, small pieces (3.5 cm × 3.5 cm) were cut out from cleaned fresh leaves and carefully glued onto a plastic Petri dish, using a double-side adhesive tape. Afterward, a liquid polymeric material (PVS, PDMS, or Epoxy resin) was slowly poured onto the leaf samples surface. After curing, leaves were carefully separated from the cured negative moulds. Developed moulds, after applying an intermediate anti-stiction treatment, were slowly filled up with PDMS mixture. After a curing at 60°C for 4 h, the PDMS replicas were gently peeled off from the negative moulds. All the PDMS samples were treated in n-heptane and 1-dodecanethiol (0.01 wt. %) solution for overnight to remove the unreacted free chains [103, 104]. After the treatment, samples were examined under SEM to check for any surface structural defects. Elaborate details on replication methods are given in manuscript A and manuscript B.

2.3 Model adhesive system

In the study, we took inspiration from the stick insect (*Carausius morosus*), which has smooth type attachment pads consisting of a soft cuticle (Figure 2.3) [28, 30]. Weighing of the adult insects measured a body mass of 800 ± 90 mg, resulting in a load of about 1.5 mN on a single

foot (assuming a uniform weight distribution over six feet of insect) [28, 30]. Furthermore, the material of smooth pad of insects is found to be demonstrating viscoelastic behaviour [28, 32, 33]. Here, PDMS, a viscoelastic soft polymer, was used to develop the model adhesive system (Figure 2.3). A moulding process was used to fabricate the PDMS half-spherical (radius of 1.5 mm) tip on a Polymethyl methacrylate (PMMA) mould. PDMS tip was embedded in a special tip holder assembly consisting of an external screw thread and nut attachment, thus ensuring a strong fixation (Figure 2.3). More details of model adhesive system fabrication are given in the Manuscript C. The same tip was used for both adhesion and friction mechanics investigations.

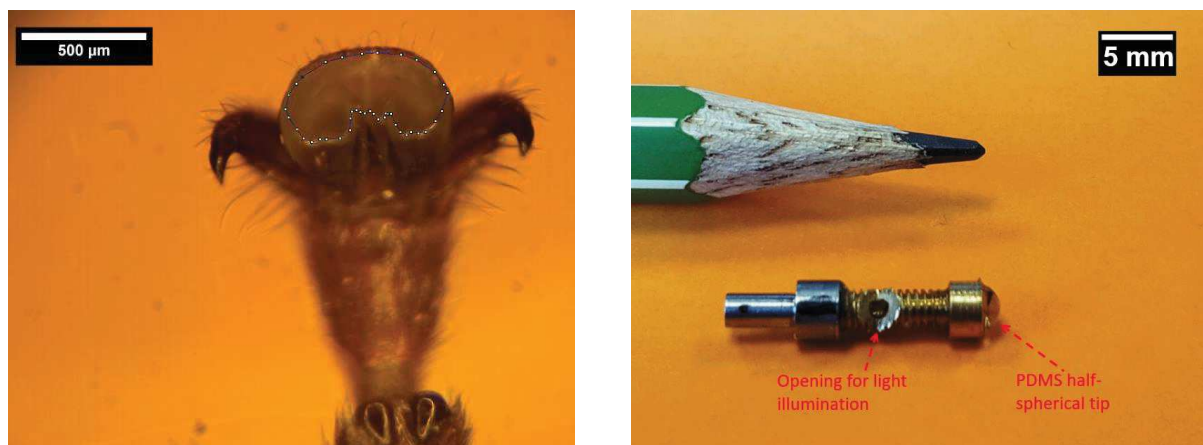


Figure 2.3. (Left) Stereo microscope image of tarsus of a stick insect (*Carausius morosus*) with paired claws and the intervening smooth adhesive pad (Arolium). (Right) Photograph of the model adhesive system with a half- spherical PDMS tip is embedded within the tip holder.

2.4 Surface morphology characterization

All the surface investigations for replication quality analysis and examination of the samples were performed using scanning electron microscopy (SEM) and confocal laser scanning microscopy (CLSM) techniques.

2.4.1 Scanning electron microscopy

The surface visualization and examination of surface morphology of original plant leaves, technical surfaces, and their polymeric replicas (negative and positive) were performed using a scanning electron microscope (SEM). SEM technique offers to capture high-resolution surface images with a high depth of focus and capable of resolving very fine surface details down to nano-meter scale [105]. SEM investigation of biological samples requires an appropriate sample preparation protocol. At first, all fresh plant leaves were dehydrated with methanol and then dried in a critical point drier [48, 53]. All the samples (plant leaves, negative moulds, and

n-heptane PDMS replicas) were mounted on aluminium stubs, and coated with a conductive thin (ca. 10 nm) film of gold. All SEM investigations were performed at a tilting angle in the range 30°-45°.

2.4.2 Confocal laser scanning microscopy

To accomplish a quantitative characterization of surface topography of all samples, a confocal laser scanning microscope (LEXT) was used. The key advantages with LEXT microscope are: no need of specific sample preparation, non-contact measurements, and three-dimensional topographical measurements. By using the LEXT microscope software, we directly analysed and quantified the geometric dimensions (height, width, inter-spacing between cuticular folds, cells diameter etc.) of the investigated samples.

2.5 Strategy to accomplish real contact visualization

One to the primary objective of this work was to accomplish the *in-situ* visualization of real contact areas, while doing the adhesion and friction investigation on biological structured surfaces. In the past, a lot of research has been done to realise the real contact visualization on smooth surfaces or on technical micro-structures with defined topographies [62, 64, 98, 100, 106–108]. However, the real contact visualization could not be achieved this way on biological structured surfaces considering the highly heterogeneous and complex structuring on biological surfaces at a sub-micron scale: indeed, the application of classical *in-situ* visualization approaches (using a laser beam or reflecting light) did not permit to visualize real contact junctions, as light beams got randomly diffuses due to the highly complex structuring.

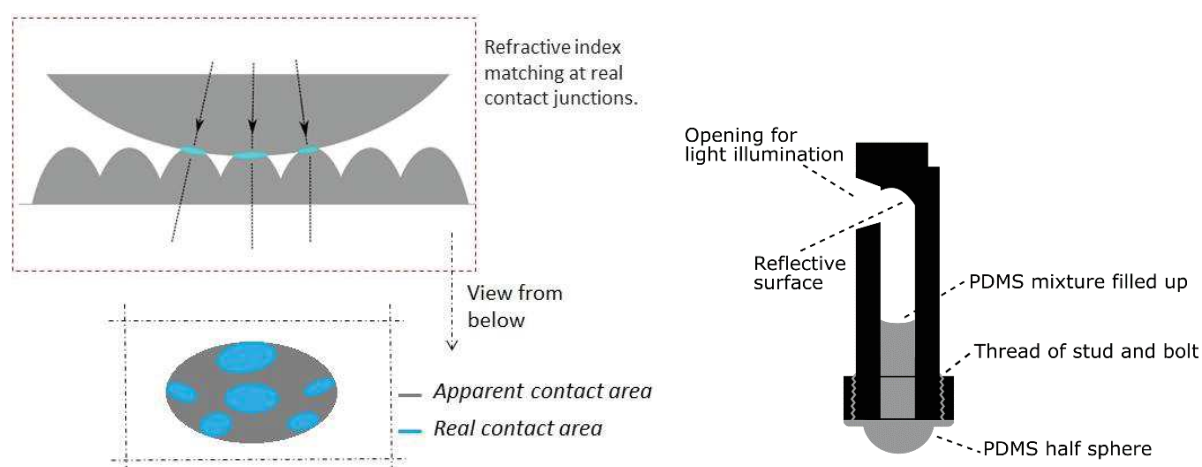


Figure 2.4. Simplified schematic sketch (left) exhibiting how the *in-situ* real contact visualization was achieved by using a high-resolution differential contrast microscopy approach based on transmission light microscopic principle. A sketch of the model adhesive tip assembly (right).

Finally, after considering various optical approaches, we successfully made use of a transmitting light microscopy principle [109]: a light beam was shined from the adhesive tip, that transmitted preferentially through the real contact junctions (matching of both material's refractive index) and later received from another side with a high definition microscope camera. The spots, which formed true contact junctions, appeared as high contrast bright spots, and rest came out as dark domains. As in our investigation theme, size of tip probe (half sphere of 1.5 mm radius) was small, it has been complicated to incorporate the optical setup with-in the adhesion and friction device. A special tip (as shown in Figure 2.4) was designed with an internal micro hole so that the light beam follows a path in the direction to the soft probe. The same *in-situ* visualization system was used in both adhesion and friction investigations.

2.6 Modified adhesion force tester

In general, the force range corresponding to insect-plant interactions falls in few mN (as measured ca. 1.5 mN for stick insect). Therefore, such contact mechanics investigations inspiring from insect-plant interactions need for a highly sensitive and low force range setup, to systematically answer the scientific questions [28]. Such a low force range and high sensitivity can be accomplished with a nano-indenter like apparatus [110, 111]. All the adhesion investigations in this work were performed with a JKR contact mechanics based apparatus [58]. An ultra-nanoindentation setup (UNHT³, Anton Paar Tritec, Switzerland) was modified to perform these low range adhesion force measurements, along with *in-situ* real contact visualization, as shown in Figure 2.5.

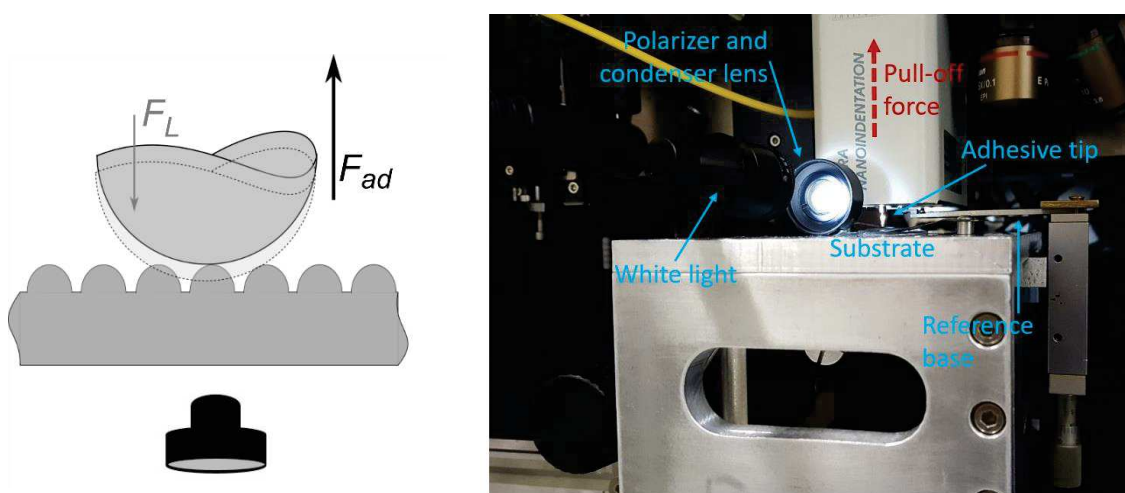


Figure 2.5. (Left) Schematic of a typical pull-off tests for adhesion force investigation. (Right) Photograph of the modified nanoindenter with force measurement head and additionally attached hard reference base. The optical device (oriented inward) for *in-situ* visualization comprises an objective lens, a microscope tube, and a high-resolution colour camera. F_L : pre-load, F_{ad} : adhesion force.

Furthermore, the setup was also advanced with a dedicated electronic system that enabled the simultaneous recording of the video frame in real-time synchronization with the corresponding force data point. All the measurements were performed in a climate controlled room (temperature = $22 \pm 3^\circ\text{C}$, relative humidity = $50\% \pm 10\%$). In order to ensure a precise and thermal drift free measurement, a unique surface referencing was performed (on each surface type) using a separate parallel referencing tip-head on a hard metal reference base, mounted with a high precision micrometre head, as can be seen in Figure 2.5. More details on this section can be found in Manuscript C.

For all the adhesion force measurements, substrates were placed on a rigid transparent glass slide and then fixed on the test platform. The adhesive tip was slowly approached near to the substrate surface. As soon as, the tip reached in close proximity to the substrate surface sudden snap-in (pull-in) took place. After this, the tip attained zero normal load condition, corresponding to an initial zero load state in the force-displacement graph. At this state, as a test started, the adhesive tip began forming a contact at a constant loading rate of 0.083 mN/sec , until the defined pre-load (F_L) is reached. The adhesive tip was kept under constant force F_L for a set time and then the tip was retracted at a retraction speed of $0.83 \mu\text{m/sec}$. This procedure is further described in section 3.2. The range of F_L was kept low enough and sample thickness was chosen large enough, so that the ratio of sample thickness to mean contact radius was more than about 10, thus the underlying substrate (glass slide) effect could be neglected [62, 65].

2.7 Friction force tester

For all the friction measurements in this work, the same ultra-nanoindentation setup, which was used for adhesion investigation, was modified and utilised under a new arrangement with double cantilever force sensor head and sliding bench, as shown in Figure 2.6. In this apparatus configuration, the sample was under sliding motion while the adhesive tip was kept fix. For *in-situ* real contact visualization and video frame-force data point synchronization, the same system was used as from adhesion measurements. For a friction test, the adhesive tip was slowly brought close to the sample surface and started forming a solid-solid contact until the given normal load (F_n) was reached. Subsequently, the sliding step started, moving the friction stage at a pre-set sliding speed (V) for a given sliding distance.

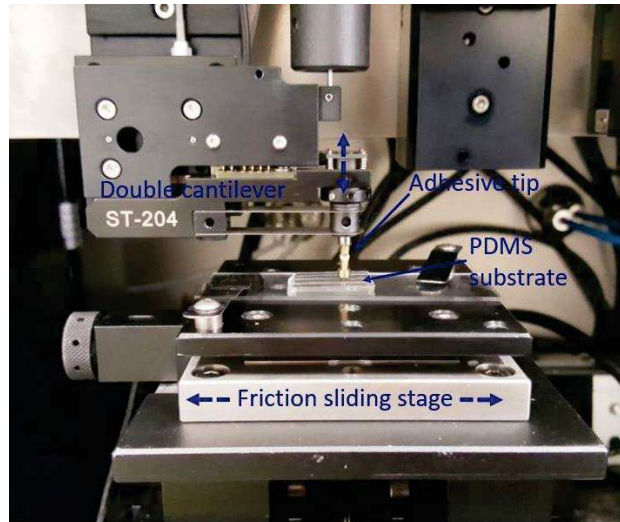
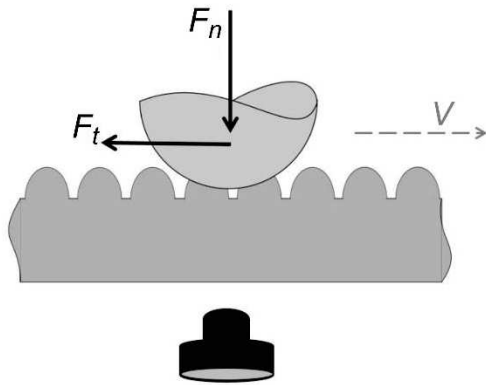


Figure 2.6. (Left) Schematic of sliding friction test on textured surfaces together with *in-situ* real contact visualization. (Right) Photograph of the modified nanoindenter setup with friction configuration to perform unidirectional sliding tests. F_n : normal force, F_t : tangential (friction) force, V : sliding velocity.

The tangential friction force (F_t) in between the tip and sample surface were measured and recorded at an acquisition rate of 100 Hz as well as F_n . All the friction measurements were carried out in a climate controlled room at a temperature of $25 \pm 3^\circ\text{C}$ and a relative humidity of $50\% \pm 10\%$. Friction tests were performed to record the effect of the normal load and the sliding speed on the friction characteristics, for all four substrates (three PDMS replicas and a smooth PDMS surface).

2.8 Image processing and analysis

Quantitative analysis and processing of all the *in-situ* videos were performed with the digital image processing tool *ImageJ* (v. 1.51p, National Institutes of Health, USA). Since, the recorded *in-situ* images could not be treated with any pre-installed standard functions due to irregular contrast all over the contact surface, dedicated macro-codes were written to perform initial homogenous filtering, to threshold, and to estimate the real contact area and apparent area as described in Figure 2.4 [112]. The real contact area was calculated by summing all the individual local real areas. For the apparent area estimation, multiple outmost peripheral point coordinates were sampled from all directions and these point-coordinates were fitted with a standard best-fit ellipse function of *ImageJ*.

3 Results and Discussion

3.1 Plants leaf replication

In this section, results of three replication techniques (PVS-PDMS, PDMS-PDMS and Epoxy-PDMS) are presented. SEM images of the surfaces of original plant leaves and of their replicas developed by Epoxy-PDMS technique are shown in Figure 3.1, and clearly illustrating the high precision of this developed replication process.

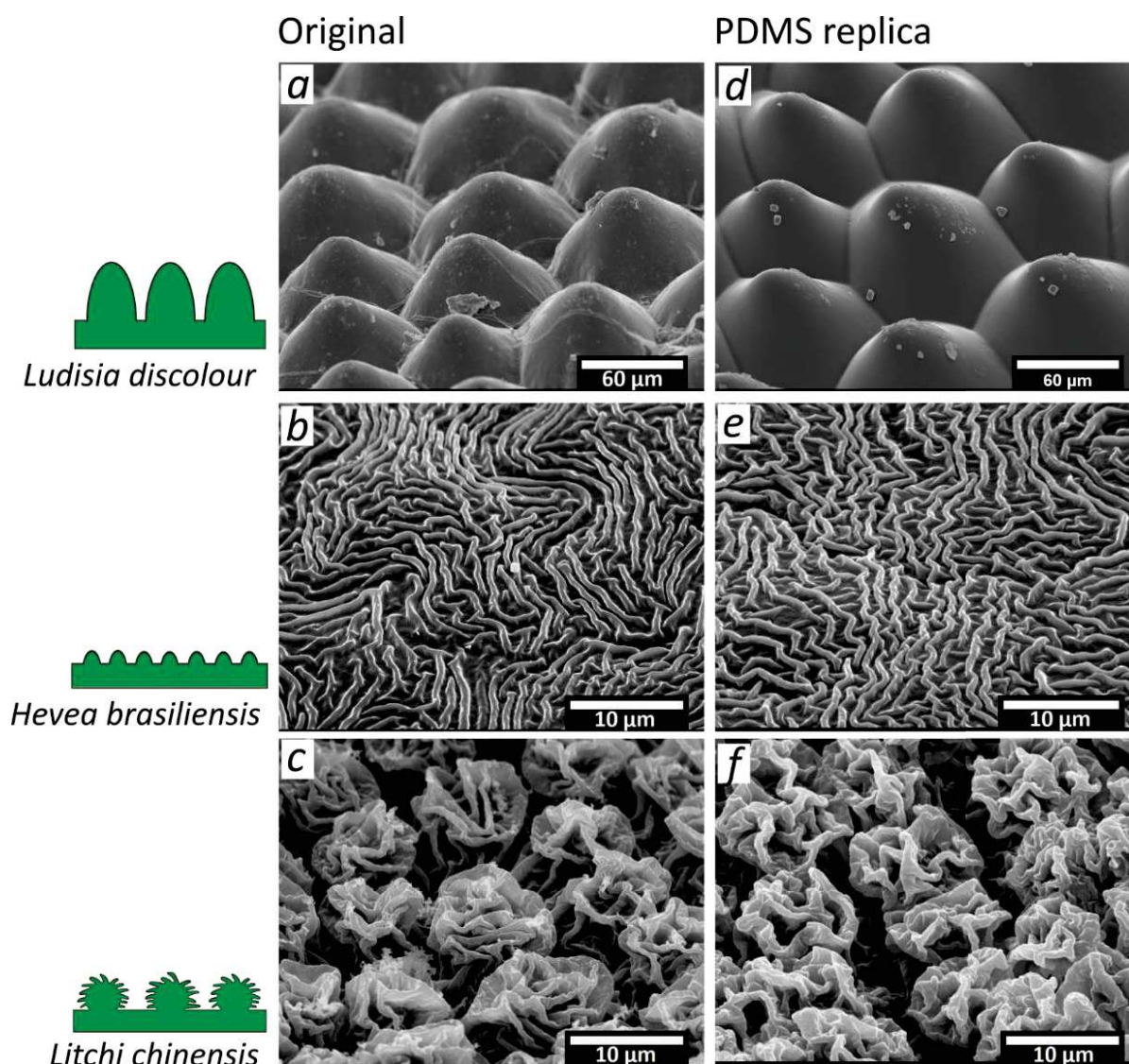


Figure 3.1. SEM images of original plant leaf surfaces (*a-c*) and their PDMS replicas (*d-f*) developed using Epoxy-PDMS replication technique. (*a, d*) *L. discolor* (coarse cone-like surface structuring), (*b, e*) *H. brasiliensis* (fine fold like microstructures) and (*c, f*) *L. chinensis* (hierarchical surface structures). Pictograms on the left side represent the type of structuring. Lower magnification images of *H. brasiliensis* and *L. chinensis* can be found in Manuscript A.

The coarse size and simplest microstructure of *L. discolor* leaf surface was replicated without exhibiting any explicit shrinkage or shape damage of the convex cell microstructures (Figure 3.1.a and 3.1.d). Very fine (less than 1 μm) surface topographies of *H. brasiliensis* leaf were successfully replicated without any fusion or overlapping of individual folds, as shown in Figure 3.1.b and 3.1.e. The most remarkable replication result in this work was obtained for *L. chinensis* leaves, where the complex hierarchical topographies with undercuts and overhanging sub-structures could be replicated precisely (Figure 3.1.c and 3.1.f). These complex structures with undercuts are usually difficult to replicate without breaking the overhanging patterns while peeling the replica from the negative mould.

The extensive investigation on comparing all three replication approaches revealed that the Epoxy-PDMS technique develops more precise positive replicas as compare to PDMS-PDMS technique, as can be realize by comparing Figure 3.2.a, 3.2.c and 3.2.d. Moreover, in case of PVS-PDMS replication, the surface morphologies of *L. chinensis* leaf were strongly damaged, causing the positive replica to loose most of the fine overhanging patterns (hierarchical patterns) as demonstrated in Figure 3.2.b.

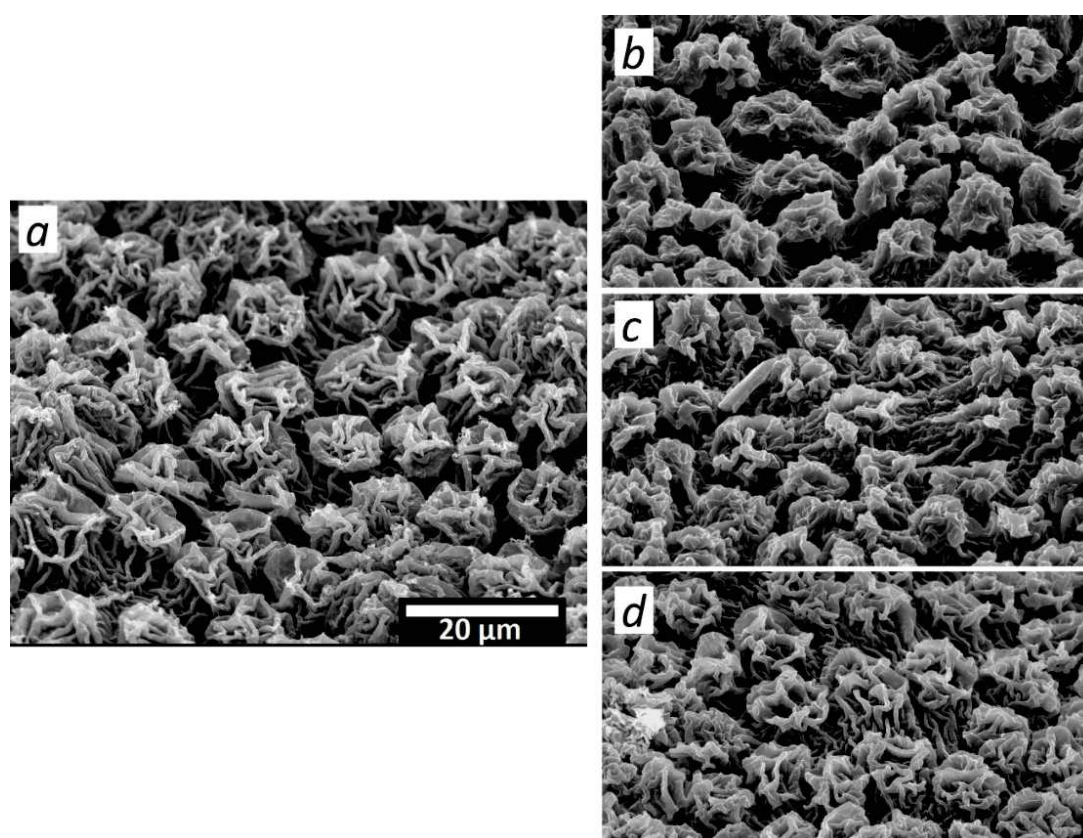


Figure 3.2. Qualitative comparison of replication quality of three techniques for *L. chinensis* leaf. SEM image of original leaf surface (a), their PDMS replicas by PVS-PDMS technique (b), by PDMS-PDMS technique (c), and by Epoxy-PDMS technique (d). Scale bar holds same for all four images.

Furthermore, after having a qualitative description of the three replication techniques, a quantitative evaluation was also done to assess the replication accuracy of each technique. For this, two quantitative parameters $ACCF_{MAX}$ and D_S were utilised, comparing the line and surface profiles from fresh leaves, negative replicas and positive replicas on the exact same spot, thanks to non-destructive and no sample preparation abilities of LEXT microscope. $ACCF_{MAX}$ is a maximized ratio between a cross-covariance function relating two profiles and their root mean squared roughnesses. D_S is defined as the root mean square roughness of a virtual profile given by A-B over the mean square roughness of a profile A (A- original profile, B- replica profile). Both parameters are compliment to each other as $ACCF_{MAX}$ quantifies the similarities in the shape of two profiles, while D_S takes into account the height differences. Results from this quantitative investigation turned out well in-line with the SEM characterization. These results are presented in details in Manuscript B.

In our opinion, the best replication results obtained from Epoxy-PDMS technique point towards the interpretation that the very low viscosity (≈ 400 mPa.s) of uncured epoxy resin and long curing time (15 h) at room temperature benefits a better filling of liquid epoxy into the fine and complex leaf structures (especially in case of *L. chinensis*), whereas for the PVS-PDMS replication approach, the high viscosity and fast polymerization of PVS result an incomplete filling of moulding material into the undercuts cavities [113]. Furthermore, the large difference in the elasticity of epoxy and PDMS (after curing) is beneficial for easy removal of the positive replica, and the soft flexible nature of PDMS prevents breaking of overhanging and damaging undercut structures. In the case of PDMS-PDMS replication, a degradation in replication quality might be because of the imperfect anti-stiction silane deposition on the undercuts and overhang structures. Due to this, the cured PDMS (positive replica) adhered with PDMS surface (places where no silane is deposited) and damaged the structures while peeling off. The lack of elastic contrast probably participates to these peeling off difficulties.

After achieving the performance comparison of these three replication techniques, PDMS replicas developed by Epoxy-PDMS replication technique were further used for the contact mechanics experiments. We also examined, prior to testing, all n-heptane treated PDMS replicas to check any structural damage caused from swelling and de-swelling events. The SEM investigation confirmed that the n-heptane treatment did not create any micro-structures damage. Corresponding SEM images can be found in Manuscript C.

3.2 Adhesion mechanics investigation

A representative graph obtained from a typical pull-off force measurement on smooth PDMS surface is present in Figure 3.3, along with real-time synchronized contact images at various stages of interest. During the unloading cycle (retraction part: *c-d-e-f*) the maximum negative force value represents the pull-off adhesion force (F_{ad}), as marked in Figure 3.3. For reading convenience, hereafter, only genus name is used to address PDMS replica samples instead of full species name: *Hevea* replica for *H. brasiliensis*, *Ludisia* replica for *L. discolor*, and *Litchi* replica for *L. chinensis*.

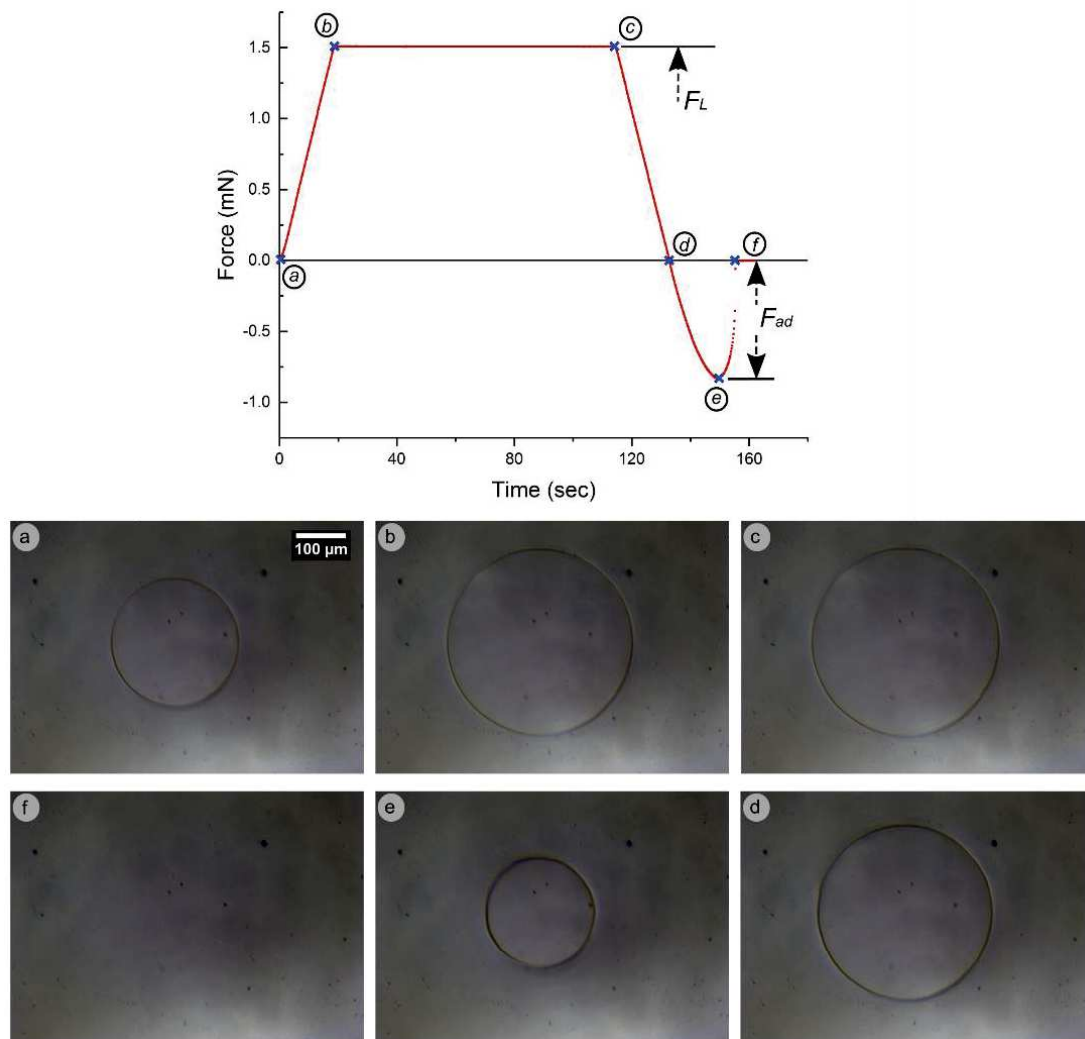


Figure 3.3. (Up) Representative force-time (displacement) curve obtained for a typical adhesion test for a whole test cycle on smooth PDMS sample, at a pre-load (F_L) of 1.5 mN. Different points of interest (*a-f*) are marked on the curve and their corresponding *in-situ* images (down).

Effect of pre-load: To investigate the effect of pre-load (F_L) on adhesion force, F_L was varied from 0.5 mN to 3.5 mN with a step size of 0.5 mN, by keeping all other parameters constant. The results of F_L influence on adhesion force characteristics are summarised in Figure 3.4. As

can be seen in Figure 3.4.a, for smooth PDMS surface F_{ad} values was quite consistent and independent ($F_{ad} \approx 0.80$ mN) with the increase in F_L , that goes in a good agreement with the well-known JKR theory [58]. This observation also validates the test protocol, which adequately complying with the standard adhesive models on a defined arrangement, *i.e.* a sphere on a flat surface. Figure 3.4.b exhibits F_{ad} characteristics obtained for the *Hevea* replica. A clear increase in F_{ad} was observed with increasing the F_L , however, the adhesion force appeared to get saturated with a further increased in F_L after 2.5 mN. This behaviour could be explained with the filling-up of fine microstructure pockets between the wrinkles (cuticular folds) with advancing F_L . Such observation has also been reported in previous studies [114–116]. This explanation was further supported by the analysis of *in-situ* real contact images and later the evaluation of normalized contact area (ratio of real contact to apparent contact area). This analysis can be followed in section 6.2 of manuscript C.

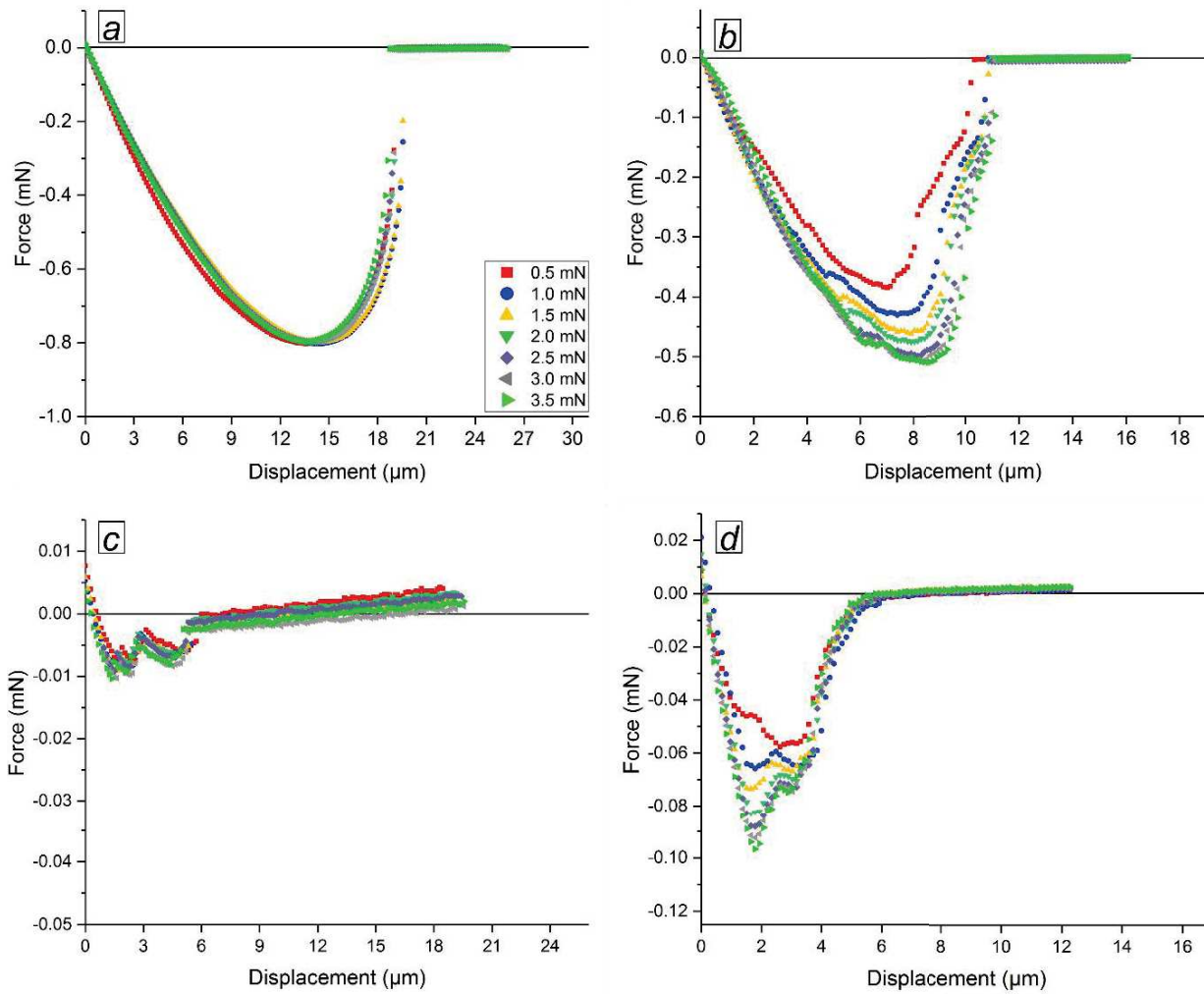


Figure 3.4. Force- displacement curve (pull-off retraction part) obtained at different normal pre-load conditions as indicated in mN. (a) Smooth PDMS, (b) *Hevea* replica, (c) *Ludisia* replica and (d) *Litchi* replica. Different pre-load color coding mentioned in graph a applies same for other three. The force scales are different on each plot, to fit graphs comparable.

For *Ludisia* replica, no detectable variation in F_{ad} was recorded with changing the F_L , as can be seen from Figure 3.4.c. One has to keep in mind that the force scale on *Ludisia* graph is highly zoomed in. As a consequence, the value of F_{ad} is very low. This behaviour could be interpreted with the validation of the *Hertzian* contact model locally (considering it as an inverted case of a half-sphere on smooth surface contact) on each cell of *Ludisia* replica and suggests that at this small scale each contacting asperity can be considered as a non-adhesive contact [117]. Corresponding analysis can be followed in the Manuscript C. One can see in Figure 3.4.d an increasing dependence behaviour of F_{ad} with raising the F_L for *Litchi* replica. Here, this dependency could be unfolded with force sensitive phenomenon associated with unique surface morphology of *Litchi* replica. For a low F_L condition, the true contact formed partially on the very top of overhanging micro-structures, whereas with increasing in F_L , more area formed the real full contact, and thus led to higher adhesion. This could be validated by examining the real contact visuals for low and high F_L conditions at the absolute zero load condition during the unloading cycling. An overall comparison of all the four samples shows that the smooth PDMS exhibited the highest value of adhesion force ($F_{ad} \simeq 0.80$ mN) as compared to the three micro-structured surfaces (Figure 3.4). This can relate to the fact that the aspect ratio of chosen micro-structured surfaces was low, therefore it lowered the adhesion compared to smooth sample, this differs to what has been demonstrated in some previous research utilising soft and compliant fibrillar geometries of high aspect ratio [118–122]. Related analyses are elaborated in Manuscript C.

Attachment and detachment mechanism from in-situ videos: The recorded *in-situ* real contact images (extracted from full test videos) at the full loading condition ($F_L = 1.5$ mN) for all four surfaces are presented in Figure 3.5. It is worthy to mention here, one key aim of this work was to achieve high-quality visualization of real contact region while performing the adhesion measurement. This was successfully achieved as can be realised from the *in-situ* results presented in Figure 3.5. For smooth PDMS contact, as anticipated, the whole surface formed the real contact (Figure 3.5.a). The real contact area increased with loading and started decreasing once the retraction part began with the well-known adhesion hysteresis. Attachment-detachment events were found homogenous and circular in shape over the whole contact cycle. Remarkably, the regions in true contact and out of contact, on the fine structured surface of *Hevea* replica, are evidently recognizable (Figure 3.5.b). During the attachment, contact formation initiated at the second level of micro-structuring (fine cuticular folds), and subsequently, as the contact formation advanced, whole cells were pulled in under a full contact

state, however, the cell boundaries were left out of contact (darker lines). In contrast, during the detachment, cell boundaries assisted in the crack initiation and further propagation: each cell in full contact behaved as a temporary contact point of stability [108]. In case of *Ludisia* replica, the real contact always occurred at the very top periphery of the conical shaped patterns of *Ludisia* replica, as illustrated in Figure 3.5.c. The real contact area was significantly lowered than the apparent area, and thus reduced the normalized contact area to 6.91%. The contact formation and separation on *Ludisia* replica, at the local cell level, was observed very smooth, homogeneously and circular in shape, similar to small smooth PDMS contact. Finally, a real contact image for *Litchi* replica can be seen in Figure 3.5.d. Here, *in-situ* visuals lacked in-detail clarity as compared to other three surfaces, indicating the limitation of visualization technique. Nevertheless, one could apparently observe that the real contacts (bright spots) were discretely distributed over the *Litchi* replica surface, attributing to its highly complex and heterogeneous surface morphology.

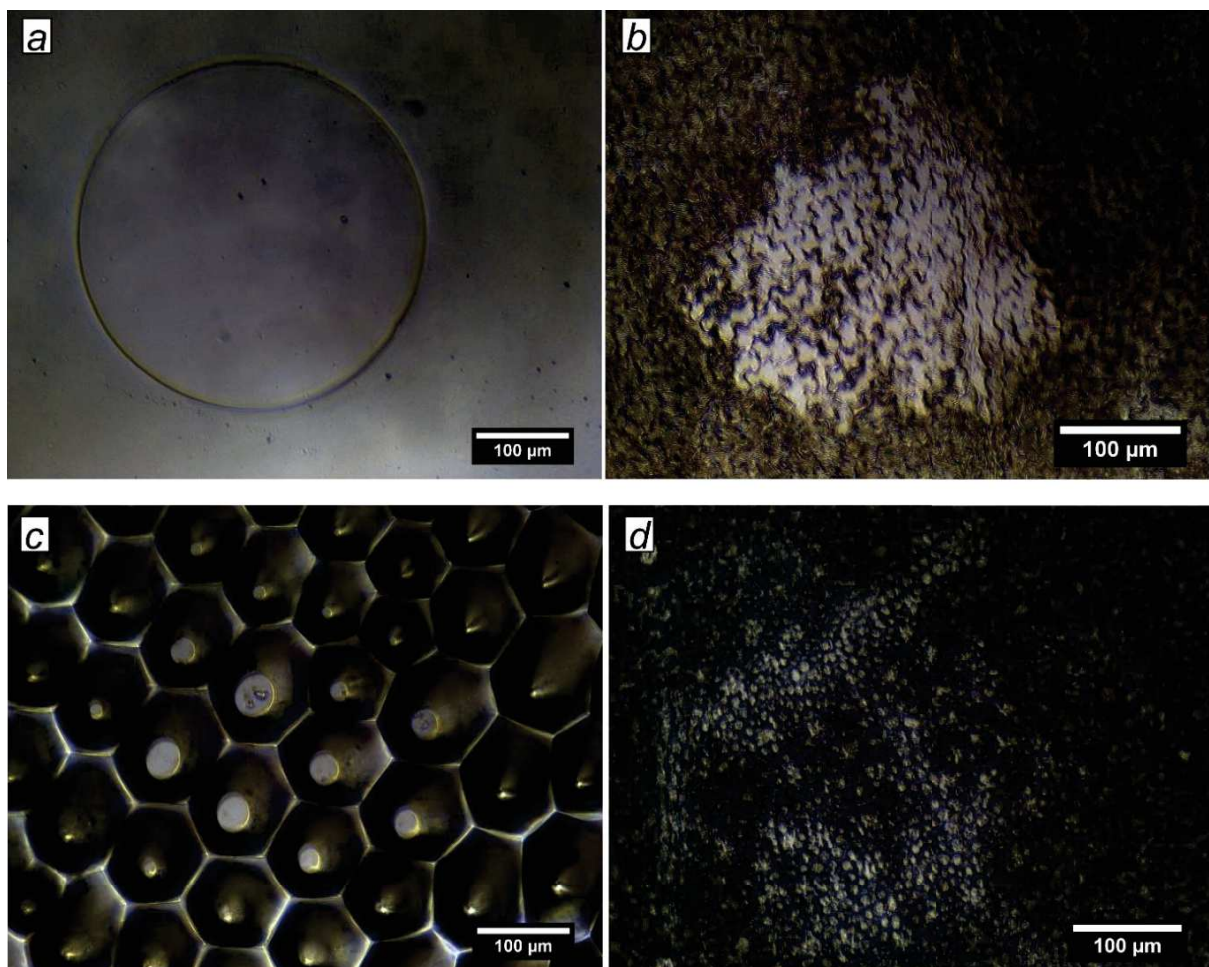


Figure 3.5. High definition real contact images recorded, at full pre-load loading stage, on all four surfaces. (a) Smooth PDMS, (b) *Hevea* replica, (c) *Ludisia* replica and (d) *Litchi* replica. Bright high contrast areas represent the real area in contact.

During the attachment stage, at first, the overhanging fine structures (cuticular folds) of a ‘*rose-flower-shaped*’ unit formed partial top-contact and later constituted a localised cluster (locally full contact) at higher loaded condition. Interestingly, for the detachment cycle, a fascinating behaviour of sudden fluctuation on adhesion response was observed, which could be attributed to a sudden release of the stored elastic energy when bended overhanging patterns and agglomerated ‘*rose-flower-shaped*’ morphologies locally popped out [123]. These results are discussed in the Manuscript C. Considering the fact that dynamic contacts were out of the scope however, it appears interesting for further studies in future.

3.3 Friction mechanics investigation

Friction tests were carried out on all four substrates (three PDMS replicas and a smooth PDMS surface) which were utilised in adhesion investigations. Friction coefficient (μ) was estimated by following the Coulomb’s friction law, $\mu = \text{tangential friction force } (F_t) / \text{normal force } (F_n)$ [75]. To investigate the effect of normal load on friction force characteristics, tests were conducted for six different normal load, 0.5-5.5 mN (step of 1 mN) at a constant sliding speed of 16.67 $\mu\text{m/s}$. In next part, the influence of sliding speed on friction response was studied by conducting the friction tests at different sliding speeds 1.67, 8.34, 16.67, 41.67, 83.34, 166.67, 416.67 and 833.34 $\mu\text{m/s}$, keeping the normal load constant. All tests were always performed over a constant sliding distance (2500 μm).

Figure 3.6 shows *in-situ* real contact visuals at sliding stage for each substrate. These snaps were singled out from complete movies captured during whole test cycles. For all four substrates, the results revealed a clear decreasing behaviour in friction coefficient with an increase in normal load. One can plot similar results as a function of friction force versus normal load. The reduction in friction coefficient behaviour could be understood with the friction force proportional dependence on the real contact area, demonstrating non-Amonton’s behaviour [76, 98]. An overall comparison of all the four substrates together (for the same normal load and sliding speed) is illustrated in Figure 3.7. Smooth PDMS showed the highest average friction coefficient ($\mu = 6.37$, at a normal load of 1.5 mN) out of all surfaces. In regards to contact dynamics, a circular (circularity parameter:1) and homogenous contact formed on smooth PDMS samples during the loading stage, however, it turned into an elliptical-like shape (with a reduction in area of 13.1 %) from static to kinetic stage (Figure 3.6.a). This behaviour attributing to the elastic stiffening of soft polymers from static to kinetic stage [124–126].

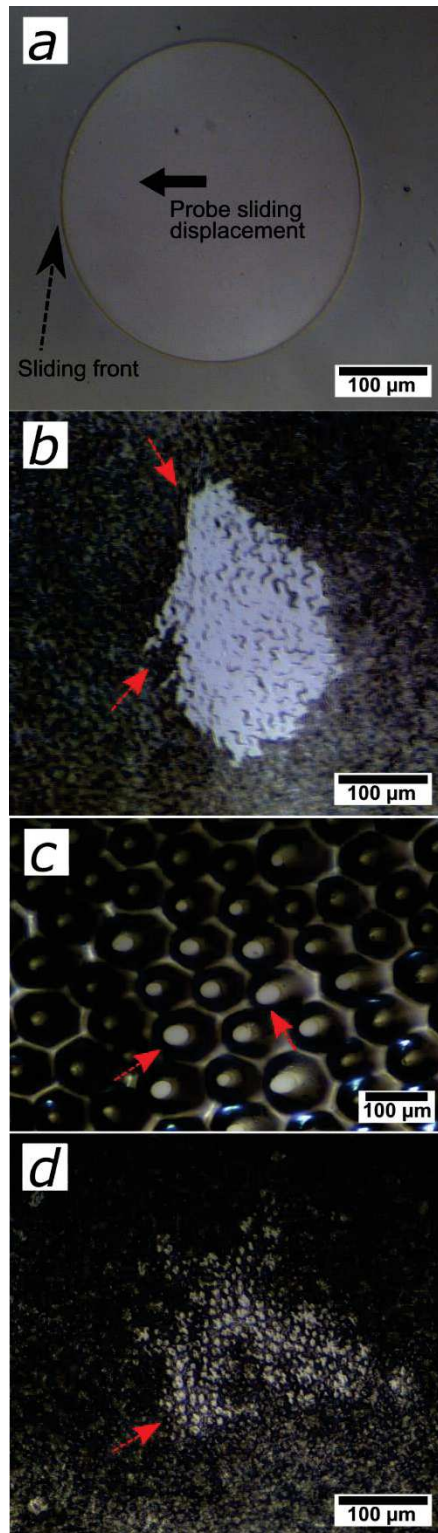


Figure 3.6. *In-situ* real contact images during sliding friction tests (under shear state) on all four substrates, at a normal load of 1.5 mN and a sliding speed of 16.67 $\mu\text{m/s}$. (a) Smooth PDMS, (b) *Hevea* replica, (c) *Ludisia* replica and (d) *Litchi* replica. Red arrows indicate different points of interest. Sliding front holds same for all four images. Modified from Manuscript D.

On *Hevea* replica, the real contact initiated just on very top of the fine cuticular folds structures and later grew over the individual cells (locally in full contact) at higher loading stage. However, during the sliding, the cells (*puzzle-shaped* bright spots) stretched under the shear

stress, and relaxed back after the tip passed away (Figure 3.6.b). An important behaviour observed on *Hevea* replica was the evolution of real contact junctions when confronting (in perpendicular orientation) with linear microstructure veins. This led to a gradual accumulation of microstructures and consequently creating more sliding resistance also inducing the semiregular instabilities on friction coefficient curve, as can be realized in Figure 3.7 (friction curve for *Hevea* replica) [127]. *In-situ* real contact videos recorded on *Ludisia* replica revealed a tremendous reduction in real contact area (normalized contact area = 7.5 %), where the real contacts always formed at the very top of its conical shaped topographies as presented in Figure 3.6.c. Moreover, the local real contact junctions showed an ellipse-like shape under shearing, without any contact instability. *Ludisia* replicas demonstrated the lowest value of friction coefficient ($\mu = 1.1$, at $F_n = 1.5$ mN), attributed to its unique surface patterning [40, 128]. *Litchi* replica, the most complex surface morphology, demonstrated a highly random distribution of real contact regions, and later the real contact evolution followed a highly random spreading (Figure 3.6.d). A slight increase in the contrast of real contact junctions was observed as soon as the sliding began, pointing toward the bending and agglomeration of its overhanging patterns when under shear [129]. Possibly, the sudden release of the strain energy stored during agglomeration deformation led to give a non-smooth friction response, as can be seen in Figure 3.7.

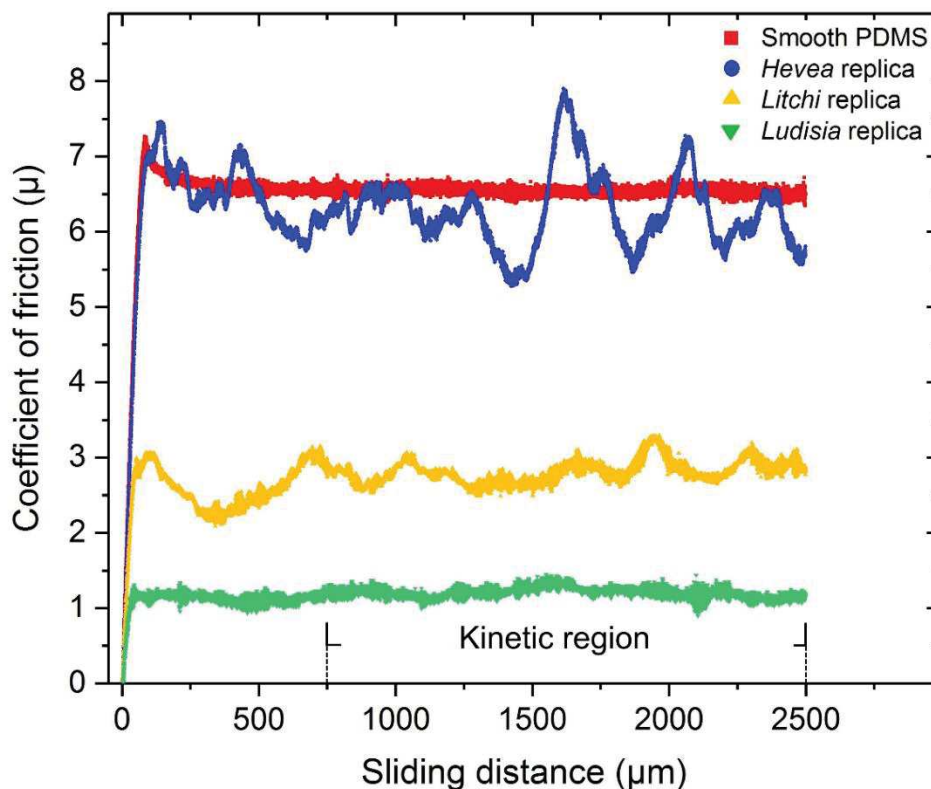


Figure 3.7. Friction coefficient versus sliding distance for all four surfaces investigated, at a constant normal load (1.5 mN) and sliding speed (16.67 $\mu\text{m/s}$).

Furthermore, results of the friction force dependence on sliding speed showed a clear increasing tendency of friction coefficient with raising the sliding speed. The same behaviour was recorded on all four substrates. Our results point out the fact that the friction characteristic of polymeric material is a speed-dependent phenomenon, which has also been observed in the past [101, 130–134]. In fact, Grosch [81] established two key mechanisms contributing to the friction on rubber: (i) the surface adhesion and (ii) energy loss arising from the material deformation. Later on, this was demonstrated by other researchers as well [133, 135, 136]. In this line, for a better understanding, one could further broaden the analysis by comparing the speed (frequency) dependent friction behaviour with loss factor plot, that was obtained from the dynamic mechanical thermal analysis of PDMS over the same frequency range [81, 133, 137, 138]. Our analysis based on a quantitative comparison noticed an unexpected deviation: a lower than anticipated increment rate of friction on smooth PDMS was obtained [135, 138]. This behaviour on smooth PDMS could be explained with the high adhesive response between soft-soft interaction, especially at low normal force range. Interestingly, *Ludisia* replica surface revealed a much higher rate of friction increment ($\mu = 0.91$ at $V = 1.67 \mu\text{m/s}$ and $\mu = 1.73$ at $V = 833.34 \mu\text{m/s}$) as compare to the smooth PDMS ($\mu = 5.39$ at $V = 1.67 \mu\text{m/s}$ and $\mu = 8.13$ at $V = 833.34 \mu\text{m/s}$), attributed to its conical shape patterns which localised the induced stresses and also significantly reduced the adhesion role [139, 140]. The *Litchi* replica demonstrated almost a similar friction increment behaviour as the smooth PDMS, but the friction coefficient on *Litchi* replica was found lower than on the smooth surface. These findings could have an important significance for particular applications requiring such friction behaviour with less adhesion force. On *Hevea* replica, a sudden increase was observed from a speed of $1.67 \mu\text{m/s}$ to $16.67 \mu\text{m/s}$, however afterwards the friction increment rate was almost retarded. Elaborated discussion of these findings can be followed in the ‘effect of sliding speed’ section of Manuscript D.

4 Summary

Within this work, the adhesion and friction mechanics on complex micro-structured surfaces were systematically investigated, where the contact interaction system was closely inspired from the insect-plant interactions. This work rather followed a contemporary approach by accommodating both sides; biological as well as contact mechanics, in parallel. Accordingly, on the one side, studying and exploring mechanics phenomena arising from unique surface morphologies and on the other side, advancing the understanding of contact formation on plant surfaces at various levels (cuticular folds, cells). The main findings and knowledge emerged from this work can be summarised as follows:

- A new bio-replication technique was needed to precisely transfer the coarse, fine (with a lateral resolution down to sub-micron), as well as complex hierarchical geometries directly from biological surfaces onto a highly transparent soft polymer material. The first part of this work includes a qualitative and quantitative evaluation of the replication ability and methodical comparison of three replication techniques (Epoxy-PDMS, PDMS-PDMS and PVS-PDMS) among a number of species of plants and a technical structured surface. Two, out of three, techniques were originally developed in this work. Along with SEM microscope examinations, two model parameters (cross-covariance function ratio and relative topography difference) were applied on the line profiles and the surface profiles recorded by confocal laser scanning microscopy. Investigation results pointed out both advantageous aspects and limitations of each technique, based on the type of surface structuring. Finally, Epoxy-PDMS resulted out the most precise replication technique to replicate complex biological morphologies, i.e. with the highest cross-covariance ratio and the lowest relative topography difference. Apart from good replication abilities, this technique offers various key advantages: simple and straightforwardness, no intermediate anti-stiction surface treatments, long durability of moulds, and multiple replicas from the same mould. This technique can be used for the rapid development of bioinspired surfaces and can also be up-scaled on a large area (cm^2).
- The second part of this work was to study pull-off adhesion mechanism, at a low force range (that closely corresponds to insect-plants interaction forces), on bio-replicated surfaces forming a contact with a model adhesive tip (soft-soft contact). An ultra-nanoindenter setup with high load and displacement precision was modified based on the JKR contact mechanics. In order to improve the understanding of the phenomena involved, we developed and successfully demonstrated an innovative technique for the *in-situ* real contact

visualization on complex biological surface morphologies (down to sub-micron sized cuticular fold level). To our knowledge, the new *in-situ* imaging system overcome previous studies limited to smooth or technical surfaces with defined structures. A significant enhancement in adhesion force with increasing in pre-load was observed on two replica surfaces: *Hevea* replica (fine micro-structuring) and *Litchi* replica (complex hierarchical morphologies), attributed to the filling-up of fine microstructure pockets on higher pre-load. However, no specific influence of pre-load was recorded on remaining two surfaces: *Ludisia* replica (coarse sized circular cone shape patterns) and smooth PDMS. Overall comparison concluded a significant reduction in adhesion force on *Ludisia* replica and *Litchi* replica as compared to other two surfaces. A close examination of real contact images revealed unique attachment-detachment phenomena, particularly on *Hevea* replica and *Litchi* replica, originating from surface-specific topographies and different pre-load conditions.

- The final part of this work investigated the friction mechanics on the same surfaces utilised in the second part under a sliding contact with a soft tip. Taking advantage of *in-situ* contact imaging technique achieved in the preceding part, visualization of real contact junctions during the sliding tests were accomplished. All four surfaces demonstrated evidently decrease in friction coefficient with increasing the normal load, however, each surface exhibited distinct decreasing behaviours. Furthermore, a clear influence of the sliding speed on friction response was recorded for all surfaces, which ascribed to the viscoelastic characteristic of PDMS. With increasing the sliding speed, friction coefficient apparently increased, however, each surface demonstrated a different rate and distinct behaviour of friction increment. Focusing on this, the speed dependent friction responses were correlated with the loss factor characteristics of PDMS material over the same frequency range. Our analysis pointed out that the localization of stresses, due to different surface topographies, led to creating different friction incremental rate with increasing the speed. For any normal load condition, *Ludisia* replica demonstrated the lowest friction coefficient, owing to its unique conical shaped patterns, which tremendously reduced the real contact area as compared to other investigated surfaces. Analysis of *in-situ* videos revealed different types of real contact evolution as well as shear strain distribution, which originating from the specific micro-structures in contact.

In this work, the same set of samples under identical contact scheme (soft-soft contact) were utilised, in both adhesion and friction investigations. It is worthwhile to mention the consistency observed between the adhesion and friction results, which suggests that the adhesion phenomenon seems to play an important role in the friction process.

Replication techniques developed in this work have perspectives for exploring biological diversity and to systematically investigate the underlying role of topography on various surface functionalities such as optical properties, wetting properties, antifouling properties, etc. In the present work, these replicas were utilised for adhesion and friction investigations. Furthermore, the replication ability evaluation tool demonstrated in this work might well be used for better accuracy evaluation of surface replication techniques. The *in-situ* imaging advancement achieved in this work could be a beneficial tool for the real contact visualization on complex structured surfaces. Furthermore, the insights gained from the adhesion and friction mechanics study on complex biological surface morphologies may provide a valuable assistance for designing bio-inspired functional surfaces and to precisely tune these functions.

In the future line, one might explore some advanced materials to precisely able to replicate plant surfaces with extreme structures with high aspect ratio, such as long hairy trichome structures, and also to enhance the robustness of replicas for the direct industrial applications. Moreover, future work could establish the individual contribution of each level of surface micro-structuring on the adhesion and friction, since the local scale has been demonstrated to be a relevant scale for understanding macroscopic characteristics. Finally, the prospect on the dynamic effect (increase local strain rate) raised during adhesion and friction studies could be addressed in further research.

Conclusions

Dans le cadre de ce travail, les mécanismes d'adhérence et de frottement sur des surfaces microstructurées complexes ont été systématiquement étudiés, où le système en contact a été inspiré par les interactions insectes-plantes. Ce travail fait à la fois intervenir des aspects de la mécanique du contact et de la biologie. Ainsi, d'une part, l'exploration des phénomènes mécaniques induits par les morphologies spécifiques de surface a été étudiée et, d'autre part, la compréhension du contact sur les surfaces végétales à plusieurs échelles (plis cuticulaires, cellules) a été améliorée. Les principales conclusions et enseignements issus de ces travaux peuvent être résumés comme suit :

- Une nouvelle technique de bio-reproduction était nécessaire pour transférer avec précision les géométries grossières, fines (avec une résolution latérale sub-micronique), ainsi que les géométries hiérarchiques complexes directement à partir de surfaces biologiques sur un matériau polymère souple hautement transparent. La première partie de ce travail comprend une évaluation qualitative et quantitative de la qualité de reproduction et une comparaison méthodique de trois techniques de reproduction (Epoxy-PDMS, PDMS-PDMS et PVS-PDMS) appliquées à plusieurs espèces végétales plus une surface technique structurée. Deux techniques sur trois sont originales car développées pour ce travail. En plus des examens au microscope électronique à balayage, deux paramètres topographiques (rapport de covariance croisée et différence topographique relative) ont été appliqués à des profils et surfaces issus de microscopie confocale à balayage laser. Les résultats ont mis en évidence à la fois les avantages et les limites de chaque technique en fonction du type de structuration de surface. Enfin, la technique Epoxy-PDMS a permis d'obtenir la reproduction la plus précise des morphologies biologiques complexes, i.e. avec le rapport de covariance croisée le plus élevé et la différence topographique relative la plus faible. Outre ses bonnes qualités de reproduction, cette technique offre de nombreux avantages : simplicité et rapidité, pas de traitement de surface anti-adhésif intermédiaire, longue durée de vie des moules, et plusieurs répliques réalisables à partir d'un même moule. Cette technique peut être utilisée pour le développement rapide de surfaces bio-inspirées et peut également être adaptée à plus grande échelle (cm²).
- La deuxième partie de ce travail consistait à étudier le mécanisme d'adhésion par décollement d'un contact obtenu à faible charge (qui correspond aux forces d'interaction insectes-plantes) entre une surface bio-répliquée et une sonde adhésive modèle (contact de matières molles). Un ultra-nanoindenteur a été dérivé comme test de contact JKR. Afin

d'améliorer la compréhension des phénomènes en jeu, une avancée a été obtenue dans la visualisation *in-situ* de contacts sur des morphologies complexes de surfaces biologiques (jusqu'au niveau du pli cuticulaire de taille sub-micronique). À notre connaissance, le nouveau système d'imagerie *in-situ* surpasse les études précédentes limitées aux surfaces lisses ou périodiquement structurées. Une augmentation significative de la force d'adhérence avec l'augmentation de la pré-charge a été observée sur deux surfaces : la réplique d'*Hévéa* (microstructuration fine) et la réplique de *Litchi* (morphologies hiérarchiques complexes), attribuée au remplissage de fines poches microstructurales à pré-charge élevée. Aucune influence spécifique de la pré-charge n'a été enregistrée sur les deux autres surfaces : la réplique de *Ludisia* (formes de cônes circulaires de taille grossière) et le PDMS lisse. La comparaison globale a montré une réduction significative de la force d'adhérence sur la réplique de *Ludisia* et la réplique de *Litchi* par rapport aux deux autres surfaces. Un examen attentif des images de contacts vrais a révélé des phénomènes originaux d'attachement-détachement, en particulier sur les répliques d'*Hévéa* et de *Litchi*, attribués à leur topographie spécifique et aux différentes conditions de pré-charge.

- La dernière partie de ce travail a porté sur la mécanique du frottement sous un contact glissant entre une pointe souple et les surfaces utilisées dans la deuxième partie. Tirant parti de la technique d'imagerie *in-situ* évoquée précédemment, la visualisation des contacts réels a été réalisée pendant les essais de glissement. Les quatre surfaces présentaient de manière nette une diminution du coefficient de frottement avec l'augmentation de la charge normale, mais chaque surface présentait des comportements distincts. De plus, une influence claire de la vitesse de glissement sur la réponse au frottement a été observée pour toutes les surfaces, ce qui a été attribuée au caractère viscoélastique du PDMS. Avec l'augmentation de la vitesse de glissement, le coefficient de frottement augmente, cependant, chaque surface induit un comportement et un incrément de frottement différent. Plus précisément, les réponses en frottement en fonction de la vitesse ont été corrélées avec les caractéristiques du facteur de perte du matériau PDMS dans la gamme de fréquences considérée. Notre analyse a montré que la distribution des contraintes, en raison des différentes topographies de surface, conduit à créer des taux d'augmentation de frottement différents avec l'augmentation de la vitesse. Pour toutes conditions de charges, la réplique de *Ludisia* a montré le coefficient de frottement le plus bas, en raison de ses textures de forme conique, qui réduit considérablement la surface de contact réelle. L'analyse des vidéos *in-situ* a révélé différents types d'évolution des aires vraies de contact ainsi que des distributions de déformation sous cisaillement, qui proviennent de la microstructure spécifique en contact.

Dans ce travail, un même ensemble d'échantillons a été soumis à des contacts identiques (contact de matières molles), tant pour des essais d'adhérence que de frottement. Il est intéressant de mentionner la cohérence observée entre les résultats d'adhérence et de frottement, ce qui suggère que le phénomène d'adhésion semble jouer un rôle important dans le processus de frottement.

Les techniques de reproduction mises au point dans le cadre de ce travail permettent d'explorer la diversité biologique et d'étudier systématiquement le rôle sous-jacent de la topographie sur diverses fonctionnalités de surface telles que les propriétés optiques, les propriétés de mouillage, les propriétés anti-salissure, etc. Dans ce travail, les répliques ont été utilisées pour des études d'adhérence et de frottement. De plus, les paramètres d'évaluation de la qualité de reproduction appliqués dans ce travail pourraient être utilisés pour une meilleure évaluation de la précision d'autres méthodes de reproduction de surfaces. Les avancées de l'imagerie *in-situ* réalisées dans le cadre de ces travaux pourraient être un outil utile pour la visualisation réelle des contacts sur des surfaces structurées complexes. De plus, les enseignements tirés de l'étude de la mécanique d'adhérence et de frottement sur les surfaces à morphologies biologiques complexes peuvent fournir une aide précieuse pour la conception de surfaces fonctionnelles bio-inspirées et pour l'ajustement précis de ces fonctions.

En perspectives, on pourrait s'intéresser à certains matériaux à fonctions avancées et tenter de les reproduire avec précision, comme les surfaces de plantes avec des structures extrêmes à rapport d'aspect élevé, telles que des structures trichomes à poils longs. Cela permettrait également d'améliorer la robustesse des répliques pour les applications industrielles directes. En outre, les travaux futurs pourraient établir la contribution individuelle de chaque niveau de microstructure de surface sur l'adhérence et le frottement, puisqu'il a été démontré que l'échelle locale est une échelle pertinente pour comprendre les caractéristiques macroscopiques. Enfin, les perspectives sur l'effet dynamique (augmentation de la vitesse de déformation locale) soulevées pendant les études d'adhérence et de frottement pourraient faire l'objet de recherches supplémentaires.

5 References

- [1] Gorb EV, Gorb SN. Contact mechanics at the insect-plant interface: how do insects stick and how do plants prevent this? In: Borodich F (ed) *IUTAM Symposium on Scaling in Solid Mechanics*. Springer, 2009, pp. 243–252.
- [2] Whitney HM, Federle W. Biomechanics of plant–insect interactions. *Current Opinion in Plant Biology* 2013; 16: 105–111.
- [3] Gorb SN. Biological attachment devices: exploring nature’s diversity for biomimetics. *Philosophical Transactions of the Royal Society of London A* 2008; 366: 1557–1574.
- [4] Koch K, Bhushan B, Barthlott W. Diversity of structure, morphology and wetting of plant surfaces. *Soft Matter* 2008; 4: 1943–1963.
- [5] Eder M, Amini S, Fratzl P. Biological composites—complex structures for functional diversity. *Science* 2018; 362: 543–547.
- [6] Koch K, Bohn HF, Barthlott W. Hierarchically sculptured plant surfaces and superhydrophobicity. *Langmuir* 2009; 25: 14116–14120.
- [7] Bargel H, Barthlott W, Koch K, et al. Plant cuticles: multifunctional interfaces between plant and environment. In: Hemsley AR, Poole I (eds) *The evolution of plant physiology*. Academic Press, London, 2004, pp. 171–194.
- [8] Barthlott W, Ehler N. Raster-elektronenmikroskopie der epidermis-oberflächen von spermatophyten. *Tropische und subtropische Pflanzenwelt* 1977; 19: 367–467.
- [9] Barthlott W, Neinhuis C, Cutler D, et al. Classification and terminology of plant epicuticular waxes. *Botanical journal of the Linnean society* 1998; 126: 237–260.
- [10] Barthlott W. Scanning electron microscopy of the epidermal surface in plants. *Scanning electron microscopy in taxonomy and functional morphology. Systematics association special volume* 1990; 69–94.
- [11] Koch K, Bhushan B, Barthlott W. Multifunctional surface structures of plants: an inspiration for biomimetics. *Progress in Materials Science* 2009; 54: 137–178.
- [12] Barthlott W, Mail M, Bhushan B, et al. Plant surfaces: structures and functions for biomimetic innovations. *Nano-Micro Letters* 2017; 9: 23.
- [13] Bhushan B. Bioinspired structured surfaces. *Langmuir* 2012; 28: 1698–1714.
- [14] Poppinga S, Koch K, Bohn HF, et al. Comparative and functional morphology of hierarchically structured anti-adhesive surfaces in carnivorous plants and kettle trap flowers. *Functional Plant Biology* 2010; 37: 952–961.
- [15] Prüm B, Seidel R, Bohn HF, et al. Plant surfaces with cuticular folds are slippery for beetles. *Journal of the Royal Society Interface* 2012; 9: 127–135.
- [16] Gorb EV, Gorb SN. Physicochemical properties of functional surfaces in pitchers of the carnivorous plant *Nepenthes alata* Blanco (Nepenthaceae). *Plant Biology* 2006; 8: 841–848.
- [17] Solga A, Cerman Z, Striffler BF, et al. The dream of staying clean: Lotus and biomimetic surfaces. *Bioinspiration & Biomimetics* 2007; 2: S126–S134.
- [18] Barthlott W, Neinhuis C. Purity of the sacred lotus, or escape from contamination in biological surfaces. *Planta* 1997; 202: 1–8.
- [19] Cerman Z, Striffler BF, Barthlott W. Dry in the water: the superhydrophobic water fern *Salvinia*—a model for biomimetic surfaces. In: Gorb SN (ed) *Functional surfaces in biology*. Springer, 2009, pp. 97–111.

- [20] Barthlott W, Schimmel T, Wiersch S, et al. The *Salvinia* paradox: superhydrophobic surfaces with hydrophilic pins for air retention under water. *Advanced Materials* 2010; 22: 2325–2328.
- [21] Prüm B, Bohn HF, Seidel R, et al. Plant surfaces with cuticular folds and their replicas: influence of microstructuring and surface chemistry on the attachment of a leaf beetle. *Acta Biomaterialia* 2013; 9: 6360–6368.
- [22] England MW, Sato T, Yagihashi M, et al. Surface roughness rather than surface chemistry essentially affects insect adhesion. *Beilstein Journal of Nanotechnology* 2016; 7: 1471–1479.
- [23] Gorb SN, Beutel RG, Gorb EV, et al. Structural design and biomechanics of friction-based releasable attachment devices in insects. *Integrative and Comparative Biology* 2002; 42: 1127–1139.
- [24] Labonte D, Federle W. Scaling and biomechanics of surface attachment in climbing animals. *Philosophical Transactions of the Royal Society B: Biological Sciences* 2015; 370: 20140027.
- [25] Bullock JMR, Drechsler P, Federle W. Comparison of smooth and hairy attachment pads in insects friction, adhesion and mechanisms for direction-dependence. *The Journal of Experimental Biology* 2008; 211: 3333–3343.
- [26] Dirks J-H. Physical principles of fluid-mediated insect attachment- Shouldn't insects slip? *Beilstein Journal of Nanotechnology* 2014; 5: 1160–1166.
- [27] Dirks J-H, Li M, Kabla A, et al. In vivo dynamics of the internal fibrous structure in smooth adhesive pads of insects. *Acta Biomaterialia* 2012; 8: 2730–2736.
- [28] Drechsler P, Federle W. Biomechanics of smooth adhesive pads in insects: influence of tarsal secretion on attachment performance. *Journal of Comparative Physiology A* 2006; 192: 1213–1222.
- [29] Gorb S. *Attachment devices of insect cuticle*. Springer Science & Business Media, 2001.
- [30] Scholz I, Baumgartner W, Federle W. Micromechanics of smooth adhesive organs in stick insects: pads are mechanically anisotropic and softer towards the adhesive surface. *Journal of Comparative Physiology A* 2008; 194: 373–384.
- [31] Zhou Y, Robinson A, Steiner U, et al. Insect adhesion on rough surfaces: analysis of adhesive contact of smooth and hairy pads on transparent microstructured substrates. *Journal of the Royal Society Interface* 2015; 11: 1–12.
- [32] Bennemann M, Backhaus S, Scholz I, et al. Determination of the Young's modulus of the epicuticle of the smooth adhesive organs of *Carausius morosus* using tensile testing. *Journal of Experimental Biology* 2014; 217: 3677–3687.
- [33] Gorb S, Jiao Y, Scherge M. Ultrastructural architecture and mechanical properties of attachment pads in *Tettigonia viridissima* (Orthoptera Tettigoniidae). *Journal of Comparative Physiology A* 2000; 186: 821–831.
- [34] Pulsifer DP, Lakhtakia A. Background and survey of bioreplication techniques. *Bioinspiration & Biomimetics* 2011; 6: 031001.
- [35] Koch K, Schulte AJ, Fischer A, et al. A fast, precise and low-cost replication technique for nano- and high-aspect-ratio structures of biological and artificial surfaces. *Bioinspiration & Biomimetics* 2008; 3: 46002–46012.
- [36] Lee S-M, Lee HS, Kim DS, et al. Fabrication of hydrophobic films replicated from plant leaves in nature. *Surface and Coatings Technology* 2006; 201: 553–559.
- [37] McDonald B, Patel P, Zhao B. Micro-structured polymer film mimicking the trembling aspen leaf. *Chemical Engineering and Process Techniques* 2013; 1(2): 1012–8.
- [38] Saison T, Peroz C, Chauveau V, et al. Replication of butterfly wing and natural lotus leaf structures by nanoimprint on silica sol–gel films. *Bioinspiration & Biomimetics* 2008; 3: 046004.

- [39] Schulte AJ, Koch K, Spaeth M, et al. Biomimetic replicas: transfer of complex architectures with different optical properties from plant surfaces onto technical materials. *Acta Biomaterialia* 2009; 5: 1848–1854.
- [40] Singh RA, Kim HJ, Kim J, et al. A biomimetic approach for effective reduction in micro-scale friction by direct replication of topography of natural water-repellent surfaces. *Journal of Mechanical Science and Technology* 2007; 21: 624–629.
- [41] Sun M, Luo C, Xu L, et al. Artificial lotus leaf by nanocasting. *Langmuir* 2005; 21: 8978–8981.
- [42] Hensel R, Helbig R, Aland S, et al. Tunable nano-replication to explore the omniphobic characteristics of springtail skin. *NPG Asia Materials* 2013; 5: e37.
- [43] Han Z, Li B, Mu Z, et al. Fabrication of the replica templated from butterfly wing scales with complex light trapping structures. *Applied Surface Science* 2015; 355: 290–297.
- [44] Williams M, Vesik M, Mullins M. Tissue preparation for scanning electron microscopy of fruit surfaces: comparison of fresh and cryopreserved specimens and replicas of banana peel. *Micron and Microscopica Acta* 1987; 18: 27–31.
- [45] Gao J, Liu Y, Xu H, et al. Biostructure-like surfaces with thermally responsive wettability prepared by temperature-induced phase separation micromolding. *Langmuir* 2010; 26: 9673–9676.
- [46] Pan Z, Shahsavani H, Zhang W, et al. Superhydro-oleophobic bio-inspired polydimethylsiloxane micropillared surface via FDTD coating blending approaches. *Applied Surface Science* 2015; 324: 612–620.
- [47] Zhuang G, Kutter JP. Anti-stiction coating of PDMS moulds for rapid microchannel fabrication by double replica moulding. *Journal of Micromechanics and Microengineering* 2011; 21: 105020.
- [48] Talbot MJ, White RG. Methanol fixation of plant tissue for scanning electron microscopy improves preservation of tissue morphology and dimensions. *Plant Methods* 2013; 9: 36.
- [49] Bodas D, Khan-Malek C. Hydrophilization and hydrophobic recovery of PDMS by oxygen plasma and chemical treatment—An SEM investigation. *Sensors and Actuators B: Chemical*; 123: 368–373.
- [50] Bunker BC, CarPick RW, Assink RA, et al. The impact of solution agglomeration on the deposition of self-assembled monolayers. *Langmuir* 2000; 16: 7742–7751.
- [51] Lee S-M, Kwon TH. Mass-producible replication of highly hydrophobic surfaces from plant leaves. *Nanotechnology* 2006; 17: 3189–3196.
- [52] Nagaraja P, Yao D. Rapid pattern transfer of biomimetic surface structures onto thermoplastic polymers. *Materials Science and Engineering: C* 2007; 27: 794–797.
- [53] Neinhuis C, Edelmann HG. Methanol as a rapid fixative for the investigation of plant surfaces by SEM. *Journal of Microscopy* 1996; 184: 14–16.
- [54] Johnson KL. *Contact mechanics*. Cambridge university press, 1987.
- [55] Fischer-Cripps AC. *Introduction to contact mechanics*. Springer, 2000.
- [56] Kumar C, Palacios A, Surapaneni VA, et al. Replicating the complexity of natural surfaces: technique validation and applications for biomimetics, ecology and evolution. *Philosophical Transactions of the Royal Society A* 2018; 377: 20180265.
- [57] Hertz H, Reine J. Original Hertzian mechanics ref. *Journal of Applied Mathematics and Mechanics* 1882; 92: 156.
- [58] Johnson K, Kendall K, Roberts A. Surface energy and the contact of elastic solids. *Proceedings of the Royal Society of London A Mathematical and Physical Sciences* 1971; 324: 301–313.

- [59] Barthel E. Adhesive elastic contacts: JKR and more. *Journal of Physics D: Applied Physics* 2008; 41: 163001.
- [60] Grierson D, Flater E, Carpick R. Accounting for the JKR–DMT transition in adhesion and friction measurements with atomic force microscopy. *Journal of Adhesion Science and Technology* 2005; 19: 291–311.
- [61] Horn R., Israelachvili J., Pribac F. Measurement of the deformation and adhesion of solids in contact. *Journal of Colloid and Interface Science* 1986; 115: 480–492.
- [62] Charrault E, Gauthier C, Marie P, et al. Experimental and theoretical analysis of a dynamic JKR contact. *Langmuir* 2009; 25: 5847–5854.
- [63] Chaudhury MK. Interfacial interaction between low-energy surfaces. *Materials Science and Engineering: R: Reports* 1996; 16: 97–159.
- [64] Chaudhury MK, Whitesides GM. Direct measurement of interfacial interactions between semispherical lenses and flat sheets of poly (dimethylsiloxane) and their chemical derivatives. *Langmuir* 1991; 7: 1013–1025.
- [65] Deruelle M, Hervet H, Jandean G, et al. Some remarks on JKR experiments. *Journal of Adhesion Science and Technology* 1998; 12: 225–247.
- [66] Derjaguin BV, Muller VM, Toporov YP. Effect of contact deformations on the adhesion of particles. *Journal of Colloid and Interface Science* 1975; 53: 314–326.
- [67] Maugis D. Adhesion of spheres: the JKR–DMT transition using a Dugdale model. *Journal of Colloid and Interface Science* 1992; 150: 243–269.
- [68] Tabor D. Surface forces and surface interactions. *Journal of Colloid and Interface Science* 1977; 58: 2–13.
- [69] Kroner EK. *Adhesion measurements on patterned elastomeric surfaces*. Doctoral dissertation, Saarländische Universitäts-und Landesbibliothek, 2011.
- [70] Spolenak R, Gorb S, Gao H, et al. Effects of contact shape on the scaling of biological attachments. *Proceedings of the Royal Society A: Mathematical, Physical and Engineering Sciences* 2005; 461: 305–319.
- [71] Mate CM. *Tribology on the small scale: a bottom up approach to friction, lubrication, and wear*. 6, Oxford University Press, 2008.
- [72] Myshkin N, Petrokovets M, Kovalev A. Tribology of polymers: adhesion, friction, wear, and mass-transfer. *Tribology International* 2005; 38: 910–921.
- [73] Amontons G. De la resistance causee dans les machines. *Mem de l'Academie Royal A* 1699; 275–282.
- [74] Fuller K, Tabor D. The effect of surface roughness on the adhesion of elastic solids. *Proceedings of the Royal Society of London A, Mathematical and Physical Sciences* 1975; 345: 327–342.
- [75] Bowden FP, Tabor D. *The Friction and Lubrication of Solids*. Oxford university press, 1950.
- [76] Mo Y, Turner KT, Szlufarska I. Friction laws at the nanoscale. *Nature* 2009; 457: 1116.
- [77] Roberts A, Jackson S. Sliding friction of rubber. *Nature* 1975; 257: 118.
- [78] Tiwari A, Miyashita N, Espallargas N, et al. Rubber friction: The contribution from the area of real contact. *The Journal of Chemical Physics* 2018; 148: 224701.
- [79] Briscoe BJ. Interfacial friction of polymer composites. General fundamental principles. In: *Composite materials series*. Elsevier, 1986, pp. 25–59.
- [80] McFarlane J, Tabor D. Relation between friction and adhesion. *Proceedings of the Royal Society of London A Mathematical and Physical Sciences* 1950; 202: 244–253.

- [81] Grosch K. The relation between the friction and visco-elastic properties of rubber. *Proceedings of the Royal Society of London A, Mathematical and Physical Sciences* 1963; 274: 21–39.
- [82] Moore DF. *The friction and lubrication of elastomers*. Pergamon Press, 1972.
- [83] Ludema K, Tabor D. The friction and visco-elastic properties of polymeric solids. *Wear* 1966; 9: 329–348.
- [84] Bowden F, Tabor D. Friction, lubrication and wear: a survey of work during the last decade. *British Journal of Applied Physics* 1966; 17: 1521.
- [85] Lafaye S, Gauthier C, Schirrer R. Analysis of the apparent friction of polymeric surfaces. *Journal of Materials Science* 2006; 41: 6441–6452.
- [86] Chernyak YB, Leonov A. On the theory of the adhesive friction of elastomers. *Wear* 1986; 108: 105–138.
- [87] Bely VA, Sviridenok AI, Petrokovets MI. *Friction and wear in polymer-based materials*. Pergamon Press, 1982.
- [88] Schallamach A. A theory of dynamic rubber friction. *Wear* 1963; 6: 375–382.
- [89] David Stratford D. *Frictional interaction of elastomeric materials*. Doctoral dissertation, Queen Mary University of London, 2018.
- [90] Williams ML, Landel RF, Ferry JD. The temperature dependence of relaxation mechanisms in amorphous polymers and other glass-forming liquids. *Journal of the American Chemical Society* 1955; 77: 3701–3707.
- [91] Onoda Y, Schieving F, Anten NP. A novel method of measuring leaf epidermis and mesophyll stiffness shows the ubiquitous nature of the sandwich structure of leaf laminas in broad-leaved angiosperm species. *Journal of Experimental Botany* 2015; 66: 2487–2499.
- [92] Wang S, Ren L, Liu Y, et al. Mechanical characteristics of typical plant leaves. *Journal of Bionic Engineering* 2010; 7: 294–300.
- [93] Saito T, Soga K, Hoson T, et al. The bulk elastic modulus and the reversible properties of cell walls in developing *Quercus* leaves. *Plant and Cell Physiology* 2006; 47: 715–725.
- [94] Mata A, Fleischman AJ, Roy S. Characterization of polydimethylsiloxane (PDMS) properties for biomedical micro/nanosystems. *Biomedical Microdevices* 2005; 7: 281–293.
- [95] Schneider F, Draheim J, Kamberger R, et al. Process and material properties of polydimethylsiloxane (PDMS) for Optical MEMS. *Sensors and Actuators A: Physical* 2009; 151: 95–99.
- [96] McDonald JC, Duffy DC, Anderson JR, et al. Fabrication of microfluidic systems in poly(dimethylsiloxane). *Electrophoresis* 2000; 21: 27–40.
- [97] Ghatak A, Vorvolakos K, She H, et al. Interfacial rate processes in adhesion and friction. *Journal of Physical Chemistry B* 2000; 104: 4018–4030.
- [98] Yashima S, Romero V, Wandersman E, et al. Normal contact and friction of rubber with model randomly rough surfaces. *Soft Matter* 2015; 11: 871–881.
- [99] Degrandi-Contraires É, Beaumont A, Restagno F, et al. Cassie-Wenzel-like transition in patterned soft elastomer adhesive contacts. *Europhysics Letters* 2013; 101: 14001.
- [100] Dies L, Restagno F, Weil R, et al. Role of adhesion between asperities in the formation of elastic solid/solid contacts. *The European Physical Journal E* 2015; 38: 130.
- [101] Vaenkatesan V, Li Z, Vellinga W-P, et al. Adhesion and friction behaviours of polydimethylsiloxane – A fresh perspective on JKR measurements. *Polymer* 2006; 47: 8317–8325.
- [102] Kroner E, Paretkar DR, McMeeking RM, et al. Adhesion of flat and structured PDMS samples to spherical and flat probes: a comparative study. *The Journal of Adhesion* 2011; 87: 447–465.

- [103] Amouroux N, Léger L. Effect of dangling chains on adhesion hysteresis of silicone elastomers, probed by JKR test. *Langmuir* 2003; 19: 1396–1401.
- [104] Deruelle M, Tirrell M, Marciano Y, et al. Adhesion energy between polymer networks and solid surfaces modified by polymer attachment. *Faraday Discussions* 1994; 98: 55–65.
- [105] Wischnitzer S. *Introduction to electron microscopy*. Elsevier, 2013.
- [106] Hisler V, Palmieri M, Le Houérou V, et al. Scale invariance of the contact mechanics of micropatterned elastic substrates. *International Journal of Adhesion & Adhesives* 2013; 45: 144–149.
- [107] Davis CS, Martina D, Creton C, et al. Enhanced adhesion of elastic materials to small-scale wrinkles. *Langmuir* 2012; 28: 14899–14908.
- [108] Jin C, Khare K, Vajpayee S, et al. Adhesive contact between a rippled elastic surface and a rigid spherical indenter: from partial to full contact. *Soft Matter* 2011; 7: 10728.
- [109] Salmon E, Tran P. High-resolution video-enhanced differential interference contrast light microscopy. *Methods in Cell Biology* 2007; 81: 335–364.
- [110] Nohava J, Randall N, Conté N. Novel ultra nanoindentation method with extremely low thermal drift: Principle and experimental results. *Journal of Materials Research* 2009; 24: 873–882.
- [111] Ebenstein DM, Pruitt LA. Nanoindentation of biological materials. *Nano Today* 2006; 1: 26–33.
- [112] Burger W, Burge MJ. *Digital image processing: an algorithmic introduction using Java*. Springer, 2016.
- [113] Kumar C, Le Houérou V, Speck T, et al. Straightforward and precise approach to replicate complex hierarchical structures from plant surfaces onto soft matter polymer. *Royal Society Open Science* 2018; 5: 172132.
- [114] Greiner C, Campo A del, Arzt E. Adhesion of bioinspired micropatterned surfaces: effects of pillar radius, aspect ratio, and preload. *Langmuir* 2007; 23: 3495–3502.
- [115] Dorogin L, Tiwari A, Rotella C, et al. Role of preload in adhesion of rough surfaces. *Physical Review Letters* 2017; 118: 238001.
- [116] Paretkar D, Kamperman M, Martina D, et al. Preload-responsive adhesion: effects of aspect ratio, tip shape and alignment. *Journal of The Royal Society Interface* 2013; 10: 20130171.
- [117] Romero V, Wandersman E, Debregeas G, et al. Probing locally the onset of slippage at a model multicontact interface. *Physical Review Letters* 2014; 112: 094301.
- [118] Campo A del, Greiner C, Arzt E. Contact shape controls adhesion of bioinspired fibrillar surfaces. *Langmuir* 2007; 23: 10235–10243.
- [119] Lamblet M, Verneuil E, Buguin A, et al. Adhesion enhancement through micropatterning at polydimethylsiloxane-acrylic adhesive interfaces. *Langmuir* 2007; 23: 6966–6974.
- [120] Glassmaker NJ, Jagota A, Hui C-Y, et al. Biologically inspired crack trapping for enhanced adhesion. *Proceedings of the National Academy of Sciences* 2007; 104: 10786–10791.
- [121] Huber G, Gorb SN, Hosoda N, et al. Influence of surface roughness on gecko adhesion. *Acta Biomaterialia* 2007; 3: 607–610.
- [122] Hui C-Y, Glassmaker N, Tang T, et al. Design of biomimetic fibrillar interfaces: 2. Mechanics of enhanced adhesion. *Journal of The Royal Society Interface* 2004; 1: 35–48.
- [123] Fischer SC, Groß K, Torrents Abad O, et al. Funnel-shaped microstructures for strong reversible adhesion. *Advanced Materials Interfaces* 2017; 4: 1700292.

- [124] Sahli R, Pallares G, Ducottet C, et al. Evolution of real contact area under shear and the value of static friction of soft materials. *Proceedings of the National Academy of Sciences* 2018; 115: 471–476.
- [125] Moore DF. On the decrease in contact area for spheres and cylinders rolling on a viscoelastic plane. *Wear* 1972; 21: 179–194.
- [126] Persson BN. *Sliding friction: physical principles and applications*. Springer Science & Business Media, 2013.
- [127] Suzuki K, Hirai Y, Ohzono T. Oscillating friction on shape-tunable wrinkles. *Applied Materials & Interfaces* 2014; 6: 10121–10131.
- [128] He B, Chen W, Wang QJ. Surface texture effect on friction of a microtextured poly(dimethylsiloxane) (PDMS). *Tribology Letters* 2008; 31: 187–197.
- [129] Murarash B, Itovich Y, Varenberg M. Tuning elastomer friction by hexagonal surface patterning. *Soft Matter* 2011; 7: 5553–5557.
- [130] Schallamach A. The velocity and temperature dependence of rubber friction. *Proceedings of the Physical Society Section B* 1953; 66: 386.
- [131] Cross R. Increase in friction force with sliding speed. *American Journal of Physics* 2005; 73: 812–816.
- [132] Popov VL, Voll L, Kusche S, et al. Generalized master curve procedure for elastomer friction taking into account dependencies on velocity, temperature and normal force. *Tribology International* 2018; 120: 376–380.
- [133] Barquins M. Sliding friction of rubber and Schallamach waves—a review. *Materials Science and Engineering* 1985; 73: 45–63.
- [134] McLaren K, Tabor D. Visco-elastic properties and the friction of solids: friction of polymers: influence of speed and temperature. *Nature* 1963; 197: 856.
- [135] Zhang S, Tsou A, Li J. Scratching behavior of elastomeric poly (dimethylsiloxane) coatings. *Journal of Polymer Science, Part B: Polymer Physics* 2002; 40: 1530–1537.
- [136] Nguyen D, Ramakrishna S, Frétiigny C, et al. Friction of rubber with surfaces patterned with rigid spherical asperities. *Tribology Letters* 2013; 49: 135–144.
- [137] Barquins M, Courtel R. Rubber friction and the rheology of viscoelastic contact. *Wear* 1975; 32: 133–150.
- [138] Klein G, LeHouérou V, Muller R, et al. Friction properties of acrylic-carboxylated latex films—1: Effects of acrylic acid concentration and pH. *Tribology International* 2012; 53: 142–149.
- [139] Maegawa S, Itoigawa F, Nakamura T. Effect of normal load on friction coefficient for sliding contact between rough rubber surface and rigid smooth plane. *Tribology International* 2015; 92: 335–343.
- [140] Kumar C, Damien F, Gauthier C, Speck T, Le Houérou V. *In-situ* investigation of adhesion mechanics on biological complex micro-structured surfaces. 2019; (*Under submission*).

6 Publications and Manuscripts

Manuscript A

C. Kumar, V. Le Houérou, T. Speck, and H. F. Bohn (2018).

Straightforward and precise approach to replicate complex hierarchical structures from plant surfaces onto soft matter polymer.

Royal Society Open Science, 5 (4): 172132.

This is an open access article published under the terms of the Creative Commons Attribution License, which permits unrestricted use, provided the original author and source are credited. The article is available at: <http://dx.doi.org/10.1098/rsos.172132>.

Contribution:

I, together with V. Le Houérou, T. Speck and H.F. Bohn conceived the idea and conceptually designed the experimental approach. The replica fabrication and SEM characterization of all samples were performed by me, under the direction of H.F. Bohn and V. Le Houérou. The first draft of manuscript was prepared by me in supervision of H.F. Bohn and V. Le Houérou. All authors critically evaluated and corrected the manuscript.

Manuscript B

C. Kumar, A. Palacios, V. A. Surapaneni, G. Bold, M. Thielen, E. Licht, T. E. Higham, T. Speck, and V. Le Houérou (2018).

Replicating the complexity of natural surfaces: technique validation and applications for biomimetics, ecology and evolution.

Philosophical Transactions of the Royal Society A. 377: 20180265

This article is available at: <https://doi.org/10.1098/rsta.2018.0265>

Contribution:

The very initial idea of this work was developed in a discussion with V. Le Houérou and T. Speck, and later conceptualized by everyone. I along with A. Palacios and V. A. Surapaneni conducted the replication experiments and surface characterization. A. Palacios performed the major data collection and statistical analyses together with V. A. Surapaneni and myself. Data evaluation and discussion of the results was a joint effort by all authors. Everyone contributed equally in preparing the first draft of the manuscript and improved further versions.

Manuscript C

C. Kumar, D. Favier, C. Gauthier, T. Speck, and V. Le Houérou (2019)

In-situ investigation of adhesion mechanics on biological complex micro-structured surfaces.

Under submission

Contribution:

I, together with V. Le Houérou and T. Speck developed and conceptualized the research idea. D. Favier and V. Le Houérou guided and assisted me in planning and designing the experimental techniques. All the replica preparation, surface characterization, adhesion experiments and data analyses were performed by me. The manuscript was written by myself in discussion with V. Le Houérou and T. Speck. All authors revised and corrected the final manuscript.

Manuscript D

C. Kumar, T. Speck, and V. Le Houérou (2019)

Friction during adhesive contacts on complex micro-structured surfaces.

Draft manuscript

Contribution:

I, together with V. Le Houérou and T. Speck developed and conceptualized the research idea. D. Favier and V. Le Houérou guided and assisted me in planning and designing the friction apparatus and experiment protocol. All the sample preparation, surface characterization, friction tests and data analyses were performed by me. DMTA analysis was carried out by V. Le Houérou. The manuscript was written by myself in discussion with V. Le Houérou and T. Speck. All authors revised and corrected the final manuscript.

6.1 Manuscript A

Downloaded from <http://rsos.royalsocietypublishing.org/> on April 18, 2018

ROYAL SOCIETY
OPEN SCIENCE

rsos.royalsocietypublishing.org

Research



Cite this article: Kumar C, Le Houérou V, Speck T, Bohn HF. 2018 Straightforward and precise approach to replicate complex hierarchical structures from plant surfaces onto soft matter polymer. *R. Soc. open sci.* 5: 172132. <http://dx.doi.org/10.1098/rsos.172132>

Received: 7 December 2017

Accepted: 14 March 2018

Subject Category:

Biochemistry and biophysics

Subject Areas:

biomimetics/biomechanics/biomaterials

Keywords:

biological surfaces, replication, hierarchical microstructures, epoxy mould, soft matter, PDMS replica

Author for correspondence:

Thomas Speck

e-mail:

thomas.speck@biologie.uni-freiburg.de

Straightforward and precise approach to replicate complex hierarchical structures from plant surfaces onto soft matter polymer

Charchit Kumar^{1,2,3}, Vincent Le Houérou², Thomas Speck^{1,3} and Holger F. Bohn^{1,3}

¹Plant Biomechanics Group Freiburg, Botanic Garden, Faculty of Biology, University of Freiburg, Schänzlestraße 1, 79104 Freiburg, Germany

²Institut Charles Sadron (ICS), CNRS UPR022, Université de Strasbourg, 23 rue du Loess, BP 84047, 67034 Strasbourg Cedex 2, France

³Freiburg Centre for Interactive Materials and Bioinspired Technologies (FIT), Georges-Köhler-Allee 105, D-79110 Freiburg, Germany

CK, 0000-0002-6912-3506; VLH, 0000-0001-7189-242X

The surfaces of plant leaves are rarely smooth and often possess a species-specific micro- and/or nano-structuring. These structures usually influence the surface functionality of the leaves such as wettability, optical properties, friction and adhesion in insect-plant interactions. This work presents a simple, convenient, inexpensive and precise two-step micro-replication technique to transfer surface microstructures of plant leaves onto highly transparent soft polymer material. Leaves of three different plants with variable size (0.5–100 µm), shape and complexity (hierarchical levels) of their surface microstructures were selected as model bio-templates. A thermoset epoxy resin was used at ambient conditions to produce negative moulds directly from fresh plant leaves. An alkaline chemical treatment was established to remove the entirety of the leaf material from the cured negative epoxy mould when necessary, i.e. for highly complex hierarchical structures. Obtained moulds were filled up afterwards with low viscosity silicone elastomer (PDMS) to obtain positive surface replicas. Comparative scanning electron microscopy investigations (original plant leaves and replicated polymeric surfaces) reveal the high precision and versatility of this

THE ROYAL SOCIETY
PUBLISHING

© 2018 The Authors. Published by the Royal Society under the terms of the Creative Commons Attribution License <http://creativecommons.org/licenses/by/4.0/>, which permits unrestricted use, provided the original author and source are credited.

replication technique. This technique has promising future application for the development of bioinspired functional surfaces. Additionally, the fabricated polymer replicas provide a model to systematically investigate the structural key points of surface functionalities.

1. Introduction

Surface functionalities are prominent when two counterparts come into contact and play an important role in the system's performance and efficiency [1–3]. This stands for most physical human-made as well as biological systems and two major parameters have to be taken into consideration: surface structuring and chemistry [4,5]. It is often crucial to fine-tune the frictional and adhesive properties of manufactured systems, when the surface-to-volume ratio gets tremendously increased in micro-contact applications (MEMS devices). For instance, a low adhesion for easy attachment and detachment of the devices is desired [6,7]. In this context, the surface micro- and nano-structuring is a possible solution to achieve such characteristics, besides altering the surface chemistry [7–10]. Surface structuring could also influence other surface properties of the technical systems such as optical effects, wetting, fluid flow, heat transfer, antifouling, etc. [11–14].

In nature, surfaces of plant leaves are often organized with a large variety of surface structuring; over a wide size range (from nano- to macro-scale), with distinct morphologies, and including several hierarchical levels [3,15,16]. Apart from surface chemistry, the specific and unique surface structuring gives rise to various remarkable and inspiring functionalities. For instance, self-cleaning behaviour of the sacred lotus (*Nelumbo nucifera*) leaves arise from the remarkable de-wetting ability due to the complex hierarchical structure composed of papillate epidermal cells covered with randomly oriented hydrophobic nano-scale wax crystals [17]. Anti-adhesive properties for insects attachments of the rubber tree (*Hevea brasiliensis*) leaves result from their fine micro-structuring, and the insect trapping in some carnivorous plants (e.g. *Nepenthes alata* Blanco) is caused by hierarchical structured architecture [18–20]. Within this context, biological surface structures may serve as role model to develop biomimetic and bioinspired surfaces and devices [21]. Furthermore, the production of precise polymer replicas of biological surfaces may help by allowing the investigation of structure influence on surface functionality, independently to surface chemistry [4,5].

The most commonly used technique to replicate structures from biological surfaces follows a two-step double casting process [5,22–32]. At first a negative mould is developed from a plant leaf (bio template); afterwards, this negative mould is used to transfer the structures onto the positive replica. In recent years, various approaches have been investigated to perform plant leaf replication (with different combinations of material for negative mould and positive replica). Williams *et al.* [22] introduced a technique with using polyvinyl siloxane (PVS) dental impression material as a negative mould and epoxy for the positive replica (hard material), and later this technique has been extensively investigated by other researchers [5,23,24]. In the PVS-epoxy approach, the fresh leaf was covered with PVS mixture and manually pressed down with a flat slide. The advantage of using PVS consists of its low adhesion to plant leaves which is useful to prevent artefacts. On the other hand, the quick polymerization of PVS (approximately in 2–5 min) constitutes a limitation for this technique as it could cause air to get trapped at the interface of mixture and leaf surface [23]. In another similar replication attempt, positive replicas were developed on PMMA (polymethyl methacrylate) from PDMS (polydimethylsiloxane) negative mould [25]. Here, plant leaves were exposed to high temperature during the development of negative mould. Shrinkage of the cell pattern can be seen on replicated surface, and final replicas were obtained on hard material (PMMA). Lee & Kwon [26] described an alternative approach to replicate the surface structure of bamboo leaf onto UV curable photopolymer, by using a hard negative mould of nickel. In this method, the substrate surface was first metallized by using gold sputtering and patterned by nickel electroforming [26]. For gold sputter coating, the substrate needs to be exposed under vacuum, which might induce cell shrinkage artefacts (surface distortion) [33,34]. Another replication approach has been described using PDMS to produce both the negative mould and the positive replica (PDMS–PDMS) [29,31]. The fresh leaf was filled up with PDMS mixture and cured at high temperature 80–90°C to develop a negative mould [29,30]. Again, the treatment of plant material with high temperatures is likely to facilitate shrinkage or collapse of surface structures resulting from evaporation of water from the cells. The strong adhesion (stiction) between PDMS mould and PDMS replica is the major issue for PDMS–PDMS replication, which could be overcome by creating an anti-stiction layer (organosilane monolayer deposition) on the PDMS mould [29,31,35]. In order to perform

a silane deposition, the PDMS mould needs to be treated under plasma, a procedure that can cause surface damage or instability [36]. Furthermore, during silane vapour deposition, aggregations of silane molecules can induce surface roughness [37,38]. Finally, an anti-stiction surface treatment degrades with time and replication cycles. In general, an anti-stiction treated PDMS mould can be well used to develop three or four positive replicas [35]. However, the PDMS–PDMS approach is not well explored yet for developing replica from complex biological structured surfaces with typically undercut and overhanging patterns. One may note that the PDMS, a soft matter polymer, is an interesting candidate for positive replicas because it has been extensively studied and is a widely used material in many nano- and micro-technology applications: it has easy handling, low cost, wide commercial availability and non-toxicity [39–41]. Furthermore, it offers numerous fascinating characteristics such as: high optical transparency, a low surface energy (22 mJ m^{-2}), excellent biocompatibility, chemical stability, high flexibility due to an extremely low elastic modulus ($E \approx 0.5\text{--}4 \text{ MPa}$, tunable with varying cross-linker density) [41–46].

In this paper, we present a new straightforward, inexpensive, robust and precise approach to replicate the microstructures directly from natural plant leaves in a hard and durable negative mould. It can be used as template for numerous positive soft matter replicas showing very precisely the original microstructure of the leaf surface. In this replication approach, epoxy resin (hard material) is used to develop negative mould and final positive replica is fabricated on the PDMS soft matter (hereinafter called the Epoxy–PDMS replication). A new alkaline chemical treatment is also established to wholly separate the leaf out from the negative mould in case of complex surface structures. In order to investigate the capabilities of this replication method, three different types of leaves were selected with different sizes (fine and coarse), distinct shapes and complexity (hierarchy) of their surface structures.

2. Material and methods

2.1. Plant materials

Three different model plant leaves were selected in this study: *H. brasiliensis* (Rubber tree), *Litchi chinensis* (Lychee) and *Ludisia discolor* (Jewel orchid). The leaves were chosen according to the different sizes (in the range of $0.5 \mu\text{m}$ to few $100 \mu\text{m}$) and distinct morphology of their surface microstructures (figure 2). *L. discolor* (adaxial, i.e. upper leaf surface) represents coarse microstructures (circular cone-like shape structures with a height of about $50 \mu\text{m}$ and a diameter $50\text{--}100 \mu\text{m}$). *H. brasiliensis* (adaxial, i.e. upper leaf surface) shows fine cuticular folds with both thickness and height of about $0.5\text{--}1 \mu\text{m}$, and an intermediate spacing of $0.5\text{--}1.5 \mu\text{m}$ [47]. *L. chinensis* (abaxial, i.e. lower leaf surface) has a complex hierarchical surface structuring consisting of undercuts and overhanging substructures of approximately $0.5\text{--}1 \mu\text{m}$ in thickness. All plants from which leaf samples were taken are cultivated in the Botanic Garden of the University of Freiburg, Germany. In order to keep safe natural surface features and to avoid dehydration artefacts, plant leaves were freshly picked just before each replication process. Before replication, leaf surfaces were gently washed with distilled water to remove contaminations. Immediately after washing, the leaf surfaces were carefully dried with pressurized air.

2.2. Replication procedure

The replication technique proposed in this study follows a two-step process: at first, a hard epoxy negative mould was produced directly from plant leaf, and then patterns from the negative mould were replicated onto PDMS surfaces. A schematic representation of the replication procedure is shown in figure 1. First, small pieces of approximately $3.5 \text{ cm} \times 3.5 \text{ cm}$ (larger or smaller area of sample can also be selected, the given sample area was chosen on purpose) were cut out from cleaned leaves and carefully attached onto a plastic Petri dish using double-side adhesive tape (tesa SE, Norderstedt, Germany). The two components epoxy resin (Epoxy Resin L & Hardener S, Toolcraft, Conrad Electronic SE, Hirschau, Germany) were uniformly mixed (mixing ratio of resin to hardener of 10:4.8) in a plastic cup for 3–5 min, using a glass rod. The mixture was then degassed in a vacuum chamber for 15 min to remove any dissolved and trapped air bubbles from the mixture. Afterwards, the epoxy resin was slowly and steadily (to avoid any bubbles) poured onto the leaf surface, so that mixture flows all over the Petri dish (figure 1*a*). The Petri dish filled with the epoxy resin is then kept for curing at room temperature ($23 \pm 2^\circ\text{C}$) for 15 h (figure 1*b*). Then the leaves were carefully peeled off from the cured epoxy negative moulds. During the peeling process, *H. brasiliensis* and *L. discolor* leaves were smoothly and wholly

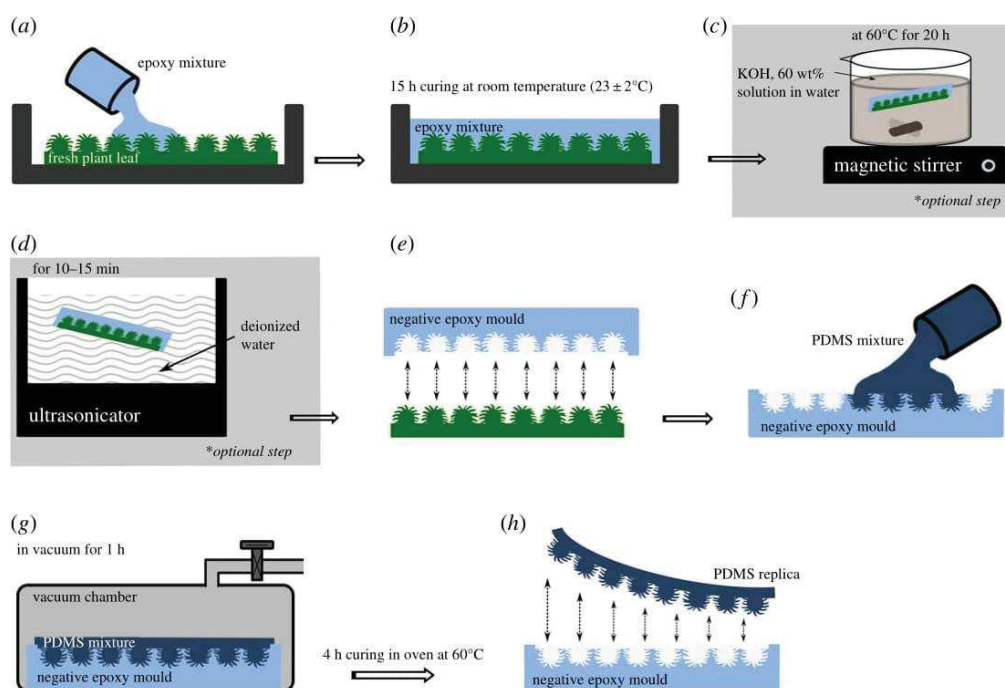


Figure 1. Schematic sketch of the two-step replication process. (a) Fresh plant leaf glued on a plastic Petri dish, filled up with epoxy resin. (b) Curing of epoxy mixture for 15 h to produce negative epoxy mould. (c)* Epoxy sample (which adhered with leaf surface) is kept for chemical treatment in potassium hydroxide solution on magnetic stirrer (at $60 \pm 3^\circ\text{C}$ for 20 h). (d)* Chemically treated sample washed in deionized water using an ultrasonicator. (e) Negative epoxy mould separated from the leaf surface. (f) Negative epoxy mould filled up with PDMS mixture. (g) Degassed in vacuum chamber to remove air trapped at the interface. (h) PDMS-positive replica peeled off from the epoxy mould. * Step c and d only necessary for complex hierarchical structured surface of *L. chinensis* leaves.

separated from cured negative epoxy moulds (figure 1e), whereas, in the case of *L. chinensis*, the leaf surface was strongly embedded in the cured epoxy mould and could not be peeled off undamaged. To separate *L. chinensis* leaf out from the cured negative epoxy mould, an alkaline chemical solution treatment was performed (figure 1c,d). A potassium hydroxide solution (KOH, $\geq 85\%$, p.a., Carl Roth GmbH & Co. KG, Karlsruhe, Germany) was prepared in distilled water at a concentration of 60 g/100 ml. The cured negative epoxy mould along with the *L. chinensis* leaf still attached was kept in a closed beaker with the KOH solution at $60 \pm 3^\circ\text{C}$ with a magnetic stirrer running at 450 ± 25 r.p.m. for 20 h (figure 1c). The sample was then removed from the solution and placed in an ultrasonicator (in deionized water) for 10–15 min (figure 1d). The leaf was carefully cut along the edges of the mould using a scalpel and then peeled off (figure 1d). Afterwards the negative mould was blown with pressurized air in order to dislodge any leftover particles and also to dry the mould.

In the next step, epoxy negative moulds (herein called negative moulds) developed from *H. brasiliensis*, *L. discolor*, and from *L. chinensis* leaves (after KOH treatment) were further used to replicate leaf surface patterns onto PDMS surfaces. Two-component PDMS elastomer (Bluesil ESA 7250 A & B kit, Bluestar Silicones GmbH, Leverkusen, Germany) was uniformly mixed (weight ratio of monomer to cross-linker of 10:1) in a plastic cup for about 5 min, using a glass rod. Then the mixture was kept in a vacuum desiccator for 30 min and was degassed (2–3 times) to remove trapped air bubbles in the mixture. The clear and bubble-free mixture was slowly poured onto the negative moulds from a corner to limit the formation of bubbles, so that the mixture flows all over the mould surface (figure 1f). Negative moulds filled up with PDMS mixture were kept in a vacuum chamber for 1 h to remove air entrapped at the interface between PDMS and micro/nano-cavities of the negative mould (figure 1g). The samples were kept in a heating oven at 60°C for 4 h and then the PDMS replicas were gently peeled off from the negative moulds (figure 1h). The PDMS replicas were washed with isopropyl alcohol ($\geq 99.95\%$, Carl Roth GmbH & Co. KG, Karlsruhe, Germany) in an ultrasonicator for 10 min, to wash off any residual particles and followed by drying with a compressed air stream.

2.3. Surface characterization

Visualization and characterization of surface morphology of the plant surfaces and their polymer replicas were performed using scanning electron microscopy (SEM). For SEM examination of the leaf surfaces, fresh leaves were dehydrated with methanol and dried by using critical point drier (LPD 030, Bal-Tec) [33]. Prior to SEM investigation, all samples (plant leaves and their replicas) were mounted on aluminium stubs (Plano GmbH, Wetzlar, Germany) using double-sided adhesive conducting tabs (Plano GmbH, Wetzlar, Germany). In addition to this, side walls of polymer replica samples were coated with highly conductive silver paint (Acheson Silver DAG 1415M, Plano GmbH, Wetzlar, Germany) to form an electron conducting path to the stubs. All samples were sputter coated with a thin (15–20 nm) layer of gold (Cressington Sputter Coater, 108 auto). Afterwards, all samples were examined using a Leo 435 vp scanning electron microscope (Leica, Wiesbaden, Germany). All SEM examinations were performed at 45° tilting angle, at an accelerating voltage of 15 kV.

3. Results and discussion

SEM images of the surfaces of original plant leaves and of their replicas are presented (side by side for better comparison) in figure 2 and illustrate the high precision of the developed replication process. The surface of the PDMS replica of *L. discolor* (figure 2f) shows microstructures (circular cones) very similar in size and shape to the original leaf surface structures (figure 2a). No explicit shrinkage or shape damage of the convex microstructures on the replica surface was observed. The surfaces of fresh *L. discolor* leaves show a shiny (glossy) optical appearance and the same optical appearance was also observed on its replica surface. The result of replications of the *H. brasiliensis* leaf surface shows that very fine (individual folds with a height and width of less than 1 µm) surface structures were successfully replicated without any fusion or overlapping of individual folds, as proved in figure 2b and figure 2g. High-resolution images of the *H. brasiliensis* leaf surface and its replica are shown in figure 2c and figure 2h confirming the high precision and spatial resolution of the new replication process. In the present investigation, the most remarkable replication result was obtained for *L. chinensis*, where complex hierarchical structures with undercuts and overhanging sub-structures could be replicated precisely (figure 2d and figure 2i). It is interesting to see in high-resolution images (figure 2e and figure 2j) that ‘rose flower-shaped’ patterns on the *L. chinensis* leaf surface were transferred to the replica undamaged. Such type of complex structures with undercuts is usually difficult to replicate without breaking the overhanging folds while peeling the replica from the negative mould.

This qualitative comparison based on SEM surface images provides evidence for the high precision and versatility of the replication technique, which is achieved due to the high compliance of PDMS (elastic modulus, $E \approx 2$ MPa [44,48]) in comparison with the elastic rigid behaviour of the cured epoxy resin. Moreover, the very low viscosity (≈ 400 mPa s) of uncured epoxy resin benefits to the better filling of liquid epoxy into the fine and complex leaf structures. This technique was even successful in the case of *L. chinensis* leaves as the epoxy mixture could completely and utterly fill the fine undercut cavities on the leaf surface. However, after complete curing of the moulding material, complex structures of leaf were tangled up in the moulding mass, with the consequence that the leaf surface was un-separably embedded (inlaid) in the cured epoxy. Therefore, the strong alkaline chemical treatment as described in detail in replication procedure section was successfully used to dissolve the plant material at the interface between leaf and epoxy mould. The low viscosity of liquid PDMS mixture also helps when filling up the negative moulding material (epoxy) (figure 1f). After polymerization (i.e. curing), the PDMS becomes a soft rubber type material. The present results strongly point towards the interpretation that the pronounced difference in the elasticity of both materials (epoxy and PDMS) is essential for easy removal of the positive replica by a simple peeling process. As a consequence, the flexible nature of PDMS prevents breaking of overhanging and damaging undercut structures. Prüm *et al.* [5] performed similar replications of complex microstructured *L. chinensis* leaf surface by using a PVS-Epoxy approach. However, some structural imperfection can be observed particularly on the overhanging cuticular folds of ‘rose flower-shaped’ hierarchical patterns [5]. This might be due to the quick curing and high viscosity of PVS impression material, which results in an incomplete filling of PVS into the undercuts cavities of the complex structure of *L. chinensis*. Our replication approach overcomes this limitation, thanks to the low viscosity of both epoxy and PDMS mixture prior to polymerization. Moreover, in some of the previously published direct replication approaches [25,26,29,30], plant leaves are exposed to vacuum or high temperatures which can produce replication errors due to shrinkage or collapse of surface structures. In the present work, no plant material was exposed to vacuum preventing early shrinkage. Furthermore, all

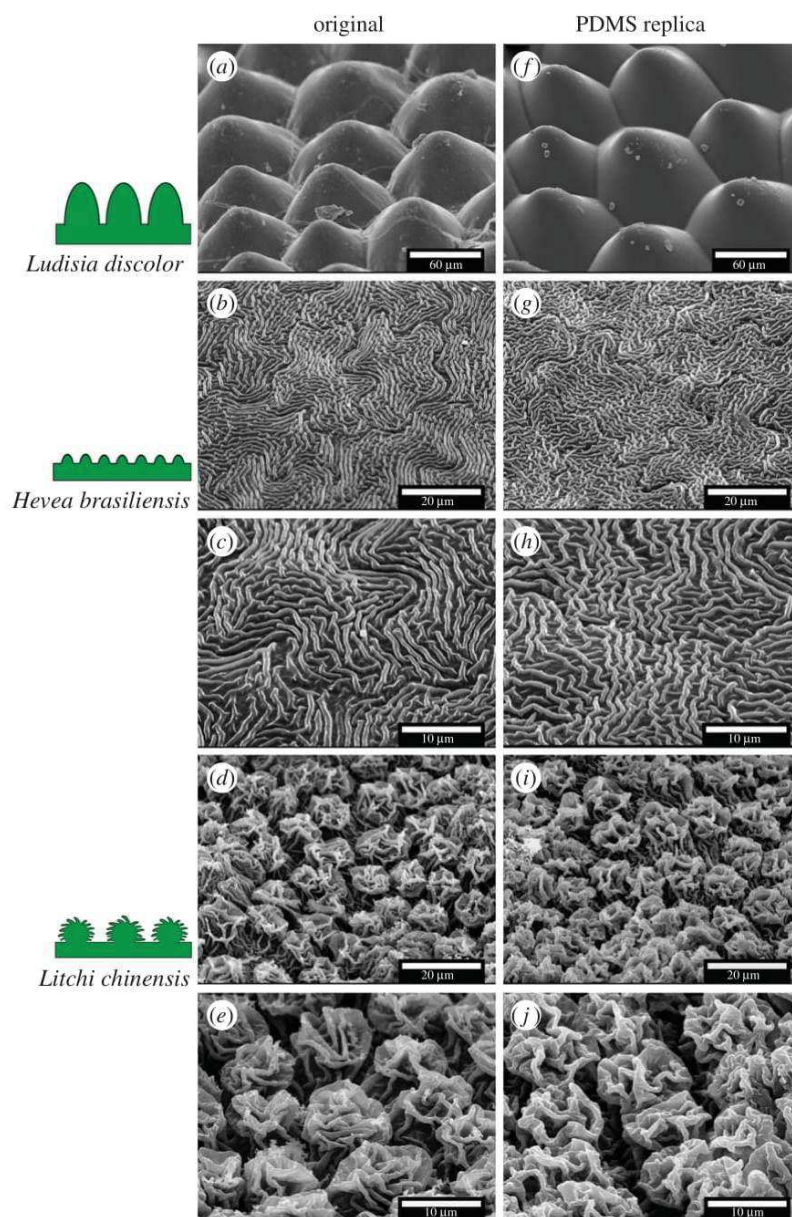


Figure 2. SEM images of original plant leaf surfaces (*a–e*) and their PDMS polymeric replicas (*f–j*). Pictograms on the left side represent the type of structuring. (*a,f*) *Ludisia discolor* (adaxial leaf surface; coarse cone-like surface structuring). (*b,g,c,h*) *Hevea brasiliensis* (adaxial leaf surface; fine fold-like microstructures). (*d,i,e,j*) *Litchi chinensis* (abaxial leaf surface; hierarchical surface structures). (*c,h,e,j*) Represent the higher magnification images of (*b,g*) and (*d,i*), respectively.

the epoxy moulds were developed at room temperature (as previously described) and because the plant samples were completely covered with epoxy resin, water loss by means of evaporation is minimized. In addition, the temperature of the moulding mass (epoxy resin) was continuously recorded during the curing process with a thermocouple probe. No noteworthy variation in ambient temperature was observed ($24 \pm 2^\circ\text{C}$).

Up to this point, the versatile replication abilities of our technique have been demonstrated. However, this technique shows some limitations which have to be discussed. The replication of a fourth plant leaf was studied to illustrate these issues. Actually, *Iris germanica* (bearded iris) plant leaf (adaxial, i.e. upper leaf surface) was chosen due to its particular surface structure made of a three-dimensional dense arrangement of perpendicularly oriented long wax platelets. One may note that the freshly hydrated leaf was used for SEM observation to avoid any wax platelets destruction that might be caused by methanol

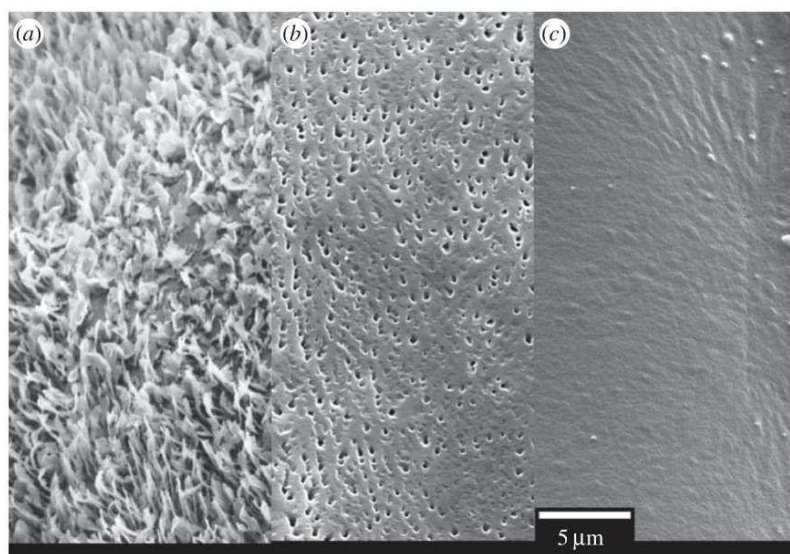


Figure 3. High-resolution SEM image of original leaf surfaces (a) of *Iris germanica* (adaxial leaf surface; covered with a dense network of perpendicularly oriented wax platelets), developed negative epoxy mould (b) and their PDMS polymeric replica (c).

dehydration protocol. The sample was quickly examined before any desiccation artefacts were observed [49]. Figure 3a shows the high-resolution image of the native *I. germanica* leaf surface covered with the dense network of high aspect ratio wax platelets, and its PDMS replica is shown in figure 3c. It shows clearly the replication flaw for the wax platelets morphology. To investigate the cause of this replication limitation, the SEM image of the negative epoxy mould is reported in figure 3b.

As can be seen on negative epoxy mould, some wax morphology partially formed a negative imprint. We believe that one possible reason might be that the liquid epoxy mixture stays on top of some wax platelets and could not completely penetrate inside the wax structures as no external pressure was applied on the moulding mass. Consequently, to this partial wetting of the fresh leaf surface by the epoxy mixture, only some wax patterns were correctly transferred onto the negative mould. We also speculate that the fragile and high-aspect-ratio wax platelets might have embedded within the cured epoxy mould and broken down during separation. It is worthy of anticipation that some leaves surface with high aspect ratio complex structures or with long, pointy slender members-like structures (such as the long hairy with pointy branches trichome microstructures on *Arabidopsis thaliana* leaf) might be difficult to replicate [50], in particular while separating of the trichomes from negative moulds.

Finally, although this new replication technique has some limitations, it demonstrates good replication abilities for various surfaces and offers extra advantageous aspects of the Epoxy–PDMS usage: (1) The negative epoxy moulds do not require any intermediate anti-stiction surface treatment (e.g. deposition of self-assembled silane monolayers), which is compulsory in some other processes such as PDMS–PDMS replication [35,38,51]. These additional surface treatments are usually time-consuming, need extra equipment and could give rise to complications. Moreover, the present replication approach eliminates the risk of chemical contamination on the positive PDMS replicas, because no chemical surface treatments have to be performed on the negative epoxy mould. (2) Our replication approach does not immensely depend on the process parameters and appears highly stable against variation in ambient conditions. This replication process can be easily performed without using costly and sophisticated laboratory machines. (3) Cured negative epoxy moulds which are hard and robust after curing (Young's modulus of the moulds approx. 3 GPa) offer long durability and high stability even of delicate surface microstructures. The same epoxy mould without any further treatment can be used repeatedly to fabricate multiple PDMS replicas.

4. Conclusion

The newly developed replication approach presented here provides a simple, inexpensive, durable and precise way to directly transfer coarse, fine (with a lateral resolution down to sub-micron), as well as

complex hierarchical geometries from biological surfaces onto PDMS soft polymer. This technique can be used for the rapid development of bioinspired functional surfaces and can also be upscaled on a large area (cm²), although limited to the size of leaves. Replicas developed by this technique have a major perspective to investigate the role of topography on the surface functionalities such as optical properties, wetting properties, tribological properties, antifouling properties, etc. Therefore, the technique presented in this work represents a relevant alternative for the micro-replication of biological surface structures.

Data accessibility. All data required to attempt a replication are provided within the manuscript, specifically in the Material and methods section and the figures presented.

Authors' contributions. C.K., V.L.H. and H.F.B. conceived the idea and designed the experimental technique. C.K. contributed towards the fabrication and characterization of samples. V.L.H. and H.F.B. supervised, and C.K. prepared the first draft of manuscript. V.L.H., T.S. and H.F.B. critically evaluated and corrected the manuscript. All authors have given approval to the final version of the manuscript.

Competing interests. We have no competing interests.

Funding. This work was financially supported by the German Research Foundation (Deutsche Forschungsgemeinschaft: DFG) under the framework of International Research Training Group (IRTG) 'Soft Matter Science - 1642'.

Acknowledgements. The authors are grateful to the German Research Foundation (Deutsche Forschungsgemeinschaft: DFG), for funding support under the framework of International Research Training Group (IRTG) 'Soft Matter Science - 1642'. We would also like to thank the gardeners of the Botanic Garden Freiburg for cultivating the plants investigated.

References

- Cao G, Wang Y. 2011 *Nanostructures and nanomaterials*. Singapore: World Scientific Publishing Company.
- Bhushan B (ed.). 2004 *Springer handbook of nanotechnology*. Berlin, Germany: Springer.
- Barthlott W, Mail M, Bhushan B, Koch K. 2017 Plant surfaces: structures and functions for biomimetic innovations. *Nano-Micro Lett.* **9**, 23. (doi:10.1007/s40820-016-0125-1)
- England MW, Sato T, Yagihashi M, Hozumi A, Gorb SN, Gorb EV. 2016 Surface roughness rather than surface chemistry essentially affects insect adhesion. *Beilstein J. Nanotechnol.* **7**, 1471–1479. (doi:10.3762/bjnano.7.139)
- Prüm B, Bohn HF, Seidel R, Rubach S, Speck T. 2013 Plant surfaces with cuticular folds and their replicas: influence of microstructuring and surface chemistry on the attachment of a leaf beetle. *Acta Biomater.* **9**, 6360–6368. (doi:10.1016/j.actbio.2013.01.030)
- Gebeshuber IC, Gordon R. 2011 Bioinspiration for tribological systems on the micro- and nanoscale: dynamic, mechanic, surface and structure related functions. *Micro Nanosyst.* **3**, 271–276. (doi:10.2174/1876402911103040271)
- Burton Z, Bhushan B. 2005 Hydrophobicity, adhesion, and friction properties of nanopatterned polymers and scale dependence for micro- and nanoelectromechanical systems. *Nano Lett.* **5**, 1607–1613. (doi:10.1021/nl050861b)
- He B, Chen W, Wang QJ. 2008 Surface texture effect on friction of a microtextured poly(dimethylsiloxane) (PDMS). *Tribol. Lett.* **31**, 187–197. (doi:10.1007/s11249-008-9351-0)
- Greiner C, del Campo A, Arzt E. 2007 Adhesion of bioinspired micropatterned surfaces: effects of pillar radius, aspect ratio, and preload. *Langmuir* **23**, 3495–3502. (doi:10.1021/la0633987)
- Poulard C, Restagno F, Weil R, Léger L. 2011 Mechanical tuning of adhesion through micro-patterning of elastic surfaces. *Soft Matter* **7**, 2543–2551. (doi:10.1039/c0sm01099e)
- Bhushan B, Jung YC. 2011 Natural and biomimetic artificial surfaces for superhydrophobicity, self-cleaning, low adhesion, and drag reduction. *Prog. Mater. Sci.* **56**, 1–108. (doi:10.1016/j.pmatsci.2010.04.003)
- Bigham S, Fazeli A, Moghaddam S. 2017 Physics of microstructures enhancement of thin film evaporation heat transfer in microchannels flow boiling. *Sci. Rep.* **7**, 1–11. (doi:10.1038/srep44745)
- Kim DE, Yu DI, Jerng DW, Kim MH, Ahn HS. 2015 Review of boiling heat transfer enhancement on micro/nanostructured surfaces. *Exp. Therm. Fluid Sci.* **66**, 173–196. (doi:10.1016/j.expthermflusc.2015.03.023)
- Zhou T, Liu X, Liang Z, Liu Y, Xie J, Wang X. 2017 Recent advancements in optical microstructure fabrication through glass molding process. *Front. Mechan. Eng.* **12**, 46–65. (doi:10.1007/s11465-017-0425-2)
- Koch K, Bhushan B, Barthlott W. 2008 Diversity of structure, morphology and wetting of plant surfaces. *Soft Matter* **4**, 1943–1963. (doi:10.1039/b804854a)
- Koch K, Bohn HF, Barthlott W. 2009 Hierarchically sculptured plant surfaces and superhydrophobicity. *Langmuir* **25**, 14 116–14 120. (doi:10.1021/la9017322)
- Barthlott W, Neinhuis C. 1997 Purity of the sacred lotus, or escape from contamination in biological surfaces. *Planta* **202**, 1–8. (doi:10.1007/s004250050096)
- Gorb EV, Gorb SN. 2006 Physicochemical properties of functional surfaces in pitchers of the carnivorous plant *Nepenthes alata* Blanco (Nepenthaceae). *Plant Biol.* **8**, 841–848. (doi:10.1055/s-2006-923929)
- Poppinga S, Koch K, Bohn HF, Barthlott W. 2010 Comparative and functional morphology of hierarchically structured anti-adhesive surfaces in carnivorous plants and kettle trap flowers. *Funct. Plant Biol.* **37**, 952–961. (doi:10.1071/FP10061)
- Prüm B, Seidel R, Bohn HF, Speck T. 2011 Plant surfaces with cuticular folds are slippery for beetles. *J. R. Soc. Interface* **9**, 127–135. (doi:10.1098/rsif.2011.0202)
- Koch K, Bhushan B, Barthlott W. 2009 Multifunctional surface structures of plants: an inspiration for biomimetics. *Prog. Mater. Sci.* **54**, 137–178. (doi:10.1016/j.pmatsci.2008.07.003)
- Williams MH, Vesik M, Mullins MG. 1987 Tissue preparation for scanning electron microscopy of fruit surfaces: comparison of fresh and cryopreserved specimens and replicas of banana peel. *Micron Microsc. Acta* **18**, 27–31. (doi:10.1016/0739-6260(87)90016-5)
- Koch K, Schulte AJ, Fischer A, Gorb SN, Barthlott W. 2008 A fast, precise and low-cost replication technique for nano- and high-aspect-ratio structures of biological and artificial surfaces. *Bioinspir. Biom.* **3**, 046 002–046 012. (doi:10.1088/1748-3182/3/4/046002)
- Schulte AJ, Koch K, Spaeth M, Barthlott W. 2009 Biomimetic replicas: transfer of complex architectures with different optical properties from plant surfaces onto technical materials. *Acta Biomater.* **5**, 1848–1854. (doi:10.1016/j.actbio.2009.01.028)
- Singh RA, Kim HJ, Kim J, Yang S, Jeong HE, Suh KY, Yoon ES. 2007 A biomimetic approach for effective reduction in micro-scale friction by direct replication of topography of natural water-repellent surfaces. *J. Mech. Sci. Technol.* **21**, 624–629. (doi:10.1007/BF03026967)
- Lee SM, Kwon TH. 2006 Mass-producible replication of highly hydrophobic surfaces from plant leaves. *Nanotechnology* **17**, 3189–3196. (doi:10.1088/0957-4484/17/13/019)
- Gao J, Liu Y, Xu H, Wang Z, Zhang X. 2010 Biostructure-like surfaces with thermally responsive wettability prepared by temperature-induced phase separation micromolding. *Langmuir* **26**, 9673–9676. (doi:10.1021/la100256b)
- Lee SM, Lee HS, Kim DS, Kwon TH. 2006 Fabrication of hydrophobic films replicated from plant leaves in

- nature. *Surf. Coat. Technol.* **201**, 553–559. (doi:10.1016/j.surfcoat.2005.12.006)
29. McDonald B, Patel P, Zhao B. 2013 Micro-structured polymer film mimicking the trembling aspen leaf. *Chem Eng Process Tech* **1**, 1012–1018.
 30. Saison T, Peroz C, Chauveau V, Berthier S, Sondergard E, Arribart H. 2008 Replication of butterfly wing and natural lotus leaf structures by nanoimprint on silica sol–gel films. *Bioinspiration Biomimetics* **3**, 046004. (doi:10.1088/1748-3182/3/4/046004)
 31. Sun M, Luo C, Xu L, Ji H, Ouyang Q, Yu D, Chen Y. 2005 Artificial lotus leaf by nanocasting. *Langmuir* **21**, 8978–8981. (doi:10.1021/la050316q)
 32. Hensel R, Helbig R, Aland S, Voigt A, Neinhuis C, Werner C. 2013 Tunable nano-replication to explore the omniphobic characteristics of springtail skin. *NPG Asia Mater.* **5**, e37. (doi:10.1038/am.2012.66)
 33. Neinhuis C, Edelmann HG. 1996 Methanol as a rapid fixative for the investigation of plant surfaces by SEM. *J. Microsc.* **184**, 14–16. (doi:10.1046/j.1365-2818.1996.d01-110.x)
 34. Talbot MJ, White RG. 2013 Methanol fixation of plant tissue for scanning electron microscopy improves preservation of tissue morphology and dimensions. *Plant Methods* **9**, 1–7. (doi:10.1186/1746-4811-9-1)
 35. Zhuang G, Kutter JP. 2011 Anti-stiction coating of PDMS moulds for rapid microchannel fabrication by double replica moulding. *J. Micromech. Microeng.* **21**, 105 020–105 026. (doi:10.1088/0960-1317/21/10/105020)
 36. Bodas D, Khan-Malek C. 2007 Hydrophilization and hydrophobic recovery of PDMS by oxygen plasma and chemical treatment—an SEM investigation. *Sens. Actuators B, Chem.* **123**, 368–373. (doi:10.1016/j.snb.2006.08.037)
 37. Bunker BC, Carpick RW, Assink RA, Thomas ML, Hankins MG, Voigt JA, Sipola D, de Boer MP, Gulley GL. 2000 The impact of solution agglomeration on the deposition of self-assembled monolayers. *Langmuir* **16**, 7742–7751. (doi:10.1021/la000502q)
 38. Pan Z, Shahsavani H, Zhang W, Yang FK, Zhao B. 2015 Superhydro-oleophobic bio-inspired polydimethylsiloxane micropillared surface via FDS coating blending approaches. *Appl. Surf. Sci.* **324**, 612–620. (doi:10.1016/j.apsusc.2014.10.146)
 39. McDonald JC, Duffy DC, Anderson JR, Chiu DT, Wu H, Schueller OJA, Whitesides GM. 2000 Fabrication of microfluidic systems in poly(dimethylsiloxane). *Electrophoresis* **21**, 27–40. (doi:10.1002/(SICI)1522-2683(20000101)21:1<27::AID-ELPS27>3.0.CO;2-C)
 40. Mata A, Fleischman AJ, Roy S. 2005 Characterization of polydimethylsiloxane (PDMS) properties for biomedical micro/nanosystems. *Biomed. Microdevices* **7**, 281–293. (doi:10.1007/s10544-005-6070-2)
 41. Schneider F, Draheim J, Kamberger R, Wallrabe U. 2009 Process and material properties of polydimethylsiloxane (PDMS) for optical MEMS. *Sens. Actuators A* **151**, 95–99. (doi:10.1016/j.sna.2009.01.026)
 42. Yoon Y, Lee DW, Lee J-B. 2013 Fabrication of optically transparent PDMS artificial lotus leaf film using underexposed and underbaked photoresist mold. *J. Microelectromech. Syst.* **22**, 1057–1157. (doi:10.1109/JMEMS.2013.2264729)
 43. Chaudhury MK, Whitesides GM. 1991 Direct measurement of interfacial interactions between semispherical lenses and flat sheets of poly(dimethylsiloxane) and their chemical derivatives. *Langmuir* **7**, 1013–1025. (doi:10.1021/la00053a033)
 44. Schneider F, Fellner T, Wilde J, Wallrabe U. 2008 Mechanical properties of silicones for MEMS. *J. Micromech. Microeng.* **18**, 065008. (doi:10.1088/0960-1317/18/6/065008)
 45. Wang Z, Volinsky AA, Gallant ND. 2014 Crosslinking effect on polydimethylsiloxane elastic modulus measured by custom-built compression instrument. *J. Appl. Polym. Sci.* **131**, 41050. (doi:10.1002/app.41029)
 46. Zhou J, Ellis AV, Voelcker NH. 2010 Recent developments in PDMS surface modification for microfluidic devices. *Electrophoresis* **31**, 2–16. (doi:10.1002/elps.200900475)
 47. Prüm B, Seidel R, Bohn HF, Speck T. 2012 Impact of cell shape in hierarchically structured plant surfaces on the attachment of male Colorado potato beetles (*Leptinotarsa decemlineata*). *Beilstein J. Nanotechnol.* **3**, 57–64. (doi:10.3762/bjnano.3.7)
 48. Dirany M, Dies L, Restagno F, Léger L, Poulard C, Miquelard-Garnier G. 2015 Chemical modification of PDMS surface without impacting the viscoelasticity: model systems for a better understanding of elastomer/elastomer adhesion and friction. *Colloids Surf. A* **468**, 174–183. (doi:10.1016/j.colsurfa.2014.12.036)
 49. Ensikat HJ, Ditsche-Kuru P, Barthlott W. 2010 Scanning electron microscopy of plant surfaces: simple but sophisticated methods for preparation and examination. *Microsc. Sci. Technol. Appl. Educ.* **1**, 248–255.
 50. Liu H, Zhou LH, Jiao J, Liu S, Zhang Z, Lu TJ, Xu F. 2016 Gradient mechanical properties facilitate arabidopsis trichome as mechanosensor. *ACS Appl. Mater. Interfaces* **8**, 9755–9761. (doi:10.1021/acsami.6b02253)
 51. Hassanin H, Mohammadkhanian A, Jiang K. 2012 Fabrication of hybrid nanostructured arrays using a PDMS/PDMS replication process. *Lab. Chip* **12**, 4160–4167. (doi:10.1039/c2lc40512a)

6.2 Manuscript B

PHILOSOPHICAL TRANSACTIONS A

royalsocietypublishing.org/journal/rsta

Research



Cite this article: Kumar C, Palacios A, Surapaneni VA, Bold G, Thielen M, Licht E, Higham TE, Speck T, Le Houérou V. 2019 Replicating the complexity of natural surfaces: technique validation and applications for biomimetics, ecology and evolution. *Phil. Trans. R. Soc. A* **377**: 20180265. <http://dx.doi.org/10.1098/rsta.2018.0265>

Accepted: 9 October 2018

One contribution of 14 to a theme issue 'Bioinspired materials and surfaces for green science and technology'.

Subject Areas:

biomechanics, biophysics, materials science

Keywords:

replication, polymers, microstructuring, biomimetics, haptics

Author for correspondence:

e-mail:
thomas.speck@biologie.uni-freiburg.de

Replicating the complexity of natural surfaces: technique validation and applications for biomimetics, ecology and evolution

Charchit Kumar^{1,2,5,†}, Alejandro Palacios^{1,2,†}, Venkata A. Surapaneni^{2,6}, Georg Bold^{2,5}, Marc Thielen^{2,6}, Erik Licht⁷, Timothy E. Higham^{2,3}, Thomas Speck^{2,5,6} and Vincent Le Houérou^{1,4}

¹Institut Charles Sadron, CNRS UPR022, Université de Strasbourg, Strasbourg, France

²Plant Biomechanics Group and Botanic Garden, University of Freiburg, Freiburg, Germany

³Department of Evolution, Ecology, and Organismal Biology, University of California, Riverside, CA, USA

⁴ICube, UMR7357, Université de Strasbourg, Strasbourg, France

⁵FIT, Freiburg Center for Interactive Materials and Bioinspired Technologies, Freiburg, Germany

⁶FMF, Freiburg Materials Research Center, Freiburg, Germany

⁷Basell Deutschland GmbH, LyondellBasell Industries, Frankfurt a.M., Germany

 CK, 0000-0002-6912-3506; VAS, 0000-0002-6241-9048; GB, 0000-0002-8020-8770; MT, 0000-0002-7773-6724; TEH, 0000-0003-3538-6671; TS, 0000-0002-2245-2636; VLH, 0000-0001-7189-242X

The surfaces of animals, plants and abiotic structures are not only important for organismal survival, but they have also inspired countless biomimetic and industrial applications. Additionally, the surfaces of animals and plants exhibit an unprecedented level of diversity, and animals often move on the surface of plants. Replicating these surfaces offers a number of advantages, such as preserving a surface that is likely to degrade over time, controlling for non-structural aspects of surfaces, such as compliance and chemistry, and being able to produce large areas

© 2018 The Author(s) Published by the Royal Society. All rights reserved.

[†]Shared first authorship.

THE ROYAL SOCIETY
PUBLISHING

of a small surface. In this paper, we compare three replication techniques among a number of species of plants, a technical surface and a rock. We then use two model parameters (cross-covariance function ratio and relative topography difference) to develop a unique method for quantitatively evaluating the quality of the replication. Finally, we outline future directions that can employ highly accurate surface replications, including ecological and evolutionary studies, biomechanical experiments, industrial applications and improving haptic properties of bioinspired surfaces. The recent advances associated with surface replication and imaging technology have formed a foundation on which to incorporate surface information into biological sciences and to improve industrial and biomimetic applications.

This article is part of the theme issue 'Bioinspired materials and surfaces for green science and technology'.

1. Introduction

Every structure, living or not, has a surface. An understanding of surfaces has inspired a myriad of applications and discoveries, incorporating disparate fields such as ecology, advanced contact mechanics, industry, biomimetics and biophysics (figure 1). The surface of an organism is a critical interface interacting with its surroundings. External surfaces are diverse and can include skin and shells (animals), but also the epidermis (with its cuticle) in plants. Internal surfaces include the gastrointestinal tract in animals or stomatal cavities in plants. From a physical point of view all surfaces of plants, animals, fungi and bacteria are interfaces between the organism and the media of its environment, which may change its aggregate state between gaseous, liquid or solid (e.g. air–water–ice), sometimes on a very short time scale (e.g. during rain). This alone shows that surfaces have to deal with highly variable physical conditions and represent very important interfaces between an organism and its environment. In addition to protective roles, the surfaces are also important for manifold types of communication between an organism and its biotic and abiotic environment. In the case of plant surfaces, the functions of epidermis and its cuticle include, among others, control of transpiration and diffusion on the one hand and of uptake of substances on the other, control of light transmission and/or reflection and of optical properties in general, wetting or anti-wetting behaviour, protection against contaminations and biotic threats (e.g. fungus or bacteria infection), cooling by increasing turbulent flow and convection, mechanical protection (against physical damage but also against feeding animals), as well as signalling for animal and host–pathogen recognition and additional control of plant–animal interaction (e.g. animals moving on slippery and non-slippery surfaces) [1–6].

(a) Plant–animal interactions

The surfaces on which animals move or hold station are inextricably linked with many behaviours that are related to fitness. For example, terrestrial animals must move over complex surfaces in order to capture prey and escape from predators. The effective attachment is, therefore, of the utmost importance. Given this, the structure of both the substrate and the animal's propulsive structures are equally important, yet most research has focused on the animal side of the interaction. When the substrate is considered, it is often categorized as smooth or rough simply based on feel or general impression, rather than a quantitative assessment [7]. This is problematic, as it is clear that microscale differences are paramount for dictating the efficacy of animal–habitat interactions. This extends to both biotic (e.g. plants) and abiotic (e.g. rocks) surfaces, both of which are traversed by a diverse array of organisms (e.g. figure 1). Many of these organisms house an intricate microtopography on their locomotor surface, such as the adhesive systems of insects [8] and some lizards [9]. However, animals can also exhibit complex structures for holding station on rough terrain in sub-optimal environmental conditions, such as clingfish in the marine intertidal zone [10,11]. Therefore, this important interface between an animal and its habitat cannot be ignored.

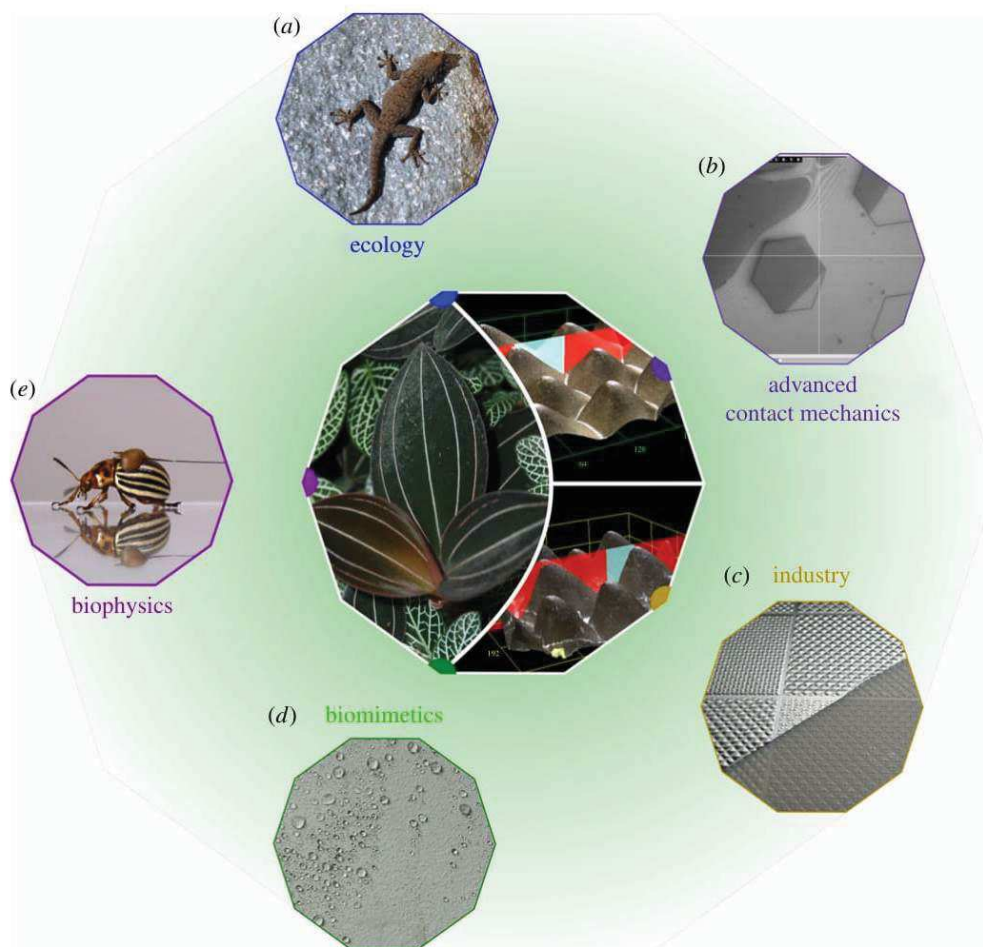


Figure 1. A schematic picture showing various research areas in which surface analyses are of importance. The decagon in the middle represents: (left) original *Ludisia discolor* leaves, (top right) Confocal Laser Scanning Microscopy (CLSM) image of a fresh leaf, and (bottom right) CLSM image of its polymeric replica; (a) shows a gecko (*Rhoptropus bradfieldi*) on a dolerite surface in Namibia; (b) exhibits the incorporation of biological microstructured surfaces (replicas) to advanced (*in situ*) contact mechanics studies; (c) shows an injection moulded polypropylene compound demonstrator (partly covered with aluminium foil); (d) shows a surface painted with self-cleaning paint Lotusan[®]; and (e) shows a locomotor experiment with a Colorado potato beetle (*Leptinotarsa decemlineata*) on a smooth glass surface.

(b) Why surface matters?

From an evolutionary and ecological perspective, identifying the relationships between organismal performance and surface topography is key to understanding how animals adapt to their surroundings. This also permits an assessment of symbiotic coevolution between biotic surfaces and the animals that use them. Biotic surfaces can defend against unwanted visitors or may promote mutualistic relationships. However, without knowledge of the surface parameters relevant to an animal, we are left to qualitative categorizations that provide little utility. This is unacceptable given that the fine-scale relationships between roughness and attachment principles (e.g. adhesion) are often nonlinear [12]. Thus, one cannot simply say that rougher is worse or better for an animal, especially when roughness is not defined quantitatively [13,14].

Surfaces relevant to terrestrial animals (or benthic marine animals) can be biotic or abiotic, as noted above. Biotic surfaces are most commonly represented by plants, but small animals

may also attach to, or move on, the surfaces of larger animals. For our paper, we will focus on plant surfaces when discussing biotic substrates. Abiotic factors can include virtually anything on Earth, from rocks to human-made structures. Rocks can exhibit the same degree of microtopography as plant surfaces [15], and it is not surprising that some animals use both rocks and plants as they move through their habitat. That said, plants and rocks differ in a number of ways, including stiffness and chemistry. Comparing plants and rocks through the use of replicated surfaces is an ideal way of eliminating the variability in variables *other* than topography.

(c) Why we need replicates?

The natural habitats of animals are rife with complexity, and this is also true for the surfaces on which the animals move. Numerous factors can vary with abiotic and biotic surfaces, including compliance, chemistry, colour and curvature, among other things. Thus, there are often confounding factors when using natural surfaces in a laboratory experiment. To control for all of the variables described above, one must generate replicas of natural surfaces. This standardizes all of the confounding parameters and allows one to explore the consequences of variation among animals using a particular surface, but also allows one to hone in on the consequences of finer variation in surface microtopography. Finally, biotic samples often dry quickly following removal from the plant, and this can cause very quick transformations in the structure. A replicate would prolong the integrity of the surface microtopography for experiments. For these reasons, surface replicates are ideal for exploring numerous questions related to ecology, evolution and biomechanics. Identifying morphological adaptations of animals to certain types of surfaces also opens the door to biomimetic applications and a deeper understanding of evolutionary patterns.

There are situations in which replicates are the only option. The fossil record is a great example of this. With the ability to create replicas, we can take information about the surfaces of extinct plants and recreate them in order to understand how extant or extinct animals may have performed on them [16]. This will shed light on the historical patterns of plant–animal interactions, therefore opening a window into the evolution of these interactions.

(d) Biomimetic applications

In the past several decades, plant surfaces (especially leaves) have attracted great attention, not only in biology but also in other disciplines. Given their various functionalities, they have been an inspiration for technical applications, including as a transport barrier, to improve anti-fouling and/or friction reduction, for controlling surface wettability and fluid flow on surfaces, for optimizing optical properties and for controlling (anti-)adhesive properties [2,3,13,17–22]. Since the first publication of the self-cleaning mechanism of plant surfaces being based on microstructured surface roughness [23], a plethora of papers has been published describing the use of this or similar effects based on surface micro- and nano-structuring for bioinspired technical applications. Most of these deal with influencing the wettability of these surfaces [2,21,24]. The same holds for air retention under water which, after its first quantitative description in *Salvinia* [25,26], inspired many attempts of biomimetic transfer [27,28]. Others describe how periodic surface structuring can induce colour effects and how these can be transferred into biomimetic applications [29–32]. Also, the interaction of insect tarsi with plant surfaces was investigated with regard to biomimetic applications. The main aim was to understand the structural and functional aspects of this interaction on a micro-level and to create technical surfaces that are difficult or impossible for insects to adhere to and, thus, to walk on [14,33]. Such bioinspired surfaces have great potential for non-chemical protection against insect infestations [34]. Except for the wetting properties, all these properties acquired through surface structuring are relatively independent of the material used [13]. Another subject that is becoming of increasing interest for biomimetics and industrial applications is that of haptic surface properties and the perception thereof. Quantitatively dealing with the questions involved, however, is at least as complex as the aforementioned topics. On the one hand, because haptic perception is very subjective, on the other

hand, because properties such as mass, geometry and material properties (modulus of elasticity, heat capacity, etc.) also play an important role in addition to surface topology [35]. An example of a plant–animal interaction involving haptic perception is that of haptic properties of fruits— notably mass and hardness—that are presumably indicators of their ripeness for certain primates [36]. Surface roughness/topography has only scarcely been analysed in this context so far and thus might represent an interesting field of future interdisciplinary research. Other vertebrates likely assess the suitability of food plants via oral assessments of surface roughness/topography and texture, which at least for humans contribute, besides appearance and flavour, markedly to the enjoyment of eating foods [37]. A very interesting study relating surface roughness and haptic perception was conducted by [38]. They found that sliding a fingertip over rough glass surfaces generated desirable positive feelings if the surface is less rough than the fingertip, whereas surfaces rougher than the fingertip generated undesirable feelings. Roughness is perceived via two types of cutaneous receptors which differentiate between surface structures with spatial periods above and below approximately 200 μm . Relatively coarse topologies with spatial periods above 200 μm are encoded spatially and transduced by slowly adapting mechanoreceptors [35,39], while finer surface structures are perceived by so-called Pacinian corpuscles that are sensitive to vibrations generated when textured surfaces and skin move relative to each other.

(e) Surface replicas as testing tool for structure–function–relationship

Most of the functional characteristics of surfaces are owing to physico-chemical properties or micro- and nano-structuring of the surfaces [3,13,21,40,41]. Sometimes, the surface function relies on the complex interplay of all properties or of both latter. Different types of techniques have been used to transfer the structures of various plant leaf surfaces and, therefore, to emulate their properties induced by topography onto technical materials such as polymers [13,29,42–48]. Certain studies have focused on reproducing the surface super-hydrophobicity (e.g. of the *Lotus* leaf) [47], while others have taken advantage of the microstructure to study novel light-harvesting systems [48], just to name a few examples. Compared to other replication techniques (atomic layer deposition, electroforming, sol–gel technique and physical vapour deposition), replica moulding is relatively advantageous not only owing to its simple and inexpensive procedure, but also because it allows direct employment of an original plant leaf as the master [49]. In general, the replica moulding is performed by pouring a liquid polymeric material onto a biological surface (master) to generate a negative replica which can then be separated from the master and be used to transfer the surface structure onto a second material (positive replica) [13,43,44,47,50–54]. The easiness and accuracy of the replication method depend on the choice of materials to be used as negative and positive replicas, respectively. It will also govern the ability of the replication technique to reproduce complex and fine structures. The mutual affinity of both materials may lead to the addition of an interfacial anti-stiction layer allowing for easy demoulding when producing the positive replica [55,56]. For instance, polydimethylsiloxane (PDMS) has been used to produce both negative and positive replicas; however, this approach involves an intermediate step of an anti-stiction treatment on the negative mould by organosilane monolayer deposition [47,51,56,57]. In the same line, some studies employed the PDMS negative replica to transfer the plants' leaf microstructures onto a hard polymer, polymethyl methacrylate (PMMA) [45,48]. Various other researchers used poly-vinylsiloxane (PVS; common imprinting material employed in dentistry) to replicate biological surface structures onto an Epoxy polymer [13,43,44,54]. Another replication approach consists in the development of the negative replica on nickel using sputtering and electroforming, and then the structures from the negative replica were further transferred to acrylonitrile–butadiene–styrene (ABS) copolymer and to a UV-curable photopolymer [50,58]. Recently, a new replication strategy suggested using an epoxy-based polymer to produce negative replicas directly from original plant leaves, before transferring the surface structure onto final positive replicas made of PDMS [53].

Much of the bio-replication research has assessed the accuracy and ability of the replication techniques by qualitatively comparing the original surface to the developed replica, using

scanning electron microscopy (SEM) or atomic force microscopy (AFM) [13,43,46,47,50,53,59]. Undoubtedly, these techniques are proven to capture high-resolution surface images, although limited to qualitative investigations and comparisons in most cases. Furthermore, SEM investigation of biological samples requires an appropriate sample preparation protocol (including chemical fixation/dehydration, critical point drier and conductive film sputter coating) which limits the further utilization of the specimen for the replication process [60–62]. As a consequence, topography comparison of the same spot on both original and replica surfaces is not feasible. With the recent advancement of high-resolution microscopy techniques over the last decade, three-dimensional laser confocal microscopy offers some beneficial advantages: three-dimensional measurement of the topography, non-contact non-destructive investigation and no pre-sample preparation requirement [63–65].

Given the need to generate an accurate way of replicating surfaces, and to assess the quality of a replicate, we employed a number of replication techniques and validation procedures on the leaves of three species of plants and one technical surface. In addition, we used a rock sample (dolerite) and a young leaf for a proof of concept. The latter is important given the sensitivity of young leaves to repeated imaging. Being able to replicate a young leaf will preserve the delicate structures to assess the functional links between them and the animals that move on them. A spot marking and tracing approach on original surfaces, using negative and positive replicas, was employed to accomplish the quantitative comparison of equivalent areas. The investigated surfaces offer distinct topographies in terms of size range, various shapes and hierarchical patterns, allowing a complete evaluation of the replication technique accuracy. Two model parameters (cross-covariance function ratio and relative topography difference) were successfully employed to evaluate the replication quality of three replication approaches applied on the surfaces investigated in this work.

2. Materials and methods

(a) Investigated surfaces

Three different plants' leaf surfaces were studied, corresponding to *Ludisia discolor* (adaxial: upper side), *Hevea brasiliensis* (adaxial: upper side) and *Litchi chinensis* (abaxial: lower side). These leaves were chosen according to their surface microstructure in order to screen the various shapes and sizes of textures: *L. discolor* represents the coarse topography (figure 2a) with circular cone-shaped microstructures between 50 and 80 μm height and diameter, *H. brasiliensis* leaves have fine wrinkle-shaped microstructures (figure 2d) in the range of 0.5–2 μm wrinkle height, width and distance, and *L. chinensis* leaves consist of complex hierarchical structures (figure 2g) with dimensions of 15–20 μm for the main patterns [13,53]. *L. chinensis* shows the most complex topography from the three selected plant leaf surfaces. All leaves were cultivated and freshly collected from the Botanic Garden of the University of Freiburg. Prior to each replication, leaves were gently cleaned with distilled water and carefully dried with pressurized air. In addition, we used a rock sample (dolerite) from Namibia and young leaves of *H. brasiliensis* for a proof of concept. The dolerite rock is a surface on which geckos move frequently, making it a relevant surface to replicate. Given the sensitivity of young leaves to repeated imaging, being able to replicate a young leaf and to preserve the delicate structures allows for assessment of the functional links between its surface and the animals that move on them. Finally, a standard technical surface was added to the samples set: a microstructured PMMA surface organized with regularly arranged circular dimples (width of 50 μm and depth of 5 μm , figure 2j) was selected.

(b) Replication techniques

The replication techniques used in this work are based on a two-step moulding approach. The full procedure has been summarized in the sketch presented in figure 3. For all four techniques, the first step was to develop a negative replica from different natural samples (plant leaves,

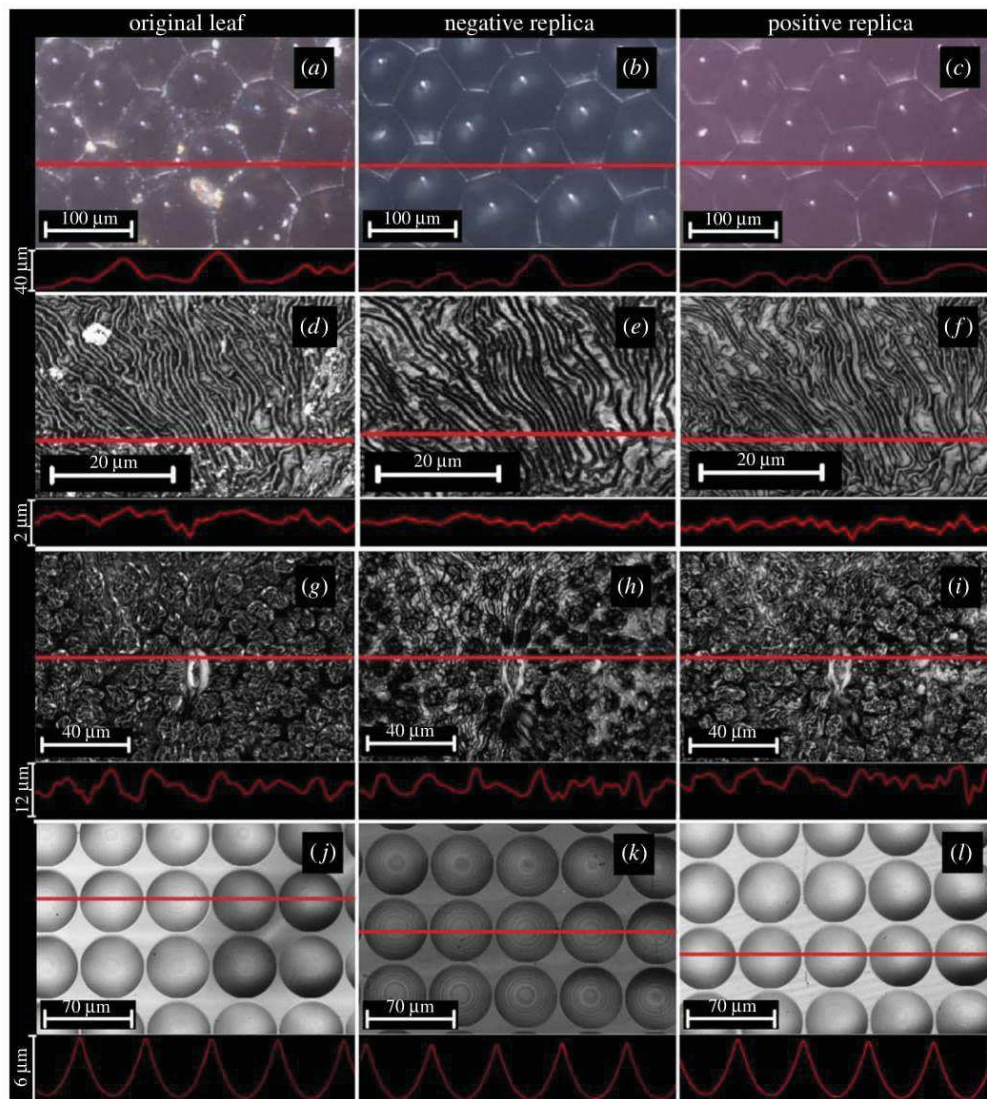


Figure 2. Confocal laser scanning microscopy (CLSM) images: surface topography of fresh plant leaves and standard structure surface (*a,d,g,j*), negative replicas (*b,e,h,k*) and positive replicas (*c,f,i,l*), for three different plant leaves replicated by Epoxy–PDMS replica moulding. (*a–c*) *L. discolor* (adaxial), (*d–f*) *H. brasiliensis* (adaxial), (*g–i*) *L. chinensis* (abaxial) and (*j–l*) standard template. The red line crossing each image represents the location of the line profile depicted under each image. The line profiles (vertical height profiles) are located such that they establish the same section on the fresh leaf, negative replica and positive replica. All images and line profiles for the negative replicas are mirrored to facilitate the qualitative visual comparison.

rock and technical standard sample). In the second step, the resulting negative replicas were used to transfer the surface structures onto the positive replicas. An additional step during the replication procedure was needed sometimes and consisted of achieving an intermediate anti-stiction treatment allowing for detachment of the positive replica from the negative mould. For the replication of young leaves of *H. brasiliensis*, the Epoxy–PDMS method has been used for reasons discussed later. While all the three replication techniques discussed above show good potential to understand leaf surfaces in general, for the rock sample, however, we find that a PDMS–Epoxy replication method prevents stiction issues on rock and consequently appears more

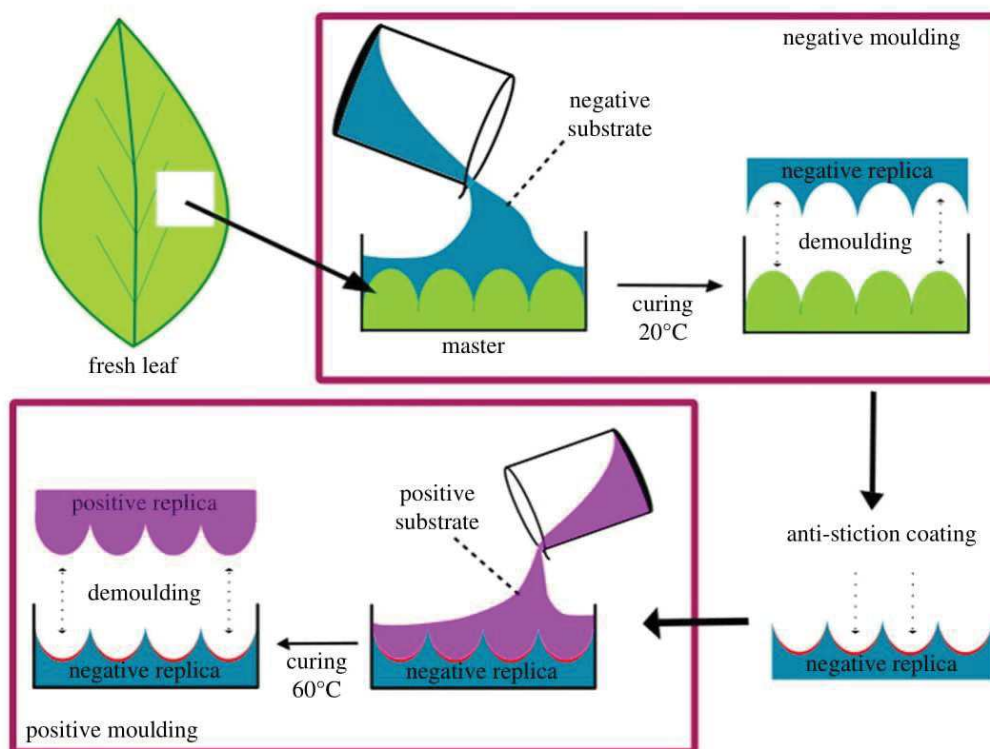


Figure 3. Schematic sketch of a replica-moulding technique using plant leaves as a master. A small piece was cut out from a fresh plant leaf and glued onto a plastic Petri dish, which was then filled up with a negative moulding material (PVS/PDMS/Epoxy). After curing of the moulding material, a negative replica was separated from the leaf sample. The negative replica was further chemically treated for anti-stiction surface coating (only in the case of PVS and PDMS). The negative replica was filled up with positive substrate material (PDMS) and the positive replica was peeled off from the mould after curing.

suitable and advantageous for further study. The different materials for negative and positive replicas used for the replication processes, are described in detail in the following sections.

(i) Materials for replication

The first material used for negative moulding was polyvinyl siloxane (PVS, President Light Body[®], Coltene Whaledent, Altstätten, Switzerland), which is normally employed in dentistry for imprinting and has also been used for replication of biological surface structures [13,43,54,66,67]. PVS has a fast polymerization time (around 10 min at room temperature), the mixing ratio of monomer and curing agent is fixed by the manufacturer as the dispenser mixes both components homogeneously when being used [43]. As the second alternative, an epoxy resin (Epoxydharz HT2, R&G Faserverbundwerkstoffe GmbH, Wandelbuch, Germany) was used to achieve the negative mould. The mixing ratio (by weight) of resin and hardener was 100:48 and the curing was performed at room temperature ($25 \pm 2^\circ\text{C}$) for 18 h. Once both materials are blended, the working time should not exceed 45 min as the viscosity increases rapidly. The third material used for negative moulding was PDMS (RTV 141 A & B-monomer and catalyst, Bluestar Silicones, Saint-Fons, France). The mixing ratio (by weight) of monomer to catalyst was 10:1 and the mixture was cured at room temperature for 24 h. To generate positive replicas, only PDMS was utilized in all the three processes. The PDMS elaboration procedure for the positive replicas was the same as the one used for negative replicas except for the curing which was done at $60 \pm 5^\circ\text{C}$ for 4 h.

(ii) Negative moulding

In order to obtain a negative replica, a small piece was cut out from a fresh plant leaf and glued onto a plastic Petri dish. The negative moulding material was slowly poured onto the leaf sample. When carrying out the process with epoxy and PDMS, a pre-degasification was done in a vacuum chamber for 20 min, to remove air bubbles trapped from the mixture. Since the plants leaf surface (master) are quite sensitive to high temperature, all the negative mouldings were conducted at room temperature. The demoulding process to obtain the negative replica was done directly after the curing was completed. The only exception was for the moulding with epoxy resin using *L. chinensis* leaves as master. Here, the complex microstructures of the leaf lead to entanglement with the negative replica (as the cured epoxy resin is highly rigid as compared with cured PDMS or PVS). In this case, the demoulding was fulfilled by treating the sample (negative replica entangled with leaf) in an aqueous solution (60 g/100 ml) of potassium hydroxide (KOH, greater than or equal to 85%, p.a., Carl Roth GmbH & Co. KG, Karlsruhe, Germany) at 60°C for 20 h. Thereafter, it was submerged in an ultrasonic bath of deionized water for 15 min to completely remove the master from the negative replica [53]. In the case of the rock sample, after the pre-degasification process, the PDMS-filled sample was kept in a heating oven for curing at 60°C for 4 h and then peeled off gently. Later on, all the negative replicas (for all three moulding materials: PVS, PDMS and epoxy resin) were used to replicate the leaf surface pattern to the PDMS surface (or Epoxy surface in the case of rock), as described in the following steps. While developing a negative replica on Epoxy from the standard structured surface, a gentle effort was needed to demould, given that both Epoxy negative replica and standard sample are made of stiff materials.

(iii) Anti-stiction coating

An intermediate step between negative and positive moulding consists in the application of an anti-stiction coating on the negative replica, which allows easy demoulding of the positive replica from the negative [55,56,68,69]. The kind of anti-stiction coating depends on the nature of the materials used for negative and positive replicas. In the case of PVS/PDMS, this coating was developed by forming a thin film coating of gold. A gold sputter coater device (108 auto, Cressington Sputter Coater, UK) was used for this purpose. Coating was performed at a current of 20 mA, a pressure of 20 Pa, and a distance of 45 mm between the sputter target and the sample. An exposure time of 60 s was maintained for the *L. discolor* and *H. brasiliensis* negative replicas, and 120 s for the *L. chinensis* negative replicas. In regard to PDMS/PDMS demoulding, an anti-stiction monolayer silanization process was applied using a home-built vapour deposition set-up as described in [56]. The silane monolayer deposition was carried out by placing the PDMS negative replicas along with a few (5–6) drops of Trichloro(1H,1H,2H,2H-perfluorooctyl)silane (FOTS, 97% Sigma-Aldrich Chemicals, USA) in a partial vacuum (40 kPa) for 5 h. In the case of Epoxy/PDMS demoulding, there was no need to apply any anti-stiction coating as the positive replica could be separated directly once it was cured.

(iv) Positive moulding

The final step to produce the positive replicas in all the three replication approaches for leaves and standard samples was done with the PDMS material. The PDMS mixture that was free from air bubbles was slowly poured onto the negative replicas (after sputtering anti-stiction coatings when needed). The samples filled with PDMS mixture were then placed in a vacuum desiccator for 1 h, to remove air bubbles formed at the interface of negative replica and PDMS mixture. The samples were kept in a heating oven for curing at 60°C for 4 h. Then the positive replicas were gently peeled off from the negative moulds. For the rock sample, the epoxy mixture after degasification for 20 min was gently poured onto the PDMS mould and was allowed to set overnight before peeling off.

(c) Surface visualization and characterization

(i) Confocal laser scanning microscopy

Surface morphology of all the fresh plant leaf surfaces, their negative replicas and final positive replicas was visualized and characterized with a confocal laser scanning microscope (LEXT OLS4000, Olympus Corporation, Japan). All measurements were performed in such a way that the same segment (spot) of the leaf surface was measured on the negative replica and the positive replica, to allow the systematic quantitative comparison of all three morphologies. For tracking the same spot from the original fresh leaf sample to negative replica and positive replica, a unique spot marking (with a tiny drop of PVS) was achieved. *L. discolor* samples were examined at a magnification of 20 \times , while the samples from *H. brasiliensis* (both young and adult), *L. chinensis* and rock were examined at 100 \times , 50 \times and 40 \times magnification, respectively. Confocal Laser Scanning Microscopy (CLSM) is one of the few methods which is not invasive to characterize biological samples at a consistent scale because it requires no sample preparation, the measurement causes no damage to the surface, and the leaf specimens can still be used afterwards [70].

3. Replication quality quantification models

(a) Parameters

Two model parameters, proposed by the National Institute of Standards and Technology (NIST), were used to quantitatively compare the line and surface profiles obtained from CLSM. The first parameter is called cross-covariance ratio ($ACCF_{MAX}$) and it is a maximized ratio between a cross-covariance function relating two profiles and their root mean squared roughnesses (Rq) [71], as described in equation (3.1):

$$ACCF_{MAX} = \frac{\sum_{i,j} [(Z_A(i,j) - \bar{Z}_A)(Z_B(i,j) - \bar{Z}_B)]}{\sqrt{\sum_{i,j} (Z_A(i,j) - \bar{Z}_A)^2} \sqrt{\sum_{i,j} (Z_B(i,j) - \bar{Z}_B)^2}}, \quad (3.1)$$

where Z is referred to as a particular height of a profile at the point ' i,j ' when analysing surface profiles or ' i ' in the case of line profiles. By convention, A is the original profile and B is the replicated one (negative replica or positive replica), and \bar{Z} is the average value for each profile. $ACCF_{MAX}$ varies from 0 to 1: it reaches 1 when two profiles are identical and 0 when they are completely unrelated [71]. The $ACCF_{MAX}$ is normally calculated in terms of a continuous integral, but the $ACCF_{MAX}$ in this investigation was used in the discrete form using summations because it is adapted to resulting CLSM data, as presented in equation (3.1) [72]. $ACCF_{MAX}$ has a disadvantage related to scale factors; therefore, the parameter must always be calculated when the two profiles are in phase to assure that the value is maximized. Nonetheless, it is not sensitive to the differences, if one of the profiles is, for example, twice as high as the other one. Scale factors can be propagated to profiles owing to calibration problems with the equipment used for characterization [72]. As a consequence, the NIST proposed a second parameter sensitive to vertical scale differences, called relative topography difference (D_S). D_S is defined as the root mean square roughness of a virtual profile given by $A-B$ over the mean squared roughness of a profile A (original profile), as shown in equation (3.2).

$$D_S = \frac{\sum_{i,j} [(Z_A(i,j) - \bar{Z}_A) - (Z_B(i,j) - \bar{Z}_B)]^2}{\sum_{i,j} (Z_A(i,j) - \bar{Z}_A)^2}, \quad (3.2)$$

D_S also varies from 0 to 1, but it tends to 0 when two profiles are identical and to 1 when they are unrelated. Both $ACCF_{MAX}$ and D_S are complements to each other as the first one quantifies the similarities in the shape of two profiles, while the second one takes into account the height differences.

(b) Line profiles and surface

The LEXT microscope software (OLS400, version 2.2.3) directly allows extraction of raw data of selected line profiles. Before extracting the information, all profiles were adjusted to remove the waviness by applying a cut-off of 400 μm for *L. discolor* profiles, 50 μm for *L. chinensis*, 25 μm for adult *H. brasiliensis*, and 80 μm for young *H. brasiliensis* leaves and rock. These cut-off values were chosen manually with the help of the microscope software, which can plot primary roughness and waviness profiles when changing the input cut-off value. With the purpose of calculating average values of line profiles for ACCF_{MAX} and D_S , a total of five to six profiles distributed in two different samples of each plant leaf were analysed and then averaged. The second set of profiles associated with surface analysis was obtained from the fresh leaves and the replicas in which surface profiles (height data in two axes) were extracted. In this case, a fixed area was selected over the images and matrices of raw data were taken for analysis; the extraction also took into consideration the same cut-off values previously mentioned for analysis of line profiles. For the computation of surface profiles only one sample per leaf and replicas was selected owing to the high density of data (one single matrix could contain up to one million data points).

4. Results

Figure 2 shows a qualitative comparison of the different CLSM images (fresh leaves, negative replicas and positive replicas) obtained for the three biological morphologies investigated when replicated by the Epoxy–PDMS replication approach. Figure 4 displays some examples when the replication is done by PDMS–PDMS and PVS–PDMS moulding.

L. discolor, having the simplest, largest and most regular microstructure out of the three plant leaves investigated, seems to show the best results in terms of accuracy of profiles and topography similarities between original leaf, negative and positive replicas (figure 2*a–c*). The difference in the profiles displayed for *L. discolor* is rather subtle but perceptible. In *H. brasiliensis*, the development of profiles shows a decrease in the height of the profile and some imperfections that can also be detected by contrasting the three images (figure 2*d–f*), especially when fresh leaf and positive replica are compared. The surface of *L. chinensis* replicas, with the most complex morphology is notably more affected, as larger areas show visible defects and the line profile undergoes large changes in shape and height, as can be compared in (figure 2*g–i*). The regularly distributed coarse-size surface structures from the standard technical surface were replicated very precisely (figure 2*j–l*).

On the other hand, by comparing the respective images shown in figures 2 and 4, it can be noted in the case of *H. brasiliensis* that the PDMS–PDMS replication approach (figure 4*a,b*) brings more topographic inaccuracies in the positive replica compared to the Epoxy–PDMS procedure. In the case of PVS–PDMS replica moulding, the topography of *L. chinensis* is strongly damaged causing the positive replica to lose most of the fine overhanging features (hierarchical patterns), as can be seen in figure 4*d*. Nevertheless, a qualitative description is not sufficient to assess the accuracy of the three different methods under evaluation.

The results of the quantitative evaluation using the two parameters ACCF_{MAX} and D_S for line profiles are plotted in figure 5 comparing negative and positive replicas against fresh leaves. For reading convenience, the relative topography difference is presented as $(1-D_S)$, so that the values corresponding to better replication would tend towards 100% instead of 0%. In the same way, the results regarding the quantitative assessment of surface profiles with ACCF_{MAX} and D_S are plotted in figure 6. By contrasting both types of measurement, the surface profile results have greater statistical significance than the line profiles, because one surface measurement contains around 900 line profiles. Surface profiles are also significantly more sensitive when considering larger topographic defects, whereas line profiles only evaluate similarities between two fixed points. Still, one can note that results from both figures 5 and 6 are consistent and show the same ranking quality between the different samples.

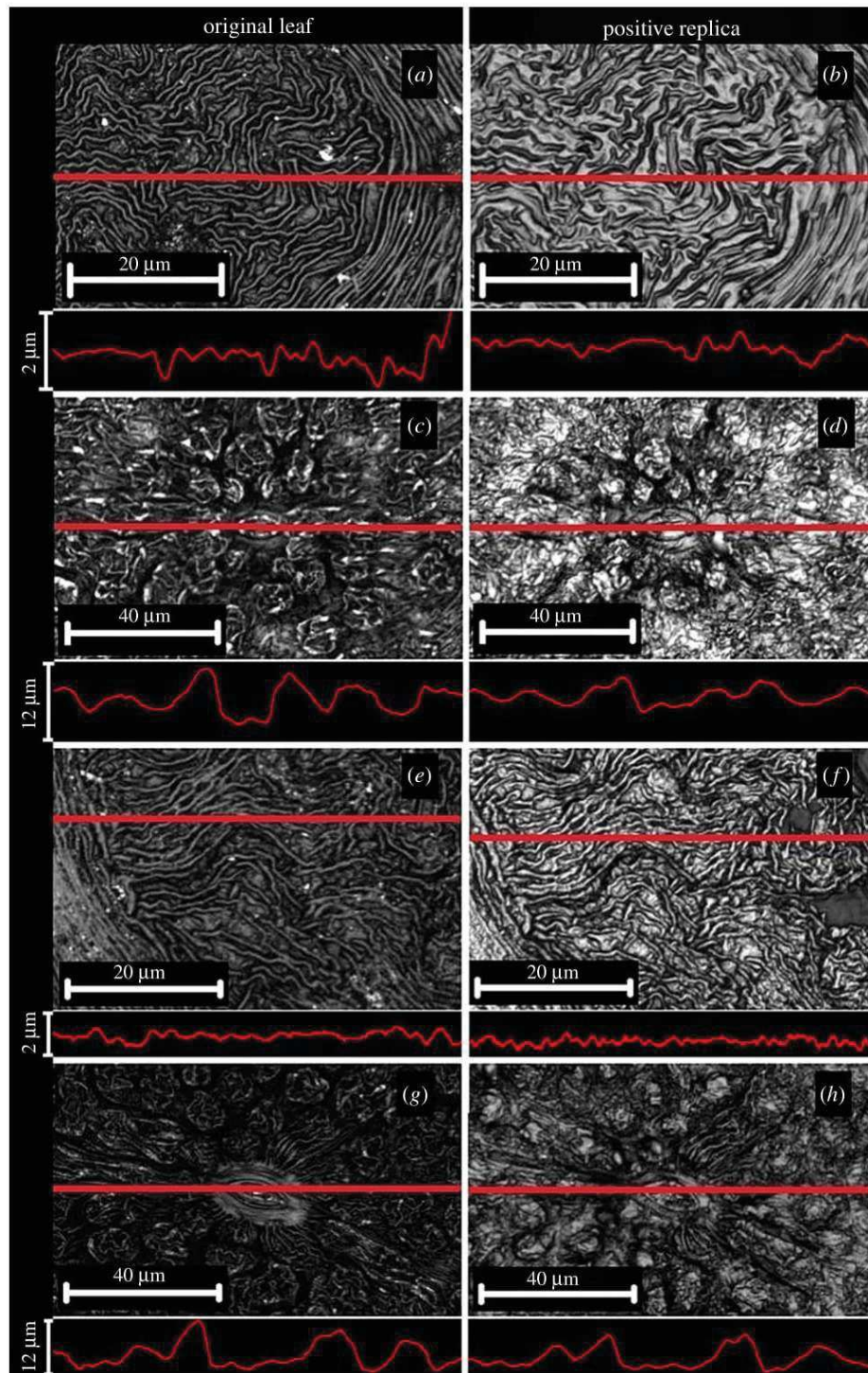


Figure 4. CLSM images showing the topography of the original leaf surfaces and their positive replicas. (a,b) *H. brasiliensis* replicated by PDMS–PDMS moulding. (c,d) *L. chinensis* replicated by PDMS–PDMS. (e,f) *H. brasiliensis* replicated by PVS–PDMS. (g,h) *L. chinensis* replicated by PVS–PDMS. Line profiles were inserted as described in figure 2. (Online version in colour.)

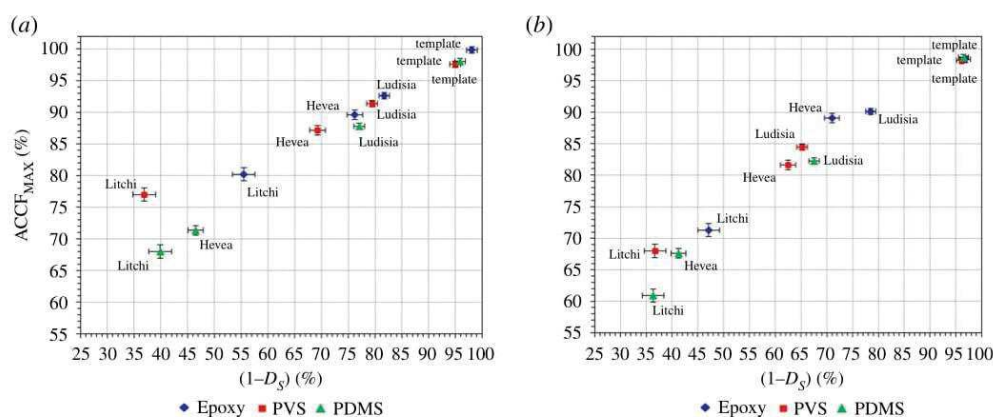


Figure 5. Quantitative evaluation of the surface structures using line profiles. (a) Comparison of negative replicas versus fresh leaves and standard template versus its negative replica by plotting $ACCF_{MAX}$ versus $(1-D_S)$. (b) $ACCF_{MAX}$ versus $(1-D_S)$ comparing positive replicas against fresh leaves and standard template and its positive replica. Epoxy, PVS and PDMS on the label refer to the negative moulding material used before positive moulding with PDMS. The error bar calculations were based on the accuracy to obtain the same line profile during repetitive measurements. For better graphical visualization, only the genus name is mentioned instead of the full species name: Ludisia for *Ludisia discolor*, Hevea for *Hevea brasiliensis* and Litchi for *Litchi chinensis*.

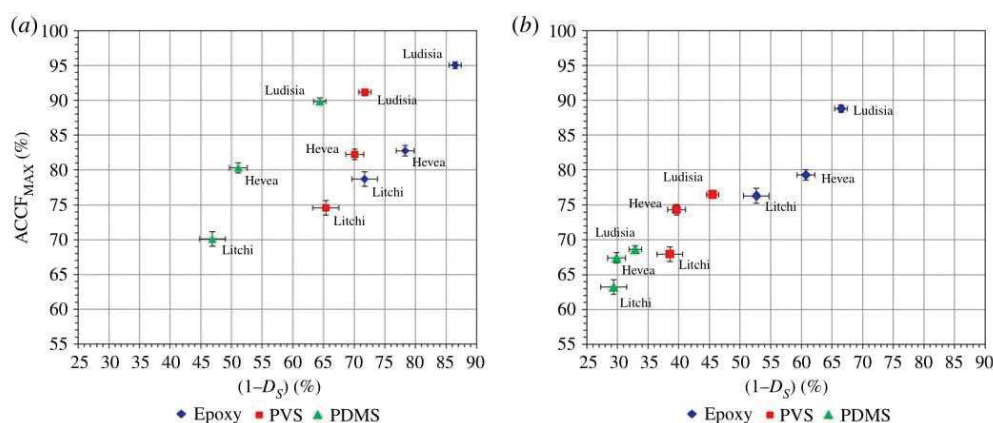


Figure 6. Quantitative evaluation of the surface structures using surface profiles. (a) Comparison of negative replicas versus fresh leaves by plotting $ACCF_{MAX}$ versus $(1-D_S)$. (b) $ACCF_{MAX}$ versus $(1-D_S)$ comparing positive replicas and fresh leaves. The error bars were calculated as in figure 5. For better graphical visualization, only the genus name is mentioned instead of the full species name: Ludisia for *Ludisia discolor*, Hevea for *Hevea brasiliensis* and Litchi for *Litchi chinensis*.

By analysing the results shown in figures 5 and 6, it can be concluded that Epoxy–PDMS replica moulding is the most precise method to replicate the morphology of the three biological samples used in this investigation. *L. discolor* shows the microstructure with the highest topographic replicability ($ACCF_{MAX} = 88.8\%$ and $1-D_S = 66.5\%$ in figure 6b). *H. brasiliensis* and *L. chinensis* have lower values for $ACCF_{MAX}$ and $1-D_S$, because the replicability is reduced to $ACCF_{MAX} = 79.3\%$, $1-D_S = 60.7\%$ (for *H. brasiliensis*) and $ACCF_{MAX} = 76.3\%$, $1-D_S = 52.6\%$ (for *L. chinensis*), respectively (figure 6b). PVS–PDMS replication is not as good as Epoxy–PDMS but it is considerably better than PDMS–PDMS. However, all three techniques were able to precisely replicate the surface structures from the standard template, resulting in high quantitative values of both parameters. For example, $ACCF_{MAX} = 98.4\%$ and $1-D_S = 96.5\%$ were calculated for the

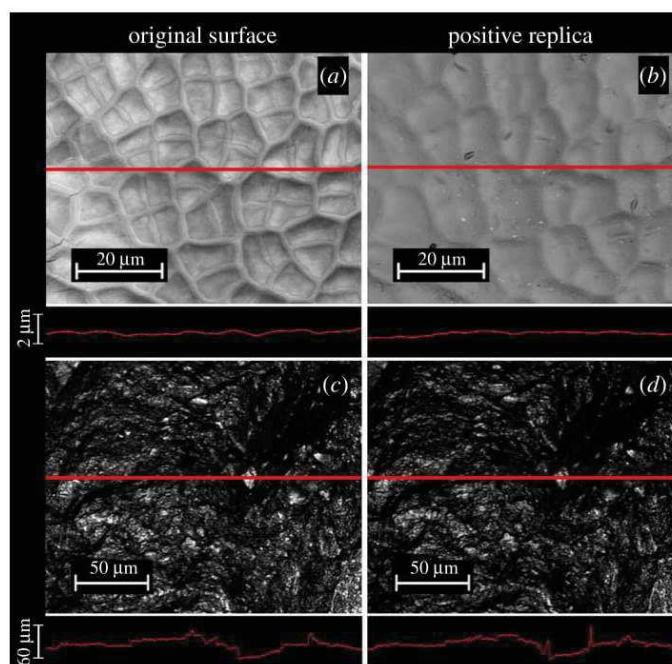


Figure 7. CLSM images. Comparison of the topography of the original and positive replicas of (a,b) young leaves of *H. brasiliensis* replicated by Epoxy–PDMS moulding and (c,d) dolerite rock replicated by PDMS–Epoxy moulding. Line profiles were inserted as described in figure 2.

Epoxy–PDMS replication approach as shown in figure 5b and a similar value range was found for the other two approaches (PVS–PDMS and PDMS–PDMS).

By taking into consideration the replica moulding process, in the negative moulding step we believe that the curing time and how fast viscosity increases are the most important factors in the accuracy of the replication. Whereas PVS cures extremely fast, it might not be as precise as epoxy resin owing to diffusion limitation to completely fill the cavities on the topography of the leaf surface (epoxy resin is about 10% more precise reproducing *L. chinensis* microstructures in terms of D_S results as compared to PVS). To increase the performance of PVS, Koch *et al.* [43] discussed the inclusion of cooling to increase its curing time, as well as the alternative of using a vacuum to remove air bubbles trapped in the microstructures. However, the use of lower pressures might accelerate the loss of humidity from the plant leaf and by this deteriorate the replication results.

An additional important fact is that while epoxy resin and PDMS have the same curing time, the increase in viscosity is extensively faster in epoxy resin, which reduces the working time to about 45 min, whereas in PDMS the increase in viscosity is much slower. This is relevant when working with biological samples, considering that the loss in humidity can highly affect the shape of the topographies of the leaf surface used as a master, thereby longer times of curing will lead to greater deformation of the leaves. If the negative moulding material does not harden quickly enough, the changes in the topography of the leaf master could eventually be transferred to the negative replica. This could explain why PDMS used for negative moulding shows the lowest values for $ACCF_{MAX}$ and $1-D_S$ in all three plant leaf surfaces. This issue may be confronted by including the monomer to curing agent ratio as a variable for PDMS during negative moulding to decrease the curing time of PDMS at room temperature. With regard to the PDMS positive moulding process, as all positive replicas underwent the same conditions, the reduction in accuracy can only be attributed to the complexity of the topography in each plant leaf species.

Figure 7 shows topographical differences between originals and replicas of a young *H. brasiliensis* leaf and dolerite rock sample. As discussed earlier, the Epoxy–PDMS replication process showed better replication quality for leaf surfaces and was used to replicate young leaves of *H. brasiliensis*. The young leaves show replication quality with values $ACCF_{MAX} = 84.2\%$ and $1 - D_S = 57.4\%$. These leaves as opposed to the adult ones have smooth cellular surfaces without any wrinkled microstructures. However, the relatively lower values of $1 - D_S$ could be attributed to the difficulty in replicating the delicate surfaces of young leaves. Nevertheless, replication of such leaves would help in surface microstructure analysis during leaf ontogeny, as the thin and translucent cuticles of young leaves makes this difficult otherwise. On the other hand, the PDMS–Epoxy replication of rock resulted in high values of $ACCF_{MAX} = 93.7\%$ and $1 - D_S = 84.6\%$, similar to the results for the standard technical samples, suggesting the effectiveness of replicating stiff and hard samples.

5. Discussion

Our study identified reliable methods for replicating the surface topologies of living (plant) and non-living (rock) surfaces and presents a method for assessing the quality of a replica. According to the results obtained in the present study, the surface topology of *L. discolor* leaves exhibits the highest replicability owing to its quasi-regularity and relatively large microstructures. The complex surface morphology of *L. chinensis* leaves makes the replication more complicated and, therefore, the negative and positive replicas exhibited a large number of defects that were correctly pointed out by the quantitative analysis. By contrast, *H. brasiliensis* surface morphology could be reproduced with higher precision than *L. chinensis*. However, a few small detail failures and imperfections were observed over the studied profiles. It is possible that the microscope measurements on *L. chinensis* surfaces suffer from some optical artifacts arising from the technique limitations, in particular when attempting to access the undercuts and overhanging structures.

Using the LEXT microscope software, we calculated the surface roughness with standard parameters such as arithmetic mean height (R_c), arithmetic mean deviation (R_a) and root mean squared deviation (R_q). However, the results obtained with these parameters (not reported in this paper) did not exhibit any clear tendency when negative and positive replicas were compared with fresh leaf profiles. Moreover, $ACCF_{MAX}$ and D_S already take into consideration the effect of surface roughness by including R_q in the calculation [71]. The use of $ACCF_{MAX}$ and D_S quantification parameters revealed that the replication process is more sensitive to loss of height and depth whereas there is a good reproducibility of profile shape (particularly for *L. discolor* and *H. brasiliensis*).

Concerning the effectiveness of $ACCF_{MAX}$ and D_S as quantification parameters, our data demonstrated that $ACCF_{MAX}$ shows the same tendencies as D_S , but the latter is more sensitive to height/depth differences (as seen in figures 5 and 6). This might indicate that the compared replication techniques are better at reproducing the shape of the structures and less effective at keeping the same height of structures over the surface. This inference is particularly notable in *H. brasiliensis* (see the line profiles in figure 2*d–f*). What is also interesting from this approach is that the $ACCF_{MAX}$ and D_S profile comparison results obtained with fresh leaves against negative moulds and fresh leaves against positive moulds consistently show deteriorated results for positive moulds (i.e. for the second moulding step), thus validating the consistency of the quantitative analysis as well as the utility of both model parameters.

With regard to quantification of the accuracy of surface replicas, $ACCF_{MAX}$ and D_S are advantageous parameters for characterizing and comparing the surface morphologies. For our study, both values were appropriate to use (with a relatively small margin of error), given the fact that standard parameters (e.g. surface roughness) are not descriptive enough when comparing two different surface morphologies, especially when the replication is done with biological samples.

Now that we can quantify the accuracy of surface replicas, we must determine what level of accuracy is necessary to answer different scientific questions related to biological surfaces and

for using the replicates for bioinspired applications. The answer is not straightforward and is completely dependent on the desired outcome of a study or application. For example, it is difficult to know what a value of 90% for $ACCF_{MAX}$ and D_S means for an animal. If adhesive performance is measured on the original and the replicate in this scenario, the outcome will dictate the level of accuracy needed. If the same adhesive performance is achieved, then one would conclude that 90% is perfectly reasonable. However, future work must quantitatively test the importance of accuracy in real-world situations. This study attempted to cover surfaces with a broad range in terms of size, shape and complexity of their surface topography; however, surfaces with extreme structures, such as long hairy trichome structures or fragile wax crystal structures, still need further investigation.

(a) Using surface replicas to study evolution, ecology and biomechanics of plant–animal interactions and for improving haptic properties of bioinspired technical surfaces

We have presented a reliable way of replicating natural surfaces and for assessing the quality of the replicas quantitatively. Keeping in mind that these surfaces are instrumental in shaping the evolution of the animals that move on them, the question that arises is how to implement the replication procedures to explore evolutionary, ecological and biomechanical phenomena. We outline potential avenues of research below.

When we think of animals adhering to surfaces, geckos are likely to spring to mind. The adhesive apparatus of geckos has been intensely investigated over the past two decades, and has been characterized as being ‘overbuilt’. However, this idea was challenged when the microtopography of the natural surfaces on which geckos move was examined in concert with the adhesive morphology [15,73]. These studies examined the morphology of geckos from the genus *Rhoptropus* in Namibia and compared this to the topography of different types of rocks from their natural habitat. When considering the available contact area between the setal fields of the gecko toe and the surface roughness, it is clear that geckos can encounter situations in which contact is dramatically reduced, which in turns bring the safety factor down considerably. A separate study found that different populations of this species exhibit differences in their adhesive microstructure in relation to habitat structure [74], highlighting how these interactions can influence the evolution of animal morphology. This also highlights the importance of considering ecology when measuring adhesive performance, and signals that replicating surfaces across different habitat types will help investigators determine which factors cause a shift in adhesive performance. Although geckos are highlighted here as an example, this idea applies to any animal that uses an adhesive system to attach to surfaces, as is the case for many invertebrates.

(i) Some like it smooth, some like it rough

The type of surface that is ideal for an animal depends on the type of attachment employed. In both benthic aquatic habitats and terrestrial environments, some species will attach more effectively on smooth surfaces whereas others will benefit from rougher surfaces. For example, intertidal marine organisms that rely on attachment mechanisms for holding station under high-force wave action will be impacted by the microtopography of the substrate. Among fishes, this is clearly important for clingfish [10] and sculpin [75]. These two groups also reflect the differences observed among terrestrial animals. Clingfish will do better on smooth surfaces, much like geckos [12]. Sculpin rely on their hooked pectoral fins to interdigitate with the rough rocky substrate [75], much like lizards that rely on claws for attachment [76]. Thus, surface roughness matters, and qualitative lumping of surfaces into smooth and rough categories is not sufficient as has been also proven recently for the attachment of leeches [77].

Several studies have examined the impact of surface topography and microstructuring on the ability of animals to cling. This includes, for example, studies of beetles [13,78], aquatic insect larvae [79], other insects [80], geckos and other lizards [7,12], and fishes [11]. All of these studies find that smoother surfaces are generally better for the animal if adhesion is being used. For those

animals that use claws, rougher substrates are beneficial. For example, claw removal in dock beetles (*Gastrophysa viridula*) resulted in a reduction in attachment force on rough surfaces [78]. Given that many terrestrial vertebrates and invertebrates have both claws and adhesive systems, they might exhibit a shift in reliance on a given system as the substrate type changes.

Using replications with defined surface roughness, a recent study examined the ability of mayfly larvae to attach to surfaces using their tarsal claws [79]. They identified a minimum roughness value that is needed before the claws can grip the substrate. Thus, some animals that use adhesion require a certain degree of smoothness, whereas other animals may require a certain degree of roughness in order to grip rough surfaces with their claws. This highlights the divergent attachment mechanisms that have evolved, and the potential for coevolution between animals and the biotic surfaces on which they attach.

(ii) Surface topography and locomotor biomechanics

Although much of the focus of attachment studies is on the ability to grip or adhere, it is clear that many animals are moving around on surfaces in their natural habitat. Therefore, locomotor experiments are necessary for determining the impact of surface topography on organismal performance. Replicated surfaces can provide flat and possibly enlarged areas that facilitate accurate assessments of locomotor ability. Without replication, many studies simply use manufactured surfaces to mimic natural surfaces in order to provide flat running trackways. For example, sandpaper, cork and mesh wire are often used for running experiments in lizards [81–83]. Sandpaper is thought to mimic rocky surfaces, but the effective similarity depends on the microtopography and the specific type of rock and grit of sandpaper. We propose that future studies should standardize the running trackways by either replicating the surfaces of interest or at least quantifying the topography and roughness of the surfaces used.

(iii) Improving haptic properties of bioinspired technical surfaces

Over the last two decades, plant surfaces have been used widely as inspiration for the development of novel biomorphic, bioinspired and biomimetic demonstrators and products by applying different process sequences of biomimetic research [84,85]. Examples include so-called 'Lotus-Effect-Surfaces' and 'Salvinia-Effect-Surfaces' [2,21,28] and biomimetic surfaces with optical properties inspired by plant surfaces [30], which have been briefly exemplified in §1. Haptics is a field of application in which inspiration from plant surfaces is of increasing interest. Potential fields of applications are wide-ranging, examples of which include the interiors of automobiles and aeroplanes, medical devices, touch-pads of computers and entertainment electronics, and interfaces of soft-robotics and controls of kitchen appliances. The need for novel and adaptive haptic surfaces becomes even more evident in an ageing community if one keeps in mind that tactile spatial acuity drastically decreases with age, as does visual capacity. Spatial resolving capacity of cutaneous receptors, measured by the two-point touch threshold (i.e. spatial separation between two stimuli to the skin that can be detected), not only varies significantly across the body surface (approx. 1 mm–several cm) but also changes with age. From the age of 12 to 85 it declines by about 1% per year [35]. This seems to be a potential target for age-adapted biomimetic products with self-explanatory haptic properties.

(iv) Industrial applications

In industry, thermoplastics have widely been used to produce finished parts for a number of things (e.g. automotive interiors) for decades. This stems from the ability to produce complex parts using cost-effective injection moulding processes, the low density (compared to metal, for example), low costs of thermoplastics and their recyclability. The most important thermoplastic is polypropylene (PP, for example, homopolymers and copolymers), which has customizable properties like stiffness and impact performance. These properties are modified by blending different kinds of PP as well as adding reinforcing mineral fillers like talc, colouring pigments

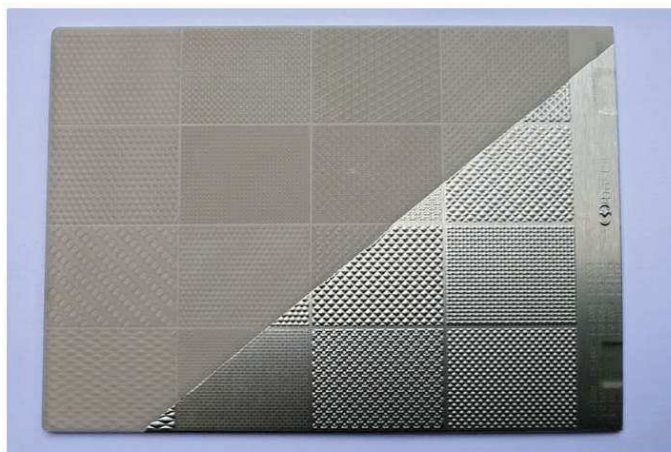


Figure 8. Injection-moulded polypropylene compound (20% talc reinforced Hostacom grade) demonstrator (size: 20.3 cm \times 14.5 cm) produced by LyondellBasell with a prototype tool grained by Eschmann Textures. The grey area is the polypropylene compound while the metallic area is aluminium (0.2 mm foil using in-mould graining technology bonded by LyondellBasell's Plastic Interface Technology). It shows typical grain structures that can be produced using injection-moulding techniques.

and stabilizing additives in a compounding process. The final PP compound, in this way, can be tailored for a specific task. In order to get to a finished part that is both functional and has an optically attractive surface with good haptics, a steel surface from an injection moulding tool is structured with the negative image of a certain grain to produce, for example, an instrument panel. By melting and injecting the PP compound into the mould, the finished part with the positive grain is produced. Interestingly, 'natural' based leather grains have been common for 'technical' interior trim parts for many years, mimicking the surface optics and haptics of the natural leather product. In recent years, a trend to use technical and geometrical grains for additional applications has been observed. Regardless of the type of grain, currently only a few examples of functional grains are known. The most popular example for functionality is the low wettability of 'Lotus-Effect-Surfaces'. As many kinds of features suitable for a biomimetic transfer are known in nature, it seems to be desirable to use these more efficiently for industrially produced finished parts in the future.

In order to structure the steel surface of a tool for the production of finished parts, etching and, more recently, laser graining techniques are applied as industrial processes. There is an imaging quality limitation of these techniques caused by the layer-wise shaping process of a grain leading to a stair-like tool surface structure. This limits the resolution to dimensions between 1 mm and 100 μm , this typically being much coarser than many (functional) structures found on leaf surfaces (figure 8). A novel technique called Cerashibo, developed by the company Eschmann Textures together with its Japanese partner some years ago, overcomes the limitations of the techniques described above and enables an exact image of nearly every kind of grain without such stair-like effects. As Cerashibo is allowing grains into injection-moulding tools in an industrially effective manner, this technique is opening up new possibilities, including the imaging and transfer of bioinspired surfaces in the low μm -range into injection-moulding tools.

LyondellBasell, Eschmann Textures and the University of Freiburg have started to work together to explore the potential of transferring surface structures from plant to bioinspired injection-moulded thermoplastic plaques. With this method, we will not only be able to develop new biomimetic products, but also to create as reference surfaces for basic research, for example, large surfaces with identical topography but different mechanical properties that can be used in locomotor experiments.

In order to evaluate the surface quality of the injected test specimen, it is essential to use and potentially further develop complementary techniques for a comprehensive surface characterization as presented in this paper. This will be the basis of ensuring the effective transfer and subsequent well-performing bioinspired functionality on finished parts at a high and well-defined level of quality.

6. Conclusion

In terms of the accuracy of the three different replication techniques presented in this work, Epoxy–PDMS appeared to be the most precise technique to replicate the three biological surfaces with the highest cross-covariance ratio and lowest relative topography difference. As for PVS–PDMS, the process was slightly less accurate, attributed to the fast curing time of PVS, which might have caused loss of replicability of the finest and more complex structures. Lastly, PDMS–PDMS replica moulding was the least accurate method studied. The result was ascribed to the long curing time and slow increase in viscosity (compared with epoxy resin) during the negative moulding process supposedly resulting in a change of topography by drying of the fresh leaf. By quantifying the surface structure of biological and other natural templates (e.g. plant leaves and rock surfaces) and of their replicas, it becomes possible not only to test plant–animal interactions on highly defined surface structures, but also to change parameters other than surface roughness by keeping the latter constant. This will allow one to quantify the impact of various surface parameters like surface chemistry, humidity and surface flooding much more accurately as to their impact on moving animals. For biomimetic applications, it will help to transfer exactly these parameters to the bioinspired technical products that are necessary for a given desirable property and/or function. Additionally, it will become possible to quantify which kind of accuracy of a surface (micro-)topography is needed to achieve a given property which will be of special importance for haptics where subjective ‘feelings’ may play a major role on the side of the human user. The precise level of accuracy needed for a specific application will largely depend on the type of application. Future work is necessary for defining these thresholds. One may also consider exploring some advanced materials that address the issue concerning the robustness of replicas for the direct industrial applications. Regardless, surface replication is a promising method for exploring biological diversity and for creating novel applications.

Data accessibility. The supplementary material and data can be viewed at: doi:10.6094/UNIFR/16790.

Authors' contributions. V.L.H., T.S. and C.K. designed the study and supervised it together with G.B. and M.T. Data collection, data assessment and statistical analyses were carried out by A.P., C.K. and V.A.S. Data evaluation and discussion of the results was a joint effort by all authors (C.K., A.P., V.A.S., G.B., M.T., E.L., T.E.H., T.S. and V.L.H.), who also contributed equally to the first draft of the manuscript and improved further versions. All authors gave final approval for publication.

Competing interests. We declare no competing interests exist.

Funding. We acknowledge funding from the European Union's Horizon 2020 research and innovation programme under the Marie Skłodowska-Curie grant agreement No. 722842 (ITN Plant-inspired Materials and Surfaces—PlaMatSu) to V.A.S., M.T., G.B. and T.S. We are also grateful to the German Research Foundation (Deutsche Forschungsgemeinschaft: DFG), for funding support under the framework of International Research Training Group (IRTG) 'Soft Matter Science—1642' to C.K., A.P., T.S. and V.L.H. T.H. gratefully acknowledges funding by the Humboldt Foundation for a one-year research stay in the laboratory of T.S.

Acknowledgements. We would like to thank the gardeners of the Botanic Garden Freiburg for cultivating the plants used in this investigation.

References

1. Bargel H, Koch K, Cerman Z, Neinhuis C. 2006 Structure-function relationships of the plant cuticle and cuticular waxes—a smart material? *Funct. Plant Biol.* **33**, 893–910. (doi:10.1071/FP06139)
2. Barthlott W, Mail M, Bhushan B, Koch K. 2017 Plant surfaces: structures and functions for biomimetic innovations. *Nano-Micro Lett.* **9**, 23. (doi:10.1007/s40820-016-0125-1)

3. Koch K, Bhushan B, Barthlott W. 2009 Multifunctional surface structures of plants: an inspiration for biomimetics. *Prog. Mater. Sci.* **54**, 137–178. (doi:10.1016/j.pmatsci.2008.07.003)
4. Bargel H, Barthlott W, Koch K, Schreiber L, Neinhuis C. 2004 Plant cuticles: multifunctional interfaces between plant and environment. In *The evolution of plant physiology* (eds AR Hemsley, I Poole), pp. 171–194. London, UK: Academic Press.
5. Whitney HM, Kolle M, Andrew P, Chittka L, Steiner U, Glover BJ. 2009 Floral iridescence, produced by diffractive optics, acts as a cue for animal pollinators. *Science* **323**, 130–133. (doi:10.1126/science.1166256)
6. Moyroud E *et al.* 2017 Disorder in convergent floral nanostructures enhances signalling to bees. *Nature* **550**, 469–474. (doi:10.1038/nature24285)
7. Tulli M, Abdala V, Cruz F. 2011 Relationships among morphology, clinging performance and habitat use in *Liolaemini* lizards. *J. Evol. Biol.* **24**, 843–855. (doi:10.1111/j.1420-9101.2010.02218.x)
8. Gorb SN *et al.* 2002 Structural design and biomechanics of friction-based releasable attachment devices in insects. *Integr. Comp. Biol.* **42**, 1127–1139. (doi:10.1093/icb/42.6.1127)
9. Ruibal R, Ernst V. 1965 The structure of the digital setae of lizards. *J. Morphol.* **117**, 271–293. (doi:10.1002/jmor.1051170302)
10. Ditsche P, Hicks M, Truong L, Linkem C, Summers A. 2017 From smooth to rough, from water to air: the intertidal habitat of Northern clingfish (*Gobiesox maeandricus*). *Sci. Nat.* **104**, 33. (doi:10.1007/s00114-017-1454-8)
11. Wainwright DK, Kleinteich T, Kleinteich A, Gorb SN, Summers AP. 2013 Stick tight: suction adhesion on irregular surfaces in the northern clingfish. *Biol. Lett.* **9**, 20130234. (doi:10.1098/rsbl.2013.0234)
12. Huber G, Gorb SN, Hosoda N, Spolenak R, Arzt E. 2007 Influence of surface roughness on gecko adhesion. *Acta Biomater.* **3**, 607–610. (doi:10.1016/j.actbio.2007.01.007)
13. Prüm B, Bohn HF, Seidel R, Rubach S, Speck T. 2013 Plant surfaces with cuticular folds and their replicas: influence of microstructuring and surface chemistry on the attachment of a leaf beetle. *Acta Biomater.* **9**, 6360–6368. (doi:10.1016/j.actbio.2013.01.030)
14. Prüm B, Seidel R, Bohn HF, Speck T. 2012 Plant surfaces with cuticular folds are slippery for beetles. *J. R. Soc. Interface* **9**, 127–135. (doi:10.1098/rsif.2011.0202)
15. Russell AP, Johnson MK. 2014 Between a rock and a soft place: microtopography of the locomotor substrate and the morphology of the setal fields of Namibian day geckos (Gekkota: Gekkonidae: *Rhoptropus*). *Acta Zool.* **95**, 299–318. (doi:10.1111/azo.12028)
16. Taylor TN. 1968 Application of the scanning electron microscope in paleobotany. *Trans. Am. Microsc. Soc.* **87**, 510–515. (doi:10.2307/3224225)
17. Bhushan B, Jung YC. 2011 Natural and biomimetic artificial surfaces for superhydrophobicity, self-cleaning, low adhesion, and drag reduction. *Prog. Mater. Sci.* **56**, 1–108. (doi:10.1016/j.pmatsci.2010.04.003)
18. Koch K, Barthlott W. 2009 Superhydrophobic and superhydrophilic plant surfaces: an inspiration for biomimetic materials. *Phil. Trans. R. Soc. A* **367**, 1487–1509. (doi:10.1098/rsta.2009.0022)
19. Koch K, Bhushan B, Barthlott W. 2008 Diversity of structure, morphology and wetting of plant surfaces. *Soft Matter* **4**, 1943–1963. (doi:10.1039/B804854A)
20. Koch K, Bohn HF, Barthlott W. 2009 Hierarchically sculptured plant surfaces and superhydrophobicity. *Langmuir* **25**, 14116–14120. (doi:10.1021/la9017322)
21. Barthlott W, Mail M, Bhushan B, Koch K. 2017 Plant surfaces: structures and functions for biomimetic applications. In *Springer handbook of nanotechnology* (ed B Bhushan), pp. 1265–1305. Berlin, Germany: Springer.
22. Vignolini S, Bruns N. 2018 Bioinspiration across all length scales of materials. *Adv. Mater.* **30**, 1801687. (doi:10.1002/adma.201801687)
23. Barthlott W, Neinhuis C. 1997 Purity of the sacred lotus, or escape from contamination in biological surfaces. *Planta* **202**, 1–8. (doi:10.1007/s004250050096)
24. Barthlott W, Mail M, Neinhuis C. 2016 Superhydrophobic hierarchically structured surfaces in biology: evolution, structural principles and biomimetic applications. *Phil. Trans. R. Soc. A* **374**, 20160191. (doi:10.1098/rsta.2016.0191)
25. Cerman Z, Striffler BF, Barthlott W. 2009 Dry in the water: the superhydrophobic water fern *Salvinia* – a model for biomimetic surfaces. In *Functional surfaces in biology* (ed SN Gorb), pp. 97–111. Berlin, Germany: Springer.

26. Barthlott W *et al.* 2010 The *Salvinia* paradox: superhydrophobic surfaces with hydrophilic pins for air retention under water. *Adv. Mater.* **22**, 2325–2328. (doi:10.1002/adma.200904411)
27. Babu DJ, Mail M, Barthlott W, Schneider JJ. 2017 Superhydrophobic vertically aligned carbon nanotubes for biomimetic air retention under water (*Salvinia* effect). *Adv. Mater. Interfaces* **4**, 1700273. (doi:10.1002/admi.201700273)
28. Busch J, Barthlott W, Brede M, Terlau W, Mail M. 2019 Bionics and green technology in maritime shipping: an assessment of the effect of *Salvinia* air-layer hull coatings for drag and fuel reduction. *Phil. Trans. R. Soc. A* **377**, 20180263. (doi:10.1098/rsta.2018.0263)
29. Gao H, Liu Z, Zhang J, Zhang G, Xie G. 2007 Precise replication of antireflective nanostructures from biotemplates. *Appl. Phys. Lett.* **90**, 123115. (doi:10.1063/1.2715094)
30. Vignolini S, Moyroud E, Glover BJ, Steiner U. 2013 Analysing photonic structures in plants. *J. R. Soc. Interface* **10**, 20130394. (doi:10.1098/rsif.2013.0394)
31. Kolle M, Lethbridge A, Kreysing M, Baumberg JJ, Aizenberg J, Vukusic P. 2013 Bio-inspired band-gap tunable elastic optical multilayer fibers. *Adv. Mater.* **25**, 2239–2245. (doi:10.1002/adma.201203529)
32. Dumanli AG, Savin T. 2016 Recent advances in the biomimicry of structural colours. *Chem. Soc. Rev.* **45**, 6698–6724. (doi:10.1039/c6cs00129g)
33. Prüm B, Seidel R, Bohn HF, Speck T. 2012 Impact of cell shape in hierarchically structured plant surfaces on the attachment of male Colorado potato beetles (*Leptinotarsa decemlineata*). *Beilstein J. Nanotechnol.* **3**, 57–64. (doi:10.3762/bjnano.3.7)
34. Graf C, Kesel AB, Gorb EV, Gorb SN, Dirks J-H. 2018 Investigating the efficiency of a bio-inspired insect repellent surface structure. *Bioinspir. Biomim.* **13**, 056010. (doi:10.1088/1748-3190/aad061)
35. Lederman SJ, Klatzky RL. 2009 Haptic perception: a tutorial. *Atten. Percept. Psychophys.* **71**, 1439–1459. (doi:10.3758/app.71.7.1439)
36. Valenta K, Miller CN, Monckton SK, Melin AD, Lehman SM, Styler SA, Jackson DA, Chapman CA, Lawes MJ. 2016 Fruit ripening signals and cues in a Madagascan dry forest: haptic indicators reliably indicate fruit ripeness to dichromatic lemurs. *Evol. Biol.* **43**, 344–355. (doi:10.1007/s11692-016-9374-7)
37. Chen J. 2007 Surface texture of foods: perception and characterization. *Crit. Rev. Food Sci. Nutr.* **47**, 583–598. (doi:10.1080/10408390600919031)
38. Barnes C, Childs T, Henson B, Southee C. 2004 Surface finish and touch—a case study in a new human factors tribology. *Wear* **257**, 740–750. (doi:10.1016/j.wear.2004.03.018)
39. Hollins M, Bensmaïa SJ. 2007 The coding of roughness. *Can. J. Exp. Psychol.* **61**, 184–195. (doi:10.1037/cjep.2007020)
40. Gorb EV, Gorb SN. 2006 Physicochemical properties of functional surfaces in pitchers of the carnivorous plant *Nepenthes alata* blanco (Nepenthaceae). *Plant Biol.* **8**, 841–848. (doi:10.1055/s-2006-923929)
41. Gorb E, Gorb S. 2009 Effects of surface topography and chemistry of *Rumex obtusifolius* leaves on the attachment of the beetle *Gastrophysa viridula*. *Entomol. Exp. Appl.* **130**, 222–228. (doi:10.1111/j.1570-7458.2008.00806.x)
42. Koch K, Domisse A, Barthlott W, Gorb SN. 2007 The use of plant waxes as templates for micro- and nanopatterning of surfaces. *Acta Biomater.* **3**, 905–909. (doi:10.1016/j.actbio.2007.05.013)
43. Koch K, Schulte AJ, Fischer A, Gorb SN, Barthlott W. 2008 A fast, precise and low-cost replication technique for nano- and high-aspect-ratio structures of biological and artificial surfaces. *Bioinspir. Biomim.* **3**, 46002–46012. (doi:10.1088/1748-3182/3/4/046002)
44. Schulte AJ, Koch K, Spaeth M, Barthlott W. 2009 Biomimetic replicas: transfer of complex architectures with different optical properties from plant surfaces onto technical materials. *Acta Biomater.* **5**, 1848–1854. (doi:10.1016/j.actbio.2009.01.028)
45. Singh A, Yoon E-S, Kim HJ, Kim J, Jeong HE, Suh KY. 2007 Replication of surfaces of natural leaves for enhanced micro-scale tribological property. *Mater. Sci. Eng. C* **27**, 875–879. (doi:10.1016/j.msec.2006.10.007)
46. Singh RA, Kim HJ, Kim J, Yang S, Jeong HE, Suh KY, Yoon E-S. 2007 A biomimetic approach for effective reduction in micro-scale friction by direct replication of topography of natural water-repellent surfaces. *J. Mech. Sci. Technol.* **21**, 624–629. (doi:10.1007/BF03026967)

47. Sun M, Luo C, Xu L, Ji H, Ouyang Q, Yu D, Chen Y. 2005 Artificial lotus leaf by nanocasting. *Langmuir* **21**, 8978–8981. (doi:10.1021/la050316q)
48. Huang Z, Yang S, Zhang H, Zhang M, Cao W. 2015 Replication of leaf surface structures for light harvesting. *Sci. Rep.* **5**, 14281. (doi:10.1038/srep14281)
49. Pulsifer DP, Lakhtakia A. 2011 Background and survey of bioreplication techniques. *Bioinspir. Biomim.* **6**, 031001. (doi:10.1088/1748-3182/6/3/031001)
50. Lee S-M, Kwon TH. 2006 Mass-producible replication of highly hydrophobic surfaces from plant leaves. *Nanotechnology* **17**, 3189–3196. (doi:10.1088/0957-4484/17/13/019)
51. McDonald B, Patel P, Zhao B. 2013 Micro-structured polymer film mimicking the trembling Aspen leaf. *Chem. Eng. Process Tech.* **1**, 1012–1018.
52. Saison T, Peroz C, Chauveau V, Berthier S, Sondergard E, Arribart H. 2008 Replication of butterfly wing and natural lotus leaf structures by nanoimprint on silica sol–gel films. *Bioinspir. Biomim.* **3**, 046004. (doi:10.1088/1748-3182/3/4/046004)
53. Kumar C, Le Hou  rou V, Speck T, Bohn HF. 2018 Straightforward and precise approach to replicate complex hierarchical structures from plant surfaces onto soft matter polymer. *R. Soc. open sci.* **5**, 172132. (doi:10.1098/rsos.172132)
54. Williams M, Vesik M, Mullins M. 1987 Tissue preparation for scanning electron microscopy of fruit surfaces: comparison of fresh and cryopreserved specimens and replicas of banana peel. *Micron Microsc. Acta* **18**, 27–31. (doi:10.1016/0739-6260(87)90016-5)
55. Hassanin H, Mohammadkhania A, Jiang K. 2012 Fabrication of hybrid nanostructured arrays using a PDMS/PDMS replication process. *Lab. Chip* **12**, 4160–4167. (doi:10.1039/c2lc40512a)
56. Zhuang G, Kutter JP. 2011 Anti-stiction coating of PDMS moulds for rapid microchannel fabrication by double replica moulding. *J. Micromech. Microeng.* **21**, 105020. (doi:10.1088/0960-1317/21/10/105020)
57. Pan Z, Shahsavan H, Zhang W, Yang FK, Zhao B. 2015 Superhydro-oleophobic bio-inspired polydimethylsiloxane micropillared surface via FDTS coating/blending approaches. *Appl. Surf. Sci.* **324**, 612–620. (doi:10.1016/j.apsusc.2014.10.146)
58. Nagaraja P, Yao D. 2007 Rapid pattern transfer of biomimetic surface structures onto thermoplastic polymers. *Mater. Sci. Eng. C* **27**, 794–797. (doi:10.1016/j.msec.2006.08.021)
59. Lee S-M, Lee HS, Kim DS, Kwon TH. 2006 Fabrication of hydrophobic films replicated from plant leaves in nature. *Surf. Coat. Technol.* **201**, 553–559. (doi:10.1016/j.surfcoat.2005.12.006)
60. Ensikat H, Ditsche-Kuru P, Barthlott W. 2010 Scanning electron microscopy of plant surfaces: simple but sophisticated methods for preparation and examination. *Microsc. Sci. Technol. Appl. Educ.* **1**, 248–255.
61. Neinhuis C, Edelmann HG. 1996 Methanol as a rapid fixative for the investigation of plant surfaces by SEM. *J. Microsc.* **184**, 14–16. (doi:10.1046/j.1365-2818.1996.d01-110.x)
62. Talbot MJ, White RG. 2013 Methanol fixation of plant tissue for scanning electron microscopy improves preservation of tissue morphology and dimensions. *Plant Methods* **9**, 36. (doi:10.1186/1746-4811-9-36)
63. Carlsson K, Danielsson P-E, Liljeborg A, Majl  f L, Lenz R,   slund N. 1985 Three-dimensional microscopy using a confocal laser scanning microscope. *Opt. Lett.* **10**, 53–55. (doi:10.1364/ol.10.000053)
64. Paddock SW. 2000 Principles and practices of laser scanning confocal microscopy. *Mol. Biotechnol.* **16**, 127–150. (doi:10.1385/mb:16:2:127)
65. Kaplonek W, Nadolny K. 2012 Advanced 3D laser microscopy for measurements and analysis of vitrified bonded abrasive tools. *J. Eng. Sci. Technol.* **7**, 714–732.
66. Chee WWL, Donovan TE. 1992 Polyvinyl siloxane impression materials: a review of properties and techniques. *J. Prosthet. Dent.* **68**, 728–732. (doi:10.1016/0022-3913(92)90192-d)
67. Mandikos MN. 1998 Polyvinyl siloxane impression materials: an update on clinical use. *Aust. Dent. J.* **43**, 428–434. (doi:10.1111/j.1834-7819.1998.tb00204.x)
68. Bhushan B, Hansford D, Lee KK. 2006 Surface modification of silicon and polydimethylsiloxane surfaces with vapor-phase-deposited ultrathin fluorosilane films for biomedical nanodevices. *J. Vac. Sci. Technol. A* **24**, 1197–1202. (doi:10.1116/1.2167077)
69. Zhuang YX, Hansen O, Knieling T, Wang C, Rombach P, Lang W, Benecke W, Kehlenbeck M, Koblitz J. 2007 Vapor-phase self-assembled monolayers for anti-stiction applications in MEMS. *J. Microelectromech. Syst.* **16**, 1451–1460. (doi:10.1109/JMEMS.2007.904342)

70. Cox G. 2002 Biological confocal microscopy. *Mater. Today* **5**, 34–41. (doi:10.1016/s1369-7021(02)05329-4)
71. Song J, Vorbuerger T. 2006 Topography measurements and applications. In *Third Int. Symp. Precision Mechanical Measurements*, p. 62801T 1–8. Washington, USA: International Society for Optics and Photonics. (doi:10.1117/12.716162)
72. Zheng X, Soons J, Vorbuerger TV, Song J, Renegar T, Thompson R. 2014 Applications of surface metrology in firearm identification. *Surf. Topogr. Metrol. Prop.* **2**, 014012. (doi:10.1088/2051-672x/2/1/014012)
73. Russell A, Johnson M. 2007 Real-world challenges to, and capabilities of, the gekkotan adhesive system: contrasting the rough and the smooth. *Can. J. Zool.* **85**, 1228–1238. (doi:10.1139/z07-103)
74. Collins CE, Russell AP, Higham TE. 2015 Subdigital adhesive pad morphology varies in relation to structural habitat use in the Namib Day Gecko. *Funct. Ecol.* **29**, 66–77. (doi:10.1111/1365-2435.12312)
75. Kane EA, Higham TE. 2012 Life in the flow lane: differences in pectoral fin morphology suggest transitions in station-holding demand across species of marine sculpin. *Zoology* **115**, 223–232. (doi:10.1016/j.zool.2012.03.002)
76. Zani P. 2000 The comparative evolution of lizard claw and toe morphology and clinging performance. *J. Evol. Biol.* **13**, 316–325. (doi:10.1046/j.1420-9101.2000.00166.x)
77. Kampowski T, Eberhard L, Gallenmüller F, Speck T, Poppinga S. 2016 Functional morphology of suction discs and attachment performance of the Mediterranean medicinal leech (*Hirudo verbana* Carena). *J. R. Soc. Interface* **13**, 20160096. (doi:10.1098/rsif.2016.0096)
78. Bullock JM, Federle W. 2011 The effect of surface roughness on claw and adhesive hair performance in the dock beetle *Gastrophysa viridula*. *Insect Sci.* **18**, 298–304. (doi:10.1111/j.1744-7917.2010.01369.x)
79. Ditsche-Kuru P, Barthlott W, Koop JH. 2012 At which surface roughness do claws cling? Investigations with larvae of the running water mayfly *Epeorus assimilis* (Heptageniidae, Ephemeroptera). *Zoology* **115**, 379–388. (doi:10.1016/j.zool.2011.11.003)
80. England MW, Sato T, Yagihashi M, Hozumi A, Gorb SN, Gorb EV. 2016 Surface roughness rather than surface chemistry essentially affects insect adhesion. *Beilstein J. Nanotechnol.* **7**, 1471–1479. (doi:10.3762/bjnano.7.139)
81. Higham TE, Russell AP. 2010 Divergence in locomotor performance, ecology, and morphology between two sympatric sister species of desert-dwelling gecko. *Biol. J. Linnean Soc.* **101**, 860–869. (doi:10.1111/j.1095-8312.2010.01539.x)
82. Macrini TE, Irschick DJ. 1998 An intraspecific analysis of trade-offs in sprinting performance in a West Indian lizard species (*Anolis lineatopus*). *Biol. J. Linnean Soc.* **63**, 579–591. (doi:10.1111/j.1095-8312.1998.tb00330.x)
83. Vanhooydonck B, Van Damme R. 2001 Evolutionary trade-offs in locomotor capacities in lacertid lizards: are splendid sprinters clumsy climbers? *J. Evol. Biol.* **14**, 46–54. (doi:10.1046/j.1420-9101.2001.00260.x)
84. Speck T, Speck O. 2008 Process sequences in biomimetic research. In *Design and nature IV* (ed CA Brebbia), pp. 3–11. Southampton, UK: WIT Press.
85. Speck O, Speck D, Horn R, Gantner J, Sedlbauer KP. 2017 Biomimetic bio-inspired biomorph sustainable? An attempt to classify and clarify biology-derived technical developments. *Bioinspir. Biomim.* **12**, 011004. (doi:10.1088/1748-3190/12/1/011004)

6.3 Manuscript C

1 Title:

In-situ investigation of adhesion mechanics on biological complex micro-structured surfaces.

2 Authors and affiliations:

Charchit Kumar^{1,2,3}, Damien Favier², Christian Gauthier², Thomas Speck^{1,3}, and Vincent Le Houérou^{2,4,*}

¹ Plant Biomechanics Group and Botanic Garden, University of Freiburg, Freiburg, Germany

² Institut Charles Sadron, CNRS UPR022, University of Strasbourg, Strasbourg, France

³ Freiburg Center for Interactive Materials and Bioinspired Technologies (FIT), Freiburg, Germany

⁴ ICube, University of Strasbourg, UMR7357, Strasbourg, France

ORCID IDs:

C. Kumar- 0000-0002-6912-3506

T. Speck- 0000-0002-2245-2636

V. Le Houérou- 0000-0001-7189-242X

*Corresponding author: v.lehouerou@unistra.fr (V. Le Houérou)

3 Abstract:

In recent years, plant leaf surfaces have attracted great attention, not only in biology but also in contact mechanics. They, for sure, are a great source of inspiration given their various fascinating functionalities, particularly unique adhesive properties, which are largely resulting from the complex arrangement of diverse surface structuring and chemistry. This paper presents a contribution to experimentally investigate the adhesion mechanics on some complex biological surface morphologies, inspired from insect-plant interactions. Soft elastomeric replica of three different plant leaves, comprising surface morphologies at a broad size range (0.5-100 μm), with distinct shape and complexity (hierarchical levels), and a smooth surface were used for adhesion investigation, in contact with a model adhesive probe. To perform precise and controlled adhesion measurements at a low force range (few mN), an ultra-nanoindenter setup was modified, based on the JKR (Johnson, Kendall and Roberts) contact mechanics approach. An innovative *in-situ* real contact visualization system (down to sub-micron size consistent with a single cuticular fold level) was developed and successfully incorporated into the adhesion apparatus, to acquire in-depth understanding of true contact areas all along the adhesion tests. The adhesion force on all four surfaces was quantitatively examined and systematically analysed regarding the pre-load conditions. Furthermore, a close examination of the results from real-time synchronization of the contact image with the corresponding force value revealed unique attachment-detachment mechanisms, arising from different pre-loads and surface-specific topographies. A significant enhancement in adhesion force, with increasing in pre-load, was observed on two replica surfaces: the one with fine micro-structuring and the other with complex hierarchical morphologies. However, no specific influence of pre-load was recorded on remaining two surfaces. An overall comparison of the results clearly demonstrated a significant reduction in adhesion force for the surfaces, with coarse sized circular cone-shape patterns and with complex hierarchical structuring, in comparison to the other two surfaces. In our opinion, the advanced understanding of adhesion characteristics, arising from unique biological surface morphologies, acquired in this work may offer assistance to design bio-inspired smart interfaces with tunable adhesion.

Keywords: Adhesion, contact mechanics, PDMS replica, *in-situ* imaging, plant leaves, micro-structures

4 Introduction:

In general, interfacial adhesive phenomena are widely spread and found in numerous man-made engineering systems, as well as in almost every biological system¹⁻⁵. Undoubtedly, the adhesive characteristics of interacting surfaces are a key feature to control system's performance and durability^{4,6}. Consequently, it appears of prior importance to precisely tune adhesive properties when the surface to volume ratio gets tremendously increased, as it is the case especially in recently emerging micro- or nano-contact applications^{2,7,8}. Well-recognised ways to adjust the adhesion characteristics are by modifying the surface chemistry or by introducing surface texturing on the interacting surfaces⁹⁻¹⁵. The pioneering work by Fuller and Tabor back in 1975, proposed a reduction in adhesion force by incorporating surface roughness¹⁶. In the last four decades, various approaches have been published utilising for instance defined geometrical asperities (square, cylindrical or hexagonal pillars, spherical dimples etc.) to study influence of surface morphology on adhesive response^{9,11-13,17-22}. Few others studied adhesion characteristics and contact formation mechanisms on surfaces decorated with ripple or wrinkle shaped texturing^{7,23-27}. Regardless of all these studies the adhesion mechanisms are not completely understood yet, considering how manifestly the type and complexity of morphologies can induce unique and distinct adhesion behaviours^{7,9,13,28-37}.

In nature, adhesion also plays an important role for the interaction of animals with plant surfaces or with the inanimate environment^{1,38-40}. Broadly mentioning, insect attachment pads evolved in a manner to assist in sticking to or climbing on various plant surfaces^{39,41-43}, while on the other side, most of the green plant leaves possess surfaces obstructing or reducing insect attachment⁴⁴⁻⁴⁷. Leaf surfaces are often decorated with species-specific and unique surface structuring of different size, ranging from few nanometres to few hundreds of micrometres, having distinct shape, complexity both at various levels of hierarchy⁴⁸⁻⁵². This induces some optimised surface functionalities such as surface wettability, anti-adhesive properties, friction reduction, antifouling, slipperiness against insect attachment and optical properties, just to name a few^{41,46,48,49,53-58}. As a result, these surfaces gained a lot of attention from the contact mechanics community, to get inspired, to investigate, and later to transmit for biomimetic surface applications^{10,55,59-66}. However, the relationship between structures and functions is not straight forward, keeping in mind that almost all these plant surface phenomena are driven by a complex interplay of compound material composition, heterogeneous surface chemistry and diverse surface structuring leading to a highly sophisticated system to investigate^{49,57,58}. A possible simplification, that has been used in the past, consists in the precise replication of the

complex structural morphologies of plant surfaces onto polymeric surfaces⁴⁵. This facilitates a methodical investigation of the role of surface morphology, without the influence of physico-chemistry aspects^{45,67,68}.

Although the advancement in the micro-structured surface fabrication technologies in the past decades made possible to generate a vast kind for micro- or nano-structures^{17,69-75}, however, still far to realise the diversity and intricacy of biological surface structures^{48-50,52}. Nevertheless, several papers on methodological research have been published offering different approaches to replicate the surface structures directly from original plant leaves onto the various polymeric substrates⁷⁶⁻⁸¹. Over the recent years, there has been a growing trend and increased interest towards the *in-situ* real contact visualization, when doing adhesion mechanics investigations, and it became possible with the latest innovation in the field of optical imaging^{7,17,19,20,23,82-85}. Surely, *in-situ* imaging offers a detailed insight into the real contact formations and also makes possible to observe the real physical contact junctions over the apparent contact area, as well as attachment/detachment mechanisms. However, much of the research, up to now, that performed *in-situ* real contact visualization has been limited to either smooth surfaces^{83,86-88} or technically developed micro-structured surfaces^{7,12,17,19,21,23,29,85}. Indeed, in the past, most of the contact mechanics investigations based on biological surfaces could not achieve real-time visualization of real contact formation on the plant leaf surfaces, down to cellular or sub-micron-sized cuticular fold level^{45,67}.

Taken all together, in this work, we use the classical adhesion mechanics understanding to methodically investigate the adhesion phenomena on biological structured surfaces closely inspired from insect-plant interactions, forming contact with a model adhesive tip. Three model plant leaves were selected and replicated onto polymeric samples, considering a broad morphological range in terms of their structure's size, shape and hierarchy. By considering the various advantageous aspects and final positive replica characteristics relevant to our research specification, we employed the replication technique presented by Kumar *et al.* 2018, that use epoxy resin for generating negative moulds and producing the final replica on Polydimethylsiloxane (PDMS) substrates⁷⁶. The force range that corresponds to plant-insect interactions falls in the (few) mN range, and therefore call for a highly sensitive, controlled and low force range experimental setup^{42,89,90}. Such a low force range and high sensitivity can be accomplished with a nano-indenter like apparatus⁹¹⁻⁹³. Thus, we introduce a new dynamic adhesion force tester (modified nanoindenter) to perform low-range adhesion force measurements under precise load or displacement control. Furthermore, the newly modified apparatus allows the *in-situ* real-contact visualization on the complex micro-structured surfaces.

At first, this paper quantitatively investigates adhesion force characteristics on the PDMS leaf replicas and on a smooth PDMS surface, and critically examines the influence of pre-load and surface morphology on the adhesion force behaviour. Furthermore, by utilising the dedicated *in-situ* imaging, this investigation also offers a comprehensive insight into the real and apparent contact areas, along with the physical understanding on attachment and detachment phenomena, arising from the various type of surface structuring.

5 Materials and Methods:

5.1 Investigated Biological Surfaces:

Three different plant leaf surfaces were selected for this investigation, on the basis of different size, distinct morphology and complexity of their surface structuring. Rubber tree (*Hevea brasiliensis*; adaxial, i.e. upper leaf surface) represents two levels of structuring consisting of “puzzle piece-shaped” epidermal cells covered by fine cuticular fold microstructures (Figure 3.a), with both height and width of about 0.5-1 μm and an intermediate spacing of 0.5-1.5 μm ⁴⁵. Jewel orchid (*Ludisia discolor*; adaxial, i.e. upper leaf surface) exhibits circular cone-like shaped microstructures (Figure 3.d) with a diameter of about 50-100 μm and a height of about 50 μm ⁷⁶. Lychee (*Litchi chinensis*; abaxial, i.e. lower leaf surface) has a complex hierarchical surface structuring (Figure 3.g) consisting of ‘rose-flower-shaped’ units inducing undercuts and overhanging substructures⁴⁵. All plants used in this investigation were grown in the Botanic Garden of the University of Freiburg, Germany. All leaves were freshly collected just before processing the replication.

5.2 Preparation of PDMS Replicas and Smooth Surfaces:

PDMS, a silicon-based soft elastomer, is an appropriate and interesting system for such contact mechanics studies, offering various key advantages: easy handling, low cost, non-toxicity, a low surface energy (22 mJ m^{-2}) and an extremely low elastic modulus ($E = 0.5\text{-}4 \text{ MPa}$)⁹⁴. Furthermore, it has a very low glass transition temperature (-120 $^{\circ}\text{C}$), so it gets easily cross-linked to a very stable elastic network, showing high chemical stability at room temperature, and doesn’t show any explicit interaction with other material⁹⁵. Importantly, PDMS exhibits high optical transparency over the wide range of UV light, thus being a perfect applicant for achieving the *in-situ* real contact visualization⁹⁶. Because of its high γ/E (surface energy to elastic modulus) ratio, it is suited for adhesion mechanics studies and also has been widely used in the past by various researchers^{19-21,83,86,97}. Surface microstructures from the original plant leaves were precisely transferred onto PDMS, using a two-step replication technique, as

previously described⁷⁶. At first, negative moulds were developed with two components epoxy resin (Epoxy Resin L & Hardener S, Toolcraft, Conrad Electronic SE, Hirschau, Germany) directly from the original fresh plant leaves. Fresh plant leaves were cut into small pieces (approximately 4 cm × 4 cm), and immediately glued onto a plastic petri dish with a double-sided adhesive tape. Subsequently, the uniformly mixed bubble free epoxy mixture (resin to hardener ratio of 10: 4.8) was steadily poured onto the leaf sample surfaces. After curing for 15 h at ambient conditions (temperature = 20-25°C and relative humidity = 40-60%), plant leaves were separated from negative epoxy moulds. In step two, negative epoxy moulds were filled up with low-viscosity Polydimethylsiloxane (Bluesil ESA 7250 A & B kit, Bluestar Silicones GmbH, Leverkusen, Germany) mixture (monomer to cross-linker ratio of 10: 1) and were kept in a vacuum chamber for one hour to remove air entrapped at the interface. After curing at 75°C for 3 h, cross-linked PDMS replicas were peeled off from the negative moulds. Smooth PDMS samples were produced by curing the same PDMS mixture in a freshly opened flat bottom glass petri dish. Each replica sample was quickly quality inspected for any replication imperfection, using an optical stereo microscope. At least four samples were developed for each surface type investigated, to develop independent results and produce a detailed statistical analysis of adhesion tests.

All samples (PDMS leaf replicas as well as the smooth PDMS samples) were swollen in a solution of n-heptane and 1-dodecanethiol (0.01 %) for overnight to remove the sol fraction (to extract the remaining unreacted free chains). After then, all the swollen samples were kept at ambient room conditions for at-least 24 h to restore back to their original state⁹⁸⁻¹⁰⁰.

5.3 Surface Characterization:

Surface morphology visualization and characterization was done using scanning electron microscopy (Leo 435 vp, Leica, Wiesbaden, Germany and Hitachi SU8010, UHR FE-SEM, France). For SEM examination of the plant leaf samples, fresh leaves were dehydrated in methanol solution and dried by using critical point drier (LPD 030, Bal-Tec)^{101,102}. All the samples (plant leaves, PDMS replicas, and replicas after n-heptane solution treatment) were mounted on aluminium stubs (Plano GmbH, Wetzlar, Germany), and the side walls of samples were coated with conductive silver paint (Acheson Silver DAG 1415M, Plano GmbH, Wetzlar, Germany). In order to avoid surface charging, all samples were metalized with a thin (ca. 10 nm) coating of gold (Cressington Sputter Coater, 108 auto). All SEM examinations were performed in the 30°- 45° tilting angle range.

5.4 Adhesion Mechanical Testing:

5.4.1 Description of the Modified Adhesion Force Tester:

The adhesion investigation was performed with a JKR contact mechanics based apparatus¹⁰³, and described in-details in the following section. An ultra-nanoindentation tester (UNHT³, Anton Paar Tritec, Switzerland) with a high-resolution load-control of 3 nN and a depth resolution down to 0.3 nm was modified to perform low range adhesion force measurements, together with *in-situ* real contact visualisation, as illustrated in a simplified schematic in Figure 1. Indeed, a dedicated optical system was introduced into the equipment, permitting high-resolution differential contrast microscopy based on transmission light microscopic principle: a light beam shines from the probe and propagates through the tested substrate^{104,105}.

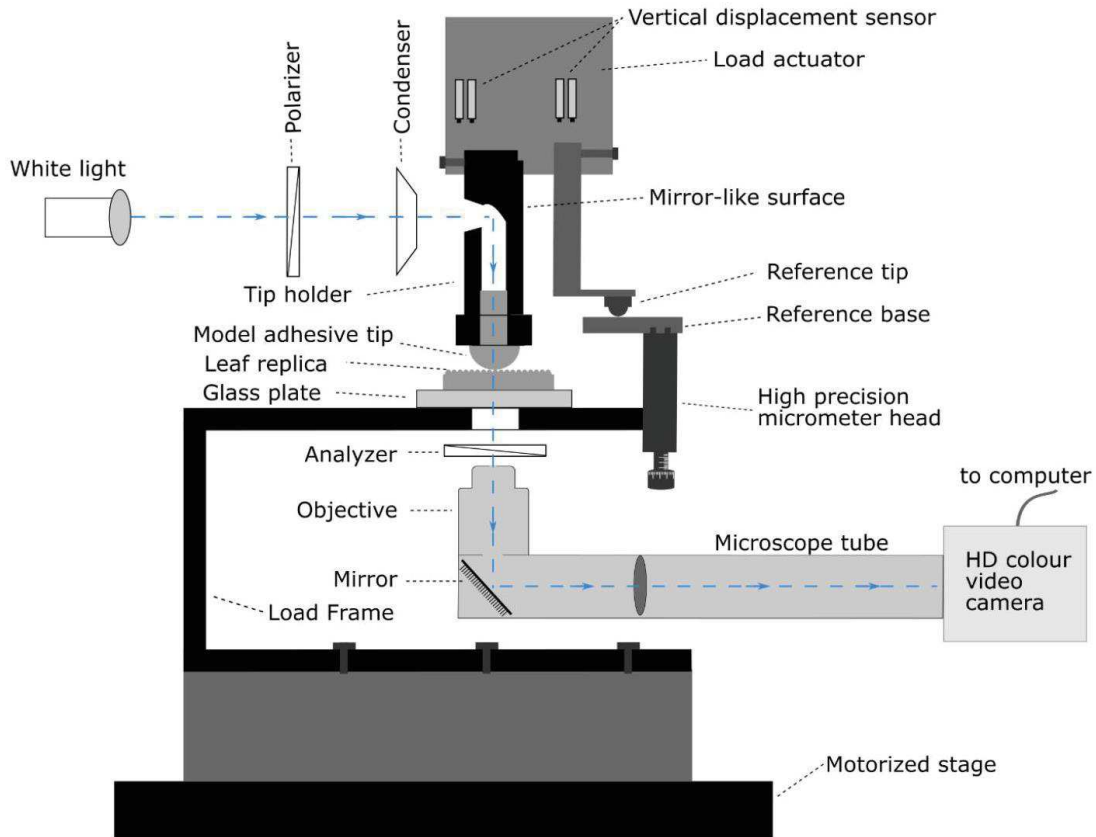


Figure 1. Simplified drawing of the modified ultra-nanoindenter setup for low-range adhesion force measurement in synchronization with *in-situ* real contact visualization. The pull-off force measurement head is additionally equipped with a vertical displacement sensor and a reference tip to perform surface referencing. A white light was shined at the tip opening, via passing through a polarizer and condenser lens. The light beam after being reflecting from an internal mirror-like surface perpendicularly bends toward the soft tip and is further transmitted through the real-contact junctions, appearing as high contrast bright spots in the recorded videos.

White light from a fibre optic cold light illumination (KL 1600 LED, Schott AG, Germany) was shined at the tip, via passing from a polarizer filter, and focused with a condenser lens onto the tip opening spot, with the purpose to get high-intensity illumination (Figure 1). A special tip (Figure 2) was fabricated with an internal micro-hole and with a micro-metal machining finished (alighted at an angle of ca. 45°) on top of the tip, so that the light beam was perpendicularly reflected and followed a path in the direction to the soft probe (Figure 1). Just under the substrate surface, an analyser along with an objective lens was attached. The objective lens was mounted on a micromanipulator, benefiting to precisely focus on contact spot. The transmitted light beams through the contact junctions, where both surfaces (PDMS-PDMS) are in real-contact with matching refractive index, appeared as high contrast bright spots and were recorded with a high definition colour camera (Basler acA3800-14uc, with a 10Mpix CMOS sensor, Germany). Moreover, light got randomly scattered over the area where no intimate contacts (PDMS-air interface) were established and thus leading to dark domains. Polarizer and analyser filters facilitated to obtain sharp yielded contact edges. Furthermore, the apparatus was also advanced with a custom-build dedicated electronic system that enabled simultaneous recording of the video frame in real-time synchronization with the corresponding force data point.

5.4.2 Model Adhesive Tip:

Since, in our investigation strategy, the entire size of the probe (half sphere of 1.5 mm radius) and the substrate system were very small, it became critically complicated to incorporate the optical prerequisites associated to transmission light microscopy within the adhesion tester. Consequently, particular caution was paid to the soft elastomeric adhesive tip which was fabricated using a two-step moulding process. In the first step, a thick Polymethyl methacrylate (PMMA) substrate (normal cast type) was slowly and locally heated up till ca. $100 \pm 5^\circ\text{C}$, with an air heating gun. Precisely, just before the material started melting, a sapphire ball (Edmund Optics, United States) with a radius of 1.5 mm was gradually pressed down until the ball is half subsided into the PMMA. After cooling for 30 min, the ball was separated out from the bulk with an indigenous vacuum suction gripper, and consequently moulded a negative impression on the PMMA surface. The developed negative mould was then filled up with a PDMS mixture (prepared with same mixing protocol as described in section 5.2) and degassed in a vacuum desiccator for 20 min to remove any air bubble that could be trapped during pouring. A homebuilt tip holder (assembly) was manufactured, by machining a micro-hole (radius = 0.5 mm) inside the tip, for a depth of about 8 mm, as shown in Figure 2. The tip holder assembly consists of an external screw thread and nut attachment at the very bottom. Tip

assembly was gradually put on top of the PDMS filled PMMA mould, by ensuring a perfect in-line central alignment, using a linear translation stage (Figure 2.b). During the PDMS curing process, the PDMS mixture was filled up in the small gaps formed at the thread in between stud and bolt, as illustrated in Figure 2.a, thus ensuring the fitting of the PDMS tip with the holder.



Figure 2 Simplified sketch of the tip assembly (a) showing that the PDMS tip is embedded within the tip assembly holder. (b) A PDMS liquid mixture is filled up inside the hole due to capillary action, and a photograph of actual the PDMS tip attached to the tip holder (in up-right corner of image b).

Additionally, we observed that the PDMS level slowly raised up inside the drilled hole, likely due to the capillarity action, consequently forming a strong bulk attachment of PDMS tip with the tip holder. Tip's centre alignment with the centre of the PMMA mould was essential to get a uniform contrast all over the whole contact image, during the *in-situ* visualization. As this perfect alignment step was crucial, the development of a perfectly aligned tip took several attempts (typically up to 4-5 tips) before final success. After development, each tip assembly was checked under optical microscope and non-aligned tips were discarded. Furthermore, to examine any surface imperfection, tips were checked with a scanning electron microscope.

5.4.3 Surface Referencing:

Another important aspect during such low range force measurements is the accurate detection of the very-top point of contact i.e. surface referencing⁹². It becomes even more crucial, when both tip and substrate samples are made up of a soft matter polymer, where long-range adhesive forces in between tip and sample surface exist, and time-dependent creep of the polymer material during the referencing process itself could greatly influence the exactness of reference position and then further affect the accuracy of adhesion measurement^{93,106}. In order to ensure a precise surface referencing, we introduced an alternative method using a separate parallel referencing tip-head on a hard metal reference base, mounted with a high precision micrometre head, as shown in Figure 1. For the referencing process, at first both the reference tip and the

adhesive tip are brought down together, in such a way so that the reference tip touched the reference base at first.

5.5 Experimental Protocol

All substrates were placed on rigid transparent glass plates and further fixed on the test platform. Prior to each set of tests, surface referencing was performed for each surface type. For each adhesion test, the adhesive tip was slowly approached just near to the substrate surface. As soon as, the tip reached in close proximity to the substrate surface, sudden snap-in (pull-in) took place. After this, the tip attained zero normal load condition, corresponding to an initial zero load state in the force-displacement graph (Figure 4). At this state, when a test started, the adhesive tip began forming contact under quasi-static loading, at a constant loading rate of 0.083 mN/sec, until the defined normal pre-load (F_L) is reached. The adhesive tip was kept under constant F_L for a set time and then the tip was retracted under displacement control motion, at a retraction speed of 0.83 $\mu\text{m}/\text{sec}$. A graph of a typical pull-off force measurement is shown in Figure 4. The range of F_L was kept low enough and substrate thickness was chosen large enough, so that the ratio of substrate thickness to mean contact radius was higher than ca. 10, thus the underlying substrate (glass slide) effect could be neglected^{86,107,108}. All measurements were conducted in a climate controlled room (temperature = $22 \pm 3^\circ\text{C}$, relative humidity = $50\% \pm 10\%$).

5.6 Image Processing:

All the recorded *in-situ* videos were processed and analysed with the digital image processing tool *ImageJ* (v. 1.51p, National Institutes of Health, USA) permitting initial homogenous filtering, thresholding, and estimating the real contact and apparent areas¹⁰⁹. The real contact area (A_r) was calculated by summing all the individual local real areas (A_{r_i}). For the apparent area (A_{ap}) estimation, multiple outmost peripheral point coordinates were sampled from all directions and fitted with a standard best-fit ellipse. The normalized contact area (A_n) is defined as:

$$A_n = \frac{\sum A_{r_i}}{A_{ap}}$$

6 Results and Discussion:

6.1 Surface Morphologies:

The results of SEM surface morphological investigation, as illustrated in Figure 3, demonstrated the high precision of PDMS replicas, made directly from original plant leaves with using Epoxy–PDMS replication. All three plant leaf surfaces, *H. brasiliensis* leaf with wrinkle-shaped fine microstructures (Figure 3.a and Figure 3.b); *L. discolor* surface with cone-shaped coarse micro-structures (Figure 3.d and Figure 3.e); and *L. chinensis* with complex hierarchical microstructures (Figure 3.g and Figure 3.h) were replicated to PDMS with high fidelity. After the n-heptane treatment, all samples were perfectly restored back by de-swelling to their original state without damage, as proved in Figure 3.c, 3.f and 3.i.

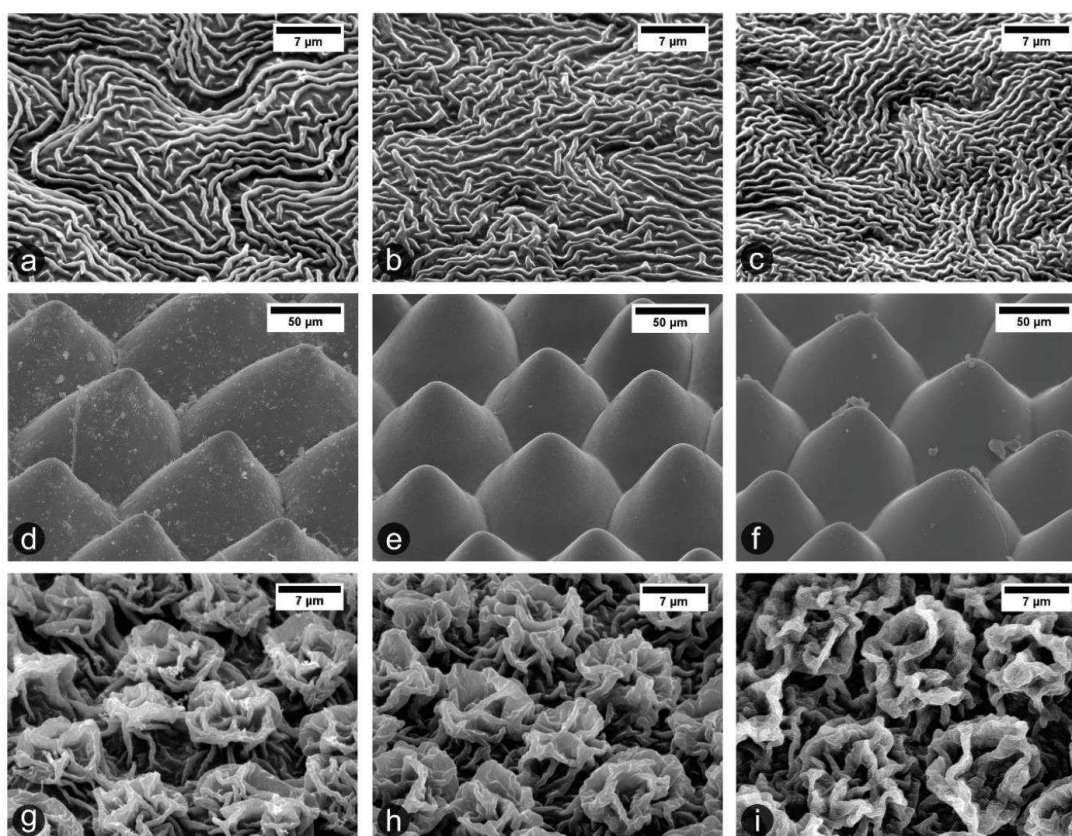


Figure 3. Scanning electron microscope images of original plant leaf surfaces (left column; a, d and g), their PDMS replicas (middle column; b, e and h), and respective PDMS replicas after n-heptane treatment (right column; c, f and i). (a-c) *Hevea brasiliensis* (adaxial, upper side surface) exhibits a micron-size wrinkled shape folds. (d-f) *Ludisia discolor* (adaxial, upper side surface) represents circular cone-like surfaces structures. (g-i) *Litchi chinensis* (abaxial, lower side surface) surface shows highly complex hierarchical structures.

6.2 Adhesion Force Characteristics:

Adhesion force measurements were carried out for each polymeric replica as well as for a smooth PDMS surface. For each type of surface, different data sets were recorded by carrying out experiments at 5-7 different spots on different samples. Figure 4 shows a plot obtained from a typical pull-off adhesion force measurement. Adopting the standard contact mechanics convention, the absolute maximum negative force value during the retraction cycle corresponds to the adhesion pull-off force (F_{ad}), as can be seen in Figure 4 for a smooth PDMS sample^{7,110}. In order to investigate the effect of pre-load (F_L), adhesion experiments were performed at the same spot, for seven different F_L values: 0.5, 1.0, 1.5, 2.0, 2.5, 3.0 and 3.5 mN, keeping all other test parameters (loading/unloading rate, retraction speeds, and time length of the test) and conditions constant. In the following sub-sections, the results on attachment and detachment mechanisms, alongside with the results from the pre-load effects on adhesion force characteristics, are presented and discussed in a sequence for each surface type. For reading convenience, hereafter, only genus name is used to address PDMS replica samples instead of full species name: *Hevea* replica for *H. brasiliensis*, *Ludisia* replica for *L. discolor*, and *Litchi* replica for *L. chinensis*.

6.2.1 Smooth PDMS:

A force-displacement (time) curve of an adhesion measurement, for a whole test cycle, on smooth PDMS sample at a pre-load (F_L) of 1.5 mN is shown in Figure 4. As can be seen from the retraction part of the force-displacement curve, the measured adhesion force (F_{ad}) was 0.827 mN. Still image sequences from the *in-situ* real contact video (see the Video 1 in additional data) of adhesion investigation at the various points of interest (a-f) are set out in Figure 4.a-f. With regard to the dynamics of smooth PDMS contact, attachment and detachment events appeared very continuous, homogenous and circular in shape over the whole contact cycle. The real contact area increased with increasing normal load and started decreasing once the retraction part began with the well-known adhesion hysteresis⁹⁸. The point (a) in the graph indicates the *just-in* contact point at zero load, right after the pull-in has taken place (not shown in the graph) ending the approach step, therefore a small contact could be seen in the corresponding *in-situ* contact image (Figure 4.a). At this state, tip and substrate already formed a solid-solid intimate contact. After this, the loading phase began and the tip slowly is pressed on the substrate surface under a highly precise load controlled loading, at a rate of 83.3 $\mu\text{N}/\text{sec}$. Point (b) in the graph represents the state where continuous loading was stopped and system was kept for relaxation. A closer observation of point b and point c, exhibited a small increase

in radius at point c. This increase in radius corresponds to the material relaxation after contact movement took place.

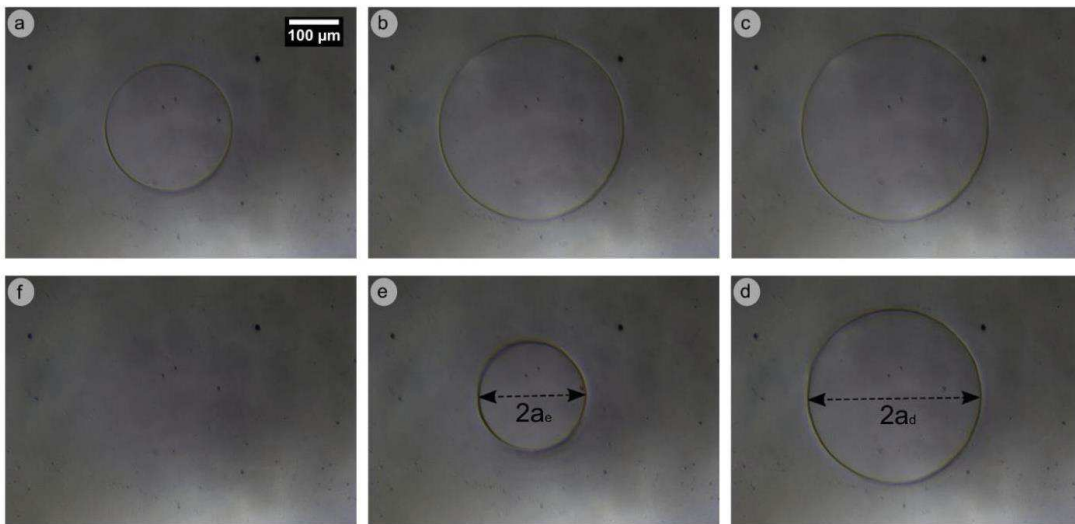
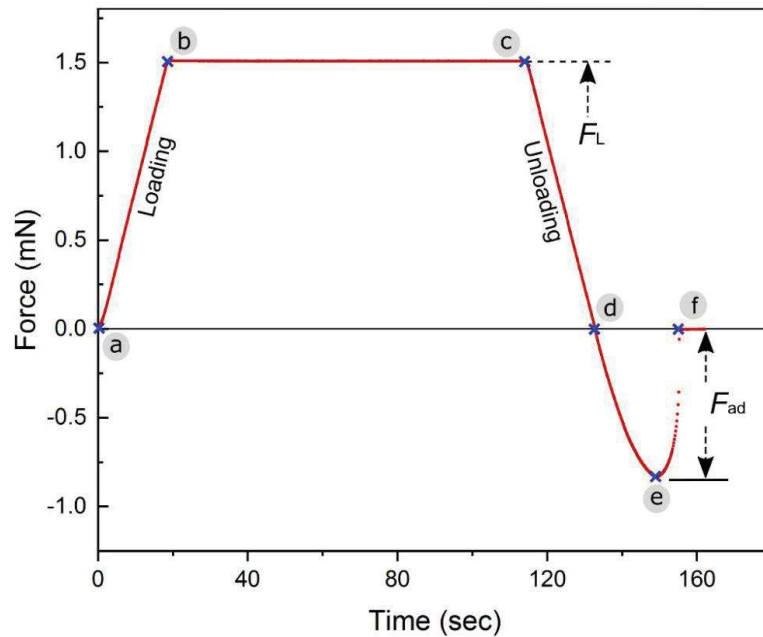


Figure 4 Graph (upper part of the figure) showing the force-time (displacement) curve for a whole test cycle on smooth PDMS sample, at a pre-load (F_L) of 1.5 mN. F_{ad} is the adhesion (pull-off) force recorded during the retraction step. Different points of interest (a-f) are marked on the curve. Phase a-b corresponds the loading stage, b-c represents to the state when interacting bodies are in full contact, c-d is the unloading phase. Phase d-e-f represents the retraction phase recording the adhesion pull-off force. On the lower part of the figure, set of in-situ contact images (a-f) corresponding to the points marked on the force-displacement curve are shown. For the full in-situ video corresponding to above images, see the supporting video 1 in additional data. The scale bar in image ‘a’ holds for all the six images.

Further investigation of the retraction part of the curve shows, that the measured value of the contact diameter ($2a_d$) at the absolute zero load condition (Figure 4.d) was found to be 348 μm . The contact diameter ($2a_e$) at the very lowest force point, *the point of detachment instability*,

where the contact diameter abruptly vanished to zero, was measured to be 219 μm (Figure 4.e). This finding is in well accordance with previously established theory, which predicts the following relation $a_e = 0.63a_d^{111,112}$. Therefore, it validates the correct establishment of our test protocol with the well-recognised theory.

Effect of pre-loading: Figure 5 shows the results from the investigation of the effect of F_L on F_{ad} . Here, F_{ad} values clearly appeared to be quite consistent and independent ($F_{ad} \approx 0.809$ mN) from variation in F_L , which is in good agreement with the Johnson, Kendall, and Roberts (JKR, 1971) model¹⁰³. The same phenomenon of the independence of adhesion force from pre-load on smooth surfaces, has been reported in previous studies^{97,113}. The relaxation time for PDMS is reported to be in the order of 0.05-0.5 s, significantly less as compare to the contact time applied in this investigation¹¹⁴. Hence, it could be assumed that this contact system behaves more likely as elastic since loading and unloading phases could be considered as quasi-static¹¹⁴. All the tests in this investigation were performed slowly enough to minimize the viscous effects of material. Moreover, no effect of loading history on the adhesion force values in the investigated force range was noticed, as supported with the results stating independence of F_{ad} from the F_L . Hence, this observation very much supports that our test protocol is adequately complying the standard JKR adhesive model.

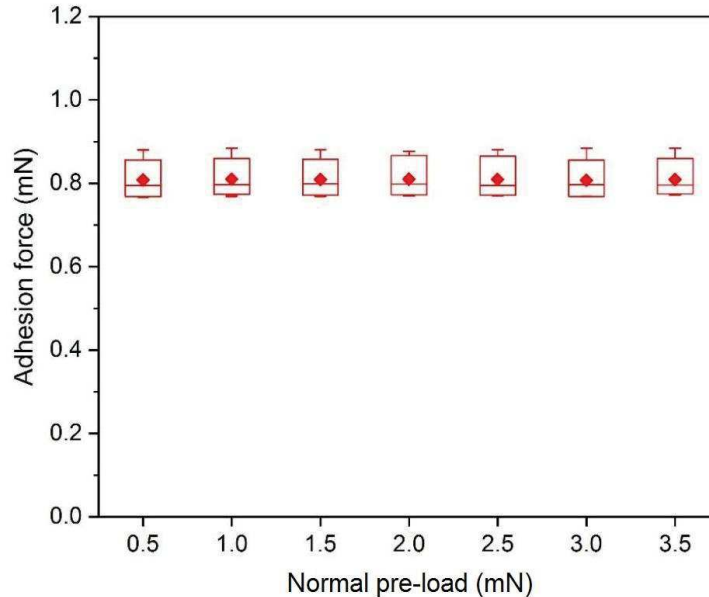


Figure 5 Box plot of the variation of adhesive pull-off force (F_{ad}) with change in applied pre-load (F_L) for smooth PDMS sample. Data points are plotted as mean and \pm standard deviation for $N=7$.

6.2.2 *Hevea* Replica:

An *in-situ* video of the adhesion test for an entire cycle on *Hevea* replica at a F_L of 1.5 mN is shown in Video 2 (additional data). The fine structured surface of *Hevea* replica is easily

recognizable, as shown in Figure 6. It is clearly possible to distinguish between the true contact area (in bright contrast) and the area out of contact (in dark contrast) on *Hevea* replica, as can be seen in Figure 6. To gain a better understanding of the attachment dynamics, we closely analysed the zoomed-in *in-situ* videos. The contact formation initiated at the second level of micro-structuring (fine cuticular folds), and as the contact formation advanced a whole cell was pulled in an intimate contact¹⁷. At the full contact state, even though a whole cell appeared to be in full contact, cell boundaries (outer line surrounding a cell, first level of structuring) were left out of contact (darker line areas). Afterwards, as the detachment event began, two distinct type of contact separation mechanisms could be identified: (i) each cell, forming the full contact, behaved as an individual contact point of stability; (ii) cell boundaries initiated and assisted the crack propagation during the detachment sequence and a cell as a whole detached at a time, as can be seen by closely observing the detachment sequences. The crack initiation began at the cell boundaries around the outer periphery of the whole contact region and then the crack further spreads toward inner areas, by following the cell boundaries. A similar kind of detachment phenomenon has been demonstrated by⁷, where adhesive contact was formed between a rigid sphere with a rippled elastic surface.

Different contrast during attachment and detachment phases: Another interesting finding from a closer observation on the zoomed-in *in-situ* videos is the distinct colour contrast at the contact periphery for the attachment and detachment cycles (Figure 6). A full video (Video 2) for better visualization of this finding is provided in additional data. Continuous *flowing-type* of the contact advancement mechanism could be evidently visualised during attachment, as can be clearly seen in Figure 6.a and Figure 6.b, while a sharp contrast on contact edge is exhibited during the detachment (Figure 6.c and Figure 6.d). We believe, that the higher edge sharpness in the detachment sequence could be attributed to an increase in local strain and thus led to make tension on edge curvatures. Such a phenomenon has also been mentioned in a previous study by Charrault *et al.*⁸⁶.

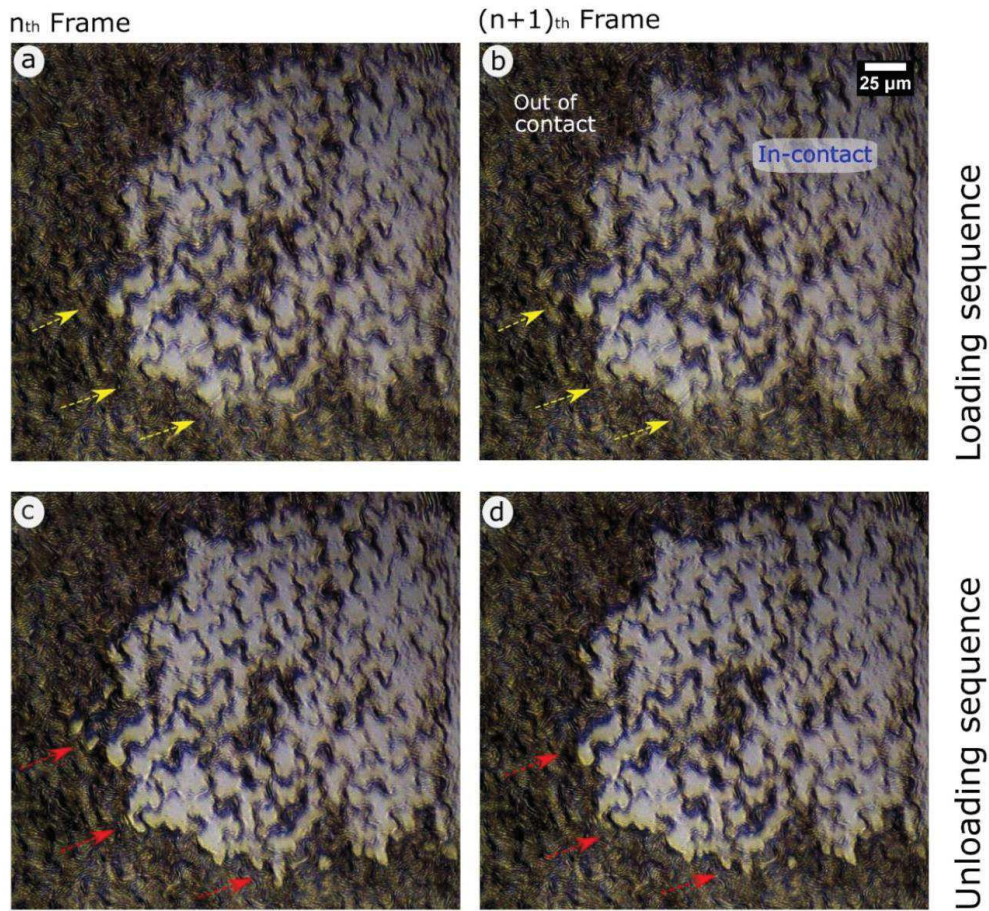


Figure 6 High magnification image sequence representing the contact formation behaviour during an attachment and detachment cycle. Bright areas represent the real area in contact. (a, b) shows the two consecutive (n_{th} and $(n+1)_{th}$) frames captured during the attachment cycle, and (c, d) for the detachment cycle. The arrows are pointing to the areas of interest with distinct colour contacts at edge for the attachment and detachment cycles. The scale bar in image b applies for all four images. A corresponding full video (Video 2) is provided in additional data.

Effect of pre-load: Figure 7 shows the results of adhesion force characteristics with increasing normal pre-load, for *Hevea* replicas. A clear increase in F_{ad} , from 0.384 mN to 0.490 mN, was observed with increasing F_L from 0.5 to 2.5 mN. However, adhesion force appeared to get saturated with a further increase in F_L above 2.5 mN^{10,20}. The increase in F_{ad} could be explained with the filling-up of fine microstructure pockets between the wrinkles (cuticular folds), with advancing the F_L . A similar phenomenon has been found also in several previous studies^{10,11,22,115}. Actually, at a low F_L (0.5 mN) value, only partial contact occurs at very top of the cuticular folds, resulting in a small normalised real contact area, $A_n = 0.44$. With further increasing F_L , tip material progressively fills up the small non-contact gaps between the wrinkles, hence resulting in an increase in adhesion force by a factor of about 30 %. One can also notice in Figure 7.I and Figure 7.II that there was an evidently large true area still left in contact even when complete load was removed (at the absolute zero load), for the higher pre-

load ($F_L = 3.5$ mN) condition in comparison to the smaller pre-load $F_L = 0.5$ mN. This clearly indicates that the observed increase of F_{ad} for *Hevea* replica is caused by its specific fine micro-structuring.

We, further, investigated the *in-situ* contact images to compute the normalized contact area (A_n) at the full loading condition, for all the F_L values (Figure 7, blue data points). Interestingly, it appeared clearly that in the beginning A_n increases with increasing F_L until 2.5 mN is reached. After this value, A_n appears to be get saturated at higher pre-loads (3.0 mN and 3.5 mN).

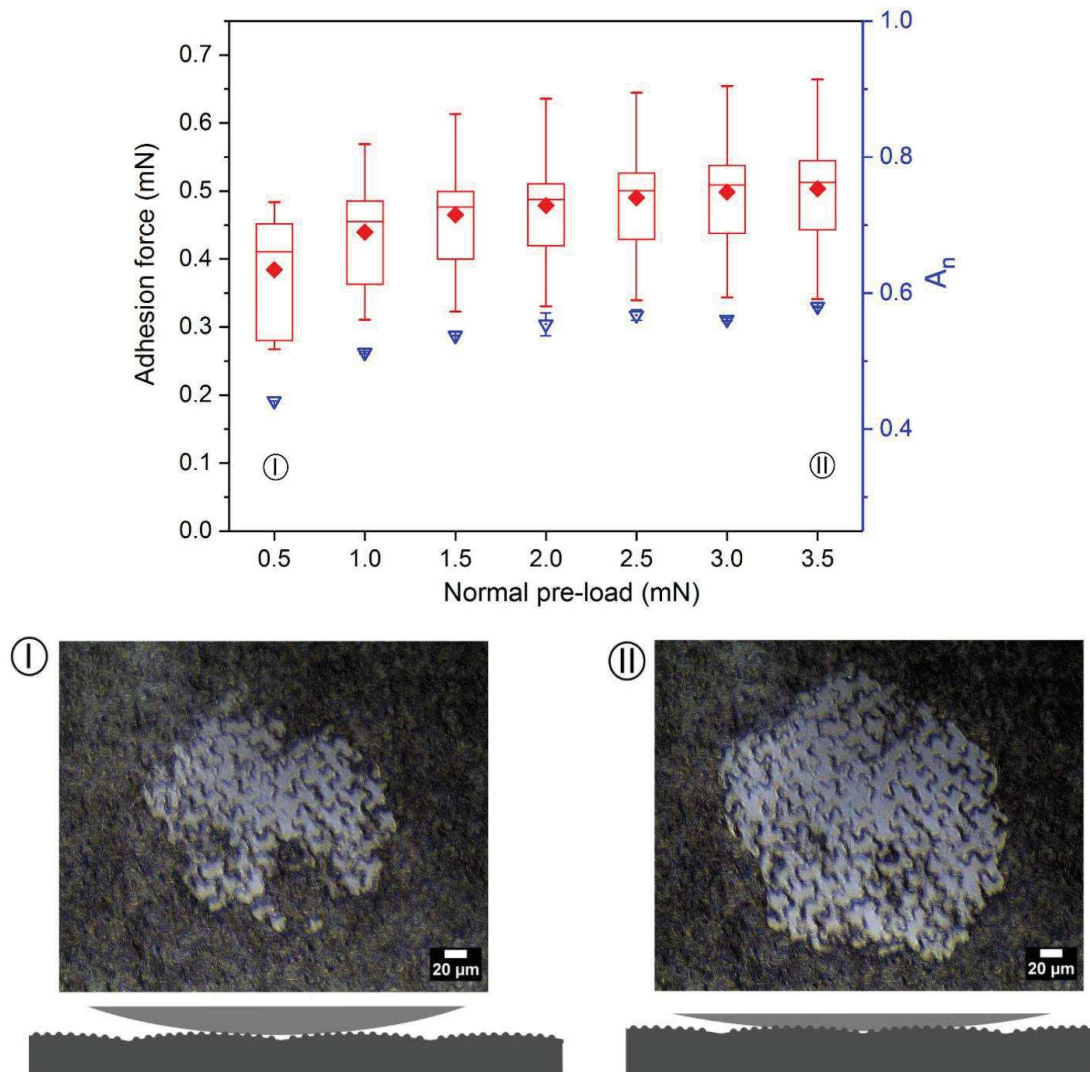


Figure 7 Upper part of the figure: Plot (in red, left-side ordinate) of the variation of adhesion pull-off force (F_{ad}) as a function of applied normal pre-load (F_L) for *Hevea* replica samples (N=6). Advancement of the normalized contact area (A_n) with increase in the pre-load (F_L), in blue on right-side ordinate. Lower part of the figure: Image I (for $F_L = 0.5$ mN) and image II (for $F_L = 3.5$ mN) show the *in-situ* contact areas at the absolute zero load condition, just before the retraction began.

A_n curve shows a similar dependency from F_L as does the adhesion force (Figure 7). This similar trend corroborates the filling of microstructures at high pre-loads, which gets saturated after a threshold value of F_L reached. A_n tends to saturate at 0.6, and never reached 1 (the latter meaning complete full contact). This can be attributed to the spherical shape of tip used in this investigation that caused a parabolic (non-flat) pressure distribution^{110,116}. This also further implies that the full intimate contact arose in the middle region, partial contact slowly spreading at the outer edges with increasing F_L ^{9,17}.

6.2.3 *Ludisia* Replica:

As illustrated and clearly evident in Figure 8.a, the real contact (the bright circular areas) always occurred at the very top periphery of the conical shaped micro-structures of the *Ludisia* replica, for the complete pre-load range (0.5-3.5 mN). Interestingly, one may note that, the real contact area was significantly lower than the apparent area, and thus is reducing A_n to 6.91% (at the full loading condition for $F_L = 1.5$ mN), owing to the specific conical shaped topography. A closer examination of *in-situ* video (supporting video 3 in additional data) for a whole test run revealed that the contact formation was continuous, and real and apparent contact grew locally and homogeneously circular in shape. The microstructures in middle region contributed more in bearing the contact pressure, as can be realised by noticing the larger size bright spots distributed in the middle area if compared to the outer side (Figure 8). This can be attributed to the *Hertzian* type pressure distribution given for two contacting bodies^{110,117}. This holds likewise for the whole F_L range investigated. As soon as the detachment step is initiated, each true contact periphery instantly started separating, without exhibiting any explicit contact hysteresis.

Further on, a local examination of the contact formation on *Ludisia* replica pointed out that, the attachment-detachment mechanism on an individual microstructure could be considered similar as to the contact on a smooth surface. It is meaningful to approximate this behaviour as an inverted case of a half-sphere pressed on a flat surface contact model. Here, at a small scale, the top of each cell tip of *Ludisia* replica behaves like a spherical asperity, that is locally forming contact against the almost flat surface of the probe. With analysing the surface topographies, average real contact densities and contact formation, one can assume, that at a defined pre-load, locally, a negligible coupling of elastic displacement from a cell microstructure to the neighbouring cells^{19,118}. Thus, we used an approach, that was nicely demonstrated by Romero *et al.* 2014 and Yashima *et al.* 2015, to validate the *Hertzian* contact theory at the local cell structures scale for *Ludisia* replica^{19,85}.

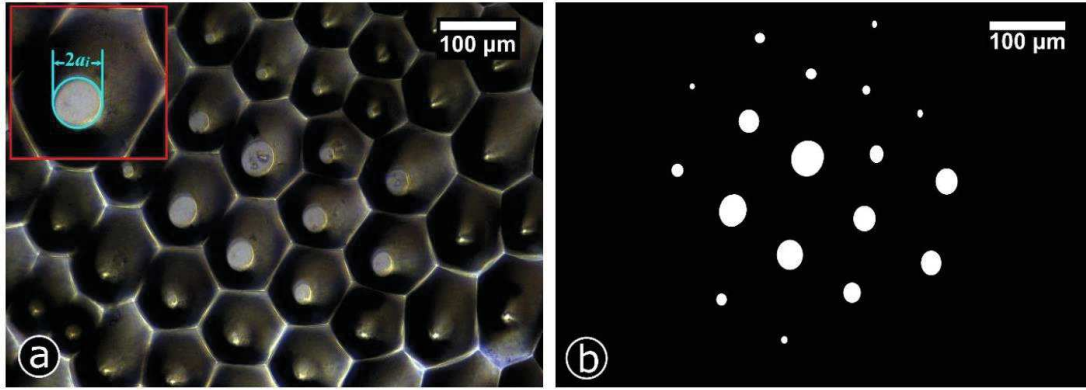


Figure 8 *In-situ* contact image for *Ludisia* replica at the full loading state for $F_L = 1.5\text{mN}$, clearly exhibiting the spatial distribution of micro-contact spots (a). Bright circular shaped spots on top of the conical structures represent the real contact area. The inset image in the upper left corner of the image indicates how the diameter ($2a$) of a real contact spot on top of a conical tip was estimated. (b) Shows the threshold image after image processing.

A standard contact state under *Hertzian* load condition for a sphere in contact with a half-space flat surface¹⁰³ can be computed using equation 1.

$$P_c = E^* \sum \frac{4 a_i^3}{3 R_i} \quad (1)$$

Here, E^* is the effective elastic modulus, which can be calculated using $E^* = E/2(1 - \nu^2)$; E is the Young's modulus and ν is the Poisson's ratio ($\nu_{PDMS} = 0.5$)^{83,86}. The E value for PDMS was calculated being 1.01 MPa by using the classical JKR model fitting on smooth PDMS substrate^{103,107}. R_i is the normalized radius of curvature of the circular cell tip of the *Ludisia* replica. a_i represents the radius of the local real contact forming at each individual tip (Figure 8.a), and was computed by locating real contact spots on the threshold image, as illustrated in Figure 8.b. F is the externally applied normal load, whereas P_c is the summation of inversely computed local (at real contact junctions) normal loads, assuming the *Hertzian* contact model obeyed locally. Using the equation 1, P_c was calculated at different load F states, for loading and unloading cycles. The P_c versus F results are plotted in Figure 9, and apparently loading and unloading data points found to be closely following a linear behaviour, with a R-square (coefficient of determination) value of 0.997.

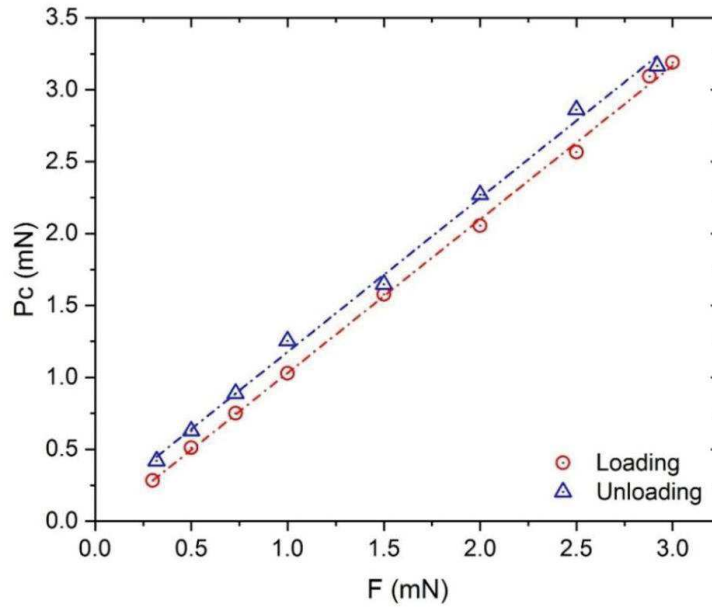


Figure 9 P_c versus F plot for the *Ludisia* replica surface. Linear slope and the overlapping of loading-unloading data points are validating the *Hertzian* contact theory locally. P_c = summation of local normal loads, F = applied load.

Moreover, P_c values for the unloading cycle perfectly trace back to zero, and nearly overlap with the loading curve, thus validating the assumption of the *Hertzian* local contact model for the *Ludisia* replica. Accordingly, our results are supporting the assumption of a negligible elastic couplings in between the neighbouring cells and that at this scale each asperity in contact can be considered as an individual non-adhesive contact.

Effect of pre-load: Here, the F_{ad} values found were the lowest if compared to all other surfaces investigated. For instance, at the pre-load condition of 1.5 mN, F_{ad} (0.014 mN) was reduced by about 98% in comparison to a smooth PDMS surface (0.809 mN). This reduction in F_{ad} followed same line for all F_L conditions. F_{ad} results as a function of F_L , are presented in Figure 10, clearly illustrating no notable variation in F_{ad} with increasing F_L . This could also be understood with the validation of the *Hertzian* contact model locally on each cell of the *Ludisia* replica surface and thus supports our assumption of non-adhesive contact at local scale. Our results suggest that loading and unloading at small scale can still be considered as quasi-static. The small asperity contacts behave similar as macro-ones but the small scale make the adhesion negligible.

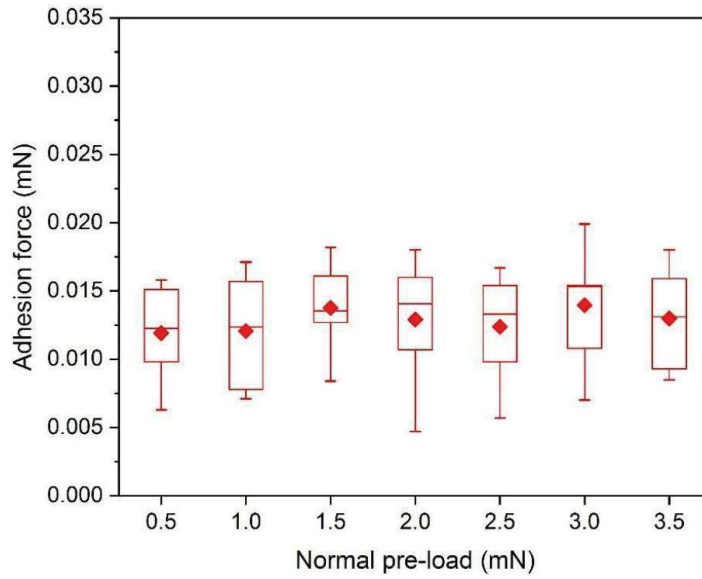


Figure 10 Variation in adhesion pull-off force (F_{ad}) with increasing applied normal pre-load (F_L) for *Ludisia* PDMS replicas, ($N = 6$).

6.2.4 *Litchi* Replica:

An *in-situ* video for a whole adhesion test cycle, on *Litchi* replica, at a F_L of 1.5 mN is presented in Video 4 (additional data). At first sight, contact mechanics appeared to be very complex, given the fact of the high complexity of surface microstructures of *Litchi* replica combined with the obvious video quality limitations. Indeed, one could point out that the *in-situ* videos on *Litchi* replica lacked in-detail clarity in comparison to other three surfaces, indicating towards the technical limitation of proposed technique for certain highly complex morphologies. Nevertheless, it was clearly visible that the real contacts (bright spots) were discretely distributed over the contact zone, related to the heterogeneous and random surface structuring. To gain a better understanding of the attachment mechanism, zoomed-in videos have been checked and the local contact zones were analysed. As soon as the loading event started, fine cuticular folds began to form partial top-contact. With further increase in pre-load, the overhanging fine structures (cuticular folds) of an individual ‘*rose-flower-shaped*’ unit accumulated together and started forming a localised cluster of units, as could be seen as close bright spots appearing in the *in-situ* video, at the fully loaded condition (dashed domain in Figure 11.II). After the full loading phase, a particular feature was observed during the retraction cycle: the sudden fluctuating behaviour and profile of the force-displacement curve, as presented in Figure 11.I, which called for further analysis. We believe, this specific behaviour visualised by the retraction curve can be attributed to the unique and complex structural morphology of the *Litchi* replicas, consisting of overhanging and undercut patterns. We further examined the *in-situ* video sequence corresponding to the position of major sudden fluctuations

on the force-displacement curve. This became possible thanks to the real-time image-data point synchronization. A series of *in-situ* contact images corresponding to various points of interest during the retraction part of the force-displacement curve are illustrated in Figure 11.II. This fluctuation behaviour could be understood by taking into account two energy factors: (1) the bending of overhanging patterns leading to localized storage of the elastic strain energy, and (2) the agglomeration of ‘*rose-flower-shaped*’ unit (micro-morphologies) gathered in a short range coupling style. During the unloading stage, the bended folds started popping out, and thus caused a sudden release of the stored elastic energy that acted against the adhesion force³⁴.

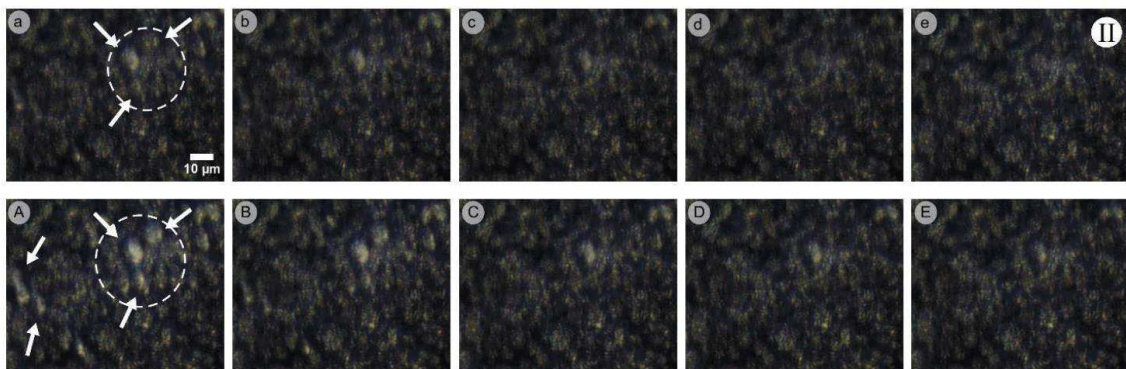
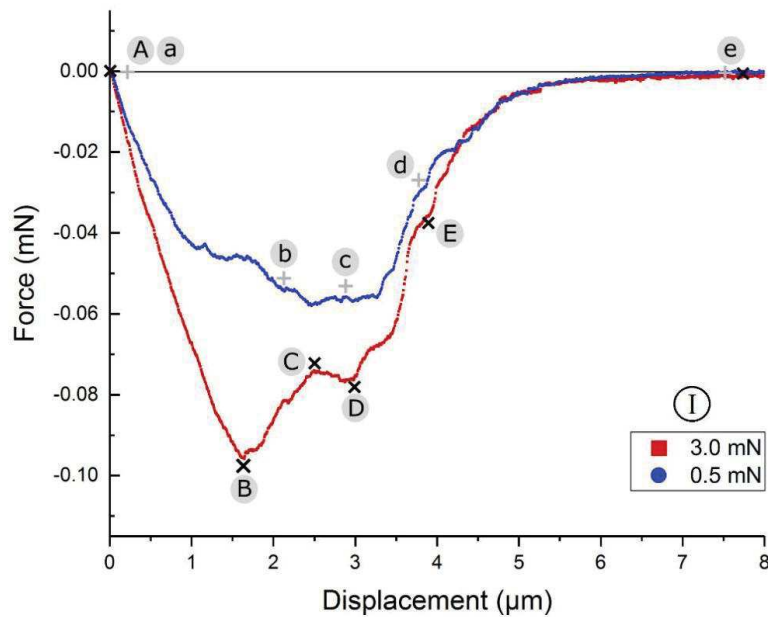


Figure 11. (I, upper part of the Figure) Diagram showing the retraction part of force-displacement curve for a *Litchi* replica sample, recorded at two different normal pre-loads, keeping all other parameters the same. (II, lower part of the figure), (a-e) and (A-E) sequences of *in-situ* contact images at high magnification, corresponding to the points marked on force-displacement curves. Images with label ‘a’ and ‘A’ correspond to contact state at the absolute zero load during unloading, for pre-load $F_L = 0.5$ and 3.0 mN respectively. White arrows in image a and A are pointing towards the high contrast region exhibiting an agglomeration of a bunch of cuticular folds on individual epidermal cells (*rose flower shaped*). Images ‘e’ represent non-contact image, being the same for both pre-load values. The scale bar corresponds for all images is 10 μm . Full video of both tests are given in additional data.

Since, these real contact morphologies are discretely distributed over the apparent contact space, thus individual agglomerated cluster released the stored energy locally with the instable separation. This behaviour appeared to be more force sensitive, and therefore, it was more pronounced and clearly visible at higher pre-load ($F_L = 3.0$ mN as compared to 0.5 mN), which can be seen in Figure 11.II. This might be attributed to similar force-dependence mechanism as found in *Hevea* replica (section 6.2.2).

Effect of pre-load: Figure 12 shows the results from the effect of F_L on F_{ad} characteristics for *Litchi* replicas. Clearly visible is an initial increase in F_{ad} with raising F_L , until 3.5 mN. Since, the previously described parameter range (F_L , 0.5-3.5 mN) did not provide enough information and no particular transition in adhesion force was observed, therefore, we continued the tests until $F_L = 5.0$ mN. By analysing the new pre-load range, F_{ad} appeared to get saturated with a minor variation from 4.0 mN onwards. This could be explained with the force sensitive phenomenon associated with the complex surface morphology of *Litchi* replicas previously discussed. At low F_L values, true contact formed partially only on the very top of overhanging micro-structures, whereas with increasing in F_L more real contact is formed leading to higher adhesion. One could note in the Figure 11.a and Figure 11.A, there was more true contact area for higher F_L (3.0 mN) as compared to low F_L (0.5 mN), at the absolute zero load condition when the normal load was completely removed during the unloading cycling.

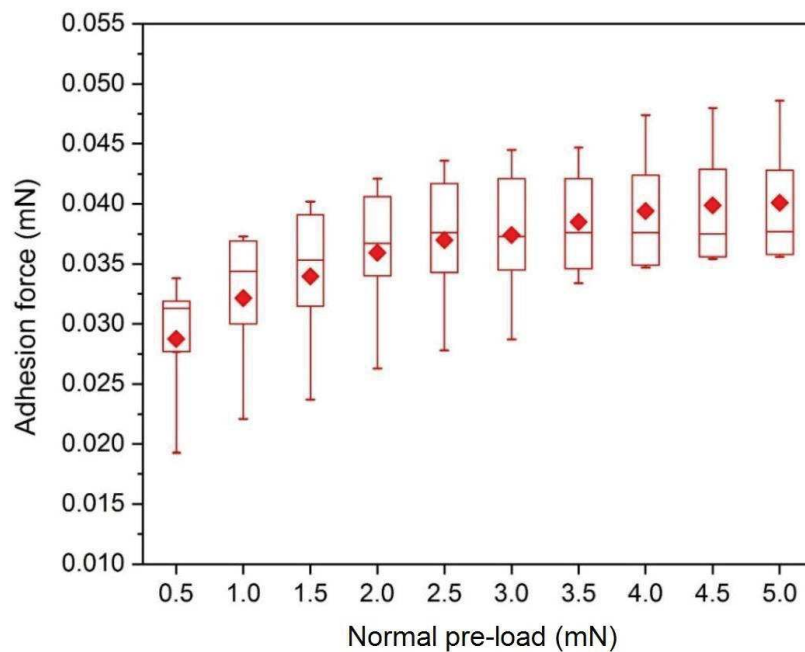


Figure 12 Plot of the variation of adhesion force (F_{ad}) with increasing applied normal pre-load (F_L) for *Litchi* replica samples, ($N = 5$). Plot shows an initial increase in F_{ad} which, however, gets saturated after 4.0 mN.

7 Overall Comparison and Conclusions:

In the present paper, a systematic study of adhesion contact mechanics at a low force range on high-precision transparent replicas of biological micro-structured surfaces is presented. For allowing such detailed investigation, we developed and successfully demonstrated an innovative technique for *in-situ* contact visualization, allowing the analysis of attachment-detachment mechanism on transparent replicas of complex biological surface morphologies. In this study we quantitatively evaluated experimentally the pull-off adhesion force of four distinct surfaces and also analysed its dependence to pre-load and surface morphology. Based on the key findings of this investigation the following conclusions can be drawn:

- A significant difference in F_{ad} between the all four surfaces was found, as presented in Figure 13, for $F_L = 1.5$ mN condition. Our data prove that the adhesion force follows the same trend for all other F_L conditions tested as well.

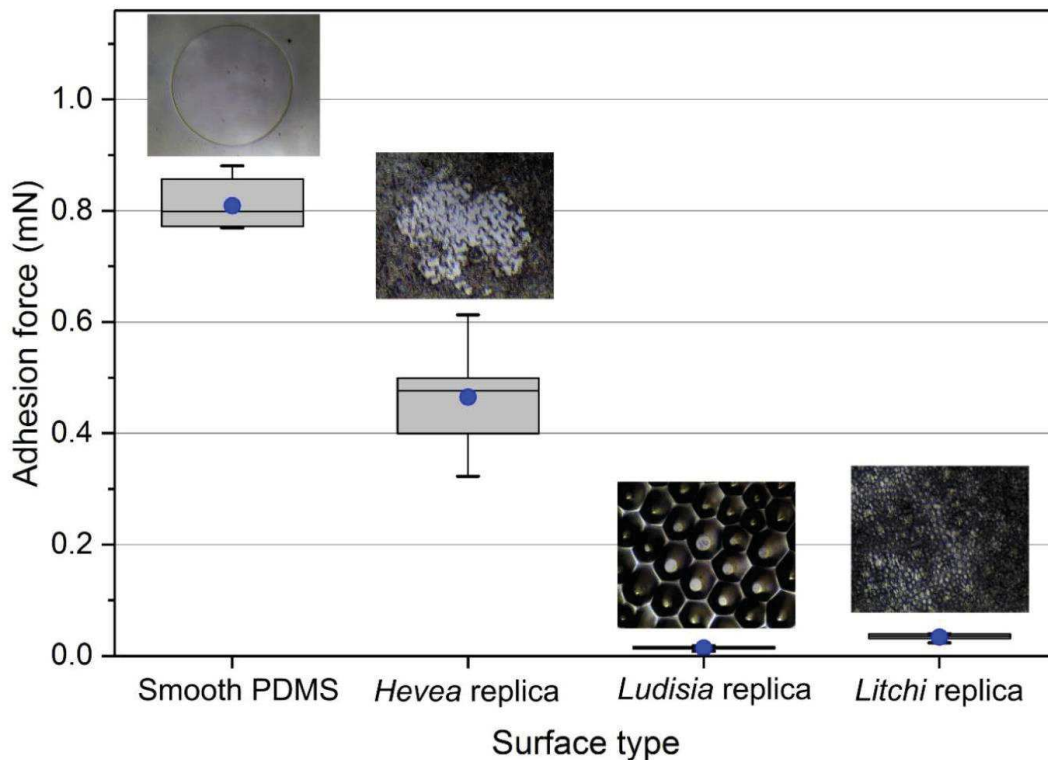


Figure 13 Overall comparison of adhesion pull-off force obtained for the four surfaces investigated, at a normal pre-load of 1.5 mN.

- Apparently, the smooth PDMS surface exhibited the highest value of adhesion force ($F_{ad} \approx 0.809$ mN, at $F_L = 1.5$ mN) out of all the four tested surfaces (Figure 13). On the surface with fine wrinkle shaped micro-structuring (*Hevea* replica) F_{ad} is reduced by 42.5 % (at $F_L = 1.5$ mN) in comparison to the smooth PDMS surface. However, the adhesion force of the *Hevea*

replica is still significantly higher in comparison to the other studied micro-structured surfaces. The surface showing coarse sized micro-structures (*Ludisia* replica) and the surface with complex hierarchical structuring (*Litchi* replica) both showed a markedly lower value of adhesion force, with $F_{ad} = 0.014$ mN and 0.035 mN respectively. The obvious reduction in adhesion force on micro-structured surfaces as compared to smooth PDMS could be attributed to the considerably low aspect ratio of patterns on the micro-structured surfaces tested. This differs to what has been demonstrated in some previous studies of adhesion enhancement by using soft and compliant fibrillar geometries with high aspect ratio^{30,33,62,119-121}.

- The investigation on the effect of pre-load demonstrated that F_{ad} enhanced for the surface of *Litchi* replicas and *Hevea* replicas by increasing in F_L . On the other hand, smooth PDMS and *Ludisia* replicas showed no influence of F_L on the adhesion force characteristics. The supposed underlying mechanism has been discussed.
- Due to the newly developed method of *in-situ* visualizations, the distribution of real contact zones reveals a high dependency from the size and morphologies of the surface structures and also exhibits distinct attachment and detachment phenomena.

The new methodological approach in contact visualisation and the results based thereon which are presented in this study – in our opinion – open up a promising direction in the understanding of contact formation on high-precision replicas of biological surface structures and by this of the biological structures themselves. This will be also of interest for the contact mechanics community in general to recognize specific adhesion phenomena arising from unique surface morphologies. The *in-situ* imaging technical advancement presented in this study could be relevant for performing real contact investigations on all kind of complex structured surfaces. Furthermore, the insights gained from this study may provide a valuable assistance for designing bio-inspired functional surfaces and for (fine-)tuning surface adhesion properties. In the future line, one could possibly assess the individual contribution of each level of hierarchical surface structuring on the adhesion force characteristics.

8 Competing Interests:

We have no competing interest.

9 Funding:

This work was financially supported by the German Research Foundation (Deutsche Forschungsgemeinschaft: DFG) under the framework of International Research Training Group (IRTG) ‘Soft Matter Science - 1642’.

10 Acknowledgements:

The authors would like to express their gratitude to the gardeners of botanical garden of the University of Freiburg for cultivating the plants used in this study. We are thankful to the electron microscopy platform of Institut Charles Sadron, Strasbourg for SEM imaging. We would also like to thank the German Research Foundation (Deutsche Forschungsgemeinschaft: DFG), for funding support under the framework of International Research Training Group (IRTG) ‘Soft Matter Science - 1642’.

11 References:

- (1) Scherge, M.; Gorb, S. *Biological micro-and nanotribology*; Springer Science & Business Media, 2001.
- (2) Bhushan, B. *Springer handbook of nanotechnology*; Springer Science & Business Media, 2010.
- (3) Kendall, K. *Molecular adhesion and its applications: the sticky universe*; Springer Science & Business Media, 2007.
- (4) Kaneko, R. Microtribology related to MEMS-Concept, measurements, applications. In *Proceedings. IEEE Micro Electro Mechanical Systems*; IEEE, 1991; p 108.
- (5) Myshkin, N.; Petrokovets, M.; Kovalev, A. Tribology of polymers: adhesion, friction, wear, and mass-transfer. *Tribology International* **2005**, *38*, 910–921.
- (6) Fischer-Cripps, A. C. *Introduction to contact mechanics*; Springer, 2000; Vol. 87.
- (7) Jin, C.; Khare, K.; Vajpayee, S.; Yang, S.; Jagota, A.; Hui, C.-Y. Adhesive contact between a rippled elastic surface and a rigid spherical indenter: from partial to full contact. *Soft Matter* **2011**, *7* (22), 10728.
- (8) Tas, N. R.; Gui, C.; Elwenspoek, M. Static friction in elastic adhesive MEMS contacts, models and experiment. In *Proceedings IEEE Thirteenth Annual International Conference on Micro Electro Mechanical Systems*; IEEE, 2000; pp 193–198.
- (9) Verneuil, E.; Ladoux, B.; Buguin, A.; Silberzan, P. Adhesion on microstructured surfaces. *The Journal of Adhesion* **2007**, *83* (5), 449–472.
- (10) Greiner, C.; Campo, A. del; Arzt, E. Adhesion of bioinspired micropatterned surfaces: effects of pillar radius, aspect ratio, and preload. *Langmuir* **2007**, *23*, 3495–3502.
- (11) Paretkar, D.; Kamperman, M.; Martina, D.; Zhao, J.; Creton, C.; Lindner, A.; Jagota, A.; McMeeking, R.; Arzt, E. Preload-responsive adhesion: effects of aspect ratio, tip shape and alignment. *Journal of The Royal Society Interface* **2013**, *10* (83), 20130171.
- (12) Fischer, S. C. L.; Arzt, E.; Hensel, R. Composite pillars with a tunable interface for adhesion to rough substrates. *Applied Materials & Interfaces* **2017**, *9* (1), 1036–1044.
- (13) Cañas, N.; Kamperman, M.; Völker, B.; Kroner, E.; McMeeking, R. M.; Arzt, E. Effect of nano- and micro-roughness on adhesion of bioinspired micropatterned surfaces. *Acta Biomaterialia* **2012**, *8*, 282–288.
- (14) Maboudian, R.; Ashurst, W. R.; Carraro, C. Self-assembled monolayers as anti-stiction coatings for MEMS characteristics and recent developments. *Sensors and Actuators* **2000**, *82*, 219–223.

- (15) Dirany, M.; Dies, L.; Restagno, F.; Léger, L.; Poulard, C.; Miquelard-Garnier, G. Chemical modification of PDMS surface without impacting the viscoelasticity: model systems for a better understanding of elastomer/elastomer adhesion and friction. *Colloids and Surfaces A: Physicochemical and Engineering Aspects* **2015**, *468*, 174–183.
- (16) Fuller, K.; Tabor, D. The effect of surface roughness on the adhesion of elastic solids. *Proceedings of the Royal Society of London. A, Mathematical and Physical Sciences* **1975**, *345* (1642), 327–342.
- (17) Hisler, V.; Palmieri, M.; Le Houérou, V.; Gauthier, C.; Nardin, M.; Vallat, M.-F.; Vonna, L. Scale invariance of the contact mechanics of micropatterned elastic substrates. *International Journal of Adhesion & Adhesives* **2013**, *45*, 144–149.
- (18) Purto, J.; Elena V. Gorb, M. S.; Gorb, S. N. Measuring of the hardly measurable adhesion properties of anti-adhesive surfaces. *Applied Physics A* **2013**, *111*, 183–189.
- (19) Yashima, S.; Romero, V.; Wandersman, E.; Frétiigny, C.; Chaudhury, M.; Chateauminois, A.; Prevost, A. Normal contact and friction of rubber with model randomly rough surfaces. *Soft Matter* **2015**, *11* (5), 871–881.
- (20) Degrandi-Contraires, É.; Beaumont, A.; Restagno, F.; Weil, R.; Poulard, C.; Léger, L. Cassie-Wenzel-like transition in patterned soft elastomer adhesive contacts. *Europhysics Letters* **2013**, *101* (1), 14001.
- (21) Dies, L.; Restagno, F.; Weil, R.; Léger, L.; Poulard, C. Role of adhesion between asperities in the formation of elastic solid/solid contacts. *The European Physical Journal E* **2015**, *38* (12), 130.
- (22) Castellanos, G.; Arzt, E.; Kamperman, M. Effect of viscoelasticity on adhesion of bioinspired micropatterned epoxy surfaces. *Langmuir* **2011**, *27* (12), 7752–7759.
- (23) Davis, C. S.; Martina, D.; Creton, C.; Lindner, A.; Crosby, A. J. Enhanced adhesion of elastic materials to small-scale wrinkles. *Langmuir* **2012**, *28* (42), 14899–14908.
- (24) Rahmawan, Y.; Chen, C.-M.; Yang, S. Recent advances in wrinkle-based dry adhesion. *Soft Matter* **2014**, *10* (28), 5028–5039.
- (25) Davis, C. S.; Crosby, A. J. Mechanics of wrinkled surface adhesion. *Soft Matter* **2011**, *7* (11), 5373–5381.
- (26) Breid, D.; Crosby, A. J. Effect of stress state on wrinkle morphology. *Soft Matter* **2011**, *7* (9), 4490–4496.
- (27) Martina, D.; Creton, C.; Damman, P.; Jeusette, M.; Lindner, A. Adhesion of soft viscoelastic adhesives on periodic rough surfaces. *Soft Matter* **2012**, *8* (19), 5350–5357.
- (28) Briggs, G.; Briscoe, B. The effect of surface topography on the adhesion of elastic solids. *Journal of Physics D: Applied Physics* **1977**, *10* (18), 2453.
- (29) Heepe, L.; Kovalev, A. E.; Gorb, S. N. Direct observation of microcavitation in underwater adhesion of mushroom-shaped adhesive microstructure. *Beilstein Journal of Nanotechnology* **2014**, *5* (1), 903–909.
- (30) Lamblet, M.; Verneuil, E.; Buguin, A.; Silberzan; Léger, L. Adhesion enhancement through micropatterning at polydimethylsiloxane-acrylic adhesive interfaces. *Langmuir* **2007**, *23*, 6966–6974.
- (31) Peressadko, A.; Hosoda, N.; Persson, B. Influence of surface roughness on adhesion between elastic bodies. *Physical Review Letters* **2005**, *95* (12), 124301.
- (32) Tiwari, A.; Dorigin, L.; Bennett, A.; Schulze, K.; Sawyer, W.; Tahir, M.; Heinrich, G.; Persson, B. The effect of surface roughness and viscoelasticity on rubber adhesion. *Soft Matter* **2017**, *13* (19), 3602–3621.
- (33) Glassmaker, N. J.; Jagota, A.; Hui, C.-Y.; Noderer, W. L.; Chaudhury, M. K. Biologically inspired crack trapping for enhanced adhesion. *Proceedings of the National Academy of Sciences* **2007**, *104* (26), 10786–10791.
- (34) Fischer, S. C.; Groß, K.; Torrents Abad, O.; Becker, M. M.; Park, E.; Hensel, R.; Arzt, E. Funnel-shaped microstructures for strong reversible adhesion. *Advanced Materials Interfaces* **2017**, *4* (20), 1700292.
- (35) Kizilkan, E.; Gorb, S. N. Combined effect of the microstructure and underlying surface curvature on the performance of biomimetic adhesives. *Advanced Materials* **2017**.
- (36) Vajpayee, S.; Khare, K.; Yang, S.; Hui, C.-Y.; Jagota, A. Adhesion selectivity using rippled surfaces. *Advanced Functional Materials* **2011**, *21* (3), 547–555.

- (37) Persson, B.; Tosatti, E. The effect of surface roughness on the adhesion of elastic solids. *The Journal of Chemical Physics* **2001**, *115* (12), 5597–5610.
- (38) Arzt, E.; Gorb, S.; Spolenak, R. From micro to nano contacts in biological attachment devices. *Proceedings of the National Academy of Sciences* **2003**, *100* (19), 10603–10606.
- (39) Gorb, E. V.; Gorb, S. N. Contact mechanics at the insect-plant interface: how do insects stick and how do plants prevent this? In *IUTAM Symposium on Scaling in Solid Mechanics*; Borodich, F., Ed.; Springer, 2009; Vol. 10, pp 243–252.
- (40) Gorb, E. V.; Purtov, J.; Gorb, S. N. Adhesion force measurements on the two wax layers of the waxy zone in *Nepenthes alata* pitchers. *Scientific Reports* **2014**, *4*.
- (41) Gorb, S. N. Biological attachment devices: exploring nature's diversity for biomimetics. *Philosophical Transactions of the Royal Society of London A* **2008**, *366* (1870), 1557–1574.
- (42) Labonte, D.; Federle, W. Scaling and biomechanics of surface attachment in climbing animals. *Philosophical Transactions of the Royal Society B: Biological Sciences* **2015**, *370* (1661), 20140027.
- (43) Whitney, H. M.; Federle, W. Biomechanics of plant–insect interactions. *Current Opinion in Plant Biology* **2013**, *16*, 105–111.
- (44) Poppinga, S.; Koch, K.; Bohn, H. F.; Barthlott, W. Comparative and functional morphology of hierarchically structured anti-adhesive surfaces in carnivorous plants and kettle trap flowers. *Functional Plant Biology* **2010**, *37*, 952–961.
- (45) Prüm, B.; Bohn, H. F.; Seidel, R.; Rubach, S.; Speck, T. Plant surfaces with cuticular folds and their replicas: influence of microstructuring and surface chemistry on the attachment of a leaf beetle. *Acta Biomaterialia* **2013**, *9*, 6360–6368.
- (46) Prüm, B.; Seidel, R.; Bohn, H. F.; Speck, T. Plant surfaces with cuticular folds are slippery for beetles. *Journal of the Royal Society Interface* **2012**, *9*, 127–135.
- (47) Wang, L.; Zhou, Q. Surface hydrophobicity of slippery zones in the pitchers of two *Nepenthes* species and a hybrid. *Scientific Reports* **2016**, *6*, 19907.
- (48) Barthlott, W.; Mail, M.; Bhushan, B.; Koch, K. Plant surfaces: structures and functions for biomimetic innovations. *Nano-Micro Letters* **2017**, *9* (2), 23.
- (49) Koch, K.; Bhushan, B.; Barthlott, W. Diversity of structure, morphology and wetting of plant surfaces. *Soft Matter* **2008**, *4*, 1943–1963.
- (50) Koch, K.; Bohn, H. F.; Barthlott, W. Hierarchically sculptured plant surfaces and superhydrophobicity. *Langmuir* **2009**, *25*, 14116–14120.
- (51) Neinhuis, C.; Barthlott, W. Characterization and distribution of water-repellent, self-cleaning plant surfaces. *Annals of Botany* **1997**, *79*, 667–677.
- (52) Barthlott, W.; Ehler, N. Raster-elektronenmikroskopie der epidermis-oberflächen von spermatophyten. *Tropische und subtropische Pflanzenwelt* **1977**, *19*, 367–467.
- (53) Barthlott, W.; Mail, M.; Neinhuis, C. Superhydrophobic hierarchically structured surfaces in biology: evolution, structural principles and biomimetic applications. *Philosophical Transactions of the Royal Society A* **2016**, *374* (2073), 20160191.
- (54) Bhushan, B.; Jung, Y. C. Natural and biomimetic artificial surfaces for superhydrophobicity, self-cleaning, low adhesion, and drag reduction. *Progress in Materials Science* **2011**, *56* (1), 1–108.
- (55) Koch, K.; Bhushan, B.; Barthlott, W. Multifunctional surface structures of plants: an inspiration for biomimetics. *Progress in Materials Science* **2009**, *54* (2), 137–178.
- (56) Barthlott, W.; Neinhuis, C. Purity of the sacred lotus, or escape from contamination in biological surfaces. *Planta* **1997**, *202* (1), 1–8.
- (57) Bargel, H.; Barthlott, W.; Koch, K.; Schreiber, L.; Neinhuis, C. Plant cuticles: multifunctional interfaces between plant and environment. In *The evolution of plant physiology*; Hemsley, A. R., Poole, I., Eds.; Academic Press, London, 2004; pp 171–194.
- (58) Eder, M.; Amini, S.; Fratzl, P. Biological composites—complex structures for functional diversity. *Science* **2018**, *362* (6414), 543–547.
- (59) Bar-Cohen, Y. Biomimetics—using nature to inspire human innovation. *Bioinspiration & Biomimetics* **2006**, *1* (1), 1–12.
- (60) Bhushan, B. Bioinspired structured surfaces. *Langmuir* **2012**, *28*, 1698–1714.
- (61) Bhushan, B. Biomimetics: lessons from nature – an overview. *Philosophical Transactions of the Royal Society A* **2009**, *367*, 1445–1486.

- (62) Campo, A. del; Greiner, C.; Arzt, E. Contact shape controls adhesion of bioinspired fibrillar surfaces. *Langmuir* **2007**, *23*, 10235–10243.
- (63) Gorb, S.; Speck, T. Biological and biomimetic materials and surfaces. *Beilstein Journal of Nanotechnology* **2017**, *8*, 403–407.
- (64) Kroner, E.; Blau, J.; Arzt, E. Note: An adhesion measurement setup for bioinspired fibrillar surfaces using flat probes. *Review of Scientific Instruments* **2012**, *83* (1), 016101.
- (65) Barthlott, W.; Mail, M.; Bhushan, B.; Koch, K. Plant surfaces: structures and functions for biomimetic applications. In *Springer handbook of nanotechnology*; Springer Nature Switzerland AG, 2017; pp 1265–1305.
- (66) Busch, J.; Barthlott, W.; Brede, M.; Terlau, W.; Mail, M. Bionics and green technology in maritime shipping: an assessment of the effect of *Salvinia* air-layer hull coatings for drag and fuel reduction. *Philosophical Transactions of the Royal Society A* **2018**, *377* (2138), 20180263.
- (67) Prüm, B.; Seidel, R.; Bohn, H. F.; Speck, T. Impact of cell shape in hierarchically structured plant surfaces on the attachment of male Colorado potato beetles (*Leptinotarsa decemlineata*). *Beilstein Journal of Nanotechnology* **2012**, *3*, 57–64.
- (68) Kumar, C.; Palacios, A.; Surapaneni, V. A.; Bold, G.; Thielen, M.; Licht, E.; Higham, T. E.; Speck, T.; Le Houérou, V. Replicating the complexity of natural surfaces: technique validation and applications for biomimetics, ecology and evolution. *Philosophical Transactions of the Royal Society A* **2018**, *377* (2138), 20180265.
- (69) Kim, M.; Kim, K.; Lee, N. Y.; Kim, K.; Shin, K.; Kim, Y. S. A simple fabrication route to a highly transparent super-hydrophobic surface with a poly(dimethylsiloxane) coated flexible mold. *Chemical Communications* **2007**, 2237–2239.
- (70) Zhuang, G.; Kutter, J. P. Anti-stiction coating of PDMS moulds for rapid microchannel fabrication by double replica moulding. *Journal of Micromechanics and Microengineering* **2011**, *21* (10), 105020.
- (71) Zhu, X.; Chen, H.; Zhu, L.; Wang, H.; Zhang, W. FDTS and PDMS fabrication of curved microlens array using a drop-on-demand droplet generator and polydimethylsiloxane replica mold. *Optical Engineering* **2014**, *53*, 117109–9.
- (72) McDonald, B.; Shahsavan, H.; Zhao, B. Biomimetic micro-patterning of epoxy coatings for enhanced surface hydrophobicity and low friction. *Macromolecular Materials and Engineering* **2014**, *299*, 237–247.
- (73) Koerner, T.; Brown, L.; Xie, R.; Oleschuk, R. D. Epoxy resins as stamps for hot embossing of microstructures and microfluidic channels. *Sensors and Actuators B: Chemical* **2005**, *107* (2), 632–639.
- (74) Shao, G.; Jiahao Wu, Z. C.; Wang, W. Fabrication of elastomeric high-aspect-ratio microstructures using polydimethylsiloxane (PDMS) double casting technique. *Sensors and Actuators A* **2012**, *178*, 230–236.
- (75) Hassanin, H.; Mohammadkhania, A.; Jiang, K. Fabrication of hybrid nanostructured arrays using a PDMS/PDMS replication process. *Lab on a Chip* **2012**, *12*, 4160–4167.
- (76) Kumar, C.; Le Houérou, V.; Speck, T.; Bohn, H. F. Straightforward and precise approach to replicate complex hierarchical structures from plant surfaces onto soft matter polymer. *Royal Society Open Science* **2018**, *5* (4), 172132.
- (77) Koch, K.; Schulte, A. J.; Fischer, A.; Gorb, S. N.; Barthlott, W. A fast, precise and low-cost replication technique for nano- and high-aspect-ratio structures of biological and artificial surfaces. *Bioinspiration & Biomimetics* **2008**, *3*, 46002–46012.
- (78) Schulte, A. J.; Koch, K.; Spaeth, M.; Barthlott, W. Biomimetic replicas: transfer of complex architectures with different optical properties from plant surfaces onto technical materials. *Acta Biomaterialia* **2009**, *5* (6), 1848–1854.
- (79) Sun, M.; Luo, C.; Xu, L.; Ji, H.; Ouyang, Q.; Yu, D.; Chen, Y. Artificial lotus leaf by nanocasting. *Langmuir* **2005**, *21* (19), 8978–8981.
- (80) Pulsifer, D. P.; Lakhtakia, A. Background and survey of bioreplication techniques. *Bioinspiration & Biomimetics* **2011**, *6* (3), 031001.
- (81) Lee, S.-M.; Kwon, T. H. Mass-producible replication of highly hydrophobic surfaces from plant leaves. *Nanotechnology* **2006**, *17*, 3189–3196.
- (82) Poulard, C.; Restagno, F.; Weil, R.; Léger, L. Mechanical tuning of adhesion through micro-patterning of elastic surfaces. *Soft Matter* **2011**, *7* (6), 2543–2551.

- (83) Vaenkatesan, V.; Li, Z.; Vellinga, W.-P.; Jeu, W. H. de. Adhesion and friction behaviours of polydimethylsiloxane – A fresh perspective on JKR measurements. *Polymer* **2006**, *47* (25), 8317–8325.
- (84) Krick, B. A.; Vail, J. R.; Persson, B. N.; Sawyer, W. G. Optical in situ micro tribometer for analysis of real contact area for contact mechanics, adhesion, and sliding experiments. *Tribology Letters* **2012**, *45* (1), 185–194.
- (85) Romero, V.; Wandersman, E.; Debregeas, G.; Prevost, A. Probing locally the onset of slippage at a model multicontact interface. *Physical Review Letters* **2014**, *112* (9), 094301.
- (86) Charrault, E.; Gauthier, C.; Marie, P.; Schirrer, R. Experimental and theoretical analysis of a dynamic JKR contact. *Langmuir* **2009**, *25* (10), 5847–5854.
- (87) Chaudhury, M. K.; Whitesides, G. M. Direct measurement of interfacial interactions between semispherical lenses and flat sheets of poly (dimethylsiloxane) and their chemical derivatives. *Langmuir* **1991**, *7* (5), 1013–1025.
- (88) Morishita, Y.; Morita, H.; Kaneko, D.; Doi, M. Contact dynamics in the adhesion process between spherical polydimethylsiloxane rubber and glass substrate. *Langmuir* **2008**, *24* (24), 14059–14065.
- (89) Drechsler, P.; Federle, W. Biomechanics of smooth adhesive pads in insects: influence of tarsal secretion on attachment performance. *Journal of Comparative Physiology A* **2006**, *192*, 1213–1222.
- (90) Bullock, J. M. R.; Drechsler, P.; Federle, W. Comparison of smooth and hairy attachment pads in insects friction, adhesion and mechanisms for direction-dependence. *The Journal of Experimental Biology* **2008**, *211*, 3333–3343.
- (91) Carrillo, F.; Gupta, S.; Balooch, M.; Marshall, S. J.; Marshall, G. W.; Pruitt, L.; Puttlitz, C. M. Nanoindentation of polydimethylsiloxane elastomers: Effect of crosslinking, work of adhesion, and fluid environment on elastic modulus. *Journal of Materials Research* **2005**, *20* (10), 2820–2830.
- (92) Nohava, J.; Randall, N.; Conté, N. Novel ultra nanoindentation method with extremely low thermal drift: Principle and experimental results. *Journal of Materials Research* **2009**, *24* (3), 873–882.
- (93) Ebenstein, D. M.; Pruitt, L. A. Nanoindentation of biological materials. *Nano Today* **2006**, *1* (3), 26–33.
- (94) Mata, A.; Fleischman, A. J.; Roy, S. Characterization of polydimethylsiloxane (PDMS) properties for biomedical micro/nanosystems. *Biomedical Microdevices* **2005**, *7* (4), 281–293.
- (95) Ghatak, A.; Vorvolakos, K.; She, H.; Malotky, D. L.; Chaudhury, M. K. Interfacial rate processes in adhesion and friction. *Journal of Physical Chemistry B* **2000**, *104*, 4018–4030.
- (96) Schneider, F.; Draheim, J.; Kamberger, R.; Wallrabe, U. Process and material properties of polydimethylsiloxane (PDMS) for Optical MEMS. *Sensors and Actuators A: Physical* **2009**, *151* (2), 95–99.
- (97) Kroner, E.; Paretkar, D. R.; McMeeking, R. M.; Arzt, E. Adhesion of flat and structured PDMS samples to spherical and flat probes: a comparative study. *The Journal of Adhesion* **2011**, *87* (5), 447–465.
- (98) Perutz, S.; Kramer, E. J.; Baney, J.; Hui, C.-Y.; Cohen, C. Investigation of adhesion hysteresis in poly(dimethylsiloxane) networks using the JKR technique. *Journal of Polymer Science, Part B: Polymer Physics* **1998**, *36* (12), 2129–2139.
- (99) Amouroux, N.; Léger, L. Effect of dangling chains on adhesion hysteresis of silicone elastomers, probed by JKR test. *Langmuir* **2003**, *19* (4), 1396–1401.
- (100) Deruelle, M.; Tirrell, M.; Marciano, Y.; Hervet, H.; Léger, L. Adhesion energy between polymer networks and solid surfaces modified by polymer attachment. *Faraday Discussions* **1994**, *98*, 55–65.
- (101) Neinhuis, C.; Edelman, H. G. Methanol as a rapid fixative for the investigation of plant surfaces by SEM. *Journal of Microscopy* **1996**, *184*, 14–16.
- (102) Talbot, M. J.; White, R. G. Methanol fixation of plant tissue for scanning electron microscopy improves preservation of tissue morphology and dimensions. *Plant Methods* **2013**, *9* (1), 36.
- (103) Johnson, K.; Kendall, K.; Roberts, A. Surface energy and the contact of elastic solids. *Proceedings of the Royal Society of London. A. Mathematical and Physical Sciences* **1971**, *324* (1558), 301–313.

- (104) Allen, R.; David, G. The Zeiss-Nomarski differential interference equipment for transmitted-light microscopy. *Zeitschrift für wissenschaftliche Mikroskopie und mikroskopische Technik* **1969**, *69* (4), 193–221.
- (105) Salmon, E.; Tran, P. High-resolution video-enhanced differential interference contrast light microscopy. *Methods in Cell Biology* **2007**, *81*, 335–364.
- (106) Gupta, S.; Carrillo, F.; Li, C.; Pruitt, L.; Puttlitz, C. Adhesive forces significantly affect elastic modulus determination of soft polymeric materials in nanoindentation. *Materials Letters* **2007**, *61* (2), 448–451.
- (107) Deruelle, M.; Hervet, H.; Jandeau, G.; Léger, L. Some remarks on JKR experiments. *Journal of Adhesion Science and Technology* **1998**, *12* (2), 225–247.
- (108) Gacoin, E.; Frétygny, C.; Chateauinois, A.; Perriot, A.; Barthel, E. Measurement of the mechanical properties of thin films mechanically confined within contacts. *Tribology Letters* **2006**, *21* (3), 245.
- (109) Burger, W.; Burge, M. J. *Digital image processing: an algorithmic introduction using Java*; Springer, 2016.
- (110) Greenwood, J.; Johnson, K. The mechanics of adhesion of viscoelastic solids. *Philosophical Magazine A* **1981**, *43* (3), 697–711.
- (111) Maugis, D. Adhesion of spheres: the JKR-DMT transition using a Dugdale model. *Journal of Colloid and Interface Science* **1992**, *150* (1), 243–269.
- (112) Horn, R. ; Israelachvili, J. ; Pribac, F. Measurement of the deformation and adhesion of solids in contact. *Journal of Colloid and Interface Science* **1986**, *115* (2), 480–492.
- (113) Paretkar, D.; Kamperman, M.; Schneider, A. S.; Martina, D.; Creton, C.; Arzt, E. Bioinspired pressure actuated adhesive system. *Materials Science and Engineering: C* **2011**, *31* (6), 1152–1159.
- (114) Cao, Y.; Yang, D.; Soboyejoy, W. Nanoindentation method for determining the initial contact and adhesion characteristics of soft polydimethylsiloxane. *Journal of Materials Research* **2005**, *20* (08), 2004–2011.
- (115) Dorogin, L.; Tiwari, A.; Rotella, C.; Mangiagalli, P.; Persson, B. Role of preload in adhesion of rough surfaces. *Physical Review Letters* **2017**, *118* (23), 238001.
- (116) Johnson, K. Adhesion and friction between a smooth elastic spherical asperity and a plane surface. *Proceedings of the Royal Society of London. Series A: Mathematical, Physical and Engineering Sciences* **1997**, *453* (1956), 163–179.
- (117) Hertz, H.; Reine, J. Original Hertzian mechanics ref. *Journal of Applied Mathematics and Mechanics* **1882**, *92*, 156.
- (118) Greenwood, J.; Williamson, J. P. Contact of nominally flat surfaces. *Proceedings of the Royal Society of London. Series A. Mathematical and Physical Sciences* **1966**, *295* (1442), 300–319.
- (119) Gorb, S.; Varenberg, M.; Peressadko, A.; Tuma, J. Biomimetic mushroom-shaped fibrillar adhesive microstructure. *Journal of the Royal Society Interface* **2007**, *4*, 271–275.
- (120) Huber, G.; Gorb, S. N.; Hosoda, N.; Spolenak, R.; Arzt, E. Influence of surface roughness on gecko adhesion. *Acta Biomaterialia* **2007**, *3* (4), 607–610.
- (121) Hui, C.-Y.; Glassmaker, N.; Tang, T.; Jagota, A. Design of biomimetic fibrillar interfaces: 2. Mechanics of enhanced adhesion. *Journal of The Royal Society Interface* **2004**, *1* (1), 35–48.

6.4 Manuscript D

1 Title:

Friction during adhesive contacts on complex micro-structured surfaces

2 Authors and affiliations:

Charchit Kumar^{1,2,3}, Thomas Speck^{2,3}, and Vincent Le Houérou^{1,4}

¹ Institut Charles Sadron (ICS), CNRS UPR022, University of Strasbourg, Strasbourg, France

² Plant Biomechanics Group (PBG) Freiburg, Botanic Garden of the University of Freiburg
Germany

³ Freiburg Center for Interactive Materials and Bio-Inspired Technologies (FIT), Germany

⁴ ICube, University of Strasbourg, CNRS UMR7357, Strasbourg, France

ORCID IDs:

C. Kumar- 0000-0002-6912-3506

T. Speck- 0000-0002-2245-2636

V. Le Houérou- 0000-0001-7189-242X

3 Abstract:

Friction characteristics are of prior importance, in technical as well as in biological systems. In this paper, we report on the friction investigation on biological micro-structured surfaces. Taking advantage of recent development on bio-replication techniques, complex and diverse surface morphologies from fresh plant leaves were directly transferred onto a soft viscoelastic polymer (PDMS). A nano-indenter setup was modified and used to perform sliding friction measurements, at a low force range configuration, on each polymeric replica and a smooth surface, forming contact with a model soft tip. Visualization and recording of real contact junctions during the sliding tests were accomplished with an original optical imaging system. Tests were carried out to study the effect of applied normal load and sliding speed on the friction characteristics. Consistent with previous studies, all four surfaces demonstrated a decrease in friction coefficient with increasing the normal load, however, each surface exhibited dissimilar decreasing behaviours. Analysis of *in-situ* videos revealed different types of real contact evolution under shearing, which originating from surface specific micro-structuring. Furthermore, our investigation results demonstrated a clear increase in friction coefficient with raising the sliding speed (frequency), although each surface showed a different rate of friction growth, attributing to their surface morphologies.

Keywords: plant leaves, micro-structures, sliding friction, PDMS, in-situ imaging, and real contacts

4 Introduction:

Frictional characteristics of interacting bodies have been a subject of great importance, as of its wide presence in a broad range of technical applications: head-disk interface in data storage drives, belts of conveyors, tires interaction against the road, rubber seals, piston rings just to name a few [1, 2]. Moreover, in all these systems, friction properties of contacting surfaces have a profound impact on their efficiency and durability. In the past several decades, surface micro- and/or nano-structuring (apart from modifying the surface chemistry) has been widely studied and well recognised as a key factor, to precisely adjust the frictional characteristics [3–8]. In most studies, a reduction in sliding friction was observed as that of a smooth surface, majorly accounting to incorporated surface patterning that led to a decrease in the true contact area as compared to the apparent area [6, 9–11]. However, a large work in this domain has primarily focused on technically developed micro-structured surfaces with defined morphologies (pillars, wrinkles, spherical dimples, squares, etc.) [9–13].

On the other hand, if we look into nature, friction plays a significant role, in particular, the interaction of biological systems between each other (e.g. feeding insects or pollinating) or with the inanimate environment [14–16]. Interestingly and inspiring both, on one side many plants possess surfaces markedly reducing insect attachment [17, 18], whereas on the other side, attachment system of insects evolved in a unique manner, so that they facilitate the insects to consciously attach-detach with, climb on or walk over different plant surfaces [19–22]. Notably, on plant leaf surfaces, highly diverse and unique surface structures with distinct shapes, of different size and at various hierarchical levels have evolved, that optimising their surface functionalities like: the slippery surface of carnivorous plants for insects trapping or drag reducing fern of *Salvinia molesta*, for example [18, 23–28]. However, one has to keep in mind that all these biological surface phenomena come from a complex interplay of surface structuring at different levels and the surface chemistry, therefore making them a complex system to investigate [17, 25, 29]. In a way, a simplification could be to transfer the surface morphologies onto to a standard material, allowing to make a systematic study which could underline the actual role of the surface structuring, independently to material surface chemistry [17, 30, 31]. Same could be accomplished for the counter system as well, that is the attachment system of insects which can be reasonably replaced by a model adhesive probe. Another important aspect to take into consideration is a realistic force range that closely follows the same scale (few mN) as of insect-plant interactions [19, 21, 32].

Moreover, from the engineering point of view, the great morphological richness of plant leaf surfaces may offer a great source to employ these structures directly for friction mechanics

studies: to grow a systematic understanding of new behaviour that resulting from complex though highly unique surface morphologies, and later on to develop a meaningful model system [29, 33–36]. In this line, the *in-situ* imaging could be an important tool to acquire greater insight into the real contact dynamics and its local exploration [37].

Considering the contexts outlined above, in this work, we present a systematic study of the friction mechanics on soft polymeric replicas, which consist of highly complex and diverse biological morphologies (different size: 0.5-100 μm , distinct shapes and hierarchical levels) against a model adhesive tip. A smooth surface was included in investigated samples as a model surface. All friction measurements were carried in unidirectional sliding configuration, with incorporating an original *in-situ* visualization of real contact junctions. In the first part, we examined the effect of applied normal load on friction characteristics, and alongside analysed the real contact dynamics under shearing and the local contribution of different micro-structures on friction behaviour. In the next part, we reported the sliding speed dependence of friction response and correlated with the material's loss factor over the same frequency range.

5 Experimental:

5.1 Investigated biological surfaces:

In this work, we focused on three different plant leaf surfaces, which were previously chosen and utilised by Kumar *et al.* (manuscript C [38]) for adhesion investigations. These plant leaves were chosen by considering the size, morphology and complexity of their surface micro-structures: coarse size conical shape patterns (50-100 μm) on *Ludisia discolor*, very fine fold like microstructures ($\approx 1 \mu\text{m}$) on *Hevea brasiliensis*, and complex hierarchical topographies comprising undercuts and overhanging patterns on *Litchi chinensis* [18, 39]. All plant species used in this investigation were collected from the Botanic Garden of the University of Freiburg. All plant leaf samples were freshly picked right before the replication procedure, to avoid any dehydration artefact.

5.2 Fabrication of PDMS replicas and smooth surface:

Recently, researchers demonstrated that the elastic modulus of plant leaves fall on a scale of few MPa, nevertheless leaves are made up of a complex material composition [40, 41]. Regarding, a close inspiration from plant leaf-insect interactions, one may note that PDMS (Polydimethylsiloxane), a widely used soft elastomer, seems appropriate material for such friction investigation, with following key advantages: extremely low elastic modulus ($E \approx 0.5-$

4 MPa, alter with varying the monomer to cross-linker ratio), low glass transition temperature (-120 °C), a low surface energy (22 mJ m⁻²), strong chemical stability, easy handling and non-toxicity [8, 42, 43]. Moreover, considering the requirements to accomplish *in-situ* visualization on highly complex biological morphologies, PDMS emerged out as an effective and realistic choice, with its high optical transparency over the wide range of UV light [44]. Taking account of the final replica's characteristics, development of polymeric replicas of all three plant leaf surfaces mentioned above was achieved by following a two-step replication technique described in detail by Kumar *et al.* [39], and shown to be suitable for this purpose [45]. Surface topographies of original plant leaves were precisely replicated onto the PDMS (Bluesil ESA 7250 A & B kit, Bluestar Silicones GmbH, Leverkusen, Germany) polymer. In addition, smooth PDMS specimens were developed by curing the PDMS mixture in a glass petri dish. All the samples (bulk substrates with a thickness of about 2 mm) were treated overnight in a solution of n-heptane and 1-dodecanethiol (0.01 %) to extract the unreacted free chains [46, 47].

5.3 Surface characterization

The morphology of the plant leaf surfaces and their PDMS replicas were examined using scanning electron microscopy (Leo 435 vp, Leica, Wiesbaden, Germany and Hitachi SU8010, UHR FE-SEM, France). In the case of plant leaves, samples were prepared by following fixation protocol in methanol solution and dried by using critical point drier (LPD 030, Bal-Tec) [48, 49]. Samples were mounted on aluminium stubs (Plano GmbH, Wetzlar, Germany), and their side walls were coated with conductive silver paint (Acheson Silver DAG 1415M, Plano GmbH, Wetzlar, Germany). All samples were sputter coated with a thin film (approximately 10 nm) of gold (Cressington Sputter Coater, 108 auto) and examined in the SEM at 30°- 45° range tilting angle.

5.4 Friction force apparatus:

Figure 1 shows a simplified scheme of the experimental device used in this study, to perform friction force measurements. An ultra-nanoindentation tester (UNHT³, Anton Paar Tritec, Switzerland) was modified to do the uni-directional linear sliding friction tests along with the *in-situ* real contact visualization. In this friction apparatus, the adhesive tip was kept fix, while the sample was moving for sliding motion. In order to perform the *in-situ* real contact visualization, a dedicated optical system was home- built and incorporated into the equipment. In-details description about *in-situ* visualization technique can be found in a previous work [38]. A custom-build electronic system was also inducted into the friction apparatus that facilitated the synchronization of the video frames with the corresponding force data points. A model

adhesive tip, PDMS half sphere of 1.5 mm radius, was fabricated with specific features to fulfill the optical necessities for *in-situ* visualization. The tip fabrication technique is described in detail elsewhere (Manuscript C [38]).

For the friction test, a sample was first mounted on the frictional translation platform, after fixing it on a supporting transparent glass plate, as shown in Figure 1. Before each set of friction tests, the sample surface and the adhesive tip (hereinafter referred to as the tip) was gently cleaned with Isopropyl alcohol and dried with pressurized air. Perfect balancing of the double cantilever beams was performed after fixing the tip with the force head. The tip was slowly brought in a close proximity to the sample surface, and then the tip gradually started forming the solid-solid contact until the given normal load (F_n) was reached. At this stage, the focus of objective lens was adjusted manually for sharp real contact view. Subsequently, the sliding step was triggered to move the friction stage at a pre-set sliding speed (V) for a sliding distance of 2500 μm . This apparatus allows to maintain the normal load constant, throughout the sliding distance. The tangential friction force (F_t) and normal load response in between the tip and sample surface were measured and recorded at an acquisition rate of 100 Hz. As the micro-structured surfaces contain a highly irregular height distribution, therefore the objective lens focus needs to be adjusted at different stages during the sliding. All the friction measurements were carried out in a climate controlled room at a temperature of $22 \pm 3^\circ\text{C}$ and a relative humidity of $50\% \pm 10\%$.

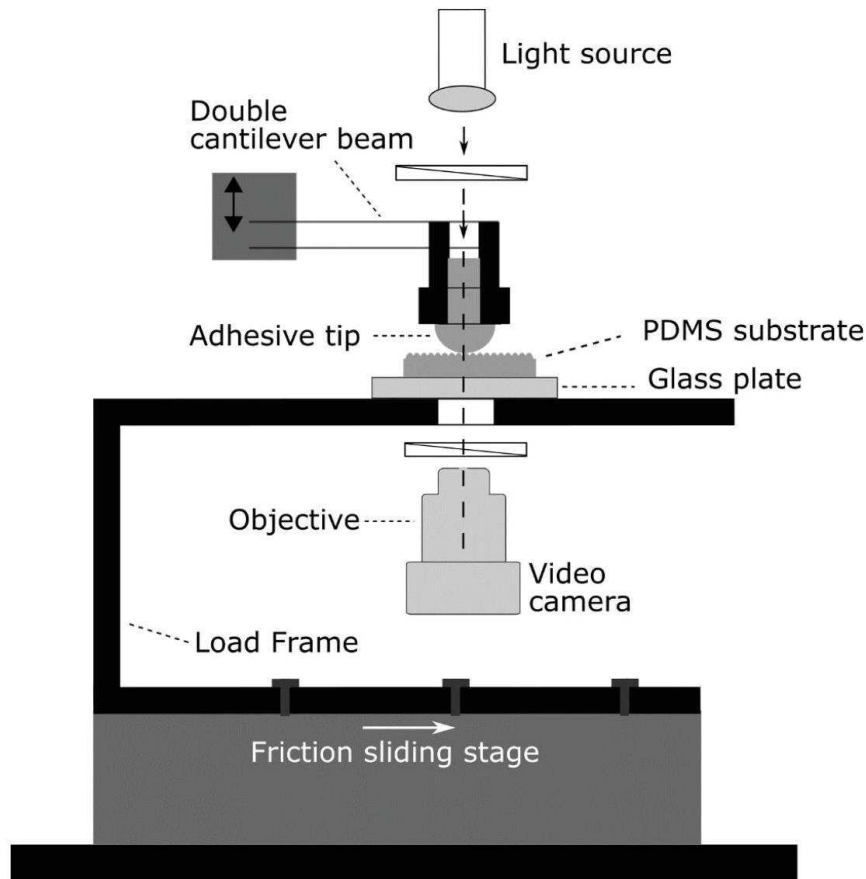


Figure 1. Simplified drawing of the friction force tester with *in-situ* real contact visualization used in this study. The sample was mounted on the sliding stage, which provides fine controlled motion. Friction force in tangential direction was recorded with a double cantilever beam sensor. A white light was shined at the tip opening after passing through optical lenses. A long working distance objective lens along with a high definition colour camera system was placed under the glass plate holding the sample.

6 Results and discussion:

6.1 Surface morphology of PDMS replicas:

PDMS replicas from all three plant leaf surfaces were replicated by following a two-step replication (Epoxy- PDMS) technique presented in a previous research [39]. This technique is proved to produce plant leaf replicas on PDMS elastomer with good precision and high fidelity [45]. SEM surface micrographs of all three PDMS replicas after doing the n-heptane treatment are presented in Figure 2. The SEM investigation confirmed that all the replicas were developed precisely from plant leaves, and also all three PDMS replicas perfectly maintained their topographies after performing the n-heptane treatment that includes swelling and de-swelling phases. Hereafter, only genus names are used when referring any PDMS replica sample, instead of full species name: *Ludisia* replica for the PDMS replica of *L. discolor*, *Hevea* replica for *H. brasiliensis*, and *Litchi* replica for *L. chinensis*.

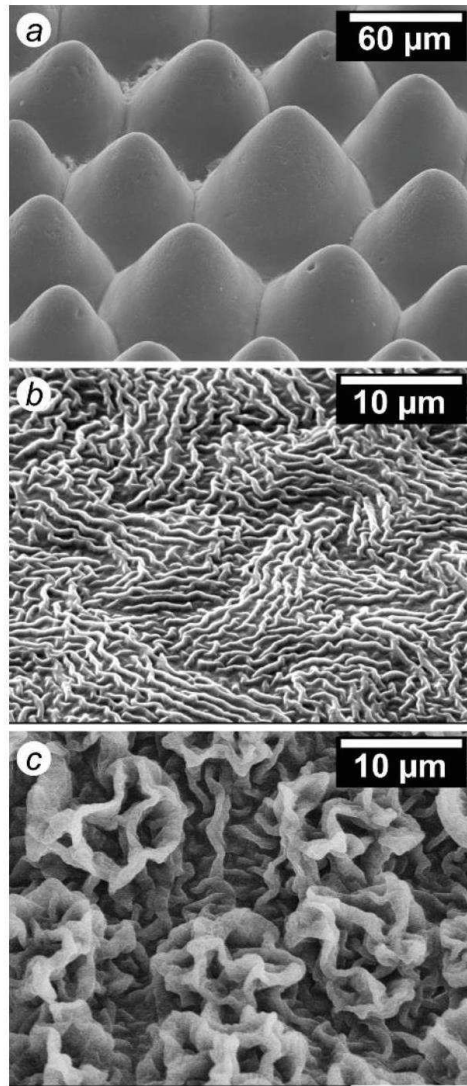


Figure 2. Scanning electron microscope image of PDMS replicas, which were replicated directly from the original plant leaves, by following a two-step replication technique (Epoxy-PDMS). (a) *Ludisia discolor* (adaxial side) with circular cone-like topographies, (b) *Hevea brasiliensis* (adaxial surface) exhibits very fine wrinkle shaped folds and (c) *Litchi chinensis* (abaxial surface) surface shows highly complex hierarchical patterns.

6.2 Friction force characteristics:

Friction investigations were performed on each PDMS replica and on the smooth PDMS surface. Experiments were conducted at 6 different spots on different samples for each surface type. A representative coefficient of friction (with normal and friction forces) *versus* sliding distance graph obtained for a typical friction experiment is shown in Figure 3. The coefficient of friction (COF) was estimated by following the Coulomb's friction law, $\text{COF} = \text{tangential friction force } (F_t) / \text{normal force } (F_n)$ [50]. In the first part, to investigate the effect of normal

load on friction force characteristics, tests were conducted for six different F_n : 0.5, 1.5, 2.5, 3.5, 4.5 and 5.5 mN, at a constant sliding speed of 16.67 $\mu\text{m/s}$. In the second part, the sliding speed influence on friction response was studied by varying the sliding velocity over three decades, $V= 1.67, 8.34, 16.67, 41.67, 83.34, 166.67, 416.67$ and 833.34 $\mu\text{m/s}$, keeping the normal load constant ($F_n = 1.5$ mN). All tests were always performed over a constant sliding distance (2500 μm). To calculate the average friction coefficient, data points were considered only in the kinetic region (after 750 μm sliding distance), as marked in Figure 3. In next two subsections, firstly the results of effect of the normal load and analysis of real contact dynamics, and later the sliding speed influence on friction characteristics are presented and discussed.

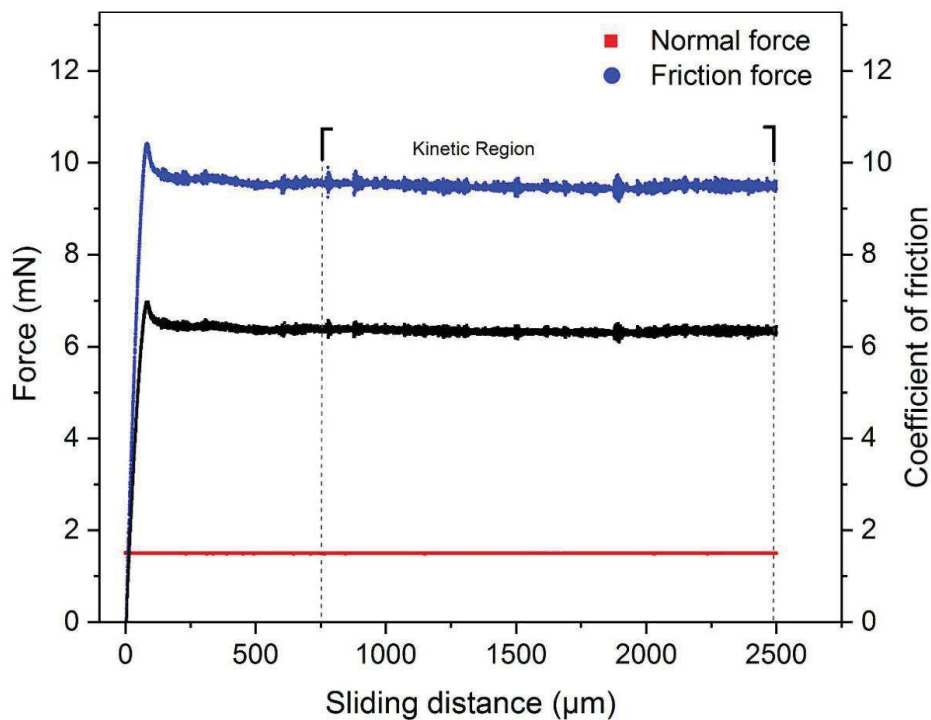


Figure 3. Representative graph of a typical friction force measurement on smooth PDMS sample, at a sliding speed of 16.67 $\mu\text{m/s}$. The coefficient of friction was calculated as a ratio of the recorded friction force to the controlled normal force.

6.2.1 Effect of the normal load and real contact dynamics:

Figure 4 shows a representative result obtained for the effect on friction response of the variation of the normal force, on all four surfaces: smooth surface, *Hevea* replica, *Ludisia* replica and *Litchi* replica. Box-plots, next to each plot, represent the mean, minima and maxima of COF values, which were calculated by computing the data points in the kinetic region. One has to keep in mind the different scaling of x-axis on all four graphs presented in Figure 4.

Comparing all the four substrates together (for a same normal load and sliding speed condition), clearly the smooth PDMS surface demonstrated the highest value of average friction coefficient (COF = 6.37, at a normal load of 1.5 mN). As one can notice in Figure 4, for each substrate the COF was found to be evidently decreasing with an increase in the normal load. However, the rate of reduction in friction coefficient changes from one to other surfaces. Figure 5 shows the *in-situ* real contact visual at different stages during sliding tests on each surface, at a normal load of 1.5 mN and a constant sliding speed of 16.67 $\mu\text{m/s}$. Full videos for the entire test cycle can be found in supporting data (Videos 1 to 4).

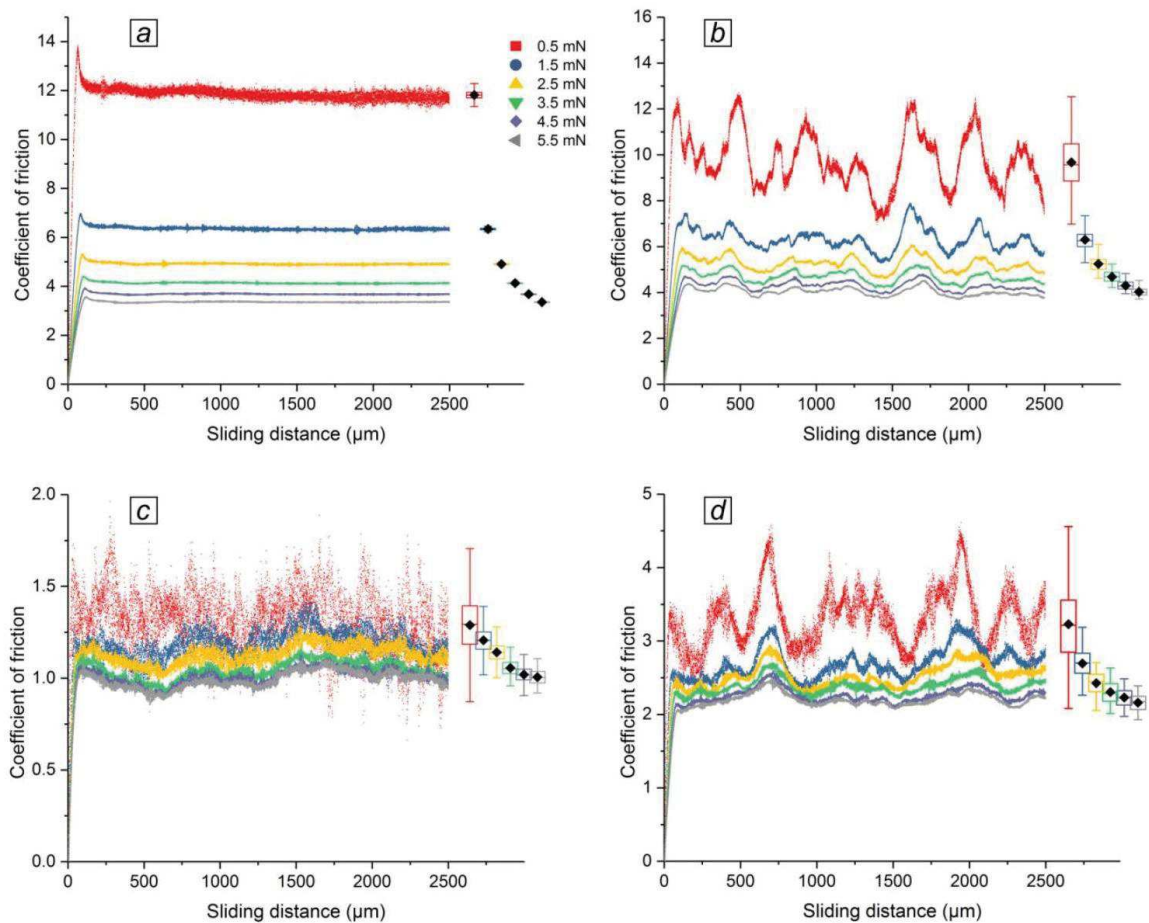


Figure 4 Coefficient of friction versus sliding distance for all four surfaces investigated. The sliding speed was kept constant (16.67 $\mu\text{m/s}$) for all tests. (a) Smooth surface, (b) *Hevea* replica, (c) *Ludisia* replica and (d) *Litchi* replica. Box plots were plotted with considering the data points after 750 μm sliding distance. The colour coding of symbols for different loading conditions hold same for all graphs, as mentioned in graph a. The x-axis scales are different on each surface to fit graphs comparable.

As shown in Figure 4.a, the friction coefficient curve behaviour on smooth PDMS was observed continuous with low noise for all normal loads (0.5 to 5.5 mN). The reduction in COF with increase in normal load could be understood with considering the tangential friction force is

proportionally dependent on the real contact area (implies an inverse dependence for friction COF), has also been observed and discussed by Zhang *et al.* [51] and Yashima *et al.* [13].

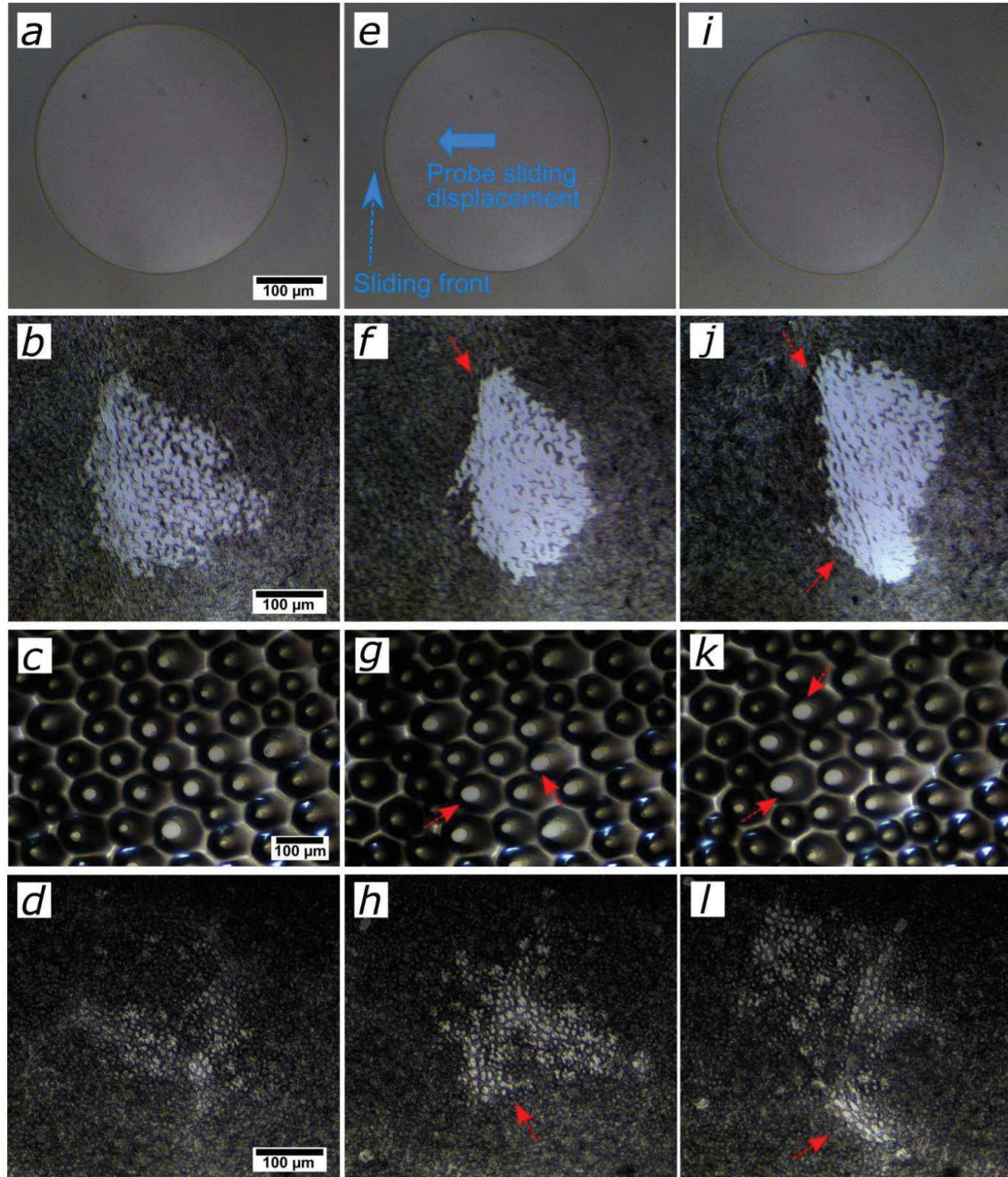


Figure 5 *In-situ* real contact images during the sliding friction tests on all four substrates, at a normal load of 1.5 mN and a sliding speed of 16.67 $\mu\text{m/s}$. From top; Smooth surface (first row), *Hevea* replica (second), *Ludisia* replica (third) and *Litchi* replica (forth). First column images represent the contact visual at static state (under full normal load), just before the sliding initiates. Red arrows indicate different points of interest. Scale bars hold the same for each surface type as mentioned on the respective static image. Sliding front applies same as stated for smooth PDMS.

For smooth PDMS samples, the contact formation during the loading stage, until the full normal load ($F_n = 1.5$ mN) established, was circular (circularity parameter:1) and continuous, as shown in Figure 5.a. As soon as sliding started, a continuous reduction in real contact area was observed (Figure 5.a, 5.e and 5.i), however, the reduction got saturated (by a drop of 13.1 %) after a certain sliding distance. The reduction could be interpreted with the effective stiffening of soft polymers on a transition from static to kinetic phase [1, 52]. What is also interesting is that the contact, which was circular during the static stage, turned into an elliptical shape and remain the same for the whole kinetic region. The similar phenomenon has also been observed in some previous research [53–55]. The circular to elliptical shape transition took place continuously. Moreover, in our investigation, no stick-slip like instability event was recorded on smooth PDMS surface, and this applies to all normal loading conditions [56].

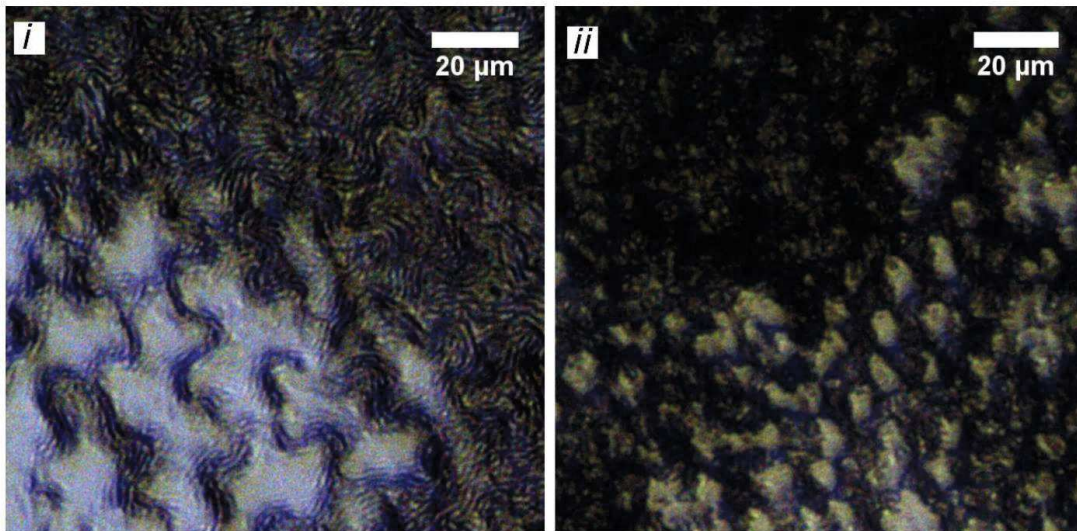


Figure 6 High-resolution zoomed-in view of *In-situ* contact images at a normal load of 1.5 mN for better visualization of the regions in real contact and out of contact. (i) *Hevea* replica, (ii) *Litchi* replica.

A similar reduction behaviour in COF was recorded on *Hevea* replica surfaces. Interestingly, as can be seen in Figure 4.b, the reduction in COF seems greater for an initial increase in normal force (0.5 mN to 1.5 mN) as compared to the further increase in F_n (from 1.5 to 5.5 mN). In regard to contact dynamics on *Hevea* replica, during the early stage of loading, the real contact took place just on very top of the fine cuticular fold structures (follow full movie ‘Video.2’ for better understanding). However, at the fully loaded static stage, real contact grew over the individual cells, this making locally full contacts yet leaving the cells boundaries out of contact (dark fine lines around the cells in full contact), as can be seen in Figure 5.b. This can be better perceived in zoomed-in real contact image presented in Figure 6.i. When sliding initiated, the

cells, which were in full intimate contact (*puzzle-shaped* bright spots) stretched under the shear stresses, and relaxed back after the tip passed away. Although not obvious on videos, we assume the micro-structures coming into the contact during the sliding exhibit continuous style evolution, whereas the separation from the back in sudden detachment style. The most striking observation that emerges from *Hevea* replica, is the evolution of real contact junctions when confronting with the specific topographies; linear microstructure veins. In particular, when these veins consisting of linear folds, which are aligned in perpendicular orientation to the sliding direction, led to create more sliding resistance, due to a gradual accumulation of microstructures, as can be seen on Figure 5.f and 5.j. Similar effects originating from the relative orientation of microstructures have been observed in previous research [57, 58]. This morphological phenomenon affected the friction force response and thus created semiregular instabilities on friction coefficient curve (Figure 4.b). On a qualitative analysis, one could relate the periodicity of friction fluctuation with the morphological distribution on *Hevea* surface (Video.2). The fluctuating behaviour on friction coefficient curve is more pronounced for lower normal load condition as supported by the boxplot in Figure 4.b. This could be understood with the crushing of fine micro-structures at higher normal load conditions and therefore diminishing the fluctuation behaviour [11].

The results of friction measurements on *Ludisia* replicas demonstrated the lowest value of friction coefficient (for the whole normal force range), attributing to its unique surface patterning [35]. Examination of the *in-situ* videos recorded on *Ludisia* replica revealed that, the real contacts always formed at the very top of the conical shaped topographies and resulted in a tremendous reduction in real contact area (ratio of real contact to apparent contact: 7.5 %), as can be clearly visualized in Figure 5.c. For the static stage, the shape of real contacts found to be normally circular in shape. However, the circular shape of individual real contact smoothly turned into an ellipse-like shape without any evidence of contact instability, as pointed out in Figure 5.g and 5.k. Based on the *in-situ* videos observation, one might note that the micro-topographies on *Ludisia* replica did not show bending behaviour, rather sheared smoothly under steady state sliding. At the local scale, its patterns limit the shear strain to the very top of each micro-asperity. Indeed, the conical shape with the continuous increase of cross-section area toward the volume is not favourable for bulk accommodation of the shear and thus leading to confine it just at the top. The friction response observed on *Ludisia* replica was rather continuous however, one could notice the noisy behaviour on friction plots in Figure 4.c, particularly at low normal load conditions. This could be correlated with the non-homogenous

height distribution of its micro-topographies, which ruggedly confront with the sliding front of the tip when coming into the contact.

The friction characteristics on *Litchi* replica demonstrated fluctuating behaviours, which were more pronounced for the lowest normal load ($F_n = 0.5$ mN). Moreover, the reduction in COF with an increase in normal load also followed a quite similar trend as noticed for *Hevea* replica. We recognised some interesting events while examining *in-situ* video of *Litchi* replica. At first, the real contact regions were distributed randomly during the loading stage itself (Figure 5.d and 6.ii), which is certainly attributed to its irregular and heterogeneous surface morphology. Interestingly, a slight increase in the contrast of real contact junctions was observed as soon as the sliding began. During the sliding stage, contact evolution on *Litchi* replica followed a highly random spreading. Furthermore, the overhanging patterns (*rose-flower-shapes*) of *Litchi* replica, in our understanding, significantly influenced the friction response. These patterns could be storing some strain energy due to the deformation under shear [8]. Actually, contrary to the sliding behaviour observed on *Ludisia* replica where the shear is just confined at the very top of its conical asperities, the kink of overhanging patterns of the *Litchi* replica favours the full bending of micro-structures. As a consequence, the thickness involved in the shear accommodation is larger in *Litchi* replica than in *Ludisia* replica relatively to the height of their structures. The patterns which came out of contact from the back end randomly released the stored energy and leading to a non-smooth friction behaviour (Figure 4.d).

6.2.2 Effect of sliding speed:

The results obtained from the investigation of the sliding speed influence on friction characteristics for all four surfaces are presented in Figure 7, where the overall-tests average COF (kinetic) is plotted as a function of the sliding speed. The results demonstrated a clear dependency on the sliding speed of friction coefficient, contrary to Coulomb's law of friction, which states that the friction coefficient is independent of the sliding speed [50]. It is clearly evident in Figure 7, that the COF increased with raising the sliding speed for all four surfaces. These results suggest that the observed friction characteristics are a speed dependence phenomenon due to the polymeric nature of the materials in contact. This has been observed by several researchers in the past [42, 59–65]. Moreover, back in 1963, pioneer research by Grosch [66] established two key mechanisms contributing to the friction on rubber: first is the adhesion between the substrate surface and the tip, and the second is the energy loss arising from the material deformation. Later on, this was demonstrated by other researchers as well [4, 51, 64]. The frictional force (and friction coefficient) dependence on sliding speed (one can convert it

as frequency also) can be directly related to the frequency dependence of the viscoelastic loss (modulus) of polymeric materials [64, 66–68].

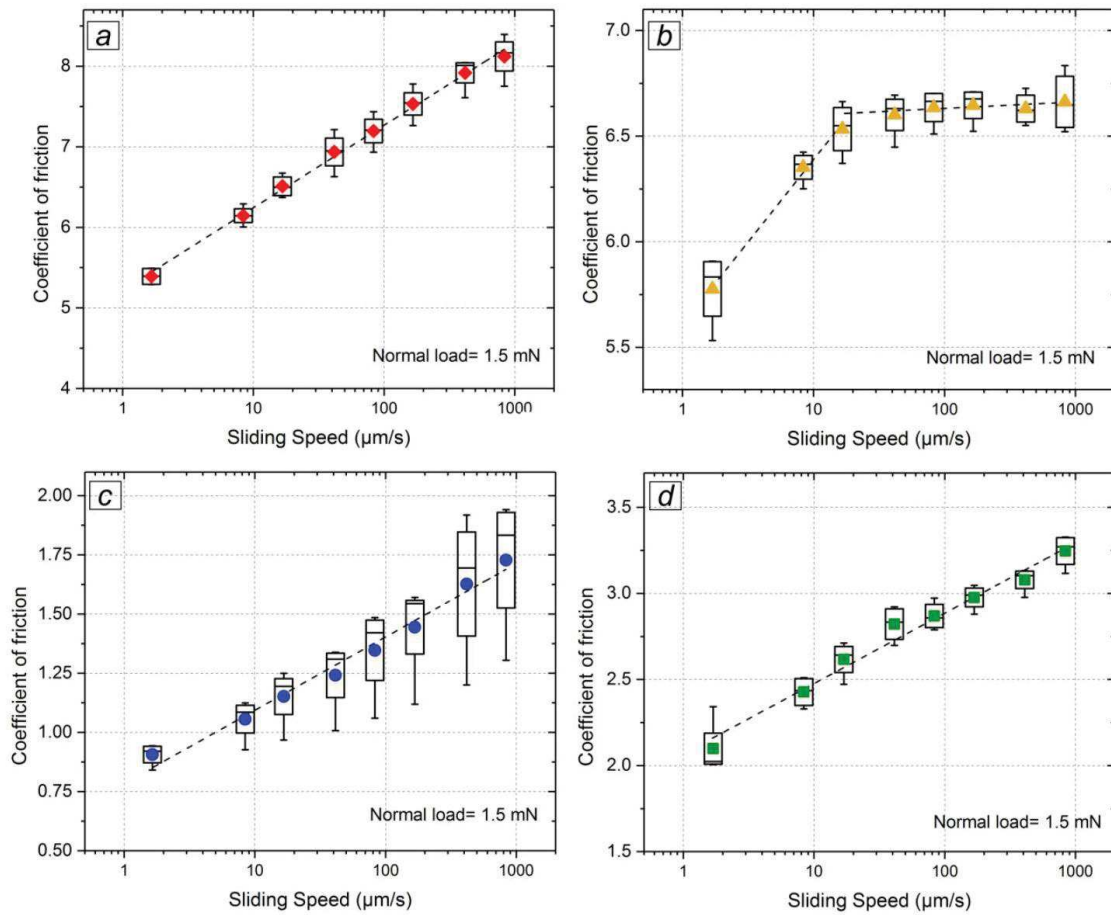


Figure 7 Plots of the coefficient of friction (μ) as a function of sliding speed (V) for all the four surfaces, keeping the normal load constant ($F_n = 1.5$ mN). (a) Smooth surface, (b) *Hevea* replica, (c) *Ludisia* replica and (d) *Litchi* replica. The friction coefficient values were estimated by calculating the arithmetic mean of the force data points after a sliding distance of 750 μm .

For the convenient understanding of speed dependent friction trends, key values of friction coefficient along with the corresponding increment (normalised by COF value at the slowest speed) are presented in Table 1. As can be seen in Figure 7.a for smooth PDMS surface, the evolution of the friction coefficient follows a linear behaviour, over the whole (log) speed range investigated. At the slowest sliding speed ($V = 1.67$ $\mu\text{m/s}$) the COF was 5.39, which increased by around 50.71 % at the fastest speed ($V = 833.34$ $\mu\text{m/s}$).

Table 1 The average friction coefficient values at slowest and highest sliding speeds, along with normalised increment of friction coefficient for all four surfaces.

Surface type	Coefficient of friction (COF)		Normalised COF increment
	Speed, 1.67 $\mu\text{m/s}$	833.34 $\mu\text{m/s}$	
Smooth PDMS	5.39	8.13	50.71 %
Hevea replica	5.75	6.71	Phase 1: 13.37 % Phase 2: 0.27 %
Ludisia replica	0.91	1.73	90.79 %
Litchi replica	2.09	3.24	54.63 %

By utilising the sliding speed (V) and the diameter ($2a$) of real contact, one could estimate the frequency of friction tests, by following the relation $f \approx V/2a$, where $2a$ could be measured from the *in-situ* real contact videos [51, 69]. This provides a frequency range varying from 0.003 to 1.3 Hz for our friction experiments. To gain a better understanding, we further extended this analysis on comparing the speed (frequency) dependence friction behaviour with the PDMS loss factor plot. The results obtained from the dynamic mechanical thermal analysis (DMTA) of PDMS, performed at room temperature, is plotted as loss factor versus frequency, shown in Figure 8.

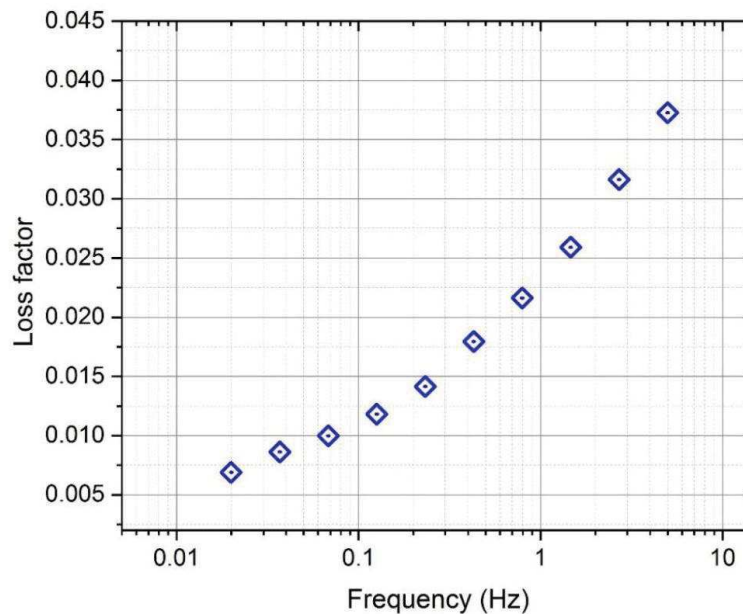


Figure 8 Plot for the loss factor as function of frequency for PDMS system at a reference room temperature ($22 \pm 3^\circ\text{C}$).

It is evident from the plot that loss factor increases with increase in frequency in DMTA analysis. However, on a quantitative comparison between the increase in COF on smooth

PDMS surface (Figure 7.a) against the increase in loss factor (Figure 8), over the same frequency interval, revealed an unexpected deviation. Increment of COF emerged out lower than as anticipated, unlike previous similar research by Klein *et al.* [68] and Zhang *et al.* [51], where their results quantitatively established a close agreement between loss factor and friction coefficient. However, their investigation was carried out for a different system (contact of a hard material tip against polymeric thin film coated substrate) and also on very high load condition. In our opinion, a possible interpretation of this unexpected behaviour on smooth PDMS could be explained with the high adhesive response between soft-soft interaction, especially at low normal force range.

Interestingly, the *Ludisia* and *Litchi* replicas revealed a higher COF increment, 90.79 % and 54.63 % respectively, as reported in Table 1. Possibly, this could be attributed to their microstructures which significantly reduced the interfacial adhesion as found in a previous study [38]. This stands if we consider the interfacial adhesion as speed independent, that could be reasonably assumed to our opinion. As a consequence, the other contribution induced by the shear may exhibit a relative larger dependence to the sliding speed. Moreover, because each pattern is not inclined to bend easily, *Ludisia* replica may confine the shear stress to a few top points of the conical tips and therefore increase the strain locally. Finally, the resulting dissipated energy may be more important in *Ludisia*'s case than in other studied microstructures, although the volume involved in the process may be smaller. Consequently, the thickness of the surface concerned by high shear is certainly lower than in other microstructures such as the *rose-flower-shaped* patterns of *Litchi* which can bend easily and accommodate the shear within a relatively large thickness inducing lower stress locally. What is interesting to point out here that, the COF increment for *Litchi* replica and smooth surface followed almost a similar behaviour (Figure 7.a and Figure 7.d), however the friction coefficient on *Litchi* replica found significantly low (2.09 to 3.24) as that of the smooth surface (5.39 to 8.13) over the whole sliding speed range (1.67 $\mu\text{m/s}$ to 833.34 $\mu\text{m/s}$). These findings on *Litchi* replica could have an important implication for specific engineering systems requiring such friction response with less adhesion force while maintaining the same COF increment with an increase in sliding speed as recorded for the smooth surface. Possibly, the easy bending of bunched overhanging patterns with a kink of the *Litchi* replica is likely to diminish the effective stiffening, contrary to the patterns of *Ludisia* replica. However, in regard to the friction response on *Hevea* replica, the increase in COF was significantly reduced, nearly to 13.37 %. One could note for the friction response from *Hevea* replica that, the linear fitting on COF data points did not accommodate satisfactorily in single line therefore, two separate linear fittings were performed (Figure 7.b).

In the beginning phase, an increase with a rate of 13.4 %, was observed from a sliding speed of 1.67 $\mu\text{m/s}$ to 16.67 $\mu\text{m/s}$. However, in the next phase from 83.34 $\mu\text{m/s}$ onwards, the gain in COF got almost saturated and could be well fitted within a horizontal line. This abnormal behaviour on *Hevea* replica could possibly be hypothesised with two distinct types of rheo-stiffening behaviours inducing from its fine micro-structures. In the first phase of slow speed, the structural induced stiffening led to slowly increase the friction coefficient. However, after an intermediate transition, on higher speeds, the fine micro-structured folds might be behaving as a fully stiffed floating bed for the sliding tip and thus resulting in a saturated friction increment. The speed dependence friction behaviour of *Hevea* replica could be considered in future research to be examined more closely. Since this original response as a function of the sliding speed might have some benefits for further applications.

7 Conclusions:

This study presents a thorough sliding friction investigation on complex biological morphologies, which were directly replicated from original plant leaf surfaces. Here, we systematically studied the effect of normal load and sliding speed on the friction characteristics.

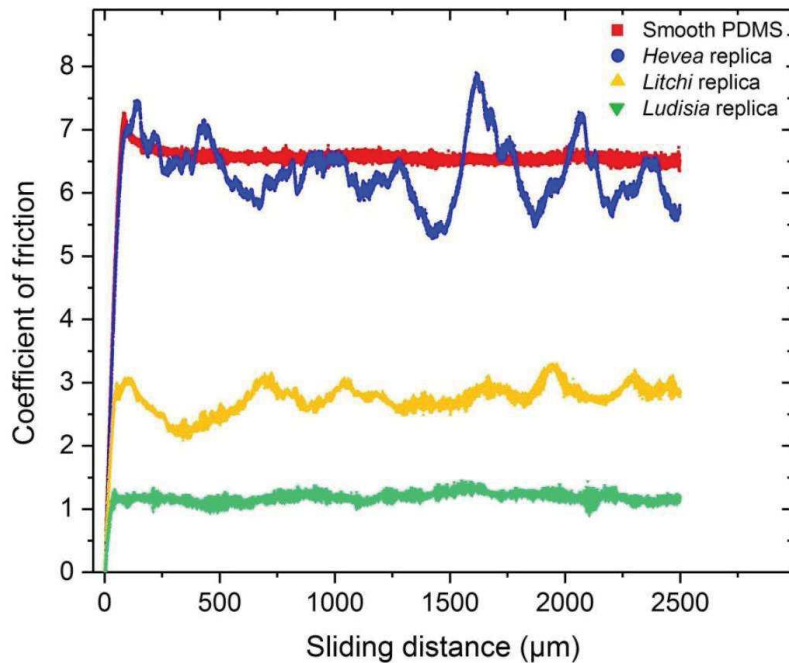


Figure 9 Overall comparison of the coefficient of friction (μ) as a function of sliding distance for all four surfaces investigated. All curves are plotted at a constant normal load (1.5 mN) and sliding speed (16.67 $\mu\text{m/s}$).

An overall comparison graph comprising representative friction responses recorded for all four surfaces is reported in Figure 9. Indeed, for any normal load condition, *Ludisia* replica (coarse structuring) and *Litchi* replica (complex morphologies) significantly lowered the friction as compared to that of smooth PDMS and *Hevea* replica (fine micro-structures). All four surfaces showed a decrease in COF with an increase in normal load however, each surface exhibited distinct COF reduction behaviour. Our examination of *in-situ* videos revealed the distinct sliding dynamics that were specifically arising from each surface topographies, and later their straight contribution transformed into different fluctuating events on friction response. Furthermore, a clear dependence on the sliding speed of friction response was recorded for all surfaces. With raising the sliding speed (frequency), friction coefficient apparently increased, however, each surface exhibited different rate and distinct behaviour of increment. To better understand the speed dependence friction dynamics, we correlated the friction response with the loss factor characteristics of standard material over the same frequency range. These results are discussed in the light of material properties and surface morphology considerations. Comparing all surfaces together, *Ludisia* replica demonstrated the lowest friction coefficient, owing to its unique conical shaped patterns, which tremendously cut down the real contact area. The understanding of unique friction behaviours, arising from complex biological surface morphologies, developed in this work may serve as an input to design bio-inspired functional surfaces. Our examination pointed out the importance of local strain induced by the different micro-structures led to creating different friction increment.

8 Funding:

This work was financially supported by the German Research Foundation (Deutsche Forschungsgemeinschaft: DFG) under the framework of International Research Training Group (IRTG) ‘Soft Matter Science - 1642’.

9 Acknowledgements:

The authors would like to thank the gardeners of botanical garden of the University of Freiburg for cultivating the plants used in this study. We are also thankful to the electron microscopy platform of Institut Charles Sadron, Strasbourg for SEM imaging. We want to thank Mr. Damien Favier (Institut Charles Sadron) for his support in modifying the friction force tester. We express our gratitude to the German Research Foundation (Deutsche Forschungsgemeinschaft: DFG), for the funding support.

10 References:

- [1] Persson BN. *Sliding friction: physical principles and applications*. Springer Science & Business Media, 2013.
- [2] Mate CM. *Tribology on the small scale: a bottom up approach to friction, lubrication, and wear*. 6, Oxford University Press, 2008.
- [3] Bhushan B. *Springer handbook of nanotechnology*. Springer Science & Business Media, 2010.
- [4] Nguyen D, Ramakrishna S, Frétiigny C, et al. Friction of rubber with surfaces patterned with rigid spherical asperities. *Tribology Letters* 2013; 49: 135–144.
- [5] Lu P, Wood RJ, Gee MG, et al. A novel surface texture shape for directional friction control. *Tribology Letters* 2018; 66: 51.
- [6] Maegawa S, Itoigawa F, Nakamura T. Effect of normal load on friction coefficient for sliding contact between rough rubber surface and rigid smooth plane. *Tribology International* 2015; 92: 335–343.
- [7] Matsuda K, Hashimoto D, Nakamura K. Real contact area and friction property of rubber with two-dimensional regular wavy surface. *Tribology International* 2016; 93: 523–529.
- [8] Murarash B, Itovich Y, Varenberg M. Tuning elastomer friction by hexagonal surface patterning. *Soft Matter* 2011; 7: 5553–5557.
- [9] Brörmann K, Barel I, Urbakh M, et al. Friction on a microstructured elastomer surface. *Tribology Letters* 2013; 50: 3–15.
- [10] Degrandi-Contraires E, Poulard C, Restagno F, et al. Sliding friction at soft micropatterned elastomer interfaces. *Faraday Discussions* 2012; 156: 255–265.
- [11] Rand CJ, Crosby AJ. Friction of soft elastomeric wrinkled surfaces. *Journal of Applied Physics* 2009; 106: 064913.
- [12] He B, Chen W, Wang QJ. Surface texture effect on friction of a microtextured poly(dimethylsiloxane) (PDMS). *Tribology Letters* 2008; 31: 187–197.
- [13] Yashima S, Romero V, Wandersman E, et al. Normal contact and friction of rubber with model randomly rough surfaces. *Soft Matter* 2015; 11: 871–881.
- [14] Koch K, Bhushan B, Barthlott W. Multifunctional surface structures of plants: an inspiration for biomimetics. *Progress in Materials Science* 2009; 54: 137–178.
- [15] Scherge M, Gorb S. *Biological micro-and nanotribology*. Springer Science & Business Media, 2001.
- [16] Bargel H, Barthlott W, Koch K, et al. Plant cuticles: multifunctional interfaces between plant and environment. In: Hemsley AR, Poole I (eds) *The evolution of plant physiology*. Academic Press, London, 2004, pp. 171–194.
- [17] Prüm B, Bohn HF, Seidel R, et al. Plant surfaces with cuticular folds and their replicas: influence of microstructuring and surface chemistry on the attachment of a leaf beetle. *Acta Biomaterialia* 2013; 9: 6360–6368.
- [18] Prüm B, Seidel R, Bohn HF, et al. Plant surfaces with cuticular folds are slippery for beetles. *Journal of the Royal Society Interface* 2012; 9: 127–135.
- [19] Drechsler P, Federle W. Biomechanics of smooth adhesive pads in insects: influence of tarsal secretion on attachment performance. *Journal of Comparative Physiology A* 2006; 192: 1213–1222.
- [20] Scholz I, Baumgartner W, Federle W. Micromechanics of smooth adhesive organs in stick insects: pads are mechanically anisotropic and softer towards the adhesive surface. *Journal of Comparative Physiology A* 2008; 194: 373–384.
- [21] Labonte D, Federle W. Scaling and biomechanics of surface attachment in climbing animals. *Philosophical Transactions of the Royal Society B: Biological Sciences* 2015; 370: 20140027.
- [22] Zhou Y, Robinson A, Steiner U, et al. Insect adhesion on rough surfaces: analysis of adhesive contact of smooth and hairy pads on transparent microstructured substrates. *Journal of the Royal Society Interface* 2015; 11: 1–12.
- [23] Koch K, Bhushan B, Barthlott W. Diversity of structure, morphology and wetting of plant surfaces. *Soft Matter* 2008; 4: 1943–1963.
- [24] Poppinga S, Koch K, Bohn HF, et al. Comparative and functional morphology of hierarchically structured anti-adhesive surfaces in carnivorous plants and kettle trap flowers. *Functional Plant Biology* 2010; 37: 952–961.

- [25] Gorb EV, Gorb SN. Physicochemical properties of functional surfaces in pitchers of the carnivorous plant *Nepenthes alata* Blanco (Nepenthaceae). *Plant Biology* 2006; 8: 841–848.
- [26] Barthlott W, Schimmel T, Wiersch S, et al. The *Salvinia* paradox: superhydrophobic surfaces with hydrophilic pins for air retention under water. *Advanced Materials* 2010; 22: 2325–2328.
- [27] Busch J, Barthlott W, Brede M, et al. Bionics and green technology in maritime shipping: an assessment of the effect of *Salvinia* air-layer hull coatings for drag and fuel reduction. *Philosophical Transactions of the Royal Society A* 2018; 377: 20180263.
- [28] Eder M, Amini S, Fratzl P. Biological composites—complex structures for functional diversity. *Science* 2018; 362: 543–547.
- [29] Barthlott W, Mail M, Bhushan B, et al. Plant surfaces: structures and functions for biomimetic innovations. *Nano-Micro Letters* 2017; 9: 23.
- [30] Prüm B, Seidel R, Bohn HF, et al. Impact of cell shape in hierarchically structured plant surfaces on the attachment of male Colorado potato beetles (*Leptinotarsa decemlineata*). *Beilstein Journal of Nanotechnology* 2012; 3: 57–64.
- [31] England MW, Sato T, Yagihashi M, et al. Surface roughness rather than surface chemistry essentially affects insect adhesion. *Beilstein Journal of Nanotechnology* 2016; 7: 1471–1479.
- [32] Gorb SN, Beutel RG, Gorb EV, et al. Structural design and biomechanics of friction-based releasable attachment devices in insects. *Integrative and Comparative Biology* 2002; 42: 1127–1139.
- [33] Bar-Cohen Y. Biomimetics—using nature to inspire human innovation. *Bioinspiration & Biomimetics* 2006; 1: 1–12.
- [34] McDonald B, Shahsavan H, Zhao B. Biomimetic micro-patterning of epoxy coatings for enhanced surface hydrophobicity and low friction. *Macromolecular Materials and Engineering* 2014; 299: 237–247.
- [35] Singh RA, Kim HJ, Kim J, et al. A biomimetic approach for effective reduction in micro-scale friction by direct replication of topography of natural water-repellent surfaces. *Journal of Mechanical Science and Technology* 2007; 21: 624–629.
- [36] Speck T, Speck O. Process sequences in biomimetic research. *Design and Nature IV* 2008; 114: 3–11.
- [37] Krick BA, Vail JR, Persson BN, et al. Optical in situ micro tribometer for analysis of real contact area for contact mechanics, adhesion, and sliding experiments. *Tribology Letters* 2012; 45: 185–194.
- [38] Kumar C, Damien F, Gauthier C, Speck T, Le Houérou V. In-situ investigation of adhesion mechanics on biological complex micro-structured surfaces. 2019; (*Under submission*).
- [39] Kumar C, Le Houérou V, Speck T, et al. Straightforward and precise approach to replicate complex hierarchical structures from plant surfaces onto soft matter polymer. *Royal Society Open Science* 2018; 5: 172132.
- [40] Wang S, Ren L, Liu Y, et al. Mechanical characteristics of typical plant leaves. *Journal of Bionic Engineering* 2010; 7: 294–300.
- [41] Saito T, Soga K, Hoson T, et al. The bulk elastic modulus and the reversible properties of cell walls in developing *Quercus* leaves. *Plant and Cell Physiology* 2006; 47: 715–725.
- [42] Vaenkatesan V, Li Z, Vellinga W-P, et al. Adhesion and friction behaviours of polydimethylsiloxane – A fresh perspective on JKR measurements. *Polymer* 2006; 47: 8317–8325.
- [43] Mata A, Fleischman AJ, Roy S. Characterization of polydimethylsiloxane (PDMS) properties for biomedical micro/nanosystems. *Biomedical Microdevices* 2005; 7: 281–293.
- [44] Schneider F, Draheim J, Kamberger R, et al. Process and material properties of polydimethylsiloxane (PDMS) for Optical MEMS. *Sensors and Actuators A: Physical* 2009; 151: 95–99.
- [45] Kumar C, Palacios A, Surapaneni VA, et al. Replicating the complexity of natural surfaces: technique validation and applications for biomimetics, ecology and evolution. *Philosophical Transactions of the Royal Society A* 2018; 377: 20180265.
- [46] Deruelle M, Léger L, Tirrell M. Adhesion at the solid-elastomer interface: influence of the interfacial chains. *Macromolecules* 1995; 28: 7419–7428.
- [47] Deruelle M, Tirrell M, Marciano Y, et al. Adhesion energy between polymer networks and solid surfaces modified by polymer attachment. *Faraday Discussions* 1994; 98: 55–65.

- [48] Neinhuis C, Edelmann HG. Methanol as a rapid fixative for the investigation of plant surfaces by SEM. *Journal of Microscopy* 1996; 184: 14–16.
- [49] Talbot MJ, White RG. Methanol fixation of plant tissue for scanning electron microscopy improves preservation of tissue morphology and dimensions. *Plant Methods* 2013; 9: 36.
- [50] Bowden FP, Tabor D. *The Friction and Lubrication of Solids*. Oxford university press, 1950.
- [51] Zhang S, Tsou A, Li J. Scratching behavior of elastomeric poly (dimethylsiloxane) coatings. *Journal of Polymer Science, Part B: Polymer Physics* 2002; 40: 1530–1537.
- [52] Moore DF. On the decrease in contact area for spheres and cylinders rolling on a viscoelastic plane. *Wear* 1972; 21: 179–194.
- [53] Sahli R, Pallares G, Ducottet C, et al. Evolution of real contact area under shear and the value of static friction of soft materials. *Proceedings of the National Academy of Sciences* 2018; 115: 471–476.
- [54] Waters JF, Guduru PR. Mode-mixity-dependent adhesive contact of a sphere on a plane surface. In: *Proceedings of the Royal Society of London A: Mathematical, Physical and Engineering Sciences*. 2117, The Royal Society, 2010, pp. 1303–1325.
- [55] Savkoor A, Briggs G. The effect of tangential force on the contact of elastic solids in adhesion. *Proceedings of the Royal Society of London A Mathematical and Physical Sciences* 1977; 356: 103–114.
- [56] Berman AD, Ducker WA, Israelachvili JN. Origin and characterization of different stick-slip friction mechanisms. *Langmuir* 1996; 12: 4559–4563.
- [57] Suzuki K, Hirai Y, Ohzono T. Oscillating friction on shape-tunable wrinkles. *Applied Materials & Interfaces* 2014; 6: 10121–10131.
- [58] Baum MJ, Heepe L, Gorb SN. Friction behavior of a microstructured polymer surface inspired by snake skin. *Beilstein Journal of Nanotechnology* 2014; 5: 83–97.
- [59] Schallamach A. The velocity and temperature dependence of rubber friction. *Proceedings of the Physical Society Section B* 1953; 66: 386.
- [60] Cross R. Increase in friction force with sliding speed. *American Journal of Physics* 2005; 73: 812–816.
- [61] Zhang S. Friction, damage and stick-slip in the scratching of polymers. In: *Tribology and Interface Engineering Series*. Elsevier, 2006, pp. 56–84.
- [62] Bahadur S, Ludema KC. The viscoelastic nature of the sliding friction of polyethylene, polypropylene and copolymers. *Wear* 1971; 18: 109–128.
- [63] Popov VL, Voll L, Kusche S, et al. Generalized master curve procedure for elastomer friction taking into account dependencies on velocity, temperature and normal force. *Tribology International* 2018; 120: 376–380.
- [64] Barquins M. Sliding friction of rubber and Schallamach waves—a review. *Materials Science and Engineering* 1985; 73: 45–63.
- [65] McLaren K, Tabor D. Visco-elastic properties and the friction of solids: friction of polymers: influence of speed and temperature. *Nature* 1963; 197: 856.
- [66] Grosch K. The relation between the friction and visco-elastic properties of rubber. *Proceedings of the Royal Society of London A, Mathematical and Physical Sciences* 1963; 274: 21–39.
- [67] Barquins M, Courtel R. Rubber friction and the rheology of viscoelastic contact. *Wear* 1975; 32: 133–150.
- [68] Klein G, LeHouérou V, Muller R, et al. Friction properties of acrylic-carboxylated latex films—1: Effects of acrylic acid concentration and pH. *Tribology International* 2012; 53: 142–149.
- [69] Kajiyama T, Tanaka K, Takahara A. Surface molecular motion of the monodisperse polystyrene films. *Macromolecules* 1997; 30: 280–285.

List of Publications

Peer-reviewed publications

C. KUMAR, T. SPECK & V. LE HOUÉROU (2019, *as manuscript*):

Friction during adhesive contacts on complex micro-structured surfaces.

C. KUMAR, D. FAVIER, C. GAUTHIER, T. SPECK & V. LE HOUÉROU (2019, *under submission*):

In-situ investigation of adhesion mechanics on biological complex micro-structured surfaces.

C. KUMAR⁺, A. PALACIOS⁺, V. A. SURAPANENI, G. BOLD, M. THIELEN, E. LICHT, T. E. HIGHAM, T. SPECK & V. LE HOUÉROU (2018):

Replicating the complexity of natural surfaces: technique validation and applications for biomimetics, ecology, and evolution, *Philosophical Transactions of the Royal Society A*. 377: 20180265.

C. KUMAR, V. LE HOUÉROU, T. SPECK & H. F. BOHN (2018):

Straightforward and precise approach to replicate complex hierarchical structures from plant surfaces onto soft matter polymers, *Royal Society Open Science* 5 (4), 172132.

Further publications

C. KUMAR, D. FAVIER T. SPECK, & V. LE HOUÉROU (2018):

Quantitative investigations of adhesion and friction on micro-textured surfaces: inspiration from insect-plant interactions, *Freiburg Centre for Interactive Materials and Bioinspired Technologies (FIT) Report 2017*, 32-33, Freiburg.

C. KUMAR, T. SPECK, H. F. BOHN & V. LE HOUÉROU (2016, 2017):

Adhesion and friction on textured surfaces: inspiration from insect-plant interactions- I & II, *Freiburg Centre for Interactive Materials and Bioinspired Technologies (FIT) Report 2015 & 2016*, Freiburg.

Conferences

C. KUMAR, D. FAVIER, T. SPECK & V. LE HOUÉROU (2018):

Adhesion on polymeric plant leaf replicas: insight into the real contact zone, using *in-situ* visualization, *9th International Plant Biomechanics Conference, Montréal Canada* (Talk).

C. KUMAR, D. FAVIER, T. SPECK, H. F. BOHN & V. LE HOUÉROU (2017):

Adhesion dynamics of polymeric leaf replicas: influence of microstructure's size, morphology, and intricacy, *6th World Tribology Congress 2017, Beijing, China* (Talk).

C. KUMAR, T. SPECK, H. F. BOHN & V. LE HOUÉROU (2017):
Adhesion investigation of bio-replicated microstructure surfaces, *SEB's Annual International Conference, Gothenburg, Sweden* (Poster).

C. KUMAR, T. SPECK, H. F. BOHN & V. LE HOUÉROU (2017):
Contact mechanics of bio-replicated polymeric surfaces: inspired from insect-plant interactions, *Swiss NanoConvention (SNC), Fribourg, Switzerland* (Poster).

C. KUMAR, T. SPECK, H. F. BOHN & V. LE HOUÉROU (2016):
Precise development of complex and hierarchical micro-structure surfaces directly from the fresh plant leaves, *The Competence Network 'Functional Nanostructures', Annual meeting-2016, Bad Herrenalb, Germany* (Poster).

C. KUMAR, T. SPECK, H. F. BOHN & V. LE HOUÉROU (2016):
Adhesion investigation on biomimetic polymer replicas: effects of size, shape and hierarchy levels of microstructures", *Beilstein Nanotechnology Symposium, Potsdam, Germany* (Poster).

C. KUMAR, V. LE HOUÉROU, T. SPECK & H. F. BOHN (2016):
A simple and low-cost method to develop micro-structured polymeric replica from anti-adhesive biological surfaces, *3rd International Conference on BioTribology (ICoBT), London, England* (Poster).

C. KUMAR, V. LE HOUÉROU, T. SPECK & H. F. BOHN (2015):
Adhesion and friction investigation on biomimetic polymer replicas: inspiration from plant surfaces. *Annual SoMaS (Soft matter science) Summer School, Mittelwihr, France* (Poster).

Appendix

Replication techniques:

1. Epoxy-PDMS replication technique:

In the Epoxy-PDMS replication approach, epoxy negative moulds were directly developed by simply peeling off the leaf samples (only for the *H. brasiliensis*, *L. discolor*) from cured epoxy (Figure 1). However, in case of *L. chinensis*, leaf samples could not be separated out from the cured epoxy (Figure 2) therefore, a dedicated chemical treatment was performed.

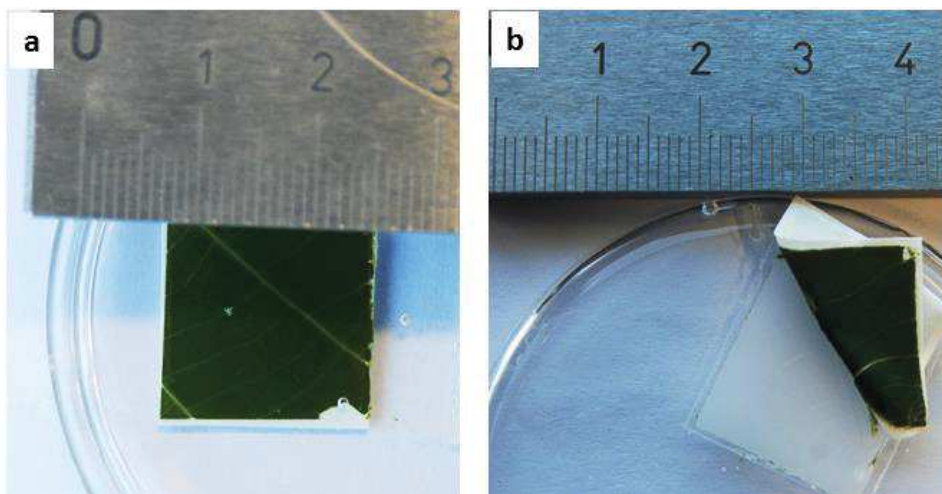


Figure 1. Preparation of negative Epoxy mould from *H. brasiliensis*. (a) Photograph of *H. brasiliensis* leaf sample filled up with epoxy resin. (b) After curing leaf sample could be easily peeled off from negative epoxy mould.

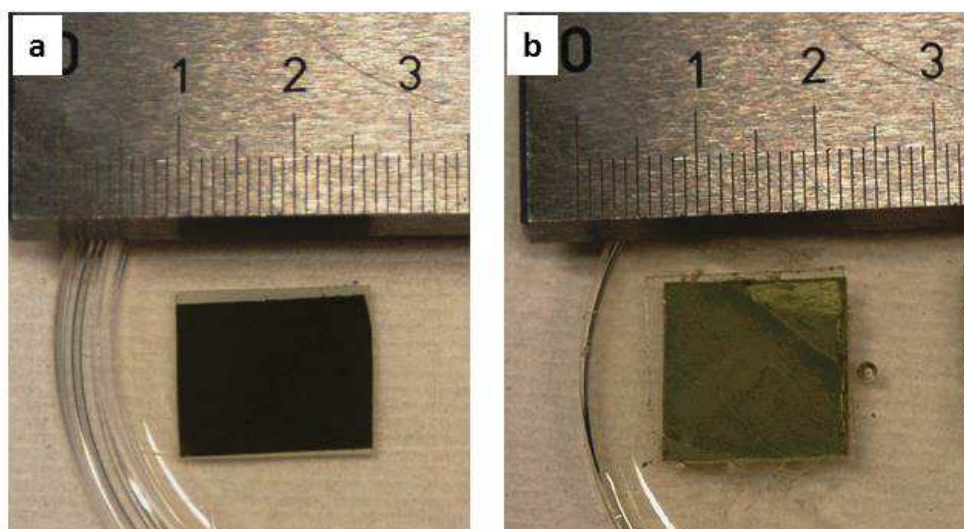


Figure 2. Preparation of negative Epoxy mould from *L. chinensis* leaf. (a) Photograph of *H. brasiliensis* leaf sample filled up with epoxy resin. (b) After curing, *L. chinensis* leaf was firmly embedded in epoxy mould and could not be separated out.

2. PVS-PDMS Replication:

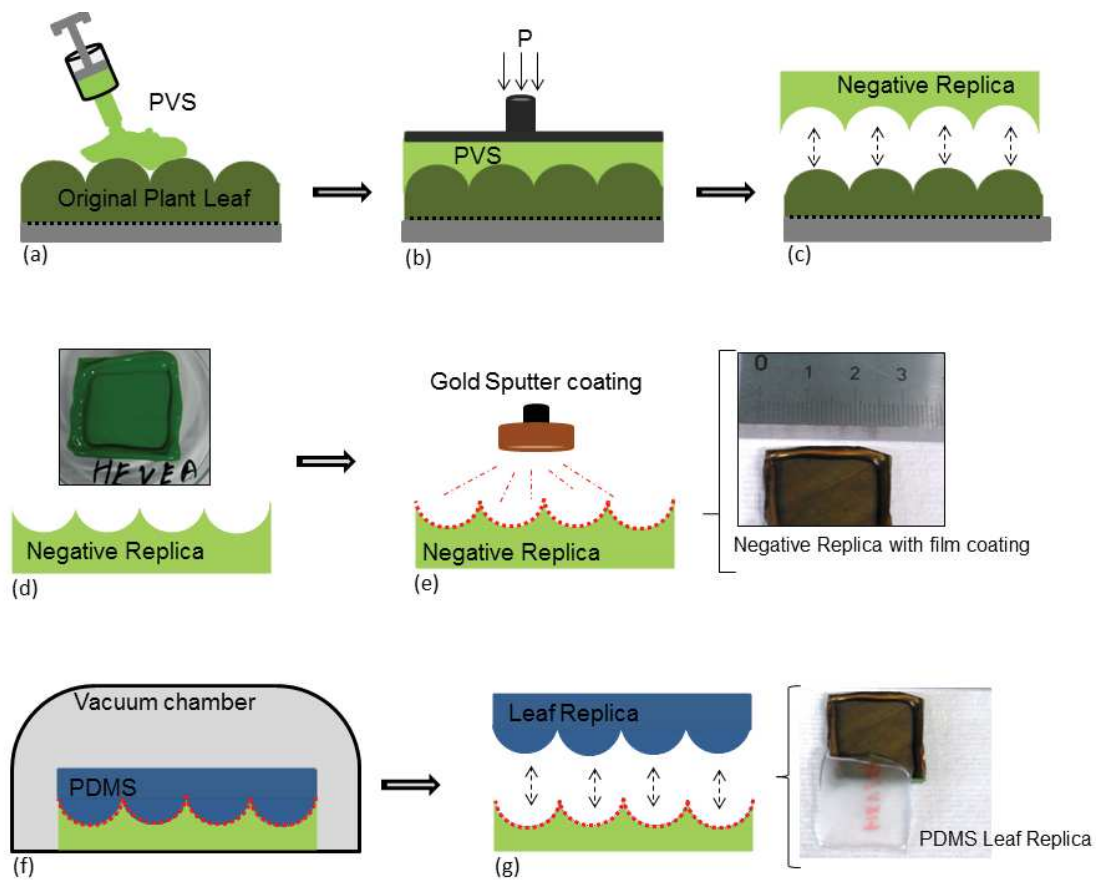


Figure 3. Schematic diagram of PVS- PDMS replication process. Pouring of PVS mixture onto original fresh plant leaf sample (a) and development of cured negative PVS mould (b). Cured PVS negative mould separated from leaf surface (c, d), and coated with gold particles thin coating (e). PVS mould filled up with PDMS mixture (e) and curing in oven. Developed PDMS replica with replicated microstructures of leaf surface (g).

3. PDMS-PDMS replication technique:

Due to high stiction in between PDMS-PDMS surface, it was not possible to peeled-off PDMS replica from negative PDMS mould. To address this issue, it was essential to make an anti-stiction surface treatment on the negative PDMS mould. A silane deposition setup (Figure 4.a) was designed in our lab and a simplified sketch of vapour phase silanization process is presented in Figure 4.b. Silanization setup consists of a vacuum pump, vacuum desiccator, absorption trap and pressure gauge. PDMS substrate (negative mould) was kept inside the desiccator with a support of side wall. 30-50 μL (few drops) of silane chemical (Trichloro 1H, 1H, 2H, 2H perfluorooctyl silane) was placed in a small petri dish. The desiccator was closed and connected to a vacuum pump for about 30 min. An adsorption filter trap was also installed in between the vacuum desiccator and the pump to avoid the contamination of the vacuum pump with toxic and corrosive silane particles (Figure 1.a). All silanization treatments were performed inside a

fume hood. After 3 hours of silanization, samples were washed with Isopropyl alcohol (IPA) and deionized water, and subsequently dried with nitrogen air. Silane treated negative PDMS mould was further used to develop positive replicas.

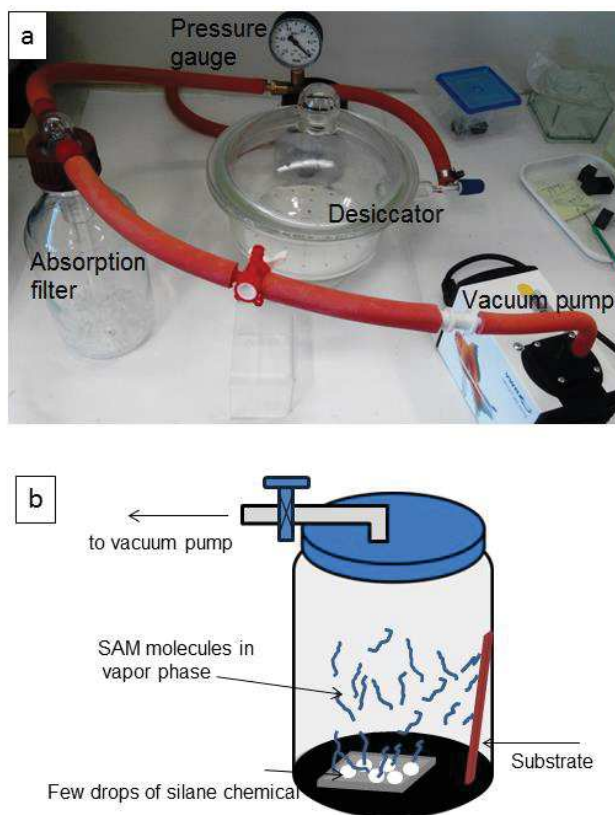


Figure 4 Photograph of silanization setup used for anti-stiction treatment of negative PDMS moulds (a), and a simplified schematic exhibiting vapour phase silanization process (b).

Quantitative and qualitative investigation of adhesion
and friction on textured surfaces: inspiration from
insect-plant interactions

Résumé

L'adhérence et le frottement existent dans de nombreux systèmes techniques ainsi que dans les systèmes naturels. Ces deux phénomènes ont une influence importante sur la durabilité et l'efficacité des dispositifs techniques. Une approche reconnue pour ajuster précisément ces caractéristiques - outre le fait de modifier les propriétés physico-chimiques - est la texturation des surfaces en contact. Les surfaces de feuilles de plantes sont souvent décorées avec des morphologies de surface diverses, et présentent ainsi des fonctionnalités de surface remarquables. Cette thèse visait à réaliser une étude systématique de la mécanique de l'adhérence et du frottement sur des surfaces micro-structurées, répliquées à partir de surfaces de feuilles végétales, en contact avec une sonde qui s'inspire de l'organe adhérent d'un insecte.

Les morphologies de surface de trois feuilles végétales différentes ont été directement transférées sur un polymère viscoélastique. Pour ce faire, trois approches différentes de reproduction ont fait l'objet d'une étude approfondie. La microscopie électronique à balayage et la microscopie confocale à balayage laser ont été utilisées pour l'évaluation qualitative et quantitative de la qualité de reproduction. Concernant l'étude de la mécanique du contact, un nano-indenteur a été modifié, permettant d'enregistrer les images *in situ* des contacts réels. Des tests de pull-off ont été menés afin d'évaluer quantitativement l'effet de la pré-charge sur la force d'adhésion et pour comprendre les modes distincts de collage/décollement. Des essais de frottement ont été effectués afin d'examiner l'effet de la charge normale et de la vitesse de glissement sur la force de frottement. Les résultats ont été discutés en fonction de la topographie de chaque surface.

Mots-clés : Feuilles végétales, microstructures, polymère PDMS, reproduction, mécanique du contact, adhésion, frottement, imagerie *in situ*

Résumé en anglais

Adhesion and friction exist in many technical systems as well as in natural ones. Both phenomena have a profound influence on the durability and efficiency of technical systems. A well-recognised way to tune these characteristics - besides altering the physicochemical properties - is the texturing of the interacting surfaces. Inspiringly, plant leaf surfaces are often decorated with diverse surface morphologies, and so show remarkable functionalities. This thesis aimed to perform a systematic investigation of adhesion and friction mechanics on micro-structured surfaces replicated from plant leaves, in contact with a probe, which was inspired from an insect's adhesive pad.

Surface morphologies of three different plant leaves were directly transferred onto a viscoelastic polymer. For this, three different replication approaches were comprehensively explored. Scanning electron microscopy and confocal laser scanning microscopy were used for the qualitative and quantitative evaluation of replication ability. For the contact mechanics investigation, a high-resolution nanoindenter was modified, with incorporating a unique feature to record the *in-situ* real-contact images. Pull-off tests were carried out to quantitatively evaluate the effect of pre-load on adhesion force characteristics and to understand distinct attachment-detachment modes. Friction investigations were performed to examine the effect of normal load and sliding speed on the friction force. Results were discussed with regard to each surface's topography.

Key-words: Plant leaves, micro-structures, PDMS polymer, replication, contact mechanics, adhesion, friction, in-situ imaging